MULTIDISCIPLINARY CENTER FOR EARTHQUAKE ENGINEERING RESEARCH
A National Center of Excellence in Advanced Technology Applications

ISSN 1520-295X

Seismic Behavior of Rail Counterweight Systems of Elevators in Buildings

by

Mahendra Pal Singh, Rildova and Luis E. Suarez
Virginia Polytechnic Institute and State University
Department of Engineering Science and Mechanics
305 Norris Hall
Blacksburg, Virginia 24061-0219

Technical Report MCEER-02-0002

May 27, 2002

This research was conducted at Virginia Polytechnic Institute and State University and was supported primarily by the Earthquake Engineering Research Centers Program of the National Science Foundation under award number EEC-9701471.

NOTICE

This report was prepared by the Virginia Polytechnic Institute and State University as a result of research sponsored by the Multidisciplinary Center for Earthquake Engineering Research (MCEER) through a grant from the Earthquake Engineering Research Centers Program of the National Science Foundation and other sponsors. Neither MCEER, associates of MCEER, its sponsors, the Virginia Polytechnic Institute and State University, nor any person acting on their behalf:

a. makes any warranty, express or implied, with respect to the use of any information, apparatus, method, or process disclosed in this report or that such use may not infringe upon privately owned rights; or

b. assumes any liabilities of whatsoever kind with respect to the use of, or the damage resulting from the use of, any information, apparatus, method, or process disclosed in this report.

Any opinions, findings, and conclusions or recommendations expressed in this publication are those of the author(s) and do not necessarily reflect the views of MCEER, the National Science Foundation, or other sponsors.

MULTIDISCIPLINARY CENTER FOR EARTHQUAKE ENGINEERING RESEARCH
A National Center of Excellence in Advanced Technology Applications

Seismic Behavior of Rail Counterweight Systems of Elevators in Buildings

by

Mahendra Pal Singh[1], Rildova[2] and Luis E. Suarez[3]

Publication Date: May 27, 2002
Submittal Date: November 6, 2000

Technical Report MCEER-02-0002

Project Numbers 98-2404, 99-2405, 00-2405 and 01-2042

NSF Grant Number EEC-9701471

1 Professor, Department of Engineering Science and Mechanics, Virginia Polytechnic Institute and State University
2 Graduate Student, Department of Engineering Science and Mechanics, Virginia Polytechnic Institute and State University
3 Professor, Department of Civil Engineering, University of Puerto Rico, Mayaguez, Puerto Rico

MULTIDISCIPLINARY CENTER FOR EARTHQUAKE ENGINEERING RESEARCH
University at Buffalo, State University of New York
Red Jacket Quadrangle, Buffalo, NY 14261

Preface

The Multidisciplinary Center for Earthquake Engineering Research (MCEER) is a national center of excellence in advanced technology applications that is dedicated to the reduction of earthquake losses nationwide. Headquartered at the University at Buffalo, State University of New York, the Center was originally established by the National Science Foundation in 1986, as the National Center for Earthquake Engineering Research (NCEER).

Comprising a consortium of researchers from numerous disciplines and institutions throughout the United States, the Center's mission is to reduce earthquake losses through research and the application of advanced technologies that improve engineering, pre-earthquake planning and post-earthquake recovery strategies. Toward this end, the Center coordinates a nationwide program of multidisciplinary team research, education and outreach activities.

MCEER's research is conducted under the sponsorship of two major federal agencies: the National Science Foundation (NSF) and the Federal Highway Administration (FHWA), and the State of New York. Significant support is derived from the Federal Emergency Management Agency (FEMA), other state governments, academic institutions, foreign governments and private industry.

MCEER's NSF-sponsored research objectives are twofold: to increase resilience by developing seismic evaluation and rehabilitation strategies for the post-disaster facilities and systems (hospitals, electrical and water lifelines, and bridges and highways) that society expects to be operational following an earthquake; and to further enhance resilience by developing improved emergency management capabilities to ensure an effective response and recovery following the earthquake (see the figure below).

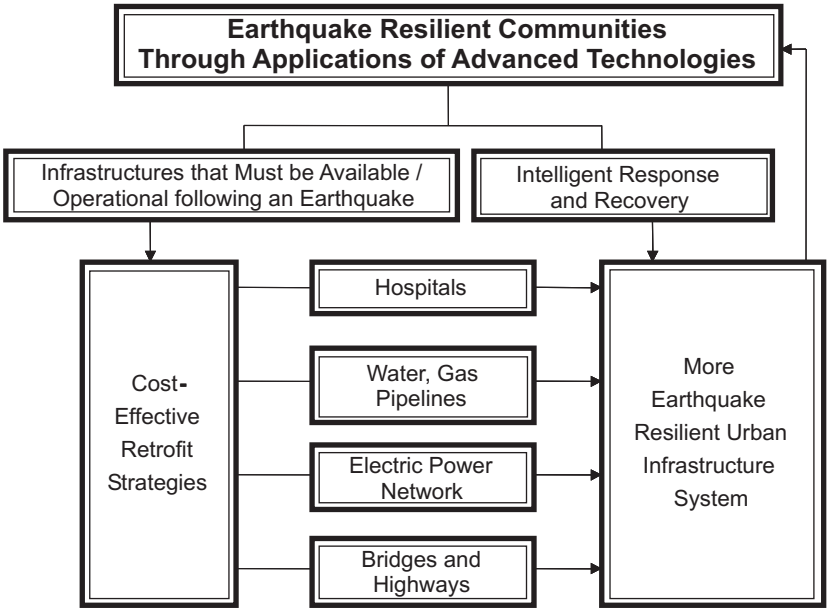

A cross-program activity focuses on the establishment of an effective experimental and analytical network to facilitate the exchange of information between researchers located in various institutions across the country. These are complemented by, and integrated with, other MCEER activities in education, outreach, technology transfer, and industry partnerships.

The study described in this report focused on the seismic performance of elevator systems. The report begins with an overview of elevator systems used in buildings, including various components of the system and their functions. From the standpoint of seismic performance, the rail-counterweights are the most vulnerable components of the system. Current code procedures used for the design of the rail and guidance system are provided, as is a survey of available literature on the seismic response and performance evaluation of elevator systems. The authors develop simple linear and more realistic nonlinear models to evaluate the seismic performance of the rail-counterweight system. The linear model provides a convenient tool for a preliminary study of the system to provide valuable insight into the dynamic behavior; it can also be conveniently used to examine protective options to improve seismic performance of the system. The nonlinear model, on the other hand, is necessary to study the performance of the system under more realistic seismic conditions. A comprehensive parametric study is conducted to evaluate the effect of various parameters on the seismic response of the system. The analytical models and approach described in the report will aid in seismic evaluation of hospitals equipped with elevators for vertical transportation. This study will also help the designers and manufacturers of the elevator systems understand why elevators behave as they do in earthquakes and will help them to evaluate the modification and design changes that may be necessary to improve their seismic performance.

ABSTRACT

Elevator systems in buildings are known to be susceptible to earthquake induced ground motions. In past earthquake events, several cases of elevator malfunctions have been reported. These disruptions have serious implication for critical facilities such as an urban hospital where the availability of critical care is seriously jeopardized by unavailability of the elevators in the facility.

Section 1 of this report provides general information about the components of an elevator system and their observed performances during past earthquakes. It is observed that in an elevator system, the counterweight being the heaviest component of the system is also the most vulnerable to earthquake induced ground motion. This section also describes the current code provisions for the design of the guide rails, evolution of various safety measures that have been proposed, and previous studies conducted on these vulnerable components.

It is noted that any study conducted to evaluate seismic performance of elevator systems must include the details of their guidance systems in the analysis. The focus of this study, therefore, has been on the development of comprehensive analytical models of the rail-counterweight systems that include these details. The analytical models for the in-plane and out-of-plane vibration analyses are developed. The models incorporate the mechanical characteristics and flexibilities of the roller guide assembly, guide rails, and support brackets. They also consider the differential inputs at the counterweight supports that filtering through the building. Both the linear and nonlinear models are developed; in the latter model, the nonlinearities caused by the closing and opening of the gaps at the restraining plates and the gap between the counterweight frame and rails are considered.

Several sets of numerical results are presented for different buildings, different earthquake motions, different rails sizes, and different flexibilities and gap sizes. The characteristics of the maximum stress response in the rails and the brackets are examined. Linear models can be useful for providing a valuable insight into the dynamic behavior of the system. They can also be conveniently used to examine different protective options that can be used to improve the seismic performance of elevator systems. For the higher levels of excitation, however, the effect of the gap closing and opening on the response must be considered. The maximum response need not occur when the counterweight is at the top of the structure even though the structure may have higher acceleration at those levels. The maximum response magnitude and location are affected in a complex manner by the dynamic characteristics of building, rail-counterweight system, nonlinearity of the roller guide assemblies, and of course the frequency characteristics of the input. It is difficult to predict any trend in the maximum response as a function of the problem parameters. For a careful evaluation of an elevator counterweight system, it is necessary to include a realistic variation of these parameters in the study with detailed time history analysis of the system.

ACKNOWLEDGEMENT

This research is supported by multidisciplinary Center for Earthquake Engineering Research through project numbers: 982404, 992405, 00-2405, and 01-2042. This support is gratefully acknowledged.

TABLE OF CONTENTS

SECTION	TITLE	PAGE
1	**ELEVATOR SYSTEMS, PAST SEISMIC PERFORMANCES AND CODES**	1
1.1	Introduction	1
1.2	Components of an Elevator System	1
1.3	Observed Performance of Elevators During Earthquakes	7
1.4	Seismic Code Provisions for Elevators	13
1.4.1	Design of Guide Rails	15
1.4.2	Design Forces for Brackets	18
1.4.3	Seismic Safety Triggers	20
1.5	Seismic Behavior of Escalators	22
1.6	Previous Studies on the Seismic Response	22
1.7	Objective and Scope of the Report	26
2	**LINEAR MODEL AND ANALYSIS**	27
2.1	Introduction	27
2.2	Analytical Model	28
2.2.1	Out-of-plane Motion	28
2.2.2	Inplane Motion	34
2.3	Equivalent Spring Coefficients	35
2.3.1	Coefficient for the Elastomer Roller	36
2.3.2	Coefficient for the Helical Spring	37
2.3.3	The Stiffness Coefficients for the Rails and Brackets	38
2.4	Solution of the Equations of Motion	38
2.5	Deformation and Stresses	40
2.6	Numerical Results	41
2.6.1	Seismic Responses	45
2.7	Concluding Remarks	54
3	**NONLINEAR MODEL AND ANALYSIS**	75
3.1	Introduction	75
3.2	Equations of Motion	76
3.2.1	Out-of-plane Motion	76
3.2.2	In-plane Motion	80
3.2.3	Damping Mechanism	84
3.3	Numerical Results	84
3.4	Concluding Remarks	92
4	**SUMMARY AND CONCLUDING REMARKS**	145
	REFERENCES	147

TABLE OF CONTENTS (cont'd)

SECTION	TITLE	PAGE
APPENDIX	**NUMERICAL INTEGRATION METHODS**	
A.1	Newmark-β	A-1
A.2	Runge-Kutta Method	A-7
A.3	Predictor-Corrector Method	A-9
A.4	Comparison of Numerical Results	A-10

LIST OF ILLUSTRATIONS

FIGURE	TITLE	PAGE
1-1	Main Components of a Typical Traction-Type Passenger Elevator	3
1-2	Nominal Cross-Section for Elevator Guide Rails According to the ASME A17.1 Code	5
1-3	A Typical Three-Wheel Roller Guide Assembly	6
1-4	Guide Rail Retainer Plate and Displacement Switch	6
1-5	Graphs for Selection of Bracket Spacing for 12-lb Guide Rails According to the A17.1 Code	16
1-6	Forces Acting at the Guide Rails Used for Seismic Design	16
1-7	Model Used to Define the Seismic Forces for Bracket Design When the Rail Span Is Equal to or Smaller than the Distance Between the Restraints Position	19
1-8	Model Used to Define the Seismic Forces for Bracket Design When the Rail Span Is Greater than the Distance Between the Restraints Position	19
2-1	Geometry of the 3-dof Model of the Rail-Counterweight System	29
2-2	The Displaced Counterweight Due to the Motion of the Four Supports	29
2-3	Plan View of the Building Slab, Elevator Shaft and Counterweight	32
2-4	Counterweight Positions Along the Rail	33
2-5	Equivalent Springs Representing the Brackets, Rails, and Roller Guides	36
2-6	Geometry of the Wheel in the Roller Guide	37
2-7	Natural Frequencies of the System for the Counterweight in the Top Story of the 10-Story Building for 18.5-lb. Rail	46
2-8	Natural Frequencies of the System for Different Counterweight Positions Along the 10-Story Building for 18.5-lb. Rail	47
2-9	Acceleration Time Histories for Northridge Earthquake	48
2-10	Seismic Input Components for Eqs. (2-11) and (2-12), for Counterweight Located in the Middle of the Top Story of the 10-Story Building, Northridge Earthquake	49
2-11	Points of Interest for Evaluation of Stresses in the Rail and Bracket	50
2-12	Maximum Stress in the Rail's Flange for the Counterweight in the Top Story of 10-Story Building for Northridge Earthquake	56
2-13	Maximum Stress in the Rail's Web for the Counterweight in the Top Story of 10-Story Building for Northridge Earthquake	57
2-14	Maximum Stress in the Rail's Flange for the Counterweight in the Top Story of 10-Story Building for Northridge Earthquake	58
2-15	Maximum Stress in the Rail's Flange for Different Counterweight Positions Along the 10-Story Building for Northridge Earthquake	59
2-16	Maximum Stress in the Rail's Web for Different Counterweight Positions Along the 10-Story Building for Northridge Earthquake	60

LIST OF ILLUSTRATIONS (cont'd)

FIGURE	TITLE	PAGE
2-17	Maximum Stress in the Brackets for Different Counterweight Positions Along the 10-Story Building for Northridge Earthquake	61
2-18	Maximum Stress in the Rail and Bracket for Different Counterweight Positions Along the 10-Story Building for Northridge Earthquake, Compared to Maximum Floor Accelerations	62
2-19	Maximum Stress in the Rail's Flange for Different Counterweight Positions Along the 10-Story Building for Northridge Earthquake, Compared to Maximum Floor Accelerations	63
2-20	Maximum Stress in the Rail's Web for Different Counterweight Positions Along the 10-Story Building for Northridge Earthquake, Compared to Maximum Floor Accelerations	64
2-21	Maximum Stress in the Bracket for Different Counterweight Positions Along the 10-Story Building for Northridge Earthquake, Compared to Maximum Floor Accelerations	65
2-22	Maximum Deformation of Roller Guide Assembly for Different Counterweight Positions Along the 10-Story Building for Northridge Earthquake, Compared to Maximum Floor Acceleration	66
2-23	Maximum Stress in the Rail's Web when the Counterweight is in the Top Story of the 10-Story Building as a Function of Stiffness Ratio α for El Centro Earthquake	67
2-24	Maximum Stress in the Rail's Flange for Different Counterweight Positions Along the of the 24-Story Building for Northridge Earthquake, Compared to Maximum Floor Acceleration	68
2-25	Maximum Stress in the Rail's Web for Different Counterweight Positions Along the of the 24-Story Building for Northridge Earthquake, Compared to Maximum Floor Acceleration	69
2-26	Maximum Stress in the Bracket for Different Counterweight Positions Along the of the 24-Story Building for Northridge Earthquake, Compared to Maximum Floor Acceleration	70
2-27	Maximum Deformation of Roller Guide Assembly for Different Counterweight Positions Along the of the 24-Story Building for Northridge Earthquake, Compared to Maximum Floor Acceleration	71
2-28	Maximum Stress in the Rail's Web, with and without Intermediate Tie-Brackets of Different Axial Stiffness, for Different Counterweight Positions Along the Top Story of 10-Story Building for Northridge Earthquake	72
2-29	Maximum Stress in the Rail's Web, with and without Intermediate Tie-Brackets of Different Axial Stiffness, for Different Counterweight Positions in the 18^{th} story for the Whittier earthquake. 24-story building.	73

LIST OF ILLUSTRATIONS (cont'd)

FIGURE	TITLE	PAGE
3-1	Free Body and Kinetic Diagram for the Out-of-Plane Motion of the Counterweight	77
3-2	The bilinear Restoring Force of the Upper Spring	78
3-3	The bilinear Restoring Force for Contact Between Rail and Counterweight Frame	81
3-4	Free Body and Kinetic Diagram for the In-Plane Motion of the Counterweight	82
3-5	In-Plane Displacement Time History at the Lower Left Roller Guide for $a_u/L = 0$, Northridge Earthquake 0.1g	85
3-6	Cross-sectional Properties of the Bracket	86
3-7	Maximum (1) Stress in the Rail Flange, (2) Rail Web, and (3) Brackets, (4) Floor Acceleration X-Direction, and (5) Floor Acceleration Y-Direction as a Function of Counterweight Position Along the Building Height, 10-Story Building; Northridge Earthquake 0.1g	95
3-8	Maximum (1) Stress in the Rail Flange, (2) Rail Web, and (3) Brackets, (4) Floor Acceleration X-Direction, and (5) Floor Acceleration Y-Direction as a Function of Counterweight Position Along the Building Height, 10-Story Building; El Centro Earthquake: 0.1g	96
3-9	Maximum (1) Stress in the Rail Web and (2) Floor Acceleration X-Direction as a Function of Counterweight Position Along the Building Height. 24-Story Building; Northridge Earthquake 0.843g	97
3-10	Maximum (1) In-Plane Force In Brackets and (2) Floor Acceleration X-Direction As A Function of Counterweight Position Along the Building Height. 24-Story Building; Northridge Earthquake 0.843g	98
3-11	Maximum Stress In The Rail As A Function of Counterweight Position For Different Values of The Clearance At Restraining Plates El Centro Earthquake 0.1g	99
3-12	Maximum Stress In The Brackets As A Function of Counterweight Position For Different Values of Clearances At The Restraining Plate El Centro 0.1g	100
3-13	Maximum In-Plane Force In The Brackets As A Function of Counterweight Position For Different Values of Clearances At The Restraining Plates. El Centro 0.1g	101
3-14	Maximum Stress In The Rail As A Function of Clearance At The Restraining Plates. El Centro Earthquake 0.1g	102
3-15	Maximum Force In The Brackets As A Function of Clearance At The Restraining Plates. El Centro Earthquake 0.1g	103

LIST OF ILLUSTRATIONS (cont'd)

FIGURE	TITLE	PAGE
3-16	Maximum Stress In The Rail As A Function of Maximum Ground Acceleration For Different Clearance Values. El Centro Earthquake	104
3-17	Maximum Inplane Forces In The Brackets As A Function of Maximum Ground Acceleration For Different Clearance Values El Centro Earthquake	105
3-18	Maximum Out-of-Plane Forces In The Brackets As A Function of Maximum Ground Acceleration For Difference Clearance Values El Centro Earthquake	106
3-19	Maximum Stress in the Rail As A Function of Maximum Ground Acceleration for Different Clearance Values. Northridge Earthquake	107
3-20	Maximum Inplane Forces in the Brackets as a Function of Maximum Ground Acceleration for Different Clearance Values Northridge Earthquake	108
3-21	Maximum Out-of-Plane Forces In The Brackets As A Function of Maximum Ground Acceleration For Different Clearance Values Northridge Earthquake	109
3-22	Maximum Stress In The Rail As A Function of The Bracket Stiffness Ratio. Northridge 0.1g	110
3-23	Maximum Forces In The Brackets As A Function of The Bracket Stiffness Ratio. Northridge Earthquake 0.1g	111
3-24	Maximum Stress In Different Rails As A Function of Counterweight Position. El Centro Earthquake 0.1g	112
3-25	Maximum Inplane Force in the Brackets for Different Rails as a Function of Counterweight Position. El Centro 0.1g	113
3-26	Maximum Out-of-Plane Force in the Bracket for Different Rail Sizes as a Function of Counterweight Position. El Centro 0.1g	114
3-27	Maximum Stress In Different Rails As A Function of Counterweight Position. As Recorded El Centro (0.348g)	115
3-28	Maximum Stress In Different Rails As A Function of Counterweight Position. As Recorded Northridge Earthquake 0.843g	116
3-29	Maximum Stress In The Rails For Different Base Inputs As A Function of Counterweight Position. All Motion Normalized To 0.1g	117
3-30	Maximum Inplane Force in the Brackets for Different Inputs as a Function of Counterweight Position. All Motions Normalized to 0.1g	118
3-31	Mean, Maximum And Minimum Values of The Stress Shown In Figure 3-29 For Different Inputs As A Function of Counterweight Position. All Motions Normalized To 0.1g	119
3-32	Mean, Maximum and Minimum Values of the Inplane Force Shown in Figure 3-30 for Different Inputs As A Function of Counterweight Position. All Motions Normalized To 0.1g	120

LIST OF ILLUSTRATIONS (cont'd)

FIGURE	TITLE	PAGE
3-33	Maximum Stress In The Rails For Different Base Inputs As A Function of Counterweight Position. All Motion Normalized To 0.5g	121
3-34	Maximum Inplane Force In Brackets For Different Inputs as a Function of Counterweight Position. All Motions Normalized To 0.5g	122
3-35	Mean, Maximum and Minimum Values of The Stress Shown in Figure 3-33 for Different Inputs as a Function of Counterweight Position. All Motions Normalized to 0.5g	123
3-36	Mean, Maximum And Minimum Values of The Inplane Force Shown in Figure 3-34 For Different Inputs As A Function of Counterweight Position. All Motions Normalized To 0.5g	124
3-37	Mean and Mean-Plus-One-Standard Deviation of Pseudo-Acceleration Spectra of 50 Sets of Synthetic Earthquakes Normalized to 0.1g	125
3-38	Mean and Mean-Plus-One-Standard Deviation of the Maximum Stress in the Rails for 50 Synthetic Earthquakes Normalized to 0.1g and 0.5g	126
3-39	The Coefficients of Variations of The Maximum Stress In The Rails for 50 Synthetic Earthquakes Normalized to 0.1g and 0.5g	127
3-40	Average of The Peak Stress In The Rails For 50 Synthetic Motions As A Function of Input Motion Intensity	128
3-41	Maximum Stress In The Rail For Different Frame Clearances As A Function of Counterweight Position For As Recorded Northridge Earthquake (0.834g)	129
3-42	Maximum In-Plane Force In The Brackets For Different Frame Clearances As A Function of Counterweight Position For As Recorded Northridge Earthquake (0.834g)	130
3-43	Maximum Stress In The Rail As A Function of The Frame Clearance For Actual Northridge (0.843g) and El Centro (0.348) Earthquakes	131
3-44	Maximum In-Plane Force In The Brackets As A Function of The Frame Clearances For Actual Northridge (0.834g) and El Centro (0.348g) Earthquakes	132
3-45	Maximum Stress In The Rails With And Without An Intermediate Tie-Bracket As A Function of Counterweight Position Northridge Earthquake 0.1g.	133
3-46	Maximum Stress In The Rails With And Without An Intermediate Tie-Bracket As A Function of Counterweight Position For As Recorded Northridge Earthquake 0.843g.	134

LIST OF ILLUSTRATIONS (cont'd)

FIGURE	TITLE	PAGE
3-47	Maximum Stress In The Rails With And Without An Intermediate Tie-Bracket As A Function of Counterweight Position For El Centro Earthquake 0.1g.	135
3-48	Maximum Stress In The Rails With And Without An Intermediate Tie-Bracket As A Function of Counterweight Position For As Recorded El Centro Earthquake 0.348g	136
3-49	Mean and Mean-Plus-One-Standard Deviation of the Maximum Stress in the Rails with an Intermediate Tie Brackets. 50 Synthetic Motions All Normalized To 0.1	137
3-50	Mean and Mean-Plus-One-Standard Deviation of the Maximum Stress in the Rails with an Intermediate Tie Brackets. 50 Synthetic Motions All Normalized to 0.5g	138
3-51	The Average of the Peak Stresses in the Rails with and without an Intermediate Tie-Bracket as a Function of Input Motion Intensity. Averaged From 50 Synthetic Earthquakes.	139
3-52	Coefficient of Variation of Maximum Stress In The Rail with Intermediate Tie-Bracket as a Function of Counterweight Position. 50 Synthetic Earthquakes Normalized to 0.1g and 0.5g.	140
3-53	Maximum Stress in the Rail for Increasing Intensity of El Centro Earthquake	141
3-54	Maximum Forces in the Bracket for Increasing Intensity of El Centro Earthquake	142
3-55	Maximum Stress in the Rail for Increasing Intensity of Northridge Earthquake	143
3-56	Maximum Forces in the Bracket for Increasing Intensity of Northridge Earthquake	144
A-1	Maximum Stress in the Rail for Counterweight in the Top Story of 10-Story Building, for Northridge 0.1g, Results from Different Numerical Methods	A-12
A-2	Maximum Stress in the Bracket for Counterweight in the Top Story of 10-Story Building, for Northridge 0.1g, Results from Different Numerical Methods	A-13
A-3	Maximum Stress in the Rail for Counterweight in the Top Story of 10-Story Building, for Actual Northridge Earthquake, Results from Different Numerical Methods	A-14
A-4	Maximum Stress in the Bracket for Counterweight in the Top Story of 10-Story Building, for Actual Northridge Earthquake, Results from Different Numerical Methods	A-15

LIST OF ILLUSTRATIONS (cont'd)

FIGURE	TITLE	PAGE
A-5	Maximum Stress in the Rail for Counterweight in the Top Story of 10-Story Building, for Northridge 0.1g, Results from Different Numerical Methods	A-16
A-6	Maximum Stress in the Bracket for Counterweight in the Top Story of 10-Story Building, for Northridge 0.1g, Results from Different Numerical Methods	A-17
A-7	Maximum Stress in the Rail for Counterweight in the Top Story of 10-Story Building, for Actual Northridge Earthquake, Results from Different Numerical Methods	A-18
A-8	Maximum Stress in the Bracket for Counterweight in the Top Story of 10-Story Building, for Actual Northridge Earthquake, Results from Different Numerical Methods	A-19
A-9	Maximum Stress in the Rail for Counterweight in the Top Story of 10-Story Building, for Northridge 0.1g, Results from Different Numerical Methods	A-20
A-10	Maximum Stress in the Bracket for Counterweight in the Top Story of 10-Story Building, for Northridge 0.1g, Results from Different Numerical Methods	A-21
A-11	Maximum Stress in the Rail for Counterweight in the Top Story of 10-Story Building, for Actual Northridge Earthquake, Results from Different Numerical Methods	A-22
A-12	Maximum Stress in the Bracket for Counterweight in the Top Story of 10-Story Building, for Actual Northridge Earthquake, Results from Different Numerical Methods	A-23

LIST OF TABLES

TABLE	TITLE	PAGE
1-1	T-Section Guide Rail Dimension	5
2-1	Properties of the 10-Story Torsional Building	42
2-2	Frequencies of the 10-Story Torsional Building	42
2-3	Properties of the 24-Story Shear Building	43
2-4	Moment of Inertia and Distance from Centroid to Outermost Point for Standard T-Sections	44
2-5	Seismic Inputs Used in the Study	48
2-6	Maximum Stress in the Rail for Different Inputs and Rail Sizes	53
2-7	Maximum Stress in the Bracket for Different Inputs and Rail Sizes	53
2-8	Maximum Displacement of Helical Spring for Different Inputs and Rail Sizes	54
3-1	Maximum Weight of Counterweight for Different Rail Size	86
3-2	Maximum Stress in the Rail's Flange	89
3-3	Maximum Stress in the Rail's Web	89

SECTION 1
ELEVATOR SYSTEMS, PAST SEISMIC PERFORMANCE AND CODES

1.1 Introduction

It is estimated that more than half a million passenger elevators in the Unites States transport people day and night every day of the year (Swerrie, 1991). Many of these elevators are located in highly seismic regions. For example, there were close to twenty thousand elevators in the area affected by the 1989 Loma Prieta earthquake in California, and this figure does not include elevators in federal buildings or private residences (Swerrie, 1991). It is thus natural to question how vulnerable the elevators are when a strong ground motion shakes the building. Indeed, the mere thought of being trapped in an elevator during an earthquake scares almost everyone. Moreover, vertical circulation systems (elevators, escalators and stairs) are essential in hospitals that must deliver crucial health services after a damaging earthquake (Highlands et al., 1975). Hospitals are just one of many other critical facilities that must remain operational after an earthquake and where elevators play an important role. It must be mentioned that so far elevators have performed very well from the point of view of safeguarding human life due to the combined efforts of industry and regulatory agencies. There are no reported direct fatalities associated with elevators failures due to earthquakes in the United States. Nevertheless, the economic losses and disruptions caused by the damage due to earthquakes are significant and therefore there is a need to enhance elevator safety and performance further.

This section presents a comprehensive review of the performance of elevators and escalators during past earthquakes in the United States and other countries. The measures adopted by the United States elevator codes to mitigate the damage suffered by elevators and to enhance their seismic performance are reviewed. All the major research studies dealing with the seismic response of elevators are also discussed. Before presenting the seismic effects on elevators, a concise description of their most important components is presented.

1.2 Components of an Elevator System

Elevators are complex mechanical and electrical systems. In order to appreciate and better understand how an earthquake can affect elevator systems, it is necessary to have knowledge of the basic components of these systems and how they work. Since many structural engineers may not be familiar with the intricacies of electric elevators, a brief description of a typical elevator system and its components is provided in this section. More information can be found in the excellent book by Janovsky (1993).

The principal design parameters of an elevator system are its rated load (or capacity) and its rated speed (measured in ft/min or m/s). Although the capacity and speed of elevators vary with the function of the building, the number of floors served, and the use of the elevator, the minimum recommended capacity for any building is 2,500 lb. For most office buildings, the 3,000-lb car is considered the minimum and for heavily traveled or prominent buildings, it is recommended to use at least 3,500-lb elevators. The suggested elevator speeds vary from 200 ft/min for small office buildings (up to 5 floors) to 1,800 ft/min for buildings over 60 floors. The analysis, design, and selection of the appropriate elevator technology to satisfy the requirements of vertical transportation of people and materials is referred to as “elevatoring”. Modern elevatoring

involves a combination of careful planning, experience, value judgment and technical calculations.

Elevators are classified according to their drive method as electric elevators, hydraulic elevators and pneumatic elevators. This report is concerned with electric elevators only since hydraulic and pneumatic elevators are mostly used for low-speed and low-rise elevators. Electric elevators are further classified according to the type of drive mechanism they use, such as traction drive, positive drive and linear induction motor drive. The positive drive or drum-drive elevators are suspended by ropes which are not driven by friction. They are not used for passenger elevators and their use is limited to low rated speeds and heights of travel. The linear induction motor drive is a relatively new concept and thus there are not many elevators of this type in use yet. The traction drive elevators are more commonly encountered in buildings, and thus they are considered in this report.

In traction drive elevators, the elevator car is supported by steel hoist ropes, sheaves and a counterweight. The weight of the car and counterweight provides sufficient traction between the sheaves and the hoist ropes so that the sheaves can grip the hoist ropes and move or hold the car securely. The main components of a typical traction elevator, shown in figure 1-1, are:

- The car
- The counterweight
- The guide rails
- The guiding members
- The suspension ropes or chains
- The compensating cables (not shown)
- The traveling cables
- The driving machine
- The motor-generator
- The safety gear
- The overspeed governor
- The buffers
- The hoistway or shaftway
- The control system
- The machine room

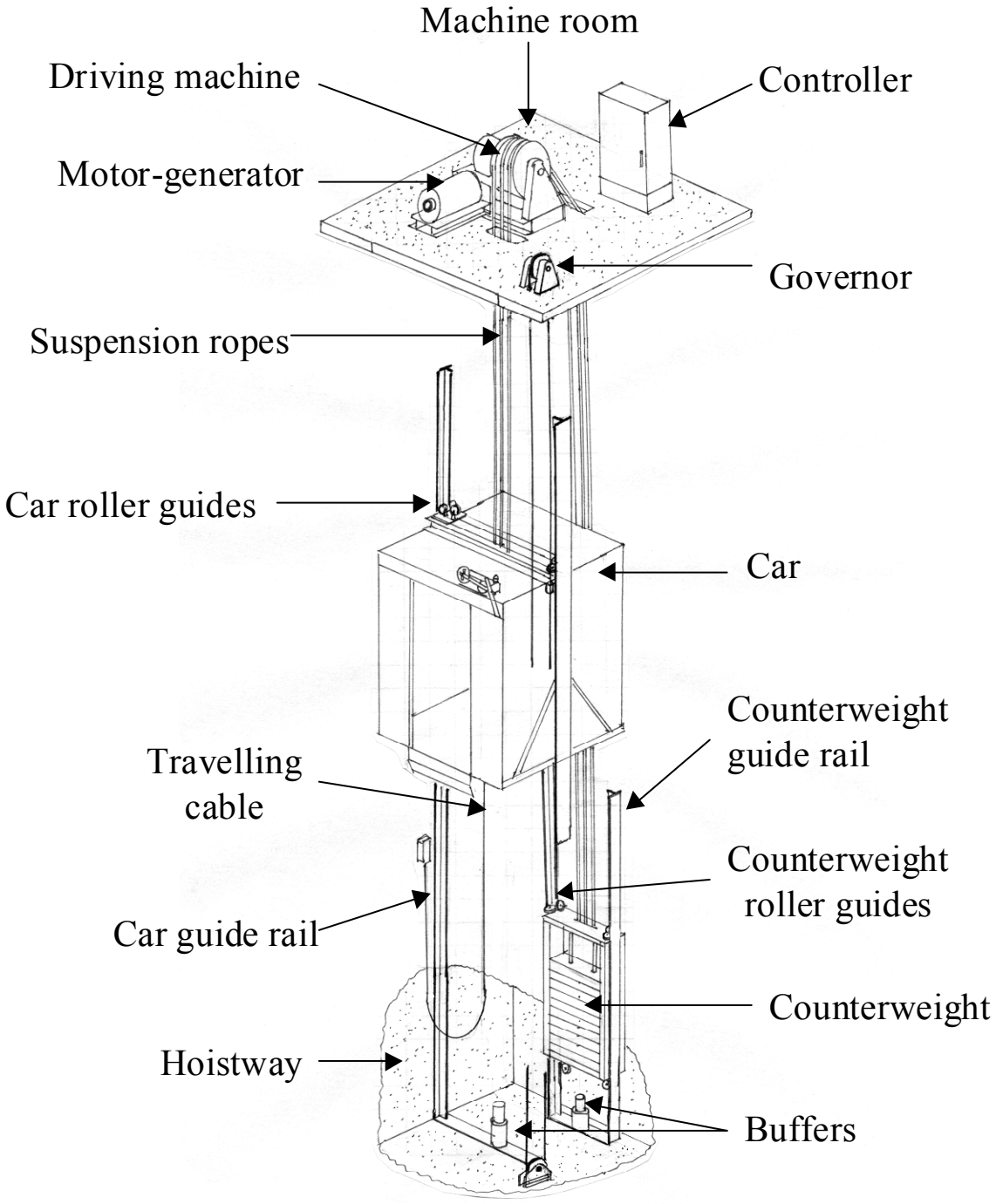

FIGURE 1-1 Main Components of a Typical Traction-Type Passenger Elevator

The car is the central component of any elevator system. The car frame is most frequently constructed as a post-side steel frame with the guide rails placed on two opposite sides of the plane of the frame. The lower member of the frame is a safety plank which supports the car platform, on which passengers and/or other loads rest during travel. The upper member of the car frame is a cross-head beam to which the suspension ropes are attached. The upper and lower

members are joined by two vertical uprights called stiles. Brace rods that extend from the car platform to the stiles are used to support and hold the platform secured in position. The car enclosure is made of metal or wood panels.

The objective of the counterweight is to balance the weight of the car and a portion (40 to 50%) of the rated load and a part of the traveling cables. Therefore, the counterweight is the component with the largest lumped mass in an elevator system. It is, thus, not surprising that the counterweight is also the element most affected by the earthquakes. The counterweight consists of a steel frame, fillers or subweights and guiding shoes. The fillers are stacked cast iron rectangular blocks or steel plates secured by two or more tie-rods. The counterweight is held by several steel ropes attached to the counterweight's frame by means of rope shackles that pass through and are fastened to its top member.

There are four guide rails in an elevator system. Two of the guide rails are used to guide the counterweight in its vertical motion as well as to minimize its horizontal motion. The other two rails accomplish the same function but guiding the car. In addition, the guide rails are used to apply the safety gear to stop the car or counterweight during an emergency and to prevent the tilting of the car when it is eccentrically loaded. The specifications in the ASME A17.1 standards (ASME, 1996) require that the guide rails must be constructed of T-sections conforming to the nominal unit weights and dimensions shown in table 1-1 and figure 1-2. The guide rails must be made of structural steel, except where this material may present accident hazards, such as in chemical factories. Nonmetallic materials can be used for these cases, provided that the cars have a speed of less than 150 ft/min. The steel used in the rail and brackets must have a tensile strength of not less than 55 ksi. The guide rails are supported at the bottom end and along its full length by equally spaced brackets. The guide rails are fixed to the brackets by means of clips.

The car and counterweight are led along the guide rails by the guiding members which consist of an assembly of components attached to the upper and lower ends of the frames. There are two types of guiding members: glide shoes and roller guides. The glide shoes are made of cast iron lined with special jibs of a material with low coefficient of friction and good wear resistance such as nylon. In this case, the guide rails must be lubricated to reduce frictional resistance and improve riding quality. This arrangement, however, can be problematic in maintaining uniform and constant lubricating properties of the fluid film. This type of guiding shoes is only used in elevators of low and medium speeds, and thus they are not of concern in this study. Roller guides, on the other hand, provide a smooth ride and savings in power due to the reduction in friction. Hence, they are used not only in high-speed elevators but also in medium speed elevators. Roller guides usually have three rollers with rubber or polyurethane tires to improve riding quality. Each roller is supported by a pivoted rocker arm and a helical steel spring which make the assembly to adjust to the guide rail and be in permanent contact with the rail (figure 1-3). Such roller assemblies have been noted to have significant influence in the seismic response of elevator systems.

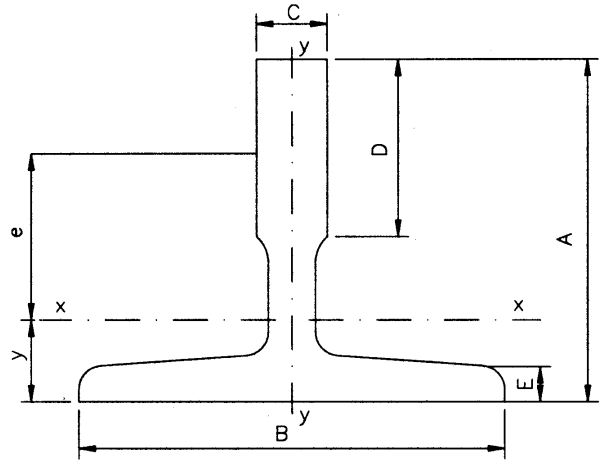

FIGURE 1-2 Nominal Cross-Section for Elevator Guide Rails According to the ASME A17.1 Code

TABLE 1-1 T-Section Guide Rail Dimensions

Nominal weight	Nominal dimensions (inches)				
(lb/ft)	A	B	C	D	E
8	2 7/16	3 ½	5/8	1 ¼	5/16
11	3 ½	4 ½	5/8	1 ½	5/16
12	3 ½	5	5/8	1 ¾	5/16
15	3 ½	5	5/8	1 31/32	½
18 ½	4 ¼	5 ½	¾	1 31/32	½
22 ½	4	5 ½	1 1/8	2	9/16
30	5	5 ½	1 ¼	2 ¼	11/16

For seismic zones 2 and higher, the A17.1 Code requires the installation of upper and lower position restraints to the car and counterweight frames. The distance between the upper and lower position restraints cannot be less than the height of the respective frame. In practice, the position restraints consist of steel flat plates bolted beneath the roller guide assembly (figure 1-4). These plates, known as retainer plates, must clear the guide rails by no more than 3/16 inches. The purpose of the retainer plates is to prevent the counterweight and car from disengaging from the rail if the roller guides fail.

The car and counterweight are suspended by a minimum of three steel wire ropes that are attached to the cross-head beam of the car frame and to the top of the counterweight's frame. There are several ways of connecting the car and counterweight with the suspension ropes. These different schemes are known as "roping systems". Usually the driving sheave is located above the hoistway. The most simple configuration is known as "single wrap drive" with "roping factor 1". In some installations, a "double wrap drive" is used to obtain sufficient traction. In this case

the ropes run from the car over the driving sheave down and around a secondary sheave, back to the driving sheave, and then back to the secondary sheave and to the counterweight.

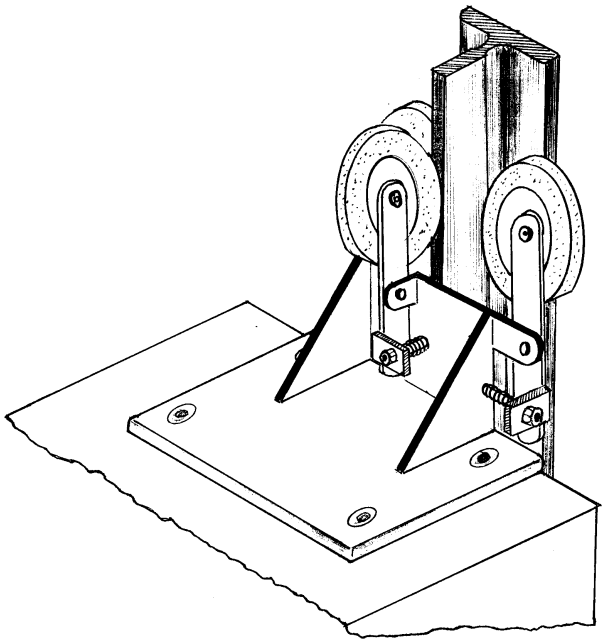

FIGURE 1-3 A Typical Three-Wheel Roller Guide

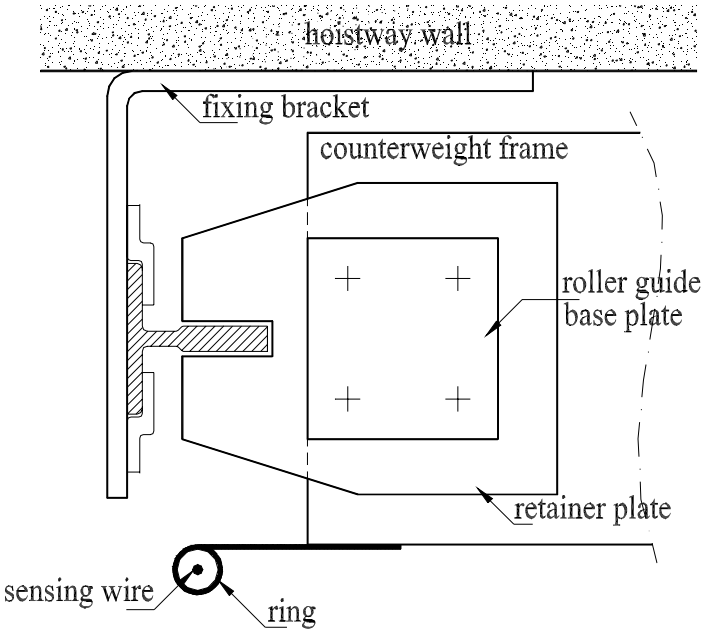

FIGURE 1-4 Guide Rail Retainer Plate and Displacement Switch

The compensating cables are a set of ropes or chains that are attached to the bottom of the car, pass around tensioning pulleys located in the pit and end up secured to the bottom of the counterweight. They are usually required on elevators with a height of travel over 100 ft. Their

purpose is to make the load on the driving sheave and motor constant regardless of the position of the car by minimizing the out-of-balance rope tension acting

The driving machine is the unit that powers the elevator system. It is composed of an electric motor, a sheave or drum, a brake and mechanical gearing and couplings. The driving machine is located in a machine room that is usually directly above the elevator hoistway. Traction drive elevators can have a geared or gearless traction system. The first system is mostly used in mid-rise installations whereas the second system is used in high-rise buildings. A geared machine has a higher-speed motor and the driving sheave is connected to the motor shaft through a gear box to reduce the rotational speed of the motor shaft to the lower driving sheave speed. A gearless machine has a low-speed motor and the driving sheave is connected directly to the motor shaft.

A multi-wire electrical cable connects the machine room to the car to feed electricity to the car and to transmit electric signals. Because the end of the cable attached to the car moves with it, this cable is called the traveling cable. All roped elevators have safety devices to back up the suspension ropes. The safety gear, or simply safety, is a mechanical device used to stop and hold the car or counterweight on the guide rails in the event of the breakage of the suspension ropes or if the speed of the descending car or counterweight exceeds a predetermined value above the rated speed. The braking action of the safety gear is triggered by an overspeed governor. The safety gear is generally located below the car frame and operates simultaneously on both guide rails. The safety gear basically comprises of a pair of jaws that grips the guide rails and applies a rapidly increasing pressure (instantaneous type) or limited pressure (progressive type) during the stopping interval, much like the brake shoes on motor vehicles. Closely related to the safety gear is the overspeed governor system. The function of the governor is to operate the safety gear, cut off power to the motor and apply the brake whenever the predetermined tripping speed is reached. It is made up of the governor sheave located in the machine room, the governor rope that passes around the sheave, down the tensioning sheave in the pit and back to the governor sheave.

Elevators are equipped with buffers for both cars and counterweights located in the pit. They are the last emergency device to stop the car or counterweight if other safety devices fail. The buffers can be of energy-accumulation type or energy-dissipation type, depending on whether they store or dissipate the kinetic energy of the car or counterweight. The energy accumulation buffers usually consist of helical springs or polyurethane cylinder blocks. The energy dissipation buffers are oil-filled cylinders with piston and compression return springs and are usually installed in high-speed elevators.

1.3 Observed Seismic Performance of Elevators

Information about damage suffered by elevators during strong ground shakings began to be collected in a systematic and organized form after the 1971 San Fernando earthquake. The damage to elevators observed during some of the past strong earthquakes in the United States and elsewhere is summarized in the following list.

- Damage to guide rail anchorage
- Bent guide rails
- Counterweights coming out of their guide rails

- Free swinging counterweights colliding with the top of the cars
- Control panels tipped or moved
- Traction machines set shaken loose from their mountings
- Motor-generator sets shifted across machine room floors
- Ropes damaged by projections or protuberances in the hoistways
- Suspension ropes jumped from drive and/or deflector sheave grooves
- Seismic switches failed to trigger.

A survey of damaged observed, documented and reported in the open technical literature during the Alaska, San Fernando, Miyagi, Carpathian, Whittier Narrows, Loma Prieta, Northridge, and Kobe earthquakes is presented next. Information about other earthquakes is scant at best, mostly reduced to a few qualitative statements and thus it is not included here.

The March 27, 1964, Alaska earthquake ($M_W = 9.2$) caused extensive damage to nonstructural elements, particularly to elevators. In a report prepared for the National Academy of Sciences, Ayres, Sun and Brown (1973) compiled a record of information on nonstructural damage with a special section on elevators. There were about 100 elevators in Anchorage during the time of the earthquake and about half of them were traction elevators. Almost all the hydraulic elevators and escalators survived the earthquake with very little damage and most of the failures were sustained by the traction elevators. The number of occurrences of each particular mode of failure was not reported; only a description of the different type of damage observed during the inspection was included in the report. According to elevator maintenance personnel, almost all the counterweights popped out of their guide rails. This was in part due to the fact that many roller guides were twisted and hammered against the rails by the counterweight's mass. The swinging counterweights often struck and deformed the spreader beams. Fortunately, there were not many collisions between cars and counterweights because power failures shut down the driving machines. The guide rails of the cars sustained little damage, primarily because they are stronger than the counterweight's guide rails. They are designed to withstand eccentric live loads and braking forces due to the action of the car safety brakes. At least 80% of the damage to elevator machinery was caused by motor-generator sets being thrown out of their vibration isolation mounts. In one case the generator was thrown out of the wall of the penthouse. Unanchored control panels falling over was another common occurrence.

After the 1971 San Fernando earthquake, the ASME A17.1 Earthquake Committee and the California Advisory Committee, in collaboration with the elevator industry, proposed what can be regarded as the first design improvements and measures to minimize damage in earthquakes. Some of these recommendations were later included in the California and ASME codes. A description of these design solutions was presented by Ayres et al. (1973) and by McGavin (1981). To avoid the damage caused by derailed counterweights, they proposed to use guide rails heavier than the 8-lb T-section. Other recommendations include the installation of guide rail brackets at more frequent intervals and placing a tie bar across from one tip of a bracket to the other. Angle brackets could also be strengthened by welding gusset plates. To protect the roller guides they proposed to bolt to the counterweight frame safety shoe assemblies similar to those used in hydraulic elevators. To prevent the rocking motion of the isolated motor generators, the vibration isolators should be bolted to the floor.

The February 9, 1971 San Fernando earthquake (M_W = 6.6) caused extensive damage to the elevators in the Los Angeles area and it was one of the first earthquakes for which the damage to elevators was systematically studied. A survey immediately following the earthquake was conducted by the Elevator Section of the California Division of Industrial Safety. A detailed account of the damage reported can be found in the report by Ayres and Sun (1973) and a summary is included in a special publication of Elevator World (Sturgeon, 1972), the trade magazine of the elevator industry. According to the results of the survey, the most common problems were the counterweights thrown out of their guide rails. The survey indicated that a total of 674 counterweights derailed, and they in turn damaged 109 cars due to collisions. In addition, other damage included 18 cars out of guides, 174 guide rail brackets broken or damaged, 286 roller guides broken or loose, 49 guide rails bent, broken or out of alignment. Other miscellaneous failures observed included 174 motor generator sets shaken loose from its mounting, 9 broken guiding shoes, 22 hoistway doors off tracks, 20 governor cables hung up or cut, 7 traveling cables hung up or broken, and 100 compensating cables out of the grooves. Two casualties were reported in hospitals due to seriously ill persons trapped between floors in elevators. It is not quite clear whether they were trapped because of the elevator damage or due to the general power failure. It is perhaps more likely that the loss of power was the cause since at that time the elevators were not required to have emergency power backup. Gates and McGavin (1998) also reported that during the San Fernando earthquake, a patient was pinned to the wall of the cab by the counterweight that had broken free and crushed through the side of the cab. A passenger in another elevator observed a counterweight penetrating through the roof of the car and passing the car after punching on through the floor.

The Miyagi Prefecture earthquake (M_W = 7.4) of June 12, 1978, was the first strong ground motion in Japan for which the extensive elevator damage was recorded (Fukuda, 1990). Out of a total of 5,462 elevators in the six prefectures affected by the earthquake, 483 (9%) suffered damaged. In the Miyagi Prefecture the percentage of failures reached 18%. The greatest problem was the derailment of the counterweights. Of the 483 elevators damaged, 282 (29%) of them experienced derailment of the car or counterweight. Other failure modes included 53 motor-generator sets displaced, 11 controllers tumbled, 54 car and counterweights guide shoes deformed, 40 guide rail brackets bent, 5 cars out of guide rails, and 23 ropes and cables damaged. Fortunately, there were no injuries or fatalities reported. Following the Miyagi earthquake, the Japan Architect Center submitted in 1980 a report to the Ministry of Construction with a set of measures to mitigate elevator failures. They include the installation of seismic sensors on each bank of elevators, similar to those required in the ASME A17.1 code discussed later. Furthermore, the design of all elevator components located in the hoistway should be done such that they can withstand a seismic force that produces a 0.6g acceleration in the horizontal direction. For design of equipment in the machine room, it is recommended to use a force producing 1g and 0.5g in the horizontal and vertical directions, respectively.

A succinct description of elevator damage during the Carpathian earthquake (M_W = 7.2) of August 31, 1986 was reported by Nazarova (1990). The author conducted a field survey of elevators in office and apartment buildings in the city of Kishinev, Moldova. It was found that out of 1590 elevators, 240 were severely damaged. The most common modes of failure were counterweights out of the guiderails, crashes between free counterweights and car cabins, broken or permanently deformed guide shoes, inelastic deformations in the frames of the car cabins and counterweights, and car cabins jammed against their guiderails. A survey conducted in other cities affected by the earthquake showed similar failure patterns. Nazarova mentioned that by the

time that the Carpathian earthquake occurred, the elevators in the former USSR territories were not explicitly designed for seismic loads.

The 1987 Whittier Narrows earthquake (M_L = 5.9) was the first earthquake to affect elevators since the provisions of the California code became effective. A survey of damaged caused by the Whittier earthquake was carried out by Schiff (1988). The survey of damage relies in part on questionnaires sent to elevator companies and interviews with maintenance managers (Schiff, 1988; 1990). The most commonly observed damage (91 cases) was the derailment of counterweights. There was a lack of information on the correlation of derailment with rail size, support spacing, bracket strength and stiffness, anchorage failure and location of the counterweight within the building. In addition, there were 19 reports of other counterweight guide rail damage and 10 reports of guide rail anchorage failure. Structural damage to the cars was minor and it usually involved collisions with derailed counterweights (11 cases). Most of these cases occurred when unauthorized persons reset the tripped seismic switches and returned the elevators to service before they were inspected for damage. There were few anchorage problems in machine rooms and no rope damage was observed. The performance of seismic switches was erratic because several switches did not trigger. Nevertheless, the overall performance of the elevators was much better than during the San Fernando earthquake.

The performance of elevators during the October 17, 1989 Loma Prieta earthquake (M_S = 7.1) is discussed in a report prepared by EERI (Ding and Arnold, 1990) and in a paper by Swerrie (1991). Similar methodologies as in the Whittier Narrows earthquake were used to collect damage statistics. Additional first-hand reports from elevator contractors and building managers can be found in the articles by Swerrie in Elevator World (1990a, b). There were 98 instances of counterweights coming out of the guide rails cited in the EERI study and 296 cases in Swerrie's paper. It must be noted that the EERI study was a preliminary assessment and more data was probably available by the time of the second study. There were several factors that were pointed out as potentially responsible for the derailment: bent rail brackets, failure of bolts holding rail brackets, and bent rail guides. It was observed that most of the derailments tended to occur when the counterweight was high on the building (Swerrie, 1991; Ding and Arnold, 1990). Practically all damaged cars were due to counterweights striking the cars when elevators with derailed counterweights were inadvertently put back in service without any repairs. As would be anticipated, most of the counterweight derailments occurred on those mounted on 8-lb guide rails. However, there were many 8-lb guides that withstood the earthquake motion without damage whereas some 11, 12 and even 15-lb guides failed. The evidence suggests that 8-lb guides can be safely used if they are adequately fastened, reinforced and bracketed (Swerrie, 1991). Once again during this earthquake, there were many instances where the seismic protective devices failed to produce the desired results (Swerrie, 1990a, b). It was suggested (Ding and Arnold, 1990) that elevators in steel frame buildings may have been subjected to more severe loads either due to the flexibility of these structures or because their fundamental frequencies may be closer to those of rail-counterweight systems. Another conclusion drawn from the analysis of damage from this and other earthquakes is that there is a lack of information on the correlation of derailment with rail size, support spacing, bracket stiffness, anchorage failure, tie spacing, tie stiffness, etc.

Information about the damage to elevators during the January 17, 1994 Northridge earthquake (M_W = 6.7) was collected by the Elevator, Tramway and Ride Unit of the Division of Occupational Safety and Health of the State of California (Pavlow, 1994; Schiff, 1994). About

100 questionnaires were sent to companies that service elevators in the area affected by the earthquake. The data shows that despite the more strict strengthening requirements imposed by the code revisions, the relative damage sustained by elevators during the Northridge earthquake was more severe than in the 1989 Loma Prieta earthquake and significantly more severe than in the 1987 Whittier Narrows earthquake. For instance, the number of counterweights that came off the guide rails was comparable to that observed during the 1971 San Fernando earthquake. In addition, there was more damage to escalators in the Northridge earthquake than in previous earthquakes. The tabulated results of the survey conducted indicate that 968 electric elevators experienced earthquake damage. There were 688 counterweights that came out of their guide rails. A total of 97 hydraulic elevators suffered damage, primarily produced by leaks due to the failure of the underground feed lines. Other observed damage include guide rails spread, counterweight roller mountings disintegration, governor ropes wrapped around limit switches, car and hoistway doors out of tracks, etc. It should be mentioned that the actual number of elevators damaged may be higher: it is estimated that the gathered statistical data covered only about 50% of the units with damage. There were about 30,000 elevators in the area affected by the earthquake and the survey covered approximately 17,000 units. Moreover, several organizations, among them some government agencies and universities, were not covered by the survey because they have their own divisions to service their elevators.

In a review of the seismic response of nonstructural systems during the Northridge earthquake, Gates and McGavin (1998) concluded that “not all the weakness identified in elevator systems were fully reorganized and compensated for in previous code revisions”. In particular, one failure mechanism observed during this earthquake and not considered in the code is the twisting and jamming of the weights in the counterweight basket or frame. This occurred because of the existing clearance between the weight blocks and the counterweight frame. This mode of failure was first observed in elevators of the Olive View Hospital during the San Fernando earthquake and 23 years later again in the new Olive View Hospital. In all these cases, however, the counterweight frame still remained in the guide rails.

After the Northridge earthquake, the Office of Statewide Health Planning and Development (OSHPD) of the state of California commissioned studies on the impact of the shaking on elevators. One of the reports was prepared by Finley et al. (1996) based on the survey of nine hospital facilities. As it was expected, this study confirmed that those elevators installed before 1973, i.e. before the California seismic provisions were enacted, sustained the majority of the structural damage. In addition to counterweight derailments, other modes of failure detected included broken cab retainer brackets, cab interior ceiling panels lying on the floor, governor anchorages pulled out of the concrete, governor ropes tangled around hoistway components, car doors jumped out of the cab sills, and diverse controller damage. The report concluded that the existing California's Title 24 seismic requirements for new hospital elevators are mostly sufficient, but minor changes should be implemented to take into account the particular modes of failure detected during the Northridge earthquake. The most pressing and strongest recommendation of the report is the need to bring the elevators installed before 1973 up to the standards for new elevators.

Similar failure mechanisms are mentioned in another report on the general performance of hospitals prepared for the Hospital Building Safety Board by OSHPD (OSHPD, 1995). A total of 24 hospitals in the area affected by the earthquake were inspected for structural damage, and also for damage to mechanical and electrical equipment, water piping, fire sprinklers, and elevators.

From the tables of damage compiled in the report, it can be seen that 20 buildings in these hospitals suffered elevator damage, such as elevator equipment shifted, elevator generators fallen over, counterweights free of the rails or out of their frames, and other unspecified damage. There were also several cases of disengagement of the stacked steel plates of the counterweights. In page 37 of the report, it is mentioned that the seismic forces acting on the plates caused the vertical channels of the frames to deflect, twist or spread apart. Nevertheless, it should be noted that in the United States, and in accordance with the A17.1 Code, the car and counterweight frames and connections are designed with a safety factor of 4 to 5 under normal (non-seismic) loading conditions. Therefore, based on U.S. experience, the failure of these frames was not observed in other earthquakes. One of the conclusions of the report is that the acceleration levels observed were four times greater than those for which the counterweight supports were designed. Also, at the time of the earthquake (very early in the morning), the cars were located at the ground floor level, and the counterweights high up in the building. Finally, it is mentioned that neither the California code nor the ASME-A17.1 code have any specific provisions for a structural design of the frames of the car or counterweight. It is argued that these conditions could account for the numerous failures that affected the elevators.

The January 17, 1995 Kobe earthquake ($M_W = 6.9$) caused widespread damage in elevators and escalators in Kobe City and surrounding districts. The significant impact upon elevator equipment was unexpected because of new antiseismic standards were implemented on January of 1983. These measures are compiled in the Standards for Elevators and Escalators of the Japan Elevator Association (or "yellow book"). A field report immediately following the earthquake was submitted by Caporale (1995) to the Elevator World magazine. The report mostly describes general damage to the infrastructure, but also provides a brief description of diverse elevator components that failed during the earthquake and includes pictures of some of them. An inventory of the elements that failed based on a more detailed study is presented next. However, an important finding reported by Caporale is that escalators were significantly affected by the shock: the bracing in the escalator trusses, the floor plates, and support bearing plates and angles were damaged. The Japan Elevator Association was in charge of investigating and analyzing the extent of elevator damage in a more comprehensive manner. Some of the results were reported by Wada and Kitamura (1995). There were approximately 66,300 elevators in the area affected by the earthquake and 728 elevators in buildings that collapsed. A total of 5,646 elevators were damaged by the quake. In Kobe City, 28.2% of the elevators designed and installed according to new regulations were damaged and this percentage rises up to almost 50% for old elevators without antiseismic measures. The most significant damage observed consisted of derailed counterweights (1001), counterweights with dislocated weights (105), derailed cars (60), deformed guide rails (323), deformed rail brackets (176), deformed or broken car frame and doors (245), deformed guide shoes (664), shifted, overturned or broken traction machines and motor generator sets (399), overturned or broken control panels and governors (137), governor ropes entangled or snagged (936), compensating ropes entangled or snagged (92), and flooding due to broken hydraulic pipings, etc. (758). This data does not include elevators in buildings that were severely damaged and thus impossible to assess.

The statistical summaries of elevator damage from past earthquakes play a very important role in formulating improvements to the elevator codes and enhancing their seismic performance. However, there are a few problems associated with the collection of detailed information. The most significant problem is the lack of collection of relevant engineering details associated with failure. The inadequate reporting of elevator damage sometimes makes it difficult to establish the

real cause of the failures. For example, sometimes it is not known whether the elevators were conformed to the code. This makes it difficult to determine if the failure was due to inadequate code provisions, or due to the poor enforcement or application of the code. Other problems associated with data collection and reporting as well as some proposed solutions are discussed by Schiff et al. (1980). The task of collecting failure information is usually done by repair service personnel at the time that the repairs are made. In the understandable rush to restore service, often the failure data is not recorded. Moreover, in general, service personnel are not engineers and they lack the training required to assess damage and identify modes of failure. In addition, the damage reports could be subpoenaed for use in litigation and hence, it may not be in the best interest of the elevator companies to collect the data. As for hospitals in California, OSHPD has legal authority to collect damage in these facilities. However, the information collected is usually limited by the lack of detailed documentation gathered at the time of the earthquake. Schiff recommended that a sample one-page report form could be included in the code to collect such important failure information. This page could be copied and used to document damage in an organized way. In addition, it is suggested that these damage reports could only be used in anonymous form.

1.4 Seismic Code Provisions

The design, construction, operation, inspection, testing, maintenance, alteration and repair of elevators, escalators and other lifting devices are covered in the A17.1 Code. This code, known as the *Safety Code for Elevators and Escalators*, was developed by a committee of the American Society of Mechanical Engineers (ASME). The A17.1 Elevator Code has been published continuously since 1921 and it has served as a model for elevator safety standards in many countries. The A17.1 Code is updated with major revisions every third year and a supplement is issued annually. A total of 15 editions have been published, the most recent one in 1996. Consensus committees formed by representatives from elevator manufacturers, insurance carriers, regulatory bodies, technical societies and professional consultants are in charge of updating the code. In the United States the role of the code is only advisory although it was intended to form the basis for local regulations. However, in the past years practically all jurisdictions with elevator codes in the United States have adopted the A17.1 Code. Until the tenth edition published in 1981, the code did not contain specific provisions for the protection of elevators during earthquakes.

The San Fernando earthquake was the first reminder to the elevator industry that strong earthquake motions can cause serious damage to their products. Following the earthquake, the California Legislature directed the California Department of Industrial Relations to convene a committee to study and propose practice, means and devices to enhance the safety of elevators during seismic motions (Swerrie, 1990). The committee proposed a number of remedies that are economical and simple ways to increase the seismic resistance of elevators. A summary of the recommendations are listed in the 1972 special issue of the Elevator Word magazine (Sturgeon, 1972). They were officially added as seismic provisions in the elevator code of the state of California in 1975. New elevators had to comply immediately and existing elevators were given seven years to implement the code requirements. The seismic provisions are now contained in the California Elevator Safety Construction Code (California Building Standards Commission, 1998), which is the seventh part of the building regulations known as the California Code of Regulations, Title 24. The code is published every three years by the International Conference of

Building Officials, with supplements issued every intervening years. The provisions in the current Elevator Safety Orders are divided into two groups: those for existing elevator installations and those for new elevators. The section on new elevators practically adopted all the regulations in the ASME A17.1-1996 Code. The section on existing elevators contains the seismic provisions intertwined with the other general regulations. Nevertheless, many of the measures in this section are similar to those of the A17.1 code, and where any difference exists between the Elevators Safety Orders and the A17.1 code, the former applies. The similarity is to be expected since many committee members that participate in the development of the California regulations are also in the earthquake committee of the ASME code. However, it is worth mentioning that there are a few regulations that are more conservative than those in the ASME code. One example is the graphs for selection of bracket spacing for a given counterweight weight.

In 1981 an appendix with seismic code provisions, known as Appendix F, was added for the first time to the National Safety Code for Elevators and Escalators (ASME, 1981). The safety requirements contained in Appendix F of ASME 17.1 were intended to serve as guide to the proper authorities in drafting regulations dealing with the design, construction installation and operation of elevators in seismic regions. In the 1993 fourteenth edition of the code the safety requirements were moved from Appendix F into a new section in the main body of the code entitled "Part XXIV: Elevator Safety Requirements for Seismic Risk Zone 2 or Greater." The provisions were originally intended for elevators located in zone 3 or greater using the classification of ANSI A581. In the 1993 edition of the code the seismic safety requirements were extended to those elevators in zone 2. In general, the code contains special requirements for bracket spacing, allowable stresses and deflections for selection and design of guide rails, brackets, and fastenings, clearances for the car and counterweight, devices for earthquake protection, and instructions for emergency operation.

Some of the most important specific recommendations of the code are:

- Providing retainer guards on all sheaves and drums.
- Guarding of snag points that could affect traveling cables, suspension ropes and chains, and compensating and governor ropes.
- Design of fastening to secure machines, control panels, etc. to withstand the simultaneous action of seismic forces that produce accelerations of 1g horizontally and ½ g vertically. The stresses due to the specified forces must not exceed 88% of the yield stress.
- Use of upper and lower position restraints attached to the counterweight and car frame. Retainer plates are usually used as position restraints. These are flat steel plates located on the car and counterweight beneath the upper and lower guides that act as a stop under earthquake loading.
- The stresses in the guide rails and in their brackets due to a force producing a horizontal acceleration of ½ g must be less that 88% of the yield stress.
- The total deflection of guide rail brackets, their fastening and supports must not exceed 1/8 in.

- Both the frames of the counterweight and car are required to have position restraints at both ends. Separate position restraints are not required if they are part of the guiding members.
- The distance between the upper and lower position restraints cannot be less than the height of the frame.

Starting with the 1994 edition, the NEHRP Provisions (BSSC, 1994) now include specific design requirements for elevators. The provisions state that "elevators shall meet the force and displacement provisions" stipulated for architectural, mechanical and electrical components. However, elevators designed in accordance with the A17.1 Code are deemed to meet these requirements. Nevertheless, the structural systems of elevators and hoistway as well as controllers are required to meet the force and displacement NEHRP provisions. For elevators with a rated speed equal to or greater than 150 ft/min, seismic switches are required. The seismic switches must be located at the highest floor serviced by the elevators, with a trigger level equal to 0.3g. Moreover, retainer plates are required for both the car and the counterweight.

1.4.1 Design of Guide Rails

The Part XXIV in the A17.1 code provides seven graphs, one for each of the nominal T-sections in table 1-1, to be used for the selection of the minimum bracket spacing (or rail span). These curves depict the maximum suspended weight of the car plus 40% of the rated load, or the maximum suspended weight of the counterweight, as a function of the rail spacing for a given size of rail. It is implied that, by using these curves, one can select the adequate guide rail that should be capable of withstanding without damage a horizontal seismic force that produces an acceleration of ½ g. The bracket spacing may exceed the values of the figures if the guide rail is reinforced, but under no circumstances the rail spacing shall exceed 16 ft (48 m). Figure 1-5 shows one of those curves for a 12-lb guide rail.

For the case when the height of the counterweight frame is less than 65% of the rail span, the specifications in Part XXIV contain an additional graph to calculate a correction factor Q to be applied to the weight of the counterweight to assure that a proper guide rail system is selected. The curve relates the correction factor $Q > 1$ to the ratio of the distance between the upper and lower position restraints and the bracket spacing. The weight of the counterweight must be multiplied by this factor to calculate a new "effective" weight that must then be used in the previous curves to select the required bracket spacing.

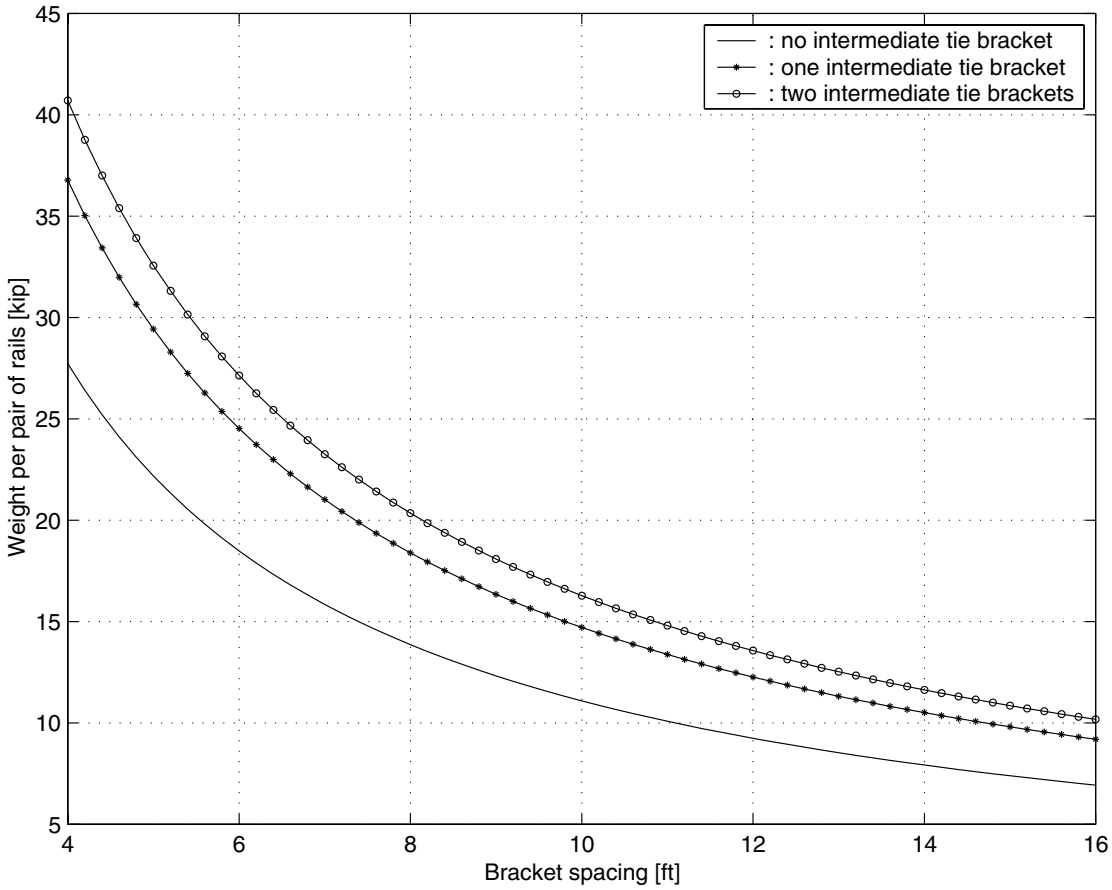

FIGURE 1-5 Graph for Selection of Bracket Spacing for 12-lb Guide Rail According to the A17.1 Code

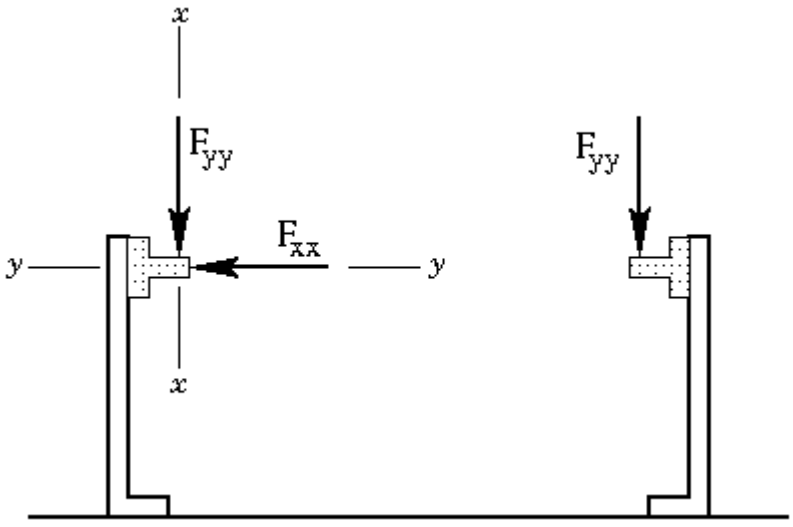

FIGURE 1-6 Forces Acting at the Guide Rails Used for Seismic Design

Part XXIV of the A17.1 Code also provides design formulas to determine the maximum allowable weight W per pair of guiderails. The formulas are divided according to the direction of the applied seismic forces. For forces applied along the web of the rail's cross-section (normal to the *x-x* axis in figure 1-6), the formulas can be summarized as follows:

For car or counterweight rails with no intermediate tie brackets:

$$W = 717,671 \frac{Z_x}{L} \alpha \tag{1-1}$$

For counterweight rails with one intermediate tie bracket at the mid-span:

$$W = 951,991 \frac{Z_x}{L} \alpha \tag{1-2}$$

For counterweight rails with two intermediate tie brackets equally spaced:

$$W = 1,053,495 \frac{Z_x}{L} \alpha \tag{1-3}$$

where α = 1 for seismic zone 3 or greater and α = 2 for zone 2. Z_x is the section modulus expressed in in^3, and L is the bracket spacing in *inches*.

The code does not provide any commentary discussing the theoretical background for these formulas. However, they seem to be based on the following development. The maximum allowable moment is given by the flexure formula:

$$M_{\max} = \sigma_{allow} Z_x \tag{1-4}$$

As mentioned before, the allowable stress is $\sigma_{allow} = 0.88 \sigma_y$. For the commonly used ASTM-36 steel, the yield stress σ_y is 36 ksi. Substituting σ_{allow} = 31680 psi the allowable moment is:

$$M_{\max} = 31680 Z_x \tag{1-5}$$

The counterweight frame can be filled up to 2/3 of its length. Therefore, the loads transmitted statically to the rail through the guiding members are P_u = 1/3 P and P_ℓ = 2/3 P, at the upper and lower positions, respectively. The force P is a fraction of the weight W and depends on the level of the input acceleration. For zones ≥ 3 the A17.1 Code recommends to use for design purposes a seismic force that produces a horizontal acceleration of the mass equal to ½ g, i.e. $P = W/2$. Therefore, the forces acting on the guiderail are $P_u = W/6$ and $P_\ell = W/3$. The moment $M_{\max}$ for a continuous beam with constant span lengths L can be expressed as:

$$M_{\max} = \gamma W L \tag{1-6}$$

The coefficient γ depends on the beam model (number of spans, etc.) and on the location of the loads on the beam. Equating (1-5) and (1-6), the maximum weight is:

$$W = \frac{31680}{\gamma} \frac{Z_x}{L} \tag{1-7}$$

As it was mentioned before, the code requires using a correction factor Q to calculate the allowable weight of a counterweight with length $\ell_c \le 0.65L$. Since for $\ell_c = 0.65L$ the correction factor is 1, it seems logical to use a counterweight with this length ratio, i.e., the two loads P_u and P_ℓ should be separated by a distance $0.65L$. By comparing (1-1) and (1-7), the value of γ to obtain the coefficient in (1-1) should be 0.0441428. It is mentioned that after trying numerous

combinations of continuous beams of different number of supports with different positions of the counterweight, we could not verify this coefficient. The closest value we found form our analyses was $\gamma = 0.04441428$. This was obtained for a three-span continuous beam with the counterweight placed symmetrically on the second support. Corresponding to the new value of γ, the coefficient in (1-1) should be 713,284 instead of 717,671.

The seismic design force for elevators in zone 2 is defined as that required to produce an acceleration of ¼ g, and thus the coefficient α in (1-1) through (1-3) is equal to 2. For forces applied normal to the web of the rail (normal to the *y*-*y* axis in figure 1-6) the numerical coefficients in (1-1) through (1-3) are multiplied by a factor of 2, because, in this case, the two rails withstand the seismic loads.

The seismic section of the A17.1 code also requires that the guide rails possess a minimum moment of inertia $I_{\min}$ when they are subjected to a seismic force that produces an acceleration of ½ g acting horizontally. The following expression is provided to calculate the minimum allowable moment of inertia for the guide rails of the car or counterweight:

$$I_{\min} = \frac{1}{249}\frac{W L^3}{\Delta E} \tag{1-8}$$

where W and L have the same meaning as before, E is the modulus of elasticity of steel, and Δ is the maximum allowable deflection. For elevators located in zone 2, the corresponding minimum moment of inertia will be ½ of the value obtained by (1-8). The maximum allowable deflection depends on the size of the rail and is provided in the specifications. The values of Δ are 0.75, 1.0, 1.25, 1.469, 1.469, 1.5 and 1.75 inches for a T-section of 8, 11, 12, 15, 18.5, 22.5 and 30-lb, respectively. The code does not provide any explanation regarding the derivation of (1-8). However, it can be obtained by considering a two-span uniform continuous beam with span length L and a force P acting at the middle of the second span. It can be shown that the deflection of the point of application of the load is given by:

$$\Delta = \frac{PL^3}{83EI} \tag{1-9}$$

Taking $P = W/3$ leads to (1-8). $W/3$ is the maximum of the two loads coming from the roller guides to the guide rail for zones 3 and higher (see figure 1-7).

1.4.2 Design Forces for Brackets

The seismic design of the guide rail brackets is consistent with the conditions on which the guide rail selection is based. The brackets must be designed to withstand the forces imposed by the car plus 40% of its rated load, or the counterweight, when they are subjected to seismic forces that produce an acceleration of ½ g acting horizontally for zone 3 and higher. The bending stresses under these circumstances must not exceed $0.88\sigma_y$, where σ_y is the yield stress of the material, and the maximum deflection must be limited to 1/10 in.

Part XXIV of the A17.1 Code provides a set of formulas to calculate the forces to be used for the bracket design. These forces are the horizontal seismic forces imposed on the faces of the guide rail by the *lower* position restraints of the car and counterweights that are consistent with the conditions stated before. Although it is not mentioned in the code, the forces are determined by assuming that the counterweight is stationed with its lower end right above the lower support of a

guide rail. The guide rail is modeled as a simply supported beam with a static seismic force equal to ½*W* (for zones 3 and higher) acting horizontally at two-third of the rail span measured from the lower support (see figures 1-7 and 1-8). Under these assumptions, the forces acting at the supports are determined as described below.

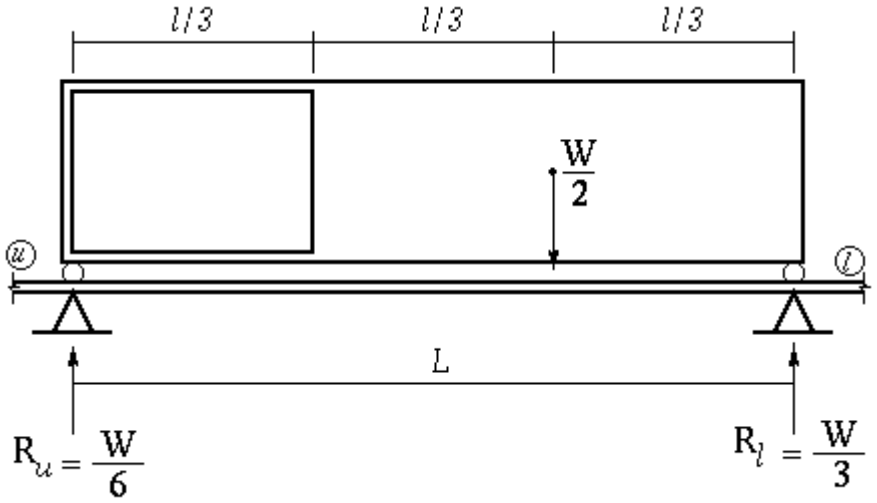

FIGURE 1-7 Model Used to Define the Seismic Forces for Bracket Design When the Rail Span is Equal to or Smaller than the Distance Between the Restraints Position

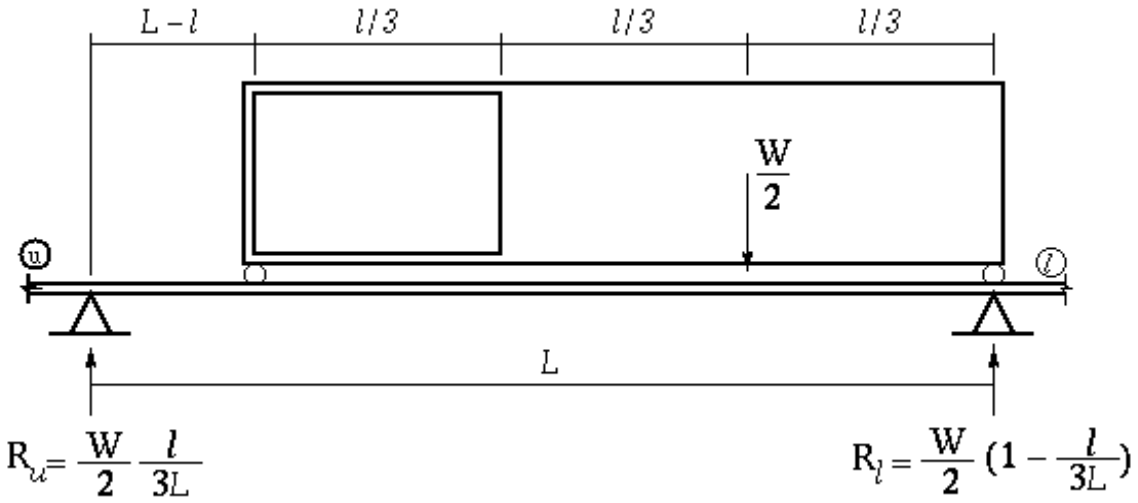

FIGURE 1-8 Model Used to Define the Seismic Forces for Bracket Design When the Rail Span is Greater than the Distance Between the Restraints Position

Let ℓ_{pr} be the distance between the upper and lower position restraints, *L* the rail span and *W* the weight of the car plus 40% of the rated load or the weight of the counterweight. The force normal to the *x*-*x* axis of the rail (see figures 1-6, 1-7 and 1-8) is:}

$$\Delta = \frac{PL^3}{83EI} \tag{1-10}$$

The force normal to the *y-y* axis of the rail (see figure 1.5) is:}

$$\Delta = \frac{PL^3}{83EI} \tag{1-11}$$

These forces are exactly half of the ones in Equations (1-10) because now two rails share the same load. The above equations are for zone 3 and higher. For zone 2 the forces should be multiplied by ½.

1.4.3 Seismic Safety Triggers

The ASME A17.1 code requires two earthquake protective devices for all traction elevators operating at a speed of 150 ft/min and above. They consist of: a) at least one seismic switch per building; and, b) a counterweight displacement switch for each elevator. All protective devices should be "fail-safe", i.e., if the devices fail to operate properly, they must default to a safe state.

A *seismic switch* was described in the Appendix F of the ASME A17.1 Code as "a device activated by ground movement to provide a signal that a potentially damaging earthquake is imminent". A *displacement switch* is defined as "a device actuated by the displacement of the counterweight at any point on the hoistway to provide a signal that the counterweight has moved from its normal plane of travel or has left its guide rails". The ASME A17.1 code requires that upon activation of seismic switch, cars in motion must proceed to the nearest available floor, open their doors, and shut down. When the counterweight displacement switch is activated, the cars in motion must stop, and then proceed to the nearest landing at reduced speed in direction away from the counterweight. A seismic switch is, in principle, a simple mechanical or electromechanical device which provides an electrical contact closure when activated by an earthquake. In practice, however, it is not simple to implement. One of the main problems is that the seismic switches may respond not only to earthquake motions but also to man-made vibrations originating from machinery, nearby traffic or construction work. Any unit with extreme sensitivity will lead to nuisance shutdowns for non-earthquake motions or microtremors. In this case, the seismic switch will activate and stop the elevators even if the elevators are not damaged. Therefore, all the elevators need to be checked before they are put back in service, and many will be out of service unnecessarily. On the other hand, the susceptibility to false triggering should not be decreased at the expense of the sensitivity to potentially damaging earthquake motions.

One of the first implementations of a combination of seismic triggers and safety control devices before it was mandatory was reported by Benuska et al. (1977). In 1972, following the San Fernando earthquake three elevators of the UCLA Public Health Building were supplemented with vertical seismic triggers EST-1 manufactured by Kinemetrics. One year later, a counterweight derailment device was also installed in one of the three elevators. The seismic trigger was anchored at the machine room floor and it was preset to provide a switch closure at 0.03g vertical acceleration with frequency in the 1.0 to 10 Hz range. Once the safety control was activated, the elevator controls responded by preventing idle elevators from running, slowing down and stopping moving elevators in the next floor, opening doors and shutting down the motor generator units. The objective of these switches was to detect the earthquake in the initial

stages by detecting the arrival of the *P*-waves, which usually cause the vertical acceleration. Although the value of 0.03g appears to be rather low, however, the authors mentioned in their paper that there were no false triggers of the system until the time that they reported their results. It should be noted that the current A17.1 Code now recommends that the seismic switches shall be activated by a vertical excitation of not more than 0.15g.

The commercially available seismic switches vary in the choice of the sensing axes (horizontal, vertical or triple sensing), the operating principle, the passive or power-supplied characteristics, the manual or automatic reset, etc. Most of them are designed to trigger when the acceleration exceeds a certain level. These conventional seismic switches based solely in acceleration measurement can, however, pose a problem in certain cases. For example, Onoda and Yamatoshi (1988, 1990) reported that during the 1983 Central Japan Sea earthquake, the oscillations at the top floor of a high-rise building exceeded 4 in (> 10 cm) causing oscillations of the traveling cables that exceeded 6.5 ft (200 cm) which in turn produced an entanglement of the cables. The seismic switch did not operate because it was set to trigger with an acceleration of 0.030g and the ground acceleration only reached 0.016g with a dominant period of 5 seconds. Two and a half months later, another earthquake hit the same building causing displacements of the top floor of only 0.2 in (0.08 cm). However, this time the seismic switches unnecessarily shutdown the elevators because the acceleration reached 0.03g with a period of 0.33 seconds.

A comparative experimental study of different types of seismic switches manufactured by four different companies was carried out by Miller (1990). The units were mounted on a shaking table and subjected to simulated earthquake motions and sine waves with varying frequencies. Although the devices performed relatively well during the sine wave testing, it was found that during the quasi-random (earthquake-like) tests, some of them showed long trip times or did not comply with the factory-specified sensitivity. Moreover, some units even tripped with the noise level of the shaking table.

The situations described above prompted a search for more effective seismic sensors. The development of a new generation of seismic sensor devices is currently an area of active research. Researchers from Hitachi Elevator Engineering reported that they achieved the proper selectivity and sensitivity by measuring what they called the “seismic-wave energy,” which is basically proportional to the product of the measured displacement and velocity (Onoda and Ikeda, 1988; Onoda and Yamatoshi, 1990; Onoda et al., 1992). Suzuki and Kishimoto (1990) from Mitsubishi Corp. developed a system that combines a *P*-wave sensor with an *S*-wave sensor. When the sensor detects the arrival of *P*-waves, the device brings the car to rest at the nearest floor and sounds an alarm to alert passengers to evacuate the car. The car then waits with its door opened until the other sensor detects the arrival of *S*-waves. At this time the doors are closed and the service is interrupted. If the *S*-waves are not detected during a certain fixed time interval, service resumes automatically.

Besides requiring that the displacement switch must be activated by the derailment of the counterweight and provide this information to the control system, the A17.1 Code does not specify the particular type of device to be used. In practice, it is common to use the so-called “ring-on-a-string” system, which consists of one (or more) taut sensing wire that runs along the hoistway, adjacent and parallel to the counterweight frame. The sensing wire is electrically charged and it is maintained at no more than 24 volts above or below the building ground potential, as required by the code. The wire is enclosed by a ring attached to the counterweight frame. The excursion of the counterweight beyond normal limits brings the sensing wire in

contact with the building ground and then closes the normally open circuit. This operates a relay, which causes the elevator to react as required by the code (see above description). On windy days, there is a possibility that these devices could be triggered by structural motion, especially in tall buildings.

1.5 Seismic Behavior of Escalators

Compared to elevators, the seismic performance of escalators did not receive a great deal of attention mostly because they were not significantly affected by past earthquakes. However, the Northridge earthquake of 1994 and the following year the Kobe earthquake caused considerable damage to many escalators. Fortunately, the fact that the Northridge earthquake occurred when local shopping malls were closed contributed to the lack of passenger injuries. Up through the 1996 edition, the A17.1 Safety Code does not contain any provisions for escalators or moving walks, but a new section will be codified in the 2000 Edition due for publication by the end of the year 2000. Recently the state of California added new requirements for escalators in Article 7-37 of the 1998 California Elevator Safety Construction Code. A summary of these requirements is presented next:

- The connections that join the escalator/moving walk to the building shall be designed to sustain loads of 0.5g in the horizontal directions.
- The design of the connections should take into account the maximum story drift.
- The handrail supports shall be designed to resist a lateral load of 50 lb/ft applied at the top of the handrail.
- A minimum of one seismic switch shall be provided in every building with an escalator or moving walk.
- The activation of the seismic switch shall remove power from the escalator/moving walk and apply the brake.
- Seismic restraints shall be provided in the longitudinal direction at one or both ends of the escalator.
- At the sliding end of the escalator, the beam seat shall be able of accommodating at least twice the story drift allowed by the code in both directions.
- Seismic restraints shall also be provided in the transverse direction at all supports.

1.6 Previous Studies on Seismic Response

Recognizing the vulnerability of elevators in buildings subjected to strong ground motions, several researchers have studied the seismic behavior of these systems. Practically all the studies were focused on the rail and counterweight systems since, as mentioned previously, experience has shown that they are the most vulnerable components of an elevator during an earthquake.

The first reported study on the seismic response of elevators was carried out by Yang and co-workers in 1983 (Yang et al., 1983). Yang and his co-authors constructed a physical model of an elevator and counterweight system to study qualitatively the response of the system when it is

subjected to a harmonic base acceleration. The experimental model consisted of a load platform that can move in a horizontal direction guided by two circular shafts. The exciter's armature is attached to the platform. The shafts were connected to a main frame used to secure the setup to a shaking table. The load platform supports the model of the counterweight and the two elements representing the rails. The rails were represented by two steel bars with rectangular cross sections. The counterweight's frame was simulated by means of a frame formed by two end plates and two flexible members representing the sides with a central bar connecting the two end plates. The central bar contained five rods normal to its axis whose function is to support the weights. The counterweight's frame was supported by four leaf springs at each corner. The bases of the leaf springs were connected to the platform by cross members. These leaf springs were intended to represent the spring loaded roller guides.

A mathematical model of the rail and counterweight system using beam elements was also developed. The rails were modeled as simply supported beams discretized with four beam elements. The frame of the counterweight was also modeled as a beam supported by two springs at each end. In addition, the frame was assumed to be connected to both rails by nonlinear parallel springs. The nonlinear springs had a constant equal to zero when the two nodal points in the rail and counterweight were not in contact and they assumed a very large value when they were in contact. These very rigid springs were provided with the intention of constraining the counterweight and rail to move together during contact. The damping matrices for the rails and frame were constructed using the Rayleigh model and 2% modal damping ratio. The equations of motion were solved using the Wilson-θ method. Because of the characteristics of the nonlinear springs, an extremely small time step ($\sim 4 \times 10^{-6}$ sec) was required in the analysis. The input for the numerical simulations was an acceleration with the form $A_g = A_o \sin(2\pi f t)$ with $A_o = 1.4\ g$ and $f = 2$, 3, and 4 *Hz*. Because the mathematical and experimental models did not have the same physical characteristics, only the general features and trends of the responses predicted by the two models could be compared. They showed good qualitative agreement. To avoid the need for a very small time step, the researchers proposed to add a viscous damper with a very high coefficient in parallel with the springs. The value of the damping coefficient was set to zero when the counterweight and rail were not in contact and set to a value that led to a damping ratio of 0.7 during contact.

In a series of papers, Tzou and Schiff (Schiff, 1980; Tzou, 1985; Tzou and Schiff, 1987; 1988) studied the seismic in-plane response of rail-counterweight systems to examine the hammering of the counterweight against the rail and roller guides. The model used for their studies is very similar to that used by Yang and his co-workers. The rails were assumed to be separated from the counterweight's frame by a small gap. The mass of the counterweight was divided into lumped masses attached to a center beam. The contact between the masses of the counterweight and their frame were not taken into account. Both ends of the beam were considered to be supported by four linear springs. The two rails were connected to the center beam by nonlinear springs and viscous dampers. The nonlinear springs had contact springs that were activated when the relative displacement of the coordinates at both ends of a contact element exceeded the gap. The dampers were used to improve the numerical stability of the integration process by reducing the high frequency oscillations of the lumped masses. In addition to the dampers, a Rayleigh damping matrix was used to provide modal damping to the beams. The counterweight was assumed to be centered between two floors and the guide rails were modeled as simply supported beams. The seismic input was a sinusoidal acceleration at the fundamental frequency of the building. The

amplitude of the harmonic acceleration was 0.4g and three excitation frequencies were considered: 1.2, 0.5, and 0.3 Hz. The dynamic response was calculated by direct integration using the Wilson-θ method. The results showed that the dynamic contact load was larger than the design load in current engineering practice. However, when an intermediate constraint in the form of a U-shaped tie rod connecting the two rails was provided, the dynamic contact load was reduced by 40%.

In related studies, Tzou and Schiff (1984, 1989) examined the seismic performance of two modified counterweight configurations. In the first case a large separation was placed between the weights and the frame of the counterweight. A mathematical model similar to that developed in their previous study was used for the numerical simulation. The frame and the rail were now modeled as a single combined beam. The authors mentioned that the large gap between the weights and the frame was initially proposed by the Hitachi Elevator Corporation. The idea behind this proposition is that the counterweights will stay still in space as the rails and the frame vibrate during the earthquake if a large separation is provided between them. As it was expected, the results from the numerical simulations showed that the large gap works well if the weights make no contact with the frame, but when contact do occur, the dynamic loading is more severe than those from the standard (small gap) configuration.

In the second modification, rubber dampers were installed between the weights and the frame to alleviate the dynamic contact and to dissipate some of the vibratory energy. The rubber dampers were modeled using the standard linear model of viscoelasticity in which a primary spring is in parallel with a series combination of a viscous damper and a secondary spring. It was found that the rubber dampers could decrease the rail loads provided that the proper values of the coefficients are selected. When the primary stiffness of the damper is increased, the contact between the counterweight and the combined beam is prevented. However, as the stiffness is increased, the absolute motion of the counterweight's mass increases and this increases the load in the rails.

Segal, Rutenberg and Levy (Segal et al., 1994; 1995; 1996; Rutenberg et al., 1996) also studied the seismic response of counterweights in a series of journal and conference papers. In all the studies it was assumed that the counterweight is guided along the rail by sliding shoes. Therefore, the counterweight hangs freely and makes contact with one rail when it oscillates in the in-plane direction and touches two rails when it moves in the out-of-plane direction. The contact elements that connect the counterweight to the building consisted of a parallel combination of a linear spring, a linear dashpot, and a Coulomb friction element. The spring represents the flexibility of the guide rail and brackets and the Coulomb friction takes into account the friction between the shoes and rail. These three elements are in series with an air gap element which represents the small clearance between the shoes and rails. One distinctive feature of these studies is that the vertical velocity of the counterweight was incorporated in the analysis. The counterweight was assumed to be moving at a constant speed. In fact, the effect of the counterweight's velocity on the response is to change the equivalent stiffness of the rail. To calculate the stiffness of the rails, it was assumed that the length of the counterweight was larger that the bracket spacing. All the brackets were assumed to be subjected to the same acceleration equal to that at the top of building. Two scaled horizontal components of the El Centro earthquake were used as input to present numerical results. In the first two studies (Segal et al., 1994; 1996) the counterweight was represented by two totally independent masses, each connected to the building by means of contact elements. The two masses were lumped at the

location of the upper and lower guiding members. The lower mass was larger (twice) that the lower mass. The structure was represented as a six degree of freedom system (three along each horizontal axis) and the counterweight had four dof (two for each mass).

In a following study (Rutenberg et al., 1996) the authors represented the counterweight as a rigid block with two degrees of freedom. The contact points between the counterweight frame and the rails were used as coordinates. The structure was represented by two uncoupled single degree of freedom systems with the properties of the first modes in the two horizontal directions. Rayleigh damping matrices were used to introduce damping to the system. The equations of motion were integrated using a 5th order Runge-Kutta method. A set of 26 earthquake records scaled to a peak ground velocity of 0.4 m/s were used as input to calculate the stresses in the rail and to compare the results with the curves in the ASME-A17.1 code. The authors found that, according to their model, the code is nonconservative by as much as 500% for low buildings and about 50% for tall buildings in Zone 4.

In another paper (Levy et al., 1996), the authors presented a more detailed comparison of the A17.1 design curves against the results obtained using with second model. To carry out the comparison, the counterweight was considered at rest at the top of the building and the distance between its guide shoes and the rail supports was assumed to be the same. The bracket flexibility was discarded. The 26 earthquake records used as excitation were scaled to have a PGV of 0.4 m/s for Zone 4 and 0.3 m/s for Zone 3. The building was represented by its first mode of vibration with two different periods: 1.0 s and 0.5 s. The weight of the counterweight that produces a rail bending stress equal to 88% of the yield stress for different bracket spacings were found using an iterative procedure. Based on these results, the authors mentioned here that the A17.1 code is nonconservative by as much as 650% for low buildings and 250% for taller buildings. However, they cautioned that if a more elaborate model of the building is used, the code may be even be less conservative, due to resonance between the rail-counterweight system and the second mode of buildings with fundamental periods of 1.0 s.

A response spectrum approach to calculate the seismic response of a rail-counterweight system was presented by Suarez and Singh (1996). They developed a three dof model of the system using as generalized coordinates the out-of-plane horizontal displacement of the center of mass and two rotations of the counterweight block. By relating the frequencies of the modes associated with the rotational dof to the translational frequency, the model was reduced to a single dof system. The formulation to calculate the acceleration floor response spectrum, originally developed by Singh to calculate the response of equipment in critical facilities, was modified to calculate the displacement of the rail-counterweight system. The NEHRP design response spectra and an accelerogram of the Loma Prieta earthquake were used to calculate the maximum displacement of the point of contact between the roller guides and the rails. It was observed that when the rail-counterweight system had a fundamental period close to the building period, the displacements became very large. These values, however, are not realistic because of the limited amount of deformation that can be sustained by the helical springs and rubber tires of the roller guides.

In a following paper, the same authors (Suarez and Singh, 1998) extended their model to consider the saturation of the springs and rubber tires. A model with bilinear springs was used to calculate the seismic response. The seismic input consisted of the acceleration time histories at the four points of attachment of the brackets to the hoistway wall. The elevator was assumed to be in a torsional building with three dof per floor. For the numerical examples a rail-

counterweight system with typical dimensions located on a 10-story building was subjected to one component of the Loma Prieta earthquake. It was found that the position of the counterweight with respect to the rail supports has a significant influence on the response. For example, when the counterweight was at the middle of a single rail span in the tenth floor, the bending stresses in the guide rails were relatively small. However, when the counterweight was covering two rail spans and located symmetrically over support at the ninth floor, the stresses exceeded the yielding stress.

After studying the failures observed during the November 22, 1995 earthquake in Israel, D'Amato (1997) recommended the following measures to protect elevators: The guiding shoes should embrace completely the guide rails, the brackets of the rails should be fixed to the building through elastic means, and the weights in the counterweights should be made of a high density material to reduce the distance between the guiding shoes. These recommendations, however, do not seem to agree with the results from the numerical simulations, in particular the last one. In fact, concentrating the mass of the counterweight is detrimental to the seismic response of the rail-counterweight system.

1.7 Objectives and Scope of the Report

It is evident from the brief review of earthquake damage to elevators that counterweights derailment is the most frequent mode of failure. Other components of elevator system suffered relatively less damage. The design forces for many of the elevator components and its attachments can be obtained from the code provisions for regular electrical and mechanical provisions, such as NEHRP, UBC, BOCA, etc. However, the rail and counterweight system is a much more complex system than a rigid block attached to the floor or even a flexibly mounted piece of equipment. Some of the special characteristics of the rail and counterweight system are the following. The rail extends over the height of the building and thus it is a system with truly multiple support excitations. The flexibility of the rail must be taken into account since it will affect the response. Moreover, the brackets supporting the rail will affect its dynamic response, at least in some directions. The fact that the counterweight frame is connected to the rail by flexible components makes the possibility of resonance more likely. The position of the counterweight will affect the response not only because the floor accelerations vary with height, but because the dynamic properties of the system depend on where it is positioned with respect to the rail supports. The characteristics of the building will have an influence on the seismic input that the rail and counterweight receives as well as the direction of the excitation relative to the counterweight's orientation.

For all the reasons stated above, it is evident that a more detailed analysis of the rail and counterweight systems is called for. Although the study must be rigorous and comprehensive, the design methodology as a result of the study must be kept as simple as possible so that it can be used in practice. This report is intended as a first step in this direction. Several simplified and more rigorous models of the rail and counterweight systems are developed. The elevator is assumed to be located in a building with torsional eccentricities to study the effect of the rotation of the building's slabs on the response.

SECTION 2
LINEAR MODEL AND ANALYSIS

2.1 Introduction

As discussed in Section 1, a rail-counterweight system consists of several mechanical parts: roller guides, guide rails, and support brackets. The roller guides themselves contain the pre-set helical spring that try to maintain a continuous contact between the roller tires and the rails. The flexibility of these components affects the dynamic response characteristics of the rail-counterweight system. It is, thus, quite important to give special attention to the details of these components while preparing a realistic analytical model for predicting the dynamic response of the system for earthquake induced ground motions. As the conclusions drawn from a study are at best as good as the model used and the assumptions made in describing the input motions, the focus of this study is on the development of an analytical model of the system which includes the: (1) physical characteristics of the counterweight frame, (2) explicit consideration of the flexibilities of the roller guide assemblies, guide rails, and supporting brackets, (3) consideration of the nonuniformity of the input motion at the counterweight frame supports, and (4) realistic earthquake induced accelerations filtered by the building and acting at the rail supports. To include the flexibility of the guide rails, they are considered as continuous beams supported on elastic supports that represent the brackets. The differential support motions caused by the torsional motion of the supporting building as well as those caused by the system being connected to different building floors are included. The simultaneous application of two orthogonal earthquake components, both causing the out-of-plane (perpendicular to the plane of the counterweight) and in-plane (in the plane of the counterweight) motions, are considered. Two building structures with different dynamic characteristics are considered to define the input to the system. The numerical results are obtained for the deformations and stresses in various vulnerable components of the system for various postions of the counterweight frame along the building height. To study the effect of the variability of ground motion characteristics on the system response, several recorded earthquake induced ground motions are used to obtain the numerical results.

In this section, it is assumed that the system remains linear during its motion. The primary sources of possible nonlinearity in the system and the limitations of the linear analysis are identified. This is followed by a study of nonlinear system in Section 3. For medium level seismic excitation, it is justified to assume that the system behaves linearly. A linear response study by itself is also quite useful as it clearly identifies important dynamic characteristics of the system and provides a clear insight into the system response. Such studies are also quite convenient for a preliminary evaluation of the effectiveness of the protective device that may be needed to strengthen a system. Although not a part of this study, this linear or an equivalent linear analysis can be used to develop a response spectrum analysis approach for a quick seismic evaluation of elevator systems.

2.2 Analytical Model

We model the counterweight frame, including the weight blocks, as a rigid block of height ℓ_c, width d, and depth e. The center of mass of the counterweight is located at a distance ℓ_m from the bottom of the frame, as shown in figure 2-1. The mass of the counterweight, including the mass of the frame, is m_c. The building's motion is transmitted to the counterweight through the brackets and guide rails and then through the rubber tires of the roller guides. The effect of the tension in the wire ropes, being of the second order for the motion of interest, is neglected in the development of the equations of motion. The analytical models for both out-of-plane and in-plane motions of the counterweight-rail system are developed. Since the in-plane and out-of-plane motions are uncoupled, their equations of motion are developed separately. Their combined effect is, however, included in the calculation of the response quantities that are influenced by the both motions.

2.2.1 Out-of-plane Motion

For the out-of-plane model, let the combined stiffnesses provided by the guide rail, bracket support, rubber tires, and helical springs at the upper and lower supports of the counterweight be represented by the stiffness coefficients k_u and k_ℓ, respectively. (The subscripts u and ℓ, respectively, denote the upper and lower supports of the counterweight frame, and this notation will be used throughout this report.) Later, these combined stiffness coefficients will be defined in terms of the individual stiffness coefficients of the roller guides, helical springs, rails, and support brackets.

The counterweight is assumed to be in the X-Z plane. The building's motion is transmitted to the counterweight through the bracket and guide rails and then through the rubber tires of the roller guides. Let the input displacements at four roller supports be denoted by $y_{u1}(t)$, $y_{u2}(t)$, $y_{\ell1}(t)$ and $y_{\ell2}(t)$. The subscripts 1 and 2 indicate the left and right locations, respectively. These displacements will be expressed in terms of the displacements and rotation of the floor slabs immediately above and below the roller supports in a later section.

For a rigid counterweight, the tips of the displacement vectors $y_{u1}(t)$, $y_{u2}(t)$, $y_{\ell1}(t)$ and $y_{\ell2}(t)$ form a plane which defines the instantaneous equilibrium position of the counterweight frame. This instantaneous equilibrium position of the counterweight is defined by the displacement of its center of mass $y_c(t)$ and its rotations about the horizontal and vertical axes, $\beta(t)$ and $\alpha(t)$, respectively. The displacement $y_c(t)$ is the displacement of the center of mass of the counterweight due to the statically applied motion of the four support points, y_{u1}, y_{u2}, $y_{\ell1}$ and $y_{\ell2}$. The base rotations $\alpha(t)$ and $\beta(t)$ are, respectively, the rotations of the rigid counterweight around the vertical and horizontal axes due to the static displacements y_{u1}, y_{u2}, $y_{\ell1}$ and $y_{\ell2}$. These quantities can be expressed in terms of $y_{u1}(t)$, $y_{u2}(t)$, $y_{\ell1}(t)$ and $y_{\ell2}(t)$ as follows:

$$y_c(t) = \frac{\ell_m}{2\ell_c}\left[y_{u1}(t) + y_{u2}(t) + \left(\frac{\ell_c}{\ell_m} - 1\right)\left(y_{\ell1}(t) + y_{\ell2}(t)\right)\right] \tag{2-1}$$

$$\alpha(t) = \frac{y_{u1}(t) - y_{u2}(t)}{d} = \frac{y_{\ell 1}(t) - y_{\ell 2}(t)}{d} \tag{2-2}$$

$$\beta(t) = \frac{y_{\ell 1}(t) - y_{u1}(t)}{\ell_c} = \frac{y_{\ell 2}(t) - y_{u2}(t)}{\ell_c} \tag{2-3}$$

Let the dynamic motion of the counterweight acting as a rigid body be described by three generalized coordinates $v_c(t)$, $\theta(t)$, and $\phi(t)$, measured from its instantaneous equilibrium position. Figure 2-2 shows these three motion coordinates with respect to the base plane that defines the instantaneous equilibrium position.

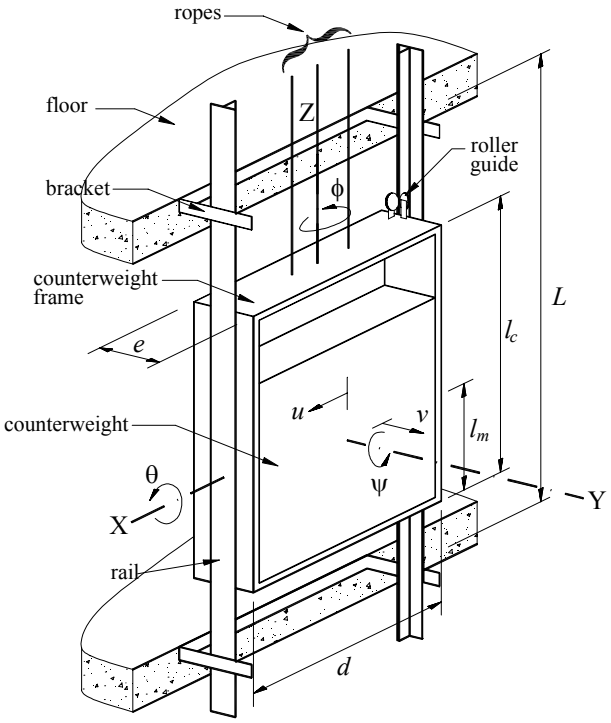

FIGURE 2-1 Geometry of the 3-dof Model of the Rail-Counterweight System

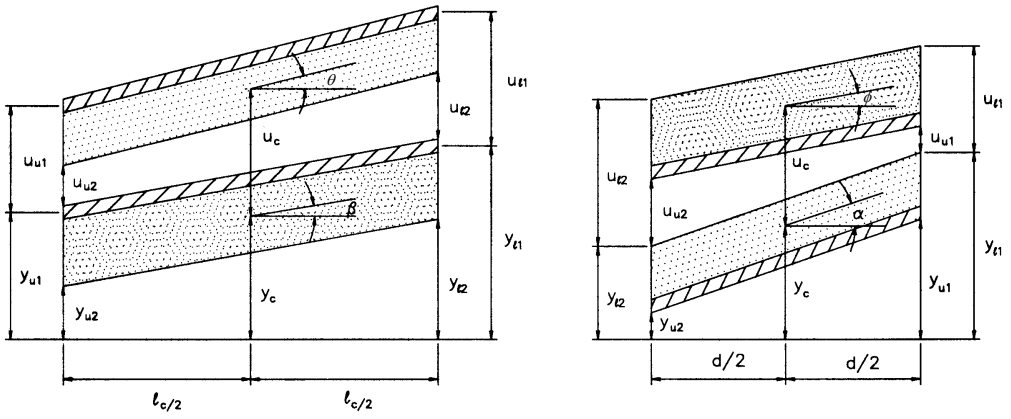

FIGURE 2-2 The Displaced Counterweight Due to the Motion of the Four Supports

Equations of Motion

In terms of the displacements and rotations defined above, the kinetic energy of the counterweight is

$$T = \frac{1}{2} m_c \left(\dot{v}_c + \dot{y}_c \right)^2 + \frac{1}{2} J_\phi \left(\dot{\phi} + \dot{\alpha} \right)^2 + \frac{1}{2} J_\theta \left(\dot{\theta} + \dot{\beta} \right)^2 \tag{2-4}$$

where J_ϕ and J_θ are, respectively, the mass moment of inertia with respect to the vertical and horizontal axes of the counterweight. They are

$$J = \frac{m_c d^2}{12} \left(1 + \frac{e^2}{d^2} \right) \tag{2-5}$$

$$J = \frac{m_c \ell_m^2}{3} \left(1 + \frac{e^2}{4\ell_m^2} \right) \tag{2-6}$$

where e is the thickness of the counterweight perpendicular to its plane.

The potential energy of the system is due to the deformation of the springs and it can be simply expressed in terms of the spring deformations as:

$$V = \frac{1}{2} k_u \left(v_{u1}^2 + v_{u2}^2 \right) + \frac{1}{2} k_\ell \left(v_{\ell 1}^2 + v_{\ell 2}^2 \right) \tag{2-7}$$

where v_{u1}, v_{u2}, $v_{\ell 1}$ and $v_{\ell 2}$ are the relative displacements (or deformations of the springs) at the four corners of the counterweight's frame. They are related to the coordinates v_c, θ, and ϕ as follows:

$$\begin{aligned} v_{u1} &= v_c + \frac{d}{2}\phi - \left(\ell_c - \ell_m \right)\theta \\ v_{u2} &= v_c - \frac{d}{2}\phi - \left(\ell_c - \ell_m \right)\theta \\ v_{\ell 1} &= v_c + \frac{d}{2}\phi + \ell_m \theta \\ v_{\ell 2} &= v_c - \frac{d}{2}\phi + \ell_m \theta \end{aligned} \tag{2-8}$$

Using the Lagrange's equations, we obtain the equations of motion for the rail-counterweight system as:

$$\begin{bmatrix} m_c & 0 & 0 \\ 0 & J_\phi & 0 \\ 0 & 0 & J_\theta \end{bmatrix} \begin{Bmatrix} \ddot{v}_c \\ \ddot{\phi} \\ \ddot{\theta} \end{Bmatrix} +$$

$$\begin{bmatrix} 2(k_u + k_\ell) & 0 & 2\left[\ell_m (k_u + k_\ell) - k_u \ell_c\right] \\ 0 & \frac{d^2}{2}(k_u + k_\ell) & 0 \\ 2\left[\ell_m (k_u + k_\ell) - k_u \ell_c\right] & 0 & 2\left[k_u (\ell_c - \ell_m)^2 - k_\ell \ell_m^2\right] \end{bmatrix} \begin{Bmatrix} u_c \\ \phi \\ \theta \end{Bmatrix} = -\begin{Bmatrix} m_c \ddot{y}_c \\ J_\phi \ddot{\alpha} \\ J_\theta \ddot{\beta} \end{Bmatrix} \tag{2-9}$$

It is noted that when the stiffness coefficients k_u and k_ℓ are equal and there is no center of mass eccentricity, the equations become uncoupled. This occurs when the counterweight is symmetrically located with respect to the supports of the guide rail. In the linear analysis, the second equation of motion is always uncoupled because of the counterweight's symmetry and the equal values of the spring stiffness coefficient at a same level.

Since we are interested in calculating the deformations of the rail and rollers, it is convenient to introduce the following coordinates:

$$v_e = \ell_m \theta \quad ; \quad v'_e = \frac{d}{2}\phi \tag{2-10}$$

In terms of these coordinates, the three equations of motion (2-9) become

$$m_c \begin{bmatrix} 1 & 0 \\ 0 & \gamma_2 \end{bmatrix} \begin{Bmatrix} \ddot{v}_c \\ \ddot{v}_e \end{Bmatrix} + 2 \begin{bmatrix} k_u + k_\ell & k_u\left(1 - \frac{\ell_c}{\ell_m}\right) + k_\ell \\ k_u\left(1 - \frac{\ell_c}{\ell_m}\right) + k_\ell & k_u\left(1 - \frac{\ell_c}{\ell_m}\right)^2 + k_\ell \end{bmatrix} \begin{Bmatrix} v_c \\ v_e \end{Bmatrix} = -m_c \begin{Bmatrix} \ddot{y}_c \\ \gamma_2 \ddot{y}_{dif} \end{Bmatrix} \tag{2-11}$$

$$m_c \gamma_1 \ddot{v}'_e + 2(k_u + k_\ell) v'_e = -m_c \gamma_1 \ddot{y}'_{dif} \tag{2-12}$$

where

$$\gamma_1 = \frac{1}{3}\left(1 + \frac{e^2}{d^2}\right); \quad \gamma_2 = \frac{1}{3}\left(1 + \frac{e^2}{4\ell_m^2}\right) \tag{2-13}$$

The three excitation terms $\ddot{y}_c$, $\ddot{y}_{dif}$ and $\ddot{y}'_{dif}$ in the equation of motion are now defined as:

$$\ddot{y}_c(t) = \frac{\ell_m}{2\ell_c}\left[\ddot{y}_{u1}(t) + \ddot{y}_{u2}(t) + \left(\frac{\ell_c}{\ell_m} - 1\right)\left(\ddot{y}_{\ell 1}(t) + \ddot{y}_{\ell 2}(t)\right)\right] \tag{2-14}$$

$$\ddot{y}_{dif} = \ell_m \ddot{\beta} = \frac{\ell_m}{\ell_c}\left(\ddot{y}_{\ell 1} - \ddot{y}_{u1}\right) \tag{2-15}$$

$$\ddot{y}'_{dif} = \frac{d}{2}\ddot{\alpha} = \frac{\ddot{y}_{u1} - \ddot{y}_{u2}}{2} \tag{2-16}$$

Input Terms in the Equations of Motion

The input acceleration terms $\ddot{y}_c$, $\ddot{y}_{dif}$ and $\ddot{y}'_{dif}$ required in Eqs. (2-11) and (2-12) can be expressed in terms of the linear and angular accelerations of the building floors. For the out-of-plane model, we are interested in the floor motions perpendicular to the counterweight's plane. That is, in figure 2-3, the motion along the Y-axis for the counterweight in the X-Z plane. If the counterweight were in the Y-Z plane, then we would be interested in floor motions in the X-direction.

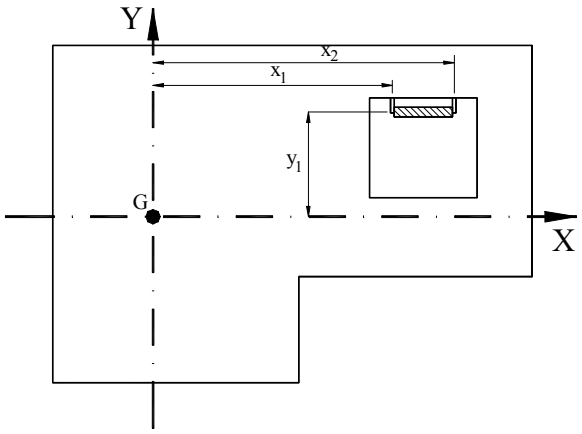

FIGURE 2-3 Plan View of the Building Slab, Elevator Shaft, and Counterweight

To define $\ddot{y}_{u1}$, $\ddot{y}_{u2}$, etc., the acceleration of the floors where the rails are supported on the brackets are required. These acceleration at the left and right bracket supports on, say the n^{th} floor can be expressed in terms of the linear and rotational acceleration of the floor center of mass as follows:

$$\begin{aligned} \ddot{V}_{n1}(t) &= \ddot{V}_n(t) + x_1\ddot{\Theta}_n(t) \\ \ddot{V}_{n2}(t) &= \ddot{V}_n(t) + x_2\ddot{\Theta}_n(t) \end{aligned} \tag{2-17}$$

where $\ddot{V}_{n1}$ and $\ddot{V}_{n2}$, respectively, are the accelerations in the Y-direction at the left and right bracket positions on the n^{th} floor.

To obtain the accelerations at a roller support of the counterweight reasonably accurately, the linear interpolation of the accelerations of the bracket location on the floors above and below the support is used. For the left and right upper rollers, located between the n^{th} and $(n\text{-}1)^{th}$ floors, the accelerations at their positions are thus obtained as:

$$\ddot{y}_{u1}(t) = \left(1 - \frac{a_u}{L}\right)\left(\ddot{V}_n(t) + x_1\ddot{\Theta}_n(t)\right) + \frac{a_u}{L}\left(\ddot{V}_{n-1}(t) + x_1\ddot{\Theta}_{n-1}(t)\right)$$
$$\ddot{y}_{u2}(t) = \left(1 - \frac{a_u}{L}\right)\left(\ddot{V}_n(t) + x_2\ddot{\Theta}_n(t)\right) + \frac{a_u}{L}\left(\ddot{V}_{n-1}(t) + x_2\ddot{\Theta}_{n-1}(t)\right) \quad (2\text{-}18)$$

where a_u is the distance of the upper rollers from the n^{th} floor.

The accelerations at the lower roller supports depend on the position of the counterweight. They are defined below for the two cases of the counterweight (1) being in a single span and (2) being in two consecutive spans as follows (see figure 2-4)

For the counterweight located within a single span

$$\ddot{y}_{\ell 1}(t) = \left(1 - \frac{a_\ell}{L}\right)\left(\ddot{V}_n(t) + x_1\ddot{\Theta}_n(t)\right) + \frac{a_\ell}{L}\left(\ddot{V}_{n-1}(t) + x_1\ddot{\Theta}_{n-1}(t)\right)$$
$$\ddot{y}_{\ell 2}(t) = \left(1 - \frac{a_\ell}{L}\right)\left(\ddot{V}_n(t) + x_2\ddot{\Theta}_n(t)\right) + \frac{a_\ell}{L}\left(\ddot{V}_{n-1}(t) + x_2\ddot{\Theta}_{n-1}(t)\right) \quad (2\text{-}19)$$

For the counterweight located on two consecutive spans (see figure 2-4b)

$$\ddot{y}_{\ell 1}(t) = \left(\frac{a_\ell}{L} - 1\right)\left(\ddot{V}_{n-1}(t) + x_1\ddot{\Theta}_{n-1}(t)\right) + \left(2 - \frac{a_\ell}{L}\right)\left(\ddot{V}_{n-2}(t) + x_1\ddot{\Theta}_{n-2}(t)\right)$$
$$\ddot{y}_{\ell 2}(t) = \left(\frac{a_\ell}{L} - 1\right)\left(\ddot{V}_{n-1}(t) + x_2\ddot{\Theta}_{n-1}(t)\right) + \left(2 - \frac{a_\ell}{L}\right)\left(\ddot{V}_{n-2}(t) + x_2\ddot{\Theta}_{n-2}(t)\right) \quad (2\text{-}20)$$

where $a_\ell = a_u + \ell_c$.

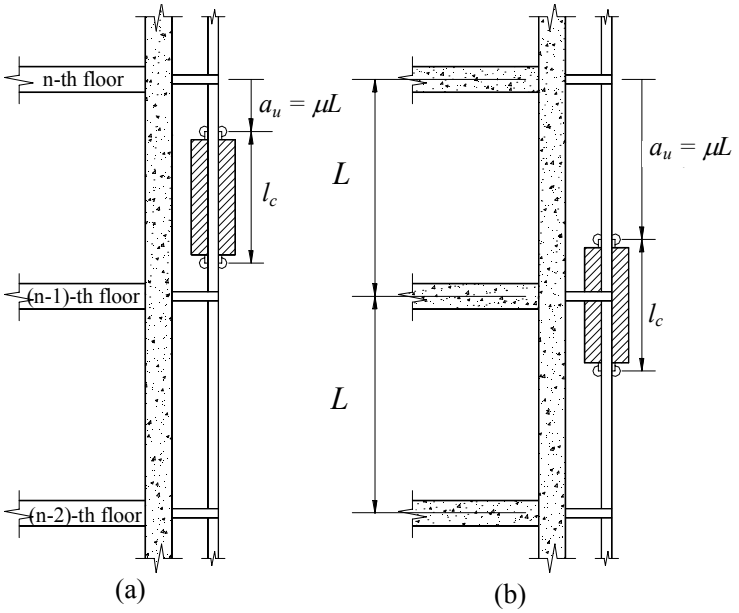

FIGURE 2-4 Counterweight Position Along the Rail in (a) A Single Span, (b) Two Consecutive Spans

2.2.2 In-plane Motion

The counterweight also receives inputs in its own plane at two point of contact with the rail. Let these input at the upper and lower roller contacts be denoted by $x_u(t)$ and $x_\ell(t)$. In terms of these displacements, the instantaneous position of the counterweight center of mass can be defined by the coordinates $x_c(t)$ and $\delta(t)$ as:

$$x_c(t) = x_\ell(t) + \frac{\ell_m}{\ell_c}\left[x_u(t) - x_\ell(t)\right] \tag{2-21}$$

$$\delta(t) = \frac{x_u(t) - x_\ell(t)}{\ell_c} \tag{2-22}$$

Let $u_c(t)$ and $\psi(t)$ be the generalized coordinates of the center of mass in the plane of the counterweight. They are measured relative to its instantaneous equilibrium position defined by equations (2-21) and (2-22). In terms of these coordinates, the kinetic and potential energies of the counterweight can be written as:

$$T = \frac{1}{2} m_c \left(\dot{x}_c + \dot{u}_c\right)^2 + \frac{1}{2} J_\psi \left(\dot{\delta} + \dot{\psi}\right)^2 \tag{2-23}$$

$$V = \frac{1}{2} s_u u_u^2 + \frac{1}{2} s_\ell u_\ell^2 \tag{2-24}$$

where s_u and s_ℓ are the combined stiffness coefficients at the upper and lower contact points, and J_ψ is the mass moment of inertia with respect to the horizontal axis perpendicular to the counterweight's plane. The quantities u_u and u_ℓ are the deformations of the springs at the upper and lower supports, respectively. They are related to the coordinates u_c and ψ as follows:

$$u_u = u_c + \left(\ell_c - \ell_m\right)\psi \;;\; u_\ell = u_c - \ell_m \psi \tag{2-25}$$

Introducing new coordinate u_e:

$$u_e = \ell_m \psi \tag{2-26}$$

one can obtain the equations of motion in terms u_c and u_e for the in-plane response as

$$m_c \begin{bmatrix} 1 & 0 \\ 0 & \gamma_3 \end{bmatrix} \begin{Bmatrix} \ddot{u}_c \\ \ddot{u}_e \end{Bmatrix} + \begin{bmatrix} s_u + s_\ell & s_u\left(\frac{\ell_c}{\ell_m} - 1\right) - s_\ell \\ s_u\left(\frac{\ell_c}{\ell_m} - 1\right) - s_\ell & s_u\left(\frac{\ell_c}{\ell_m} - 1\right)^2 + s_\ell \end{bmatrix} \begin{Bmatrix} u_c \\ u_e \end{Bmatrix} = -m_c \begin{Bmatrix} \ddot{x}_c \\ \gamma_3 \ddot{x}_{dif} \end{Bmatrix} \tag{2-27}$$

where

$$\gamma_3 = \frac{1}{3}\left(1 + \frac{d^2}{4\ell_m^2}\right) \tag{2-28}$$

The input acceleration terms in Eq. (2-27) are now defined as:

$$\ddot{x}_c(t) = \ddot{x}_\ell(t) + \frac{\ell_m}{\ell_c}\left[\ddot{x}_u(t) - \ddot{x}_\ell(t)\right] \tag{2-29}$$

$$\ddot{x}_{dif}(t) = \ell_m \ddot{\delta} = \frac{\ell_m}{\ell_c}\left(\ddot{x}_u(t) - \ddot{x}_\ell(t)\right) \tag{2-30}$$

As was done for the out-of-plane case, the accelerations $\ddot{x}_u$ and $\ddot{x}_\ell$ at the upper and lower contact points on the rails are defined by linear interpolation of the floor accelerations above and below these levels as:

$$\ddot{x}_u(t) = \left(1 - \frac{a_u}{L}\right)\left(\ddot{U}_n(t) - y_1\ddot{\Theta}_n(t)\right) + \frac{a_u}{L}\left(\ddot{U}_{n-1}(t) - y_1\ddot{\Theta}_{n-1}(t)\right) \tag{2-31}$$

For the counterweight located within a single span

$$\ddot{x}_\ell(t) = \left(1 - \frac{a_\ell}{L}\right)\left(\ddot{U}_n(t) - y_1\ddot{\Theta}_n(t)\right) + \frac{a_\ell}{L}\left(\ddot{U}_{n-1}(t) + y_1\ddot{\Theta}_{n-1}(t)\right) \tag{2-32}$$

For the counterweight located on two consecutive spans

$$\ddot{x}_\ell(t) = \left(\frac{a_\ell}{L} - 1\right)\left(\ddot{U}_{n-1}(t) - y_1\ddot{\Theta}_{n-1}(t)\right) + \left(2 - \frac{a_\ell}{L}\right)\left(\ddot{U}_{n-2}(t) - y_1\ddot{\Theta}_{n-2}(t)\right) \tag{2-33}$$

where y_1 is the y-coordinate of the bracket supports, measured from the mass centers of the floors (assumed to be on the same vertical line for each floor).

In the development of this model the inertia-related deformations of the rails are neglected. One can include the effect of inertia terms from the rails by preparing a combined dynamical model of the rail-bracket-counterweight system with multiple support inputs coming from different floors. However, because of the relatively small contribution to the inertial forces from the rails, these refinements are found to be unnecessary here. The stiffness contribution from the rails and brackets is, however, included. Also, the acceleration at the contacts of the roller supports with the guide rails are approximated by a simple linear interpolation of the floor accelerations above and below the roller locations.

2.3 Equivalent Springs Coefficients

The flexibility at the counterweight supports is provided by the four components: (1) the flexible guide rail, (2) the guide rail brackets, (3) the helical spring in the roller assembly, and (4) rubber tire rollers. Figure 2-5 shows a schematic of these spring components where the roller guide and helical springs are combinedly represented by the stiffness coefficient, k_{rs}. This combined stiffness can be defined in terms of the individual stiffness coefficients k_s and k_r of the helical springs and the rubber tires. The guide rail and bracket spring coefficients are represented by k_{bm} and k_{br}. Their combined stiffness will be denoted by k_{gr}. Also since the springs represented by k_r, k_s and k_{gr} are all in a series configuration, the stiffness coefficients of the combined equivalent upper and lower springs can be defined as:

$$k_u = \frac{\left(k_{gr}\right)_u k_r k_s}{\left(k_{gr}\right)_u\left(k_r + k_s\right) + k_r k_s} \quad ; \quad k_\ell = \frac{\left(k_{gr}\right)_\ell k_r k_s}{\left(k_{gr}\right)_\ell\left(k_r + k_s\right) + k_r k_s} \tag{2-34}$$

where subscripts u and ℓ identify the stiffness coefficients of the upper and lower springs as usual. Since the counterweight can move along the guide rails, the spring coefficient k_{gr}

associated with the rail and bracket supports will depend upon its location, and it could have different values for the upper and lower springs.

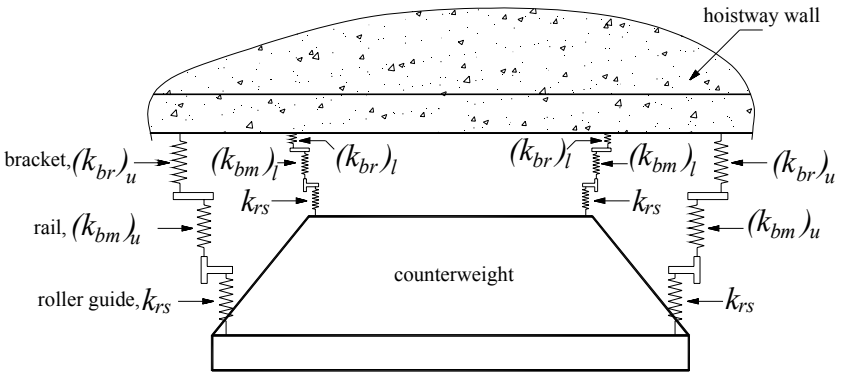

FIGURE 2-5 Equivalent Springs Representing the Brackets, Rails, and Roller Guides

In the following the methods to obtain k_r, k_s, and k_{gr} are described.

2.3.1 Coefficient for the Elastomer Roller

For medium and high speed elevators, the counterweight frame is guided on each guide rail by a pair of guide rollers attached to the frame at its top and bottom. Roller guides are composed of three spring-loaded rollers; the springs keep the rollers in permanent contact with the guide rail (Janovsky, 1993). The rollers consist of an inner steel wheel with an outer rubber tire to minimize noise and improve riding quality. Each roller is connected to a pivoted rocker arm with a helical steel spring which keeps the roller in constant contact with the rail. Depending on the direction of the relative motion of the frame with respect to the guide rail, one of the two rollers is always compressed against a rail's web in the out-of-plane motion, and against one of the two rail webs in the in-plane motion.

The force deformation characteristics of the rubber rollers are inherently nonlinear. In such a case, an accurate evaluation of their spring coefficient can only be made experimentally. However, here we assume the linear behavior and obtain the coefficient in an approximate manner. We assume that the contact area between the rubber tire and the rails remains constant. The dimensions of this contact area are $b \times c$ (see figure 2-6), where c is the web thickness of the guide rail. The average compressive stress in the rubber tire can be expressed as

$$\sigma_b = \frac{P}{bc} = E_r \frac{\delta}{e_r} \tag{2-35}$$

where E_r is the modulus of rubber, e_r is the thickness of the rubber tire, and δ is the deformation of the tire. The stiffness coefficient for the equivalent tire spring can be written as,

$$k_r = \frac{P}{\delta} = \frac{b}{e_r} cE_r \tag{2-36}$$

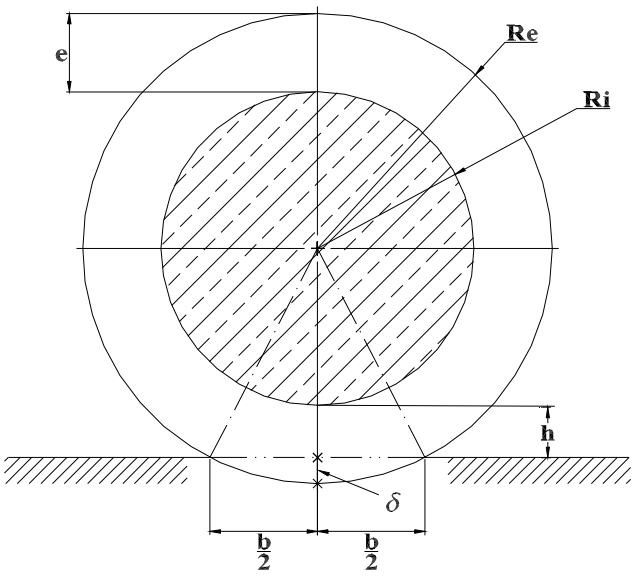

FIGURE 2-6 Geometry of the Wheel in the Roller Guide

The rail's thickness c and all other dimensions of the T-section guide rails have nominal values specified in codes (see Section 1). The value of b is not known. We assume $b/e_r = 4$ and thus

$$k_r \simeq 4cE_r \tag{2-37}$$

Equation (2-37) provides an approximate linear estimate of the spring coefficient. However, it is noted that the contact length b will actually be a nonlinear function of the tire deformation δ, thus making the roller tire spring behave nonlinearly.

2.3.2 Coefficient for the Helical Spring

The stiffness coefficient k_s of the helical springs in the roller guide can be obtained from the manufacturer's specifications. Alternatively, if the material and geometry of the springs are known, the coefficient can be calculated with the following formula (Avallone and Baumeister, 1986) for cylindrical, helical springs with circular cross sections:

$$k_s = \frac{d_s^4 G}{64 n_c r^3} \tag{2-38}$$

where d_s is the diameter of the steel wire, G is the shear modulus, n_c is the number of coils, and r is the mean radius of the coils. The helical spring coefficient in (2-38) should be multiplied by the square of the ratio of its own distance to the distance of the roller from the pivot on the rocker arm before being used in (2-34).

If the deformation of a helical spring exceeds a certain limit, the gap between the helical wire coils could be closed. The stiffness of such saturated spring will then be provided by the bearing contact between the coils rather than the torsional deformation of the wire. The stiffness coefficient associated with the bearing contact could be much larger than the stiffness due to the torsional rigidity. A similar situation will also occur in the counterweights provided with the

restraining plates. Whenever the deformation of a roller guide assembly exceeds the clearance between its restraining plate and the rail, the stiffness of the system will then be provided by the rail and the brackets and not by the roller guide assembly. This sudden change in the stiffness will introduce nonlinearity in the system. This nonlinearity caused by a change in the system stiffness is considered in section 3.

2.3.3 The Stiffness Coefficients for the Rails and Brackets

The coefficients k_{gr} at the upper or lower supports depends on the location of the counterweight along the guide rails. To calculate this for a given location, the deflection of the guide rail-bracket system for a unit load applied at the location is calculated by the finite element analysis. The inverse of this deflection defines the stiffness coefficient. In this analysis, the guide rails are modeled as continuous beams supported on linear springs that represent the flexibility of the bracket supports. It is necessary to consider the eccentric loading of the brackets in calculating their stiffness coefficients. Although the guide rails and brackets could possibly yield and thus introduce nonlinearity in the system, inclusion on such nonlinearity in the analysis is never considered necessary as a post yielding deformation analysis of the counterweight-rail system is rarely of any interest.

2.4 Solution of the Equations of Motion

Here, the equations of motion for both out-of-plane and in-plane motions are rewritten in the matrix form. To include some inevitable dissipation of energy in the system, a damping matrix is also added to the equations of motion.

$$[M]\{\ddot{q}\}+[C_d]\{\dot{q}\}+[K]\{q\}=-[M]\{U\} \tag{2-39}$$

where:

$$\{q\}=\begin{pmatrix} u_c & u_e & v_c & v_e & v_e \end{pmatrix}^T \tag{2-40}$$

$$\{U\}=\begin{pmatrix} \ddot{x}_c & \ddot{x}_{dif} & \ddot{y}_c & \ddot{y}_{dif} & \ddot{y}_{dif} \end{pmatrix}^T \tag{2-41}$$

$$[M]=m_c\begin{bmatrix} 1 & 0 & 0 & 0 & 0 \\ 0 & \gamma_3 & 0 & 0 & 0 \\ 0 & 0 & 1 & 0 & 0 \\ 0 & 0 & 0 & \gamma_2 & 0 \\ 0 & 0 & 0 & 0 & \gamma_1 \end{bmatrix} \tag{2-42}$$

$$[K]=\begin{bmatrix} s_u+s_\ell & s_u\left(\frac{\ell_c}{\ell_m}-1\right)+s_\ell & 0 & 0 & 0 \\ & s_u\left(\frac{\ell_c}{\ell_m}-1\right)^2+s_\ell & 0 & 0 & 0 \\ & & 2\left(k_u+k_\ell\right) & 2\left[k_u\left(1-\frac{\ell_c}{\ell_m}\right)+k_\ell\right] & 0 \\ & \text{symm.} & & 2\left[k_u\left(1-\frac{\ell_c}{\ell_m}\right)^2+k_\ell\right] & 0 \\ & & & & 2\left(k_u+k_\ell\right) \end{bmatrix} \tag{2-43}$$

To include some inevitable dissipation energy in the system, a damping matrix is also added to the equation of motion. In absence of any better information about the energy dissipation mechanisms, the damping matrix $[C_d]$ is traditionally defined in terms of the modal damping ratios ξ_i as follows:

$$[C_d]=[\Phi]^{-T}[2\xi_i\omega_i][\Phi]^{-1}=[M][\Phi][2\xi_i\omega_i][\Phi]^T[M] \tag{2-44}$$

where $[\Phi]$ is the matrix of eigenvectors of the undamped system in (2-39), normalized with respect to the mass matrix $[M]$.

Any suitable numerical procedure can be used to solve the equations of motion. In this study, the numerical calculations were carried out using MATLAB® (Mathworks Inc., 1992) and the program (or m-file) *lsim*. To integrate the equations of motion (2-39) by MATLAB, it is necessary to rewrite them as a set of first order differential equations with the form

$$\begin{aligned} \{\dot{X}(t)\}&=[A]\{X(t)\}+[B]\{U(t)\} \\ \{Y(t)\}&=[C]\{X(t)\} \end{aligned} \tag{2-45}$$

where $\{X(t)\}$ is a state vector, $\{Y(t)\}$ is the output vector and $\{U(t)\}$ is the input vector. The state vector and the state matrices $[A]$, $[B]$, and $[C]$ are defined in terms of the system matrices as follows:

$$\{X(t)\}=\begin{Bmatrix}\{\dot{q}\}\\ \{q\}\end{Bmatrix} \tag{2-46}$$

$$[A]=\begin{bmatrix}-[M]^{-1}[C_d] & -[M]^{-1}[K]\\ [I] & [O]\end{bmatrix} \tag{2-47}$$

$$[B]=\begin{bmatrix}-[I]\\ [O]\end{bmatrix} \tag{2-48}$$

where $[I]$ and $[O]$ are the (5 × 5) identity and null matrices, respectively. The output vector $\{Y(t)\}$ contains the deformations of the equivalent springs at the upper and lower ends of the counterweight:

$$\{Y(t)\} = \begin{pmatrix} u_u & u_\ell & v_{u1} & v_{u2} & v_{\ell 1} & v_{\ell 2} \end{pmatrix}^T \tag{2-49}$$

In view of Eqs. (2-8), and (2-25), the matrix [C] in (2-45) is thus defined as,

$$[C] = \begin{bmatrix} 0 & 0 & 0 & 0 & 0 & 1 & \frac{\ell_c}{\ell_m} - 1 & 0 & 0 & 0 \\ 0 & 0 & 0 & 0 & 0 & 1 & -1 & 0 & 0 & 0 \\ 0 & 0 & 0 & 0 & 0 & 0 & 0 & 1 & 1 - \frac{\ell_c}{\ell_m} & 1 \\ 0 & 0 & 0 & 0 & 0 & 0 & 0 & 1 & 1 - \frac{\ell_c}{\ell_m} & -1 \\ 0 & 0 & 0 & 0 & 0 & 0 & 0 & 1 & 1 & 1 \\ 0 & 0 & 0 & 0 & 0 & 0 & 0 & 1 & 1 & -1 \end{bmatrix} \tag{2-50}$$

2.5 Deformation and Stresses

The solution of the equation of motion provides v_c,v_e, and v_e' for the out-of-plane model and u_c and u_e for the in-plane model. These quantities can be used to calculate the deformations and stresses in the deformable components of the system. The deformation of the equivalent springs at the four corners of the counterweight can be calculated by using (2-8) for the out-of-plane model, and (2-25) for the in-plane model. To obtain the stresses in the deformable components of the systems, e.g., the rail-bracket system and roller guide components, these equivalent spring deformations must be resolved into the deformations $(v_{gr})_u$ and $(v_{gr})_\ell$ of the bracket-rail systems, and the deformation $(v_{rs})_u$ and $(v_{rs})_\ell$ of the roller guide assemblies. These deformations can in turn be resolved further into the deformations of their components.

Since the springs representing the rail-bracket system and the roller guide assemblies are in series we can write for the springs at an upper support as,

$$\left(k_{gr}\right)_u \left(v_{gr}\right)_{ui} = k_{rs} \left(v_{rs}\right)_{ui} \tag{2-51}$$

where the combined stiffness coefficient of the roller guide assembly can be expressed as

$$k_{rs} = \frac{k_r\, k_s}{k_r + k_s} \tag{2-52}$$

in which k_r and k_s are defined by (2-24) and (2-25), respectively. Also, since the total deformation of the equivalent spring is sum of deformations of the rail-bracket spring and the roller guide spring, we have,

$$v_{ui} = \left(v_{gr}\right)_{ui} + \left(v_{rs}\right)_{ui} \quad ; \quad i = 1, 2 \tag{2-53}$$

From (2-51) and (2-53) we obtain the separate deformations of the guide rail-bracket and roller guide assembly as follows:

$$\left(v_{gr}\right)_{ui} = \frac{k_{rs}}{k_{rs} + \left(k_{gr}\right)_u} v_{ui} \quad ; \quad i = 1, 2$$
$$\left(v_{rs}\right)_{ui} = \frac{\left(k_{gr}\right)_u}{k_{rs} + \left(k_{gr}\right)_u} v_{ui} \quad ; \quad i = 1, 2 \tag{2-54}$$

Similar expressions can be developed to calculate the deflections and deformations at the lower support of the counterweight:

$$\left(v_{gr}\right)_{\ell i} = \frac{k_{rs}}{k_{rs} + \left(k_{gr}\right)_\ell} v_{\ell i} \quad ; \quad i = 1, 2$$
$$\left(v_{rs}\right)_{\ell i} = \frac{\left(k_{gr}\right)_u}{k_{rs} + \left(k_{gr}\right)_\ell} v_{\ell i} \quad ; \quad i = 1, 2 \tag{2-55}$$

The deformations of the roller guide assemblies can be similarly resolved into the deformations of the rubber rollers and the helical springs using their stiffness coefficients. These deformations can also be used to calculate the stresses in these components if necessary.

To calculate the bending moments and stresses in the rail-bracket system we use deformations $(v_{gr})_{ui}$ and $(v_{gr})_{\ell i}$ with the finite element model of the rail-bracket system. Corresponding to each calculated deformation v_{gr}, and the equivalent static load at each roller guide location is obtained from:

$$P_{eq} = k_{gr}\, v_{gr} \tag{2-56}$$

For these equivalent loads, the finite element model of the rail-bracket system is then analyzed to obtain the required forces and stresses.

2.6 Numerical Results

In this section we present the numerical results of an elevator system used in two different building models. The first building is a ten story building described in reference 11 (Conner et al., 1987) with slight modification. The building is modeled as a torsional system with three degrees of freedom per floor: two horizontal translations and one rotation about the vertical axis. The building has a rectangular plan with a relatively small eccentricity. The mass and stiffness properties of the building are shown in table 2-1. The natural frequencies and mass matrix normalized participation factors are presented in table 2-2. The modal damping ratio for the building was assumed to be 5% for all the modes.

TABLE 2-1 Properties of the 10-Story Torsional Building

Story	Mass	Inertia	Stiffness		Eccentricity	
	$[10^6$ kg]	$[10^4$ kg.m^2]	$k_x = k_y$ $[10^9$ N/m]	k_t $[10^{12}$ N.m]	e_x [m]	e_y [m]
1	1.318	1.602	0.803	0.269	2.286	1.528
2	1.211	1.472	3.098	1.100	2.286	1.528
3	1.211	1.472	3.098	1.100	2.286	1.528
4	1.194	1.451	2.390	0.779	2.286	1.528
5	1.194	1.451	2.390	0.779	2.286	1.528
6	1.194	1.451	2.390	0.779	2.286	1.528
7	1.194	1.451	2.390	0.779	2.286	1.528
8	1.167	1.418	1.347	0.424	2.286	1.528
9	1.167	1.418	1.347	0.424	2.286	1.528
10	1.167	1.418	1.347	0.424	2.286	1.528

TABLE 2-2 Frequencies of the 10-Story Torsional Building

Mode	Frequency [rad/sec]	Period [sec]	Participation factor
1	5.70	1.1014	-139.0785
2	5.77	1.0892	208.1074
3	15.60	0.4027	-38.2893
4	15.78	0.3981	-57.2584
5	26.33	0.2386	-16.9277
6	26.63	0.2359	-25.3191
7	38.59	0.1628	-6.9129
8	39.04	0.1609	10.3518
9	47.78	0.1315	-4.7535
10	48.33	0.1300	7.1106
11	58.14	0.1081	2.9359
12	58.81	0.1068	-4.3990
13	63.23	0.0994	2.2669
14	63.96	0.0982	-3.3775
15	73.20	0.0858	-1.6666
16	74.04	0.0849	2.4912
17	83.40	0.0753	-0.7834
18	84.35	0.0745	1.1747
19	91.33	0.0688	0.9745
20	92.32	0.0681	-1.4548
21	967.84	0.0065	0.1229
22	2605.72	0.0024	0.0347
23	4400.36	0.0014	-0.0152
24	6454.48	0.00097	0.0059
25	8013.25	0.00078	-0.0042
26	9726.08	0.00065	-0.0024
27	10585.43	0.00059	0.0024
28	12336.80	0.00051	-0.0016
29	14035.72	0.00045	0.0006
30	15778.94	0.00040	0.0009

The second building is a slightly modified version of a 24-story building described by Newmark, Blume and Corning (1961). The building is modeled as a shear building, with one degree-of-freedom per floor. The building has nonuniform stiffness and mass properties along its height. They are shown in table 2-3. The modal frequencies, periods and participation factors of this building are also given in table 2-3. The modal dumping ration for this building was also assumed to be 5% for all models.

TABLE 2-3 Properties of the 24-Story Shear Building

Story / Mode	M [10^6 kg]	K [10^9 N/m]	Frequency [rad/sec]	Period [sec]	Participation factor
1	2.098	7.425	3.43	1.8316	-383.2827
2	1.977	7.425	8.30	0.7569	-177.7671
3	1.855	6.918	13.39	0.4692	119.5009
4	1.855	6.970	18.27	0.3440	88.3527
5	1.741	5.849	23.14	0.2715	61.8244
6	1.729	5.587	28.27	0.2223	49.6557
7	1.729	5.569	32.96	0.1907	48.6557
8	1.609	4.063	37.74	0.1665	-37.0350
9	1.581	3.678	41.34	0.1520	34.1981
10	1.581	3.678	45.76	0.1373	25.2754
11	1.567	3.678	50.01	0.1256	-24.6916
12	1.555	3.415	54.30	0.1157	23.9750
13	1.555	3.415	57.59	0.1091	22.1104
14	1.492	2.855	61.60	0.1020	-23.5130
15	1.475	2.469	64.96	0.0967	19.4600
16	1.475	2.469	68.89	0.0912	18.1303
17	1.455	2.329	74.26	0.0846	16.0150
18	1.434	1.769	78.24	0.0803	13.6681
19	1.434	1.769	83.06	0.0756	15.9951
20	1.345	1.524	87.97	0.0714	12.9106
21	1.338	1.278	93.23	0.0674	8.5423
22	1.345	1.261	98.51	0.0638	17.2519
23	1.343	0.928	107.44	0.0585	10.9432
24	1.396	0.771	116.55	0.0539	7.8433

The numerical results are obtained mainly for the 18.5-lb guide rails; however, other rail sizes of the rails shown in Table 1.1 have also been considered. The cross sectional properties of different rail sizes are provided in table 2.4. Although some numerical results using the 8-lb guide rails have been presented, it must be pointed out that currently the 8-lb guide rail is not recommended for use in seismic regions 3 and higher.

From the catalogs and plans of a leading elevator company, the following typical dimensions and properties for the counterweight, helical springs, roller guides, guide rails and support brackets have been selected for the analysis. The counterweight frame is considered to be two-third full of the weight blocks; thus $\ell_m = \ell_c/3$. It is mentioned that some of these properties might be different for different pay loads and elevator car designs.

TABLE 2-4 Moment of Inertia and Distance from Centroid to Outermost Point for Standard T-Sections

Rail Size [lb/ft]	Moment of Inertia [in^4]		Distance c [in]	
	I_{xx}	I_{yy}	c_x	c_y
8	1.424	1.369	1.641	1.75
11	4.279	2.885	2.376	2.25
12	4.476	3.948	2.413	2.50
15	4.797	6.294	2.544	2.50
18.5	9.743	8.400	2.998	2.75
22.5	10.924	9.627	2.652	2.75
30	22.633	11.867	3.244	2.75

Counterweight properties:
mass $m_c = 1950\ kg$,
height $\ell_c = 3.505\ m$,
width $d = 0.711m$,
depth $e = 152.4mm$.

Helical springs in the roller guides:
shear modulus of steel $G = 76.9\ GPa$,
number of coils $n_c = 5$,
diameter of the wires $d_s = 6.35\ mm$,
mean radius of the coils $r = 12.7\ mm$.

Rubber tires:
Modulus of elasticity of rubber $E_r = 20.7\ MPa$,
tire width $c = 15.875\ mm$.

Guide rails
distance between rail's supports $L = 3.66\ mm$
modulus of elasticity of steel $E_s = 200\ GPa$

Bracket that attach the rails to the hoistway walls:
cross-sectional area $A_{br} = 1612.9\ mm^2$
length of brackets $\ell_{br} = 127\ mm$

Equivalent stiffness coefficients

For these properties, Eqs. (2-37) and (2-38) yield the following values for the stiffnesses of the rubber tires and helical springs: $k_r = 1.313 \times 10^6$ *N/m*, and $k_s = 0.191 \times 10^6$ *N/m*. For these values, the combined stiffness of the roller guide is $k_{rs} = 0.167 \times 10^6$ *N/m*.

As mentioned before, the stiffness coefficients of the combined bracket-guide rail system is calculated by the finite element analysis for each position of the rollers. Several counterweight positions as the counterweight travels from the top to the bottom of the building are considered. To introduce some inherent dissipation of energy in the rail-counterweight system, a modal damping ratio of 2% was assumed for all modes.

In figure 2-7, we show the variation in the three frequencies of the rail-counterweight system, vibrating in the out-of-plane motion, as a function of the location parameter $\mu = a_u/L$. This parameter defines the position of the top rollers as it move down the top story of the building. There are two zones in the graph. The first zone is for $0 \le \mu \le 1\text{-}\ell_c/L$ when the counterweight is entirely in the upper span (see figure 2-4a). The second zone is for $1\text{-}\ell_c/L < \mu \le 1$ when the upper roller guides of the counterweight are in the upper span and the lower ones in the lower span (See figure 2-4b). Note that in typical installations the length of the counterweight ℓ_c is close to the rail span L; in this example $1\text{-}\ell_c/L=0.0417$. Therefore, most of the graphs correspond to the second case. In figure 2-8 we show the variation in the three frequencies as the counterweight traverses from the top to the bottom of the 10-story building. It is noted that the system frequencies change as the counterweight moves, but within a rather narrow range. Similar observation can be made for the in-plane model. This has some implication in the development of a single frequency-based simplified procedure for seismic evaluation of elevator system.

2.6.1 Seismic Response

Several recorded ground motions listed in Table 2-5 have been used as inputs to the building to define the seismic input to the rail-counterweight system. To compare the numerical results due to different earthquakes, the maximum acceleration of the major component of each earthquake was normalized to a value of 0.1 g. Although the numerical results were obtained for several system characteristics and response quantities, here only some representative results of the stresses in the guide rails and brackets and some response quantities are presented.

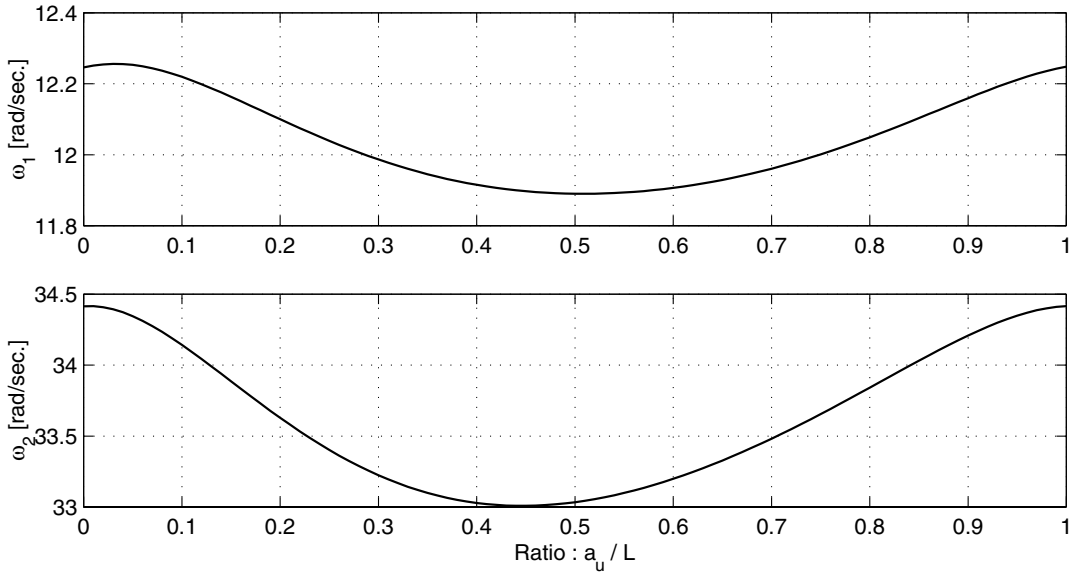

(a) In-plane motion

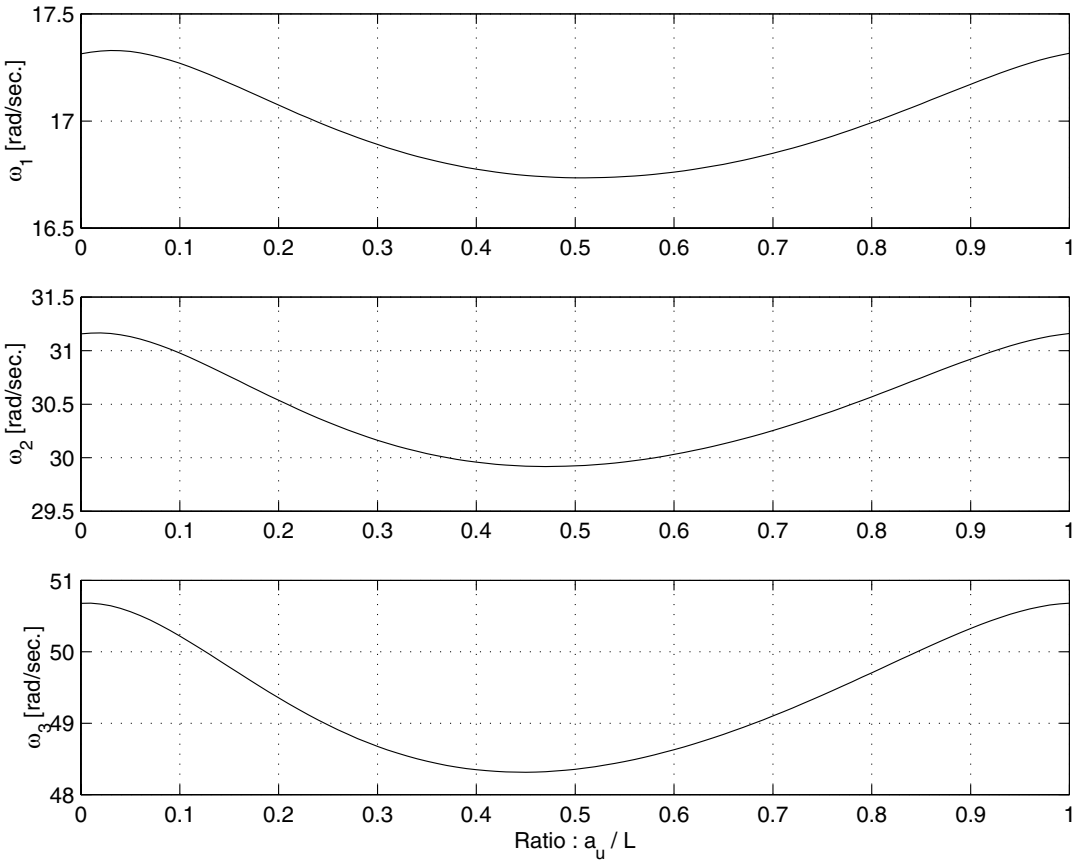

(b) Out-of-plane motion

FIGURE 2-7 Natural Frequencies of the System for the Counterweight in the Top Story of the 10-Story Building for 18.5-lb. Rail

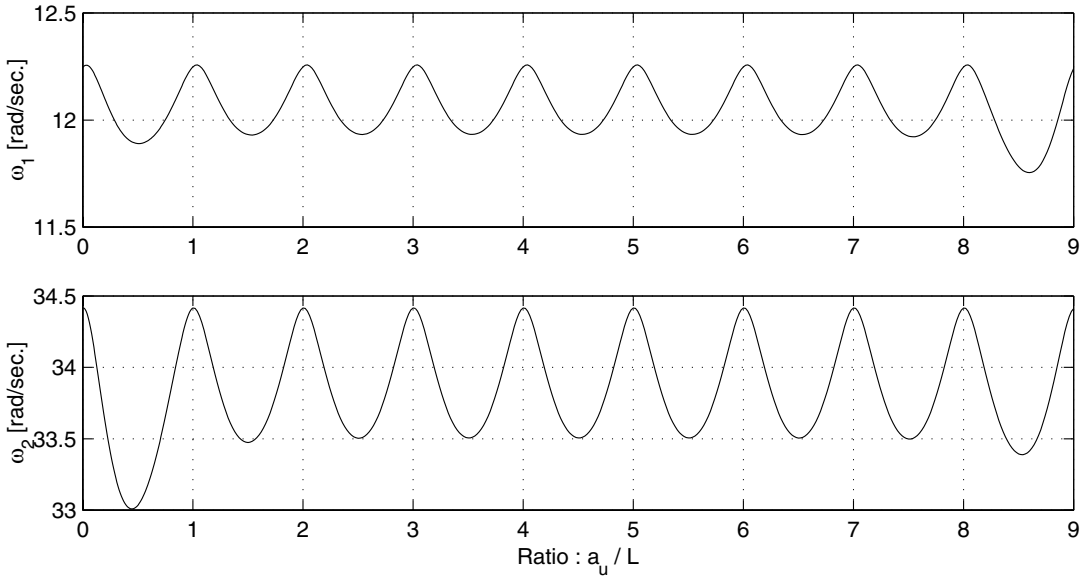

(a) In-plane motion

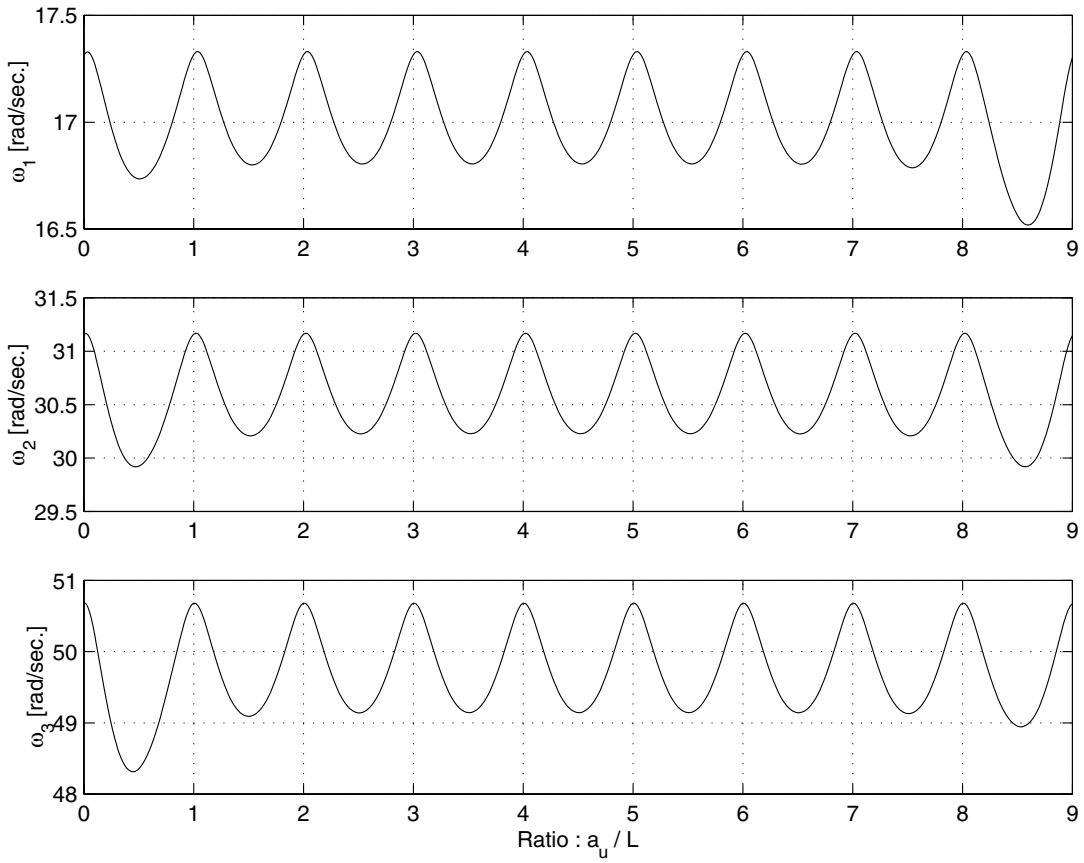

(b) Out-of-plane motion

FIGURE 2-8 Natural Frequencies of the System for Different Counterweight Positions Along the 10-Story Building for 18.5-lb. Rail

Building Motion Characteristics

In figure 2-9b we shows the absolute acceleration at the tenth floor $V_n(t)$ of the 10-story torsional building due to one of the horizontal components of the Northridge earthquake recorded in the parking lot of the Sylmar County hospital (shown in Figure 2-9a). This floor acceleration, as well as the acceleration of the lower floor $V_{n-1}(t)$ and the angular accelerations $\Theta_n(t)$ and $\Theta_{n-1}(t)$ were used in Eqs. (2-18)-(2-20) to calculate the input acceleration y_c, y_{dif} and y'_{dif} to the equations of motion in the out-of-plane model. The time histories of these inputs are shown in figure 2-10. From these figures, it is noted that, for this particular building and earthquake, the input accelerations y_{dif} and y'_{dif} in the equations of motion are negligible compared to y_c. Similar observations can be made from the response results obtained for other earthquake records as well as for the in-plane motion. This has some implication for the development of a simplified procedure.

TABLE 2-5 Seismic Inputs Used in the Study

Event	Date	Location	Max. Ground Acceleration* [g]	
			x-direction	y-direction
El Centro	05/18/1940	Imperial Valley Irrigation District	0.348	0.214
Parkfield	06/27/1966	Cholame, Shandon, CA	0.434	0.355
San Fernando	02/09/1971	Pacoima Dam	1.170	1.075
Whittier	10/01/1987	Tarzana - Cedar Hill Nursery	0.537	0.405
Loma Prieta	10/17/1989	Corralitos - Eureka Canyon Rd.	0.630	0.478
Northridge	01/17/1994	Sylmar - County Hospital Parking Lot	0.843	0.604

* For numerical results, inputs normalized to 0.1g are used.

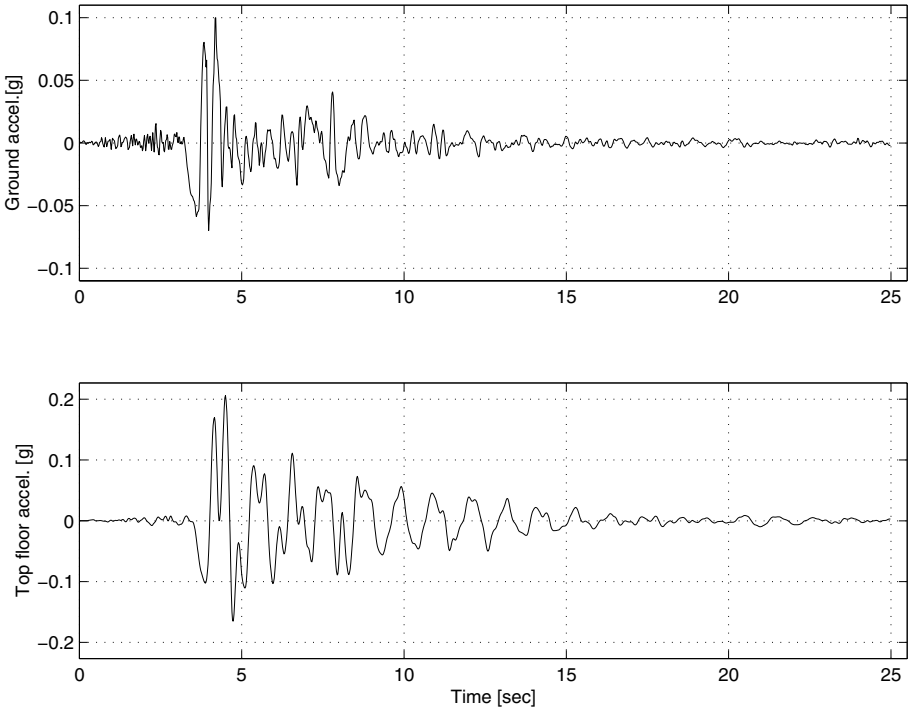

FIGURE 2-9 Acceleration Time Histories for Northridge Earthquake: a) Ground Acceleration, b) Absolute Acceleration of the Top Floor of the 10-Story Building

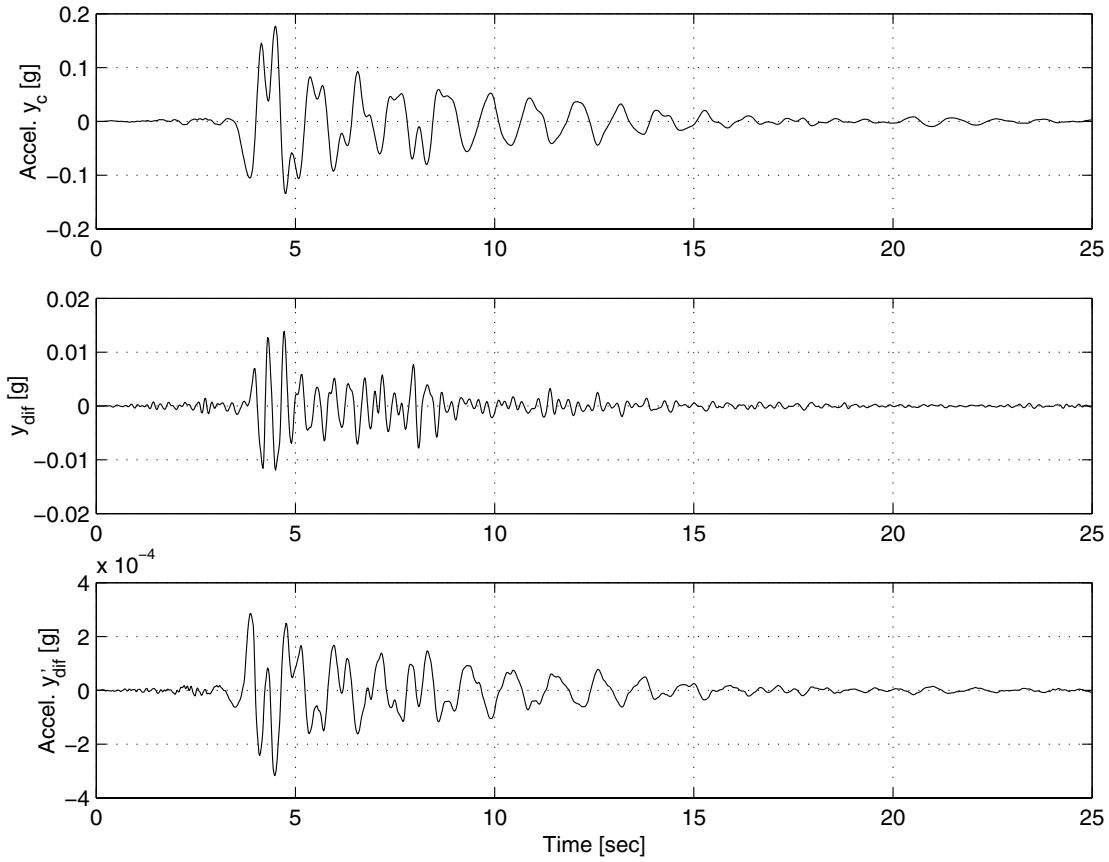

FIGURE 2-10 Seismic Input Components for Eqs. (2-11) and (2-12), for the Counterweight Located in the Middle of the Top Story of the 10-Story Building, Northridge Earthquake

Stress and Deformation Responses

Next we present some results showing the maximum stresses in the rails and brackets, and deformation in the helical springs. The stresses have been calculated at the three points shown in figures 2-11. The results in figure 2-12 through 2-23 are for the 10-story building, and those in figures 2-24 through 2-27 are for the 24-story building. Since the 10-story building has some torsional response, its effect on the stresses and deformation of the rail-counterweight components is included. For different positions of counterweight, figure 2-12 shows the maximum flexural stresses in the flange of the rail (point A, figure 2-11) for the three input scenarios: (1) x-excitation only, (2) y-excitation only, and (3) both x and y excitations, all of the Northridge earthquake. When the ratio a_u/L is zero, the top of the counterweight frame is at the top support, and when the ratio is 1, it is at the next lower support. A point on each of the three curves represents the largest of the five bending stress values: three values calculated near the three consecutive bracket supports and two calculated at the roller guide positions. Note that the maximum values for each input scenario need not occur at the same location. For each input excitation case, the calculated stress includes the contribution of both the in-plane and the out-of-plane motions. Since the stress in the rail flange (point A in figure 2-11) is affected by both input components, it is necessary to consider both earthquake components to calculate this response

quantity. The maximum stress in the web (point B, figure 2-11), on the other hand, is usually not much affected by the seismic component in the out-of-plane direction, as is shown in Figure 2-13. The relative contribution of the out-of-plane input to the in-plane response effects depends upon the coupling effect introduced by the torsional response of the building structure. If a building has strong torsional response tendencies due to a large eccentricity between the mass and stiffness centers, then the input in the out-of-plane direction may also introduce significant effects in the in-plane direction, and vice versa. It is noted that the maximum stresses in the flange and the web occur when the top roller is at about the middle of the story.

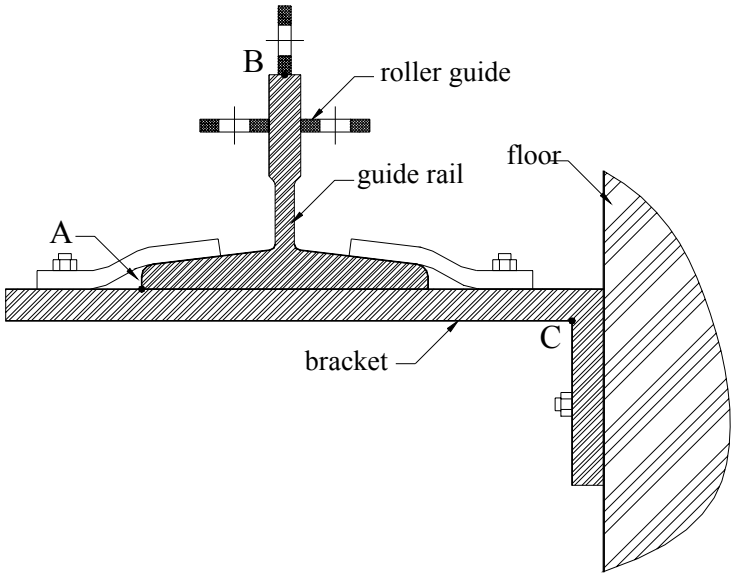

FIGURE 2-11 Points of Interest for Evaluation of Stresses in the Rail and Bracket

Figure 2-14 shows the maximum stress in the bracket (point C, Figure 2-11), again for the three input scenarios and for different positions of the counterweight. The seismic input in this case is again the Northridge earthquake, with the stronger component applied along the y-direction (out-of-plane) and the weaker component along the x-direction. The maximum stress shown in this figure is the largest of the stresses in the three consecutive brackets. In this particular case, the effect of the stronger component in the out-of-plane direction on the stress primarily caused by the in-plane vibration is quite significant. The point is that it is important to consider both horizontal components of an earthquake induced ground motion in the response analysis of a counterweight rail-system. It is especially necessary to do so when the building has a strong torsional response component.

It is also noted from Figures 2-12, 2-13 and 2-14 that the positions of the counterweight that would cause the maximum stress effects in the brackets and the rail need not be the same. Also, the maximum stresses in the rail and the bracket usually occur due to the in-plane component of the input motion, although in some other rail sizes the out-of-plane stress in the flange could also be larger than the in-plane stress in the web.

The results in Figures 2-15 through 2-17 show the effect of using different rail sizes on maximum stresses in the rails and the brackets as the upper rollers move down from the top to

the bottom of the 10th story. The rail sizes of 8-lb, 18.5-lb, and 30-lb have been used but the bracket size is kept the same. Figure 2-15 shows the stress in the flange, figure 2-16 in the web, and figure 2-17 in the brackets. As one would expect, the larger size rails help reduce the stresses but they also induce larger forces in the brackets to cause larger stresses in them.

Figures 2-18 through 2-21 show the maximum stresses in the rail and the brackets as the upper rollers of the counterweight traverses the entire height of the 10-story building. Figure 2-18 shows the maximum stress in the bracket, rail web and rail flange, whereas the figures 2-19, 2-20 and 2-21 show these three maximum stresses separately but for three different rail sizes. The effect of the rail size is the same as mentioned above. However, it is noted that these stresses need not increase monotonically with height in the building. Although the maximum stresses for this building occur when the counterweight is near the top, but this need not be the case always. We will see later from the results for the 24-story building that maximum stresses can occur at the lower levels as well. The figures also show the variation of the maximum accelerations of various floors. The maximum stresses in the rails and the bracket seem to follow the same trend as the maximum floor acceleration, but they are not directly proportional as the acceleration is usually highest in the top story but the stresses in the rails could be higher in the lower stories. Thus, the variation of the maximum stress with height depends depend upon the dynamic characteristics of the building vis-à-vis that of the counterweight-rail system, and also on the frequency content of the input motions.

Roller Guide Deformations

Figure 2.22 shows the maximum deformation of the roller guide assembly for different positions of the upper rollers in the top story. The deformation of the rubber tire will have the same trend; in fact this deformation can be easily calculated from the deformation of the roller guide assembly by simply multiplying it by a factor of $k_s/(f_r k_r+k_s)$, which in our case is equal to 0..... The factor f_r here is the square of the ratio of the distances of the roller and the spring from the pivot. These deformations are of interest to check if the restraining plate will contact the rail, or the rubber tire or helical springs are getting close to their saturation. When the gaps close, the stiffness characteristics of the springs will change drastically, introducing the nonlinearity in the system. It is noted that for the excitation intensity and example considered here, the in-plane deformation of the roller guide assembly is more than the gap between the restraining plate and the rail. Thus in this case the restraining plate will come in contact with the rails, and introduce nonlinearity in the system. This situation is considered in Section 3 where the nonlinear analysis is presented.

Effect of Roller Guide Stiffness

The total deformation of the roller guide assembly can be reduced by increasing the stiffness of the helical springs and the rubber tire stiffness, and also by increasing the distance of the of the helical spring from the pivot point in the assembly. Any changes in these parameters change the equivalent stiffness of the roller guide assembly. To examine the effect of changing the stiffness of the roller guide assembly on the stresses in the guide rails we present Figures 2-23. The figure shows the maximum stress in the webs of the 18.5-lb and 30-lb rails as a function of the roller guide stiffness ration parameter α. The stiffness coefficient k_{rs} corresponding to $\alpha = 1$ is the

same as the one used for all previous numerical results (that is, k_{rs} = 0.167 x 10^6 N/m). Thus, a value of α = 2 for the stiffness ratio implies that the roller guide is twice as stiff as the roller guide considered for the previous numerical results (that is, k_{rs} = 2 x 0.167 x 10^6 N/m). The numerical results in Figure 2-23 are shown for a wide range of the roller guide stiffness ration values varying between α = 0.1 and α =5. The results corresponding to α = 0.1 are for a very soft spring, and for α = 5 are for a rather stiff spring. As mentioned before, this parameter can be changed by choosing different rubber and helical spring stiffness combinations, and the rocker arm design. However, changing the rubber tire stiffness also changes the riding quality and noise level due to the counterweight motion. These results are for the El Centro ground motion, normalized to the maximum acceleration of 0.1g, with its stronger component in the plane of the counterweight. It is noted that the stresses can be high for very soft roller guide assemblies. The stress level can be reduced by choosing a stiffer roller guide assembly. However, a stiffer roller guide assembly may be more noisy. Roller guides with more rollers but with softer rubber tires may therefore provide a better ride with relatively smaller stresses. No such trade off investigation has been performed in this study.

The next four figures are for the 24-story shear building. They are presented just to show the affect of changing the building characteristics. The stiffness properties of the building in the x- and y- directions are assumed to be the same. Since this building does not have any torsional response, there is no coupling in the in-plane and out-of-plane responses. The stress in the web is only affected by the x- component of the motion. This stress is shown in Figure 2-24 as the counterweight travels along the building height. The stress at the flange tip is affected by the both components. Figure 2-25 shows this stress again for different positions of the counterweight along the building height. It is interesting to note that the response has no monotonic trend; several lower stories can also have high stresses. In fact, in this particular case the maximum stress did not occur in the top story but in one of the lower stories. The figures also show the maximum floor acceleration due to the ground motions. In Figure 2-24, only the maximum floor acceleration in the x-direction is shown, as this component only affects the web stress. In Figure 2-25 the maximum acceleration in both directions are shown as the flange stress is affected by both components. Figure 2-26 shows the maximum stress in the brackets, and Figure 2-27 shows the maximum deformation of the equivalent roller guide spring. Comparison of the maximum stresses with the maximum floor acceleration indicates that the lower stories with lower levels of floor accelerations than the top story can have high stresses. The roller guide deformations also do not increase monotonically; they can be high at lower levels of the buildings. That is, the maximum stresses or deformations in the elevator components may not be directly proportional to the floor acceleration; rather it is the dynamics of the rail-counterweight system that affects the response. Therefore, it is necessary to include the dynamics of the rail-counterweight system with that of the building for accurate seismic evaluation of an elevator components.

The previous set of results were obtained primarily for the Northridge earthquake. Similar results were also obtained for other recorded ground motions, and showed similar characteristics. In table 2-6, we collectively show the results for the maximum stresses in different size guide rail sizes obtained for the motions of several recorded earthquake events. Both the stresses in the web and the flanges are shown. Similarly, results for the maximum stresses in the brackets and the maximum deformations in the roller guide assemblies are shown in tables 2-7 and 2-8. The earthquake components were normalized such that the stronger component components had the maximum level of 0.1g. The stronger component was also aligned to be in the plane of the

counterweight. Although different rail sizes are used, the physical properties of the counterweight and brackets were kept the same in all cases. The last columns of the tables also give the average of the values for different rails considering different earthquakes. It is interesting to note that some earthquakes cause higher stresses in the flange and others in the web. Also, for a given earthquake the higher stress may occur in the web for some rail sizes and in the flange for other sizes. This emphasizes the need for considering different earthquakes with different frequency characteristics for evaluating the seismic performance of an elevator system. For the same counterweight size, the larger rails will experience lower bending stresses, and somewhat higher bracket stresses (except for the El Centro earthquake the reverse seems to be true.) On the whole the bracket stresses are not very sensitive to the changes in the rails sizes. The deformation response of the roller guide assembly shows, that in this example, the restraining plates will contact the rails if they were provided. To include the effect of this contact in the elevator response, the nonlinear analysis of Section 3 will be necessary.

TABLE 2-6 Maximum Stress in the Rail for Different Inputs and Rail Sizes

Rail Size	Northridge		El Centro		Loma Prieta		Parkfield		San Fernando		Whittier		Average	
	Flange	Web	Flange	Web	Flange	Web	Flange	Web	Flange	Web	Flange	Web	Flange	Web
8-lb	122.54	195.46	181.39	237.40	149.68	191.70	136.53	79.07	187.76	112.33	89.05	53.26	144.49	144.87
11-lb	70.41	89.20	90.05	118.92	68.05	85.25	88.01	53.26	124.41	50.04	60.99	26.40	83.65	70.51
12-lb	60.48	86.39	74.87	115.63	57.47	83.18	66.91	52.67	88.15	48.24	47.93	26.00	65.97	68.68
15-lb	44.74	84.85	55.52	113.93	43.74	82.32	39.43	53.25	43.49	46.87	30.03	26.10	42.83	67.89
18.5-lb	35.26	57.55	37.54	65.61	31.38	51.63	33.03	38.82	33.80	31.93	26.29	18.05	32.88	43.93
22.5-lb	33.15	46.51	33.96	51.59	28.31	40.24	30.80	31.39	29.33	26.45	23.33	14.60	29.81	35.13
30-lb	23.42	30.34	22.40	29.97	20.24	23.16	24.08	20.40	21.10	18.86	19.16	9.50	21.73	22.04

TABLE 2-7 Maximum Stress in the Bracket for Different Inputs and Rail Sizes

Rail Size	Northridge	El Centro	Loma Prieta	Parkfield	San Fernando	Whittier	Average
8-lb	142.12	137.11	107.08	105.43	90.32	60.61	107.11
11-lb	145.27	131.73	102.84	113.18	98.16	72.52	110.62
12-lb	144.87	135.47	105.37	112.09	93.82	71.11	110.46
15-lb	144.69	136.48	104.91	111.10	90.78	69.86	109.64
18.5-lb	146.86	127.66	101.59	117.12	94.18	78.58	111.00
22.5-lb	146.11	126.98	101.30	114.90	92.20	75.53	109.50
30-lb	148.09	125.77	101.38	121.42	94.74	85.07	112.74

TABLE 2-8 Maximum Displacement of Helical Spring for Different Inputs and Rail Sizes

Rail Size	Northridge		El Centro		Loma Prieta		Parkfield		San Fernando		Whittier		Average	
	Out-of-plane	In-plane	Out-of-plane	In-plane	Out-of-plane	In-plane	Out-of-plane	In-plane	Out-of-plane	In-plane	Out-of-plane	In-plane	Out-of-plane	In-plane
8-lb	11.94	37.70	17.91	34.91	12.02	27.43	16.51	24.91	25.85	22.70	17.44	12.33	16.94	26.67
11-lb	9.36	37.88	13.14	34.21	9.47	27.49	14.44	25.00	24.14	22.69	17.38	12.40	14.65	26.61
12-lb	8.59	37.88	11.47	34.13	9.26	27.49	13.29	25.01	20.12	22.69	17.45	12.40	13.36	26.60
15-lb	8.03	37.91	9.23	34.04	8.80	27.48	13.01	25.02	14.14	22.68	17.52	12.40	11.79	26.59
18.5-lb	7.93	37.98	8.23	33.24	8.55	27.51	13.07	25.06	12.36	22.67	17.40	12.44	11.25	26.48
22.5-lb	7.92	37.99	8.22	33.23	8.40	27.53	13.03	25.04	11.67	22.65	17.45	12.45	11.12	26.48
30-lb	7.97	38.02	8.24	33.21	8.30	27.51	13.12	25.08	11.50	22.67	17.28	12.47	11.07	26.49

Effect of Tie Brackets

As mentioned earlier, the intermediate tie brackets are often used with counterweight rails to reduce their seismic vulnerability. To examine the effect of the tie brackets, in Figures 2-28 and 2-29 we present the maximum stresses in the web of the rails, with and without an intermediate tie bracket. Figure 2-28 is for the counterweight rolling down in the top story of the 10-story building and Figure 2-29 for the counterweight rolling down between the 17th and 18th floors of the 24-story building. These particular building stories were chosen to present the results because the maximum stresses in the rails occur in these stories. The stress shown is the maximum of the stresses calculated at six critical locations on each rail. Each story of the building was installed with a tie bracket in the middle of the story. For the calculation of the axial stiffness of the tie brackets, the effective axial area of cross section was assumed to be 1.00 in^2. It is noted from Figures 2-28 and 2-29 that the use of one such intermediate tie bracket per span reduces the maximum bending stress in the rail by about 25% for these building. This is quite consistent with the code provisions. It is also shown that this stress reducing effect of the tie brackets is not very sensitive to assumed value of the effective area. The results shown for the effective areas of 0.1 and 0.01 in^2 in figure 11 indicate that even a nominal size tie bracket can provide an adequate axial restraint to reduce the stresses in the rails. Based on the allowable stress in the rails of 88% of the yield strength (380 MPa) in the code, this particular elevator in the 24-story building could be exposed to an acceleration level of 1.37 g of a Whittier type ground motion before the allowable stress in the rail is exceeded. However, at this level of earthquake, the linear model may not remain applicable because of the possible contacts of the restraining plates with the guide rails, as mentioned earlier. The stresses in the rails can be further reduced by using more than one intermediate tie bracket in a single span.

2.7 Concluding Remarks

A linear analytical model considering both the in-plane and out-of-plane motions is developed for calculating the seismic response of the counterweight-rail system. The supports at the corners of the counterweight with the rails are represented by equivalent springs. The method to calculate the coefficients of these equivalent springs is described. The equations of motion of the system are developed in an analytically convenient form. The differential support input motions to the counterweight are included in the formulation.

These linear models can be useful for studying the seismic response behavior of these systems. They can provide useful insight into the dynamic behavior of these systems that can further help in the development of simple procedures for analysis and design for seismic loads. They can also be helpful in the preliminary evaluations of the effectiveness of various protective schemes proposed for improving seismic performance of elevators systems.

To study and evaluate the dynamic behavior of counterweights under earthquake motions, several sets of numerical results are obtained for the stresses in the rails and brackets, and the deformation in roller guides. The results are obtained for different buildings, for different earthquake motions, and for different positions of the counterweight along the building height. It is noted that although a building may experience maximum acceleration at the top, the maximum stresses in the rails and brackets need not occur at the top; they may even occur some where in the lower stories. The location and magnitude of the maximum stresses will depend upon the dynamic characteristics of the building, rail-counterweight systems, and the earthquake input motion. The stresses are also affected by the size of the rails used, and the stiffness characteristics of the roller guide assembly. Softer roller guide assemblies may provide a smoother ride, but they usually cause higher stresses in the rails and brackets.

The numerical results are also obtained to evaluate the effectiveness of the tie brackets provided on the rails. It is observed that the use of the tie brackets can significantly reduce the maximum stresses in the rails. One can take advantage of them to either increase the bracket span, if possible, or to decrease the size of the rails as indicated in the codes. It is also observed that even a nominal size tie bracket can be quite effective in providing the restraints and a desired reduction in the stresses in the rails.

It is quite possible that the deformations of one of more roller guide assemblies at the corners of the counterweight may be more than the clearance provided between the restraining plates and the guide rails, and thus causing a contact to occur between them. This contact will occur intermittently as the system vibrates. This contact will introduce a sudden change of stiffness in the system. To evaluate such a system, with a sudden change in the stiffness, a nonlinear analysis is required. This nonlinearity can be quite important in affecting the system response. The dynamic behavior of such nonlinear counterweight systems is examined in Section 3.

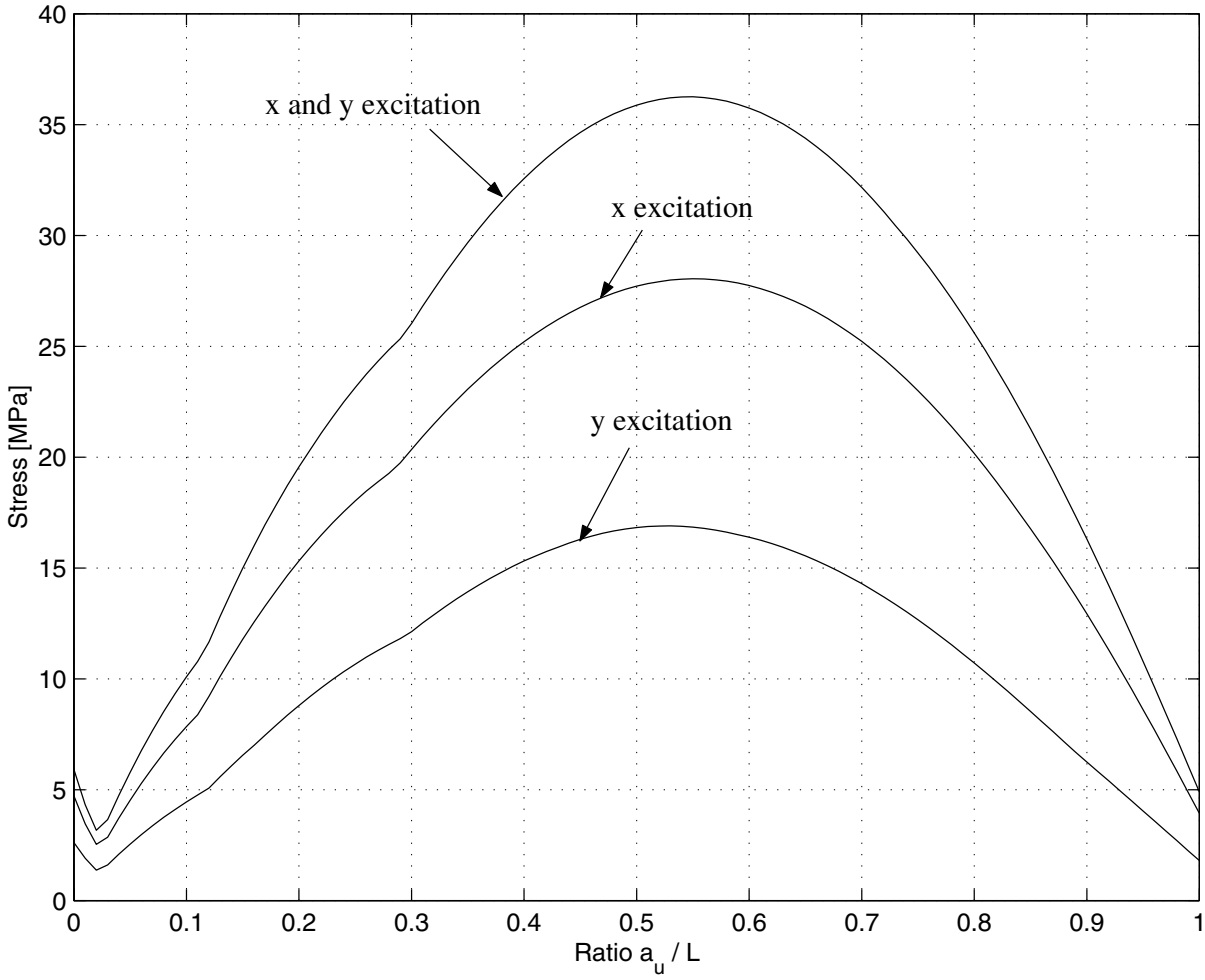

FIGURE 2-12 Maximum Stress in the Rail's Flange for the Counterweight in the Top Story of 10-Story Building for Northridge Earthquake

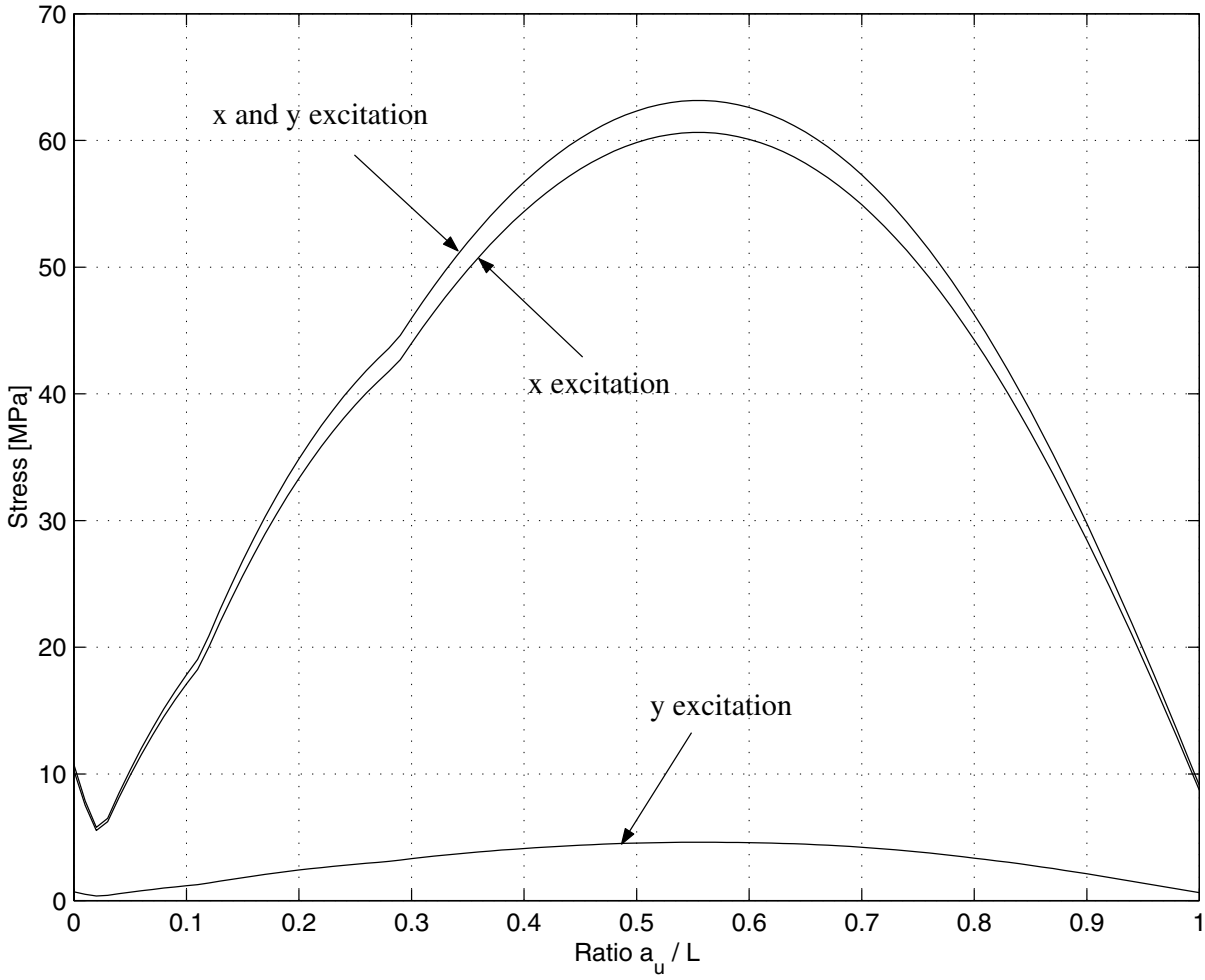

FIGURE 2-13 Maximum Stress in the Rail's Web for the Counterweight in the Top Story of 10-Story Building for Northridge Earthquake

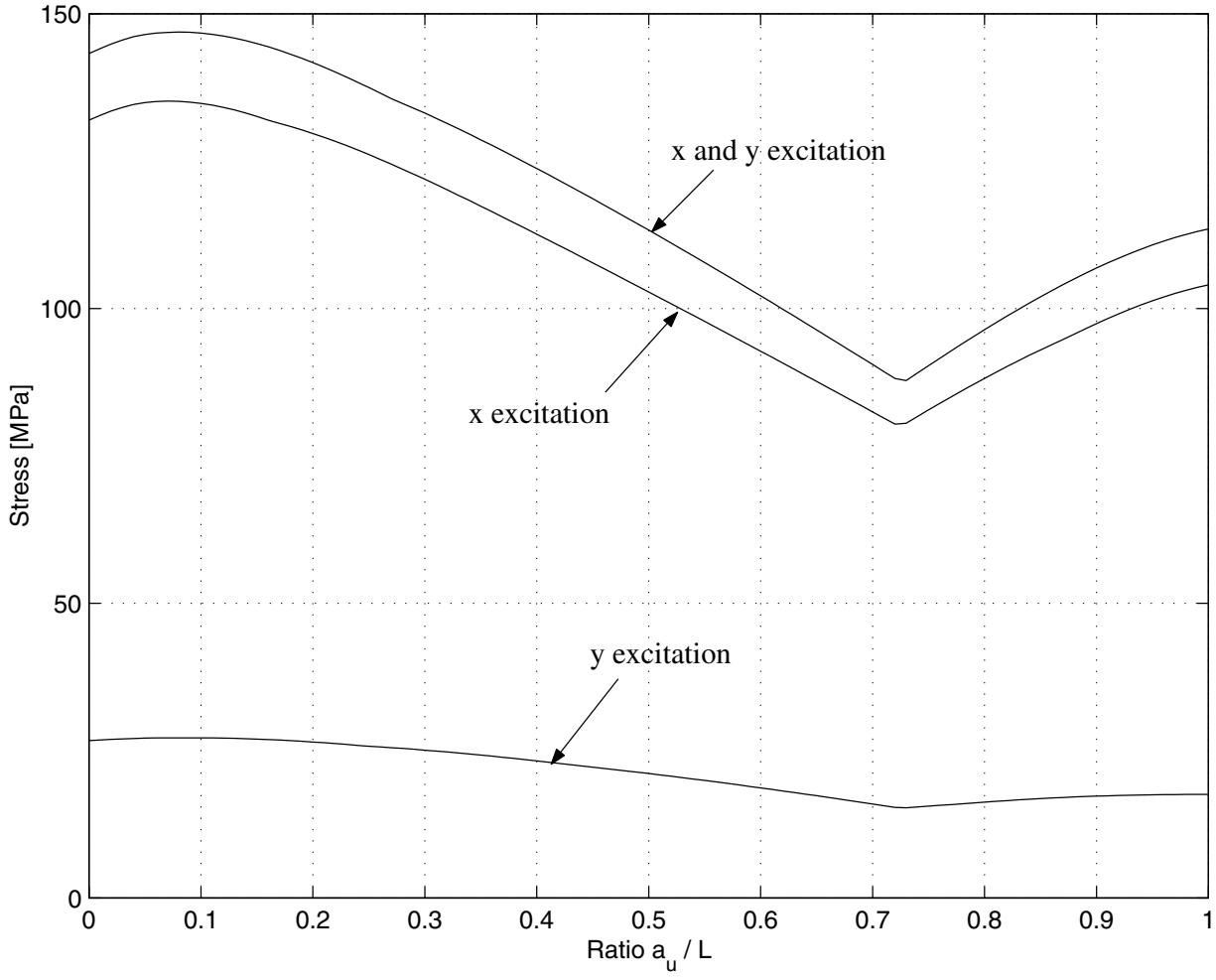

FIGURE 2-14 Maximum Stress in the Brackets for the Counterweight in the Top Story of 10-Story Building for Northridge Earthquake

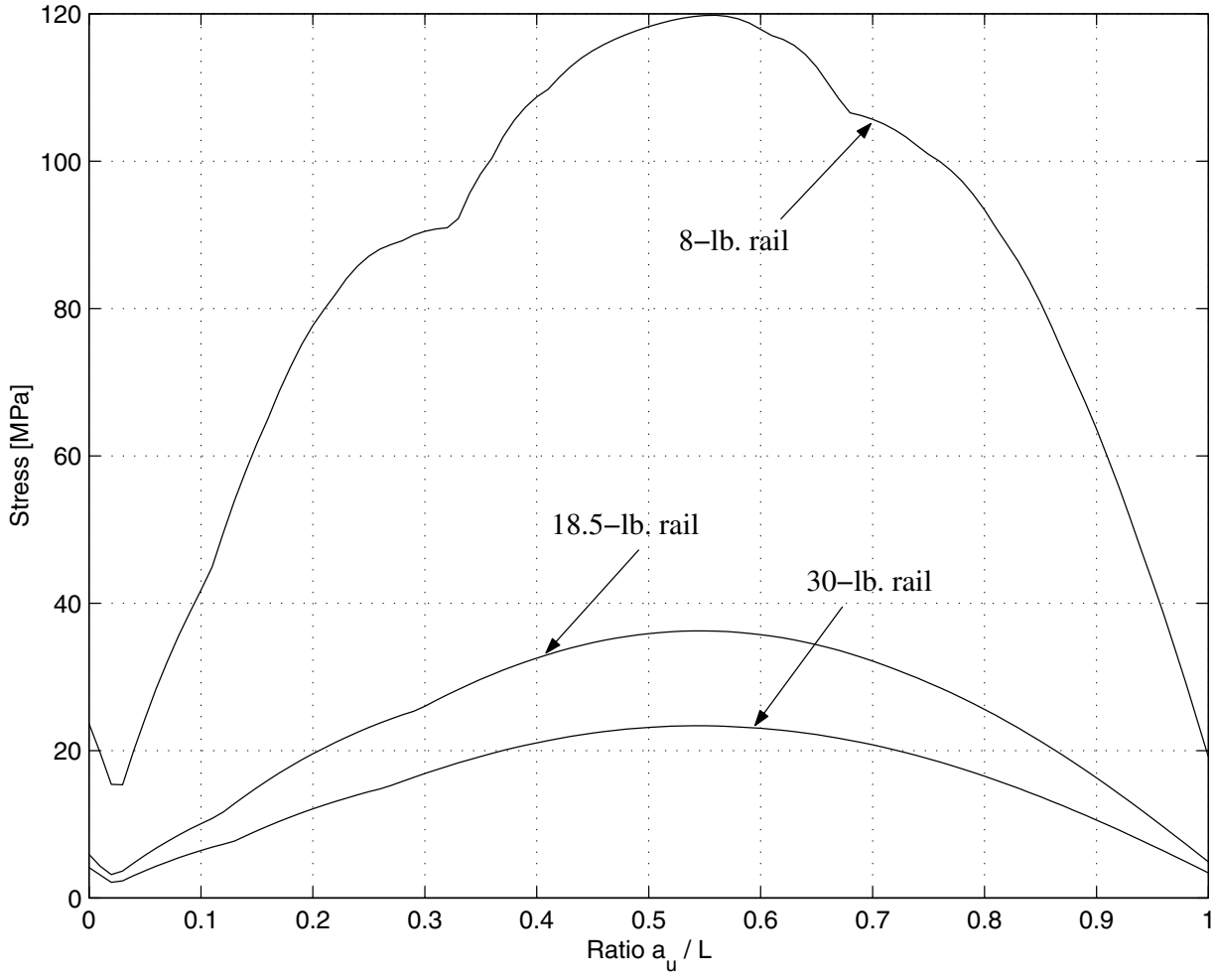

FIGURE 2-15 Maximum Stress in the Rail's Flange for Different Counterweight Positions Along the 10-Story Building for Northridge Earthquake

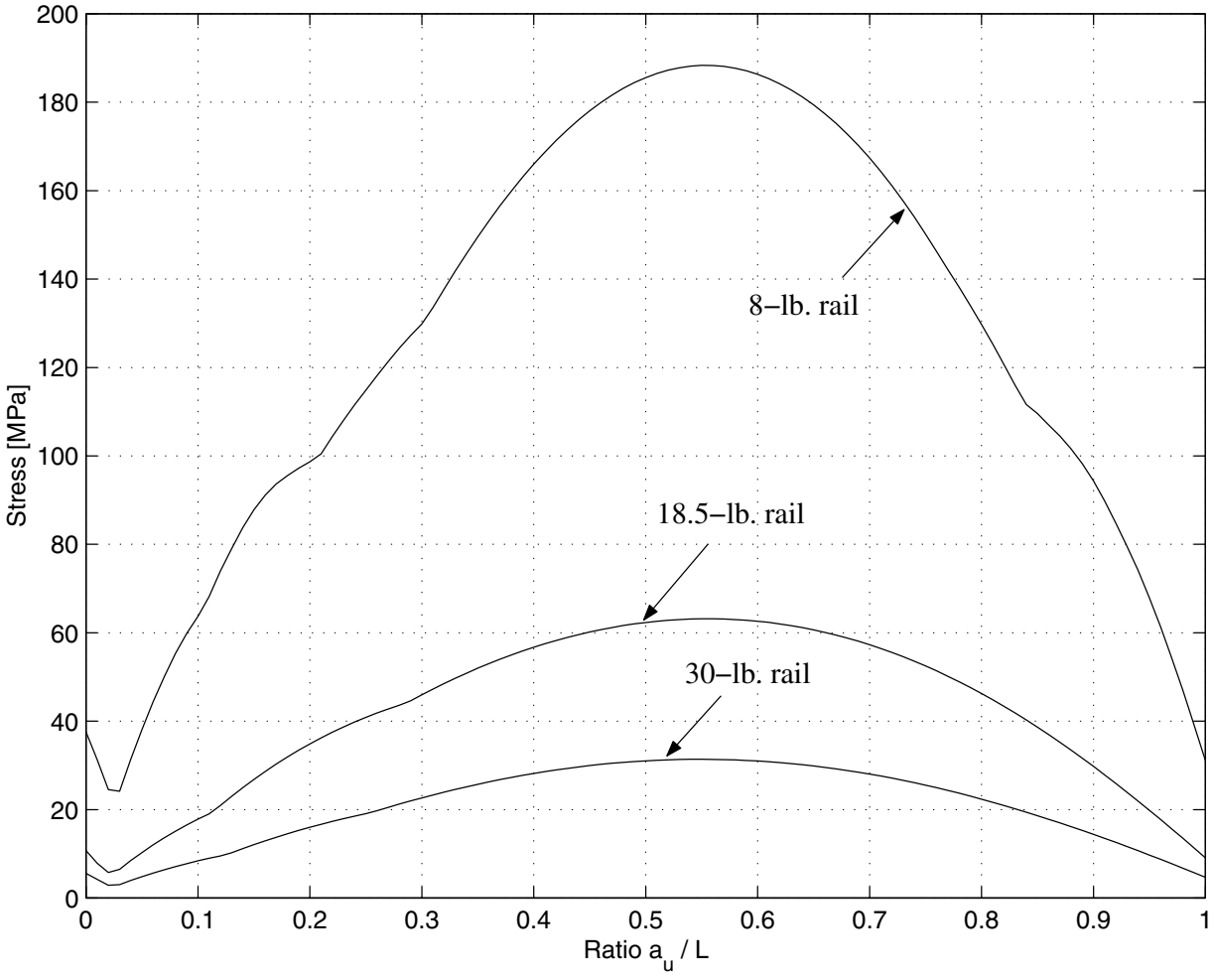

FIGURE 2-16 Maximum Stress in the Rail's Web for Different Counterweight Positions Along the 10-Story Building for Northridge Earthquake

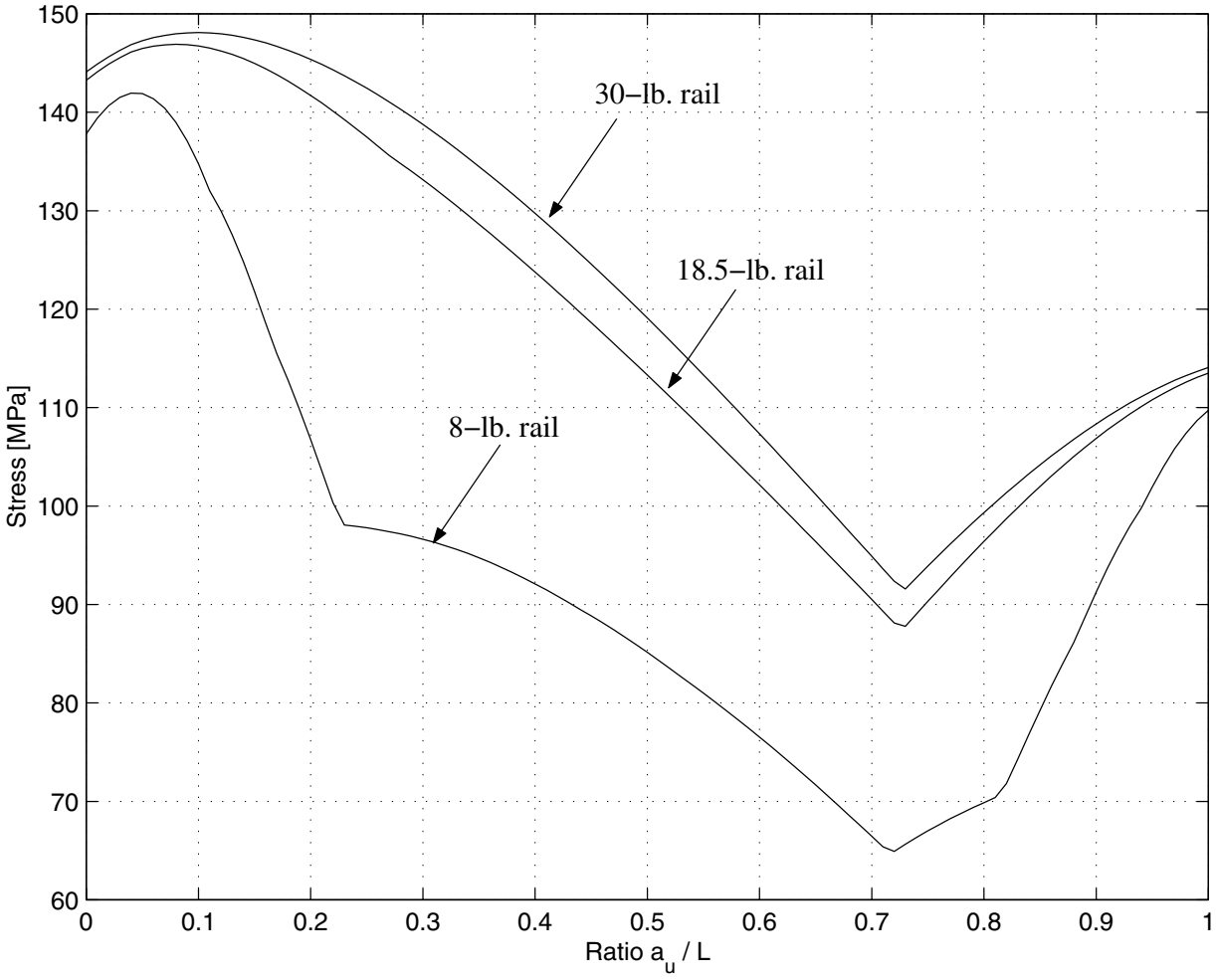

FIGURE 2-17 Maximum Stress in the Brackets for Different Counterweight Positions Along the 10-Story Building for Northridge Earthquake

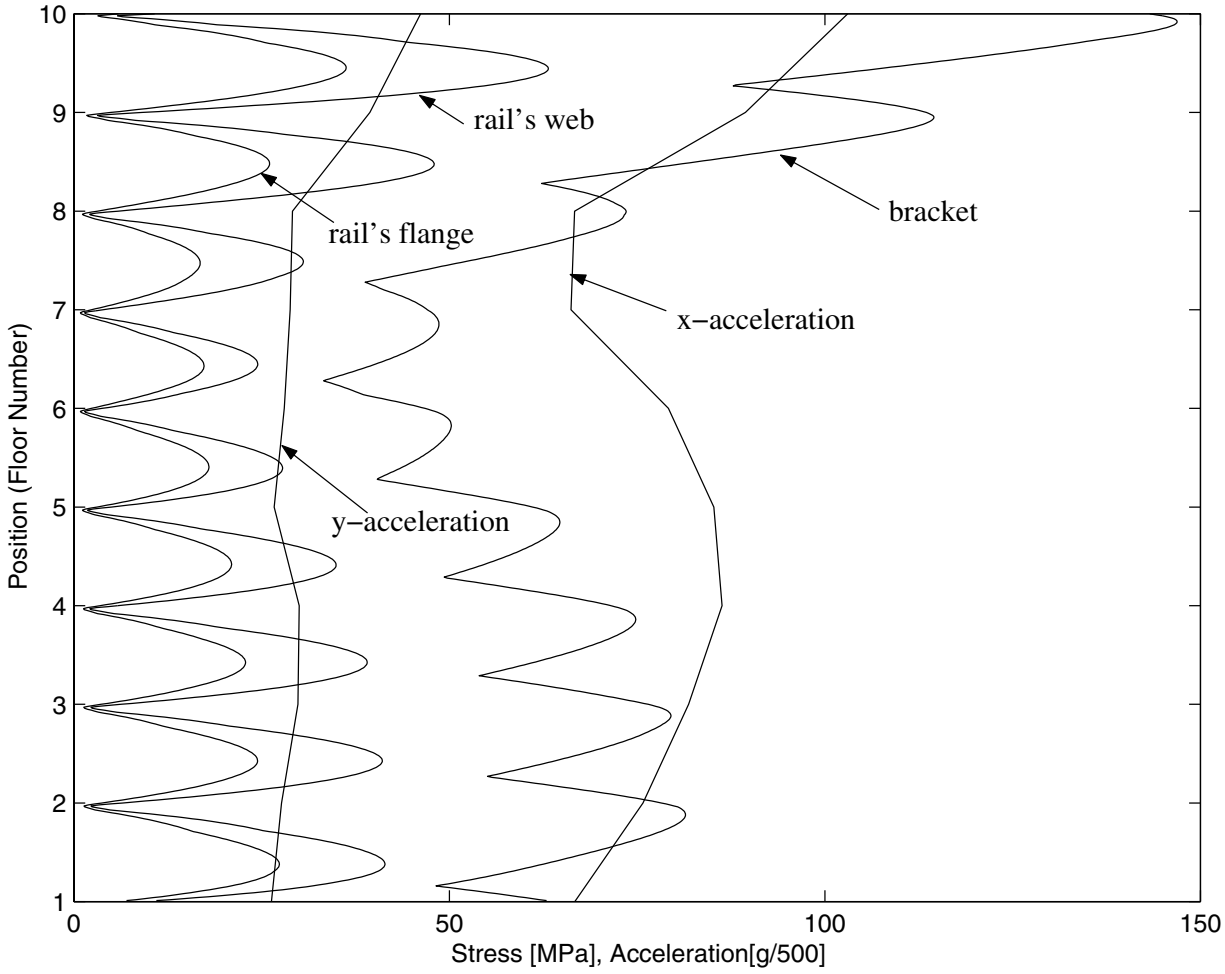

FIGURE 2-18 Maximum Stress in the Rail and Bracket for Different Counterweight Positions Along the 10-Story Building for Northridge Earthquake, Compared to Maximum Floor Accelerations

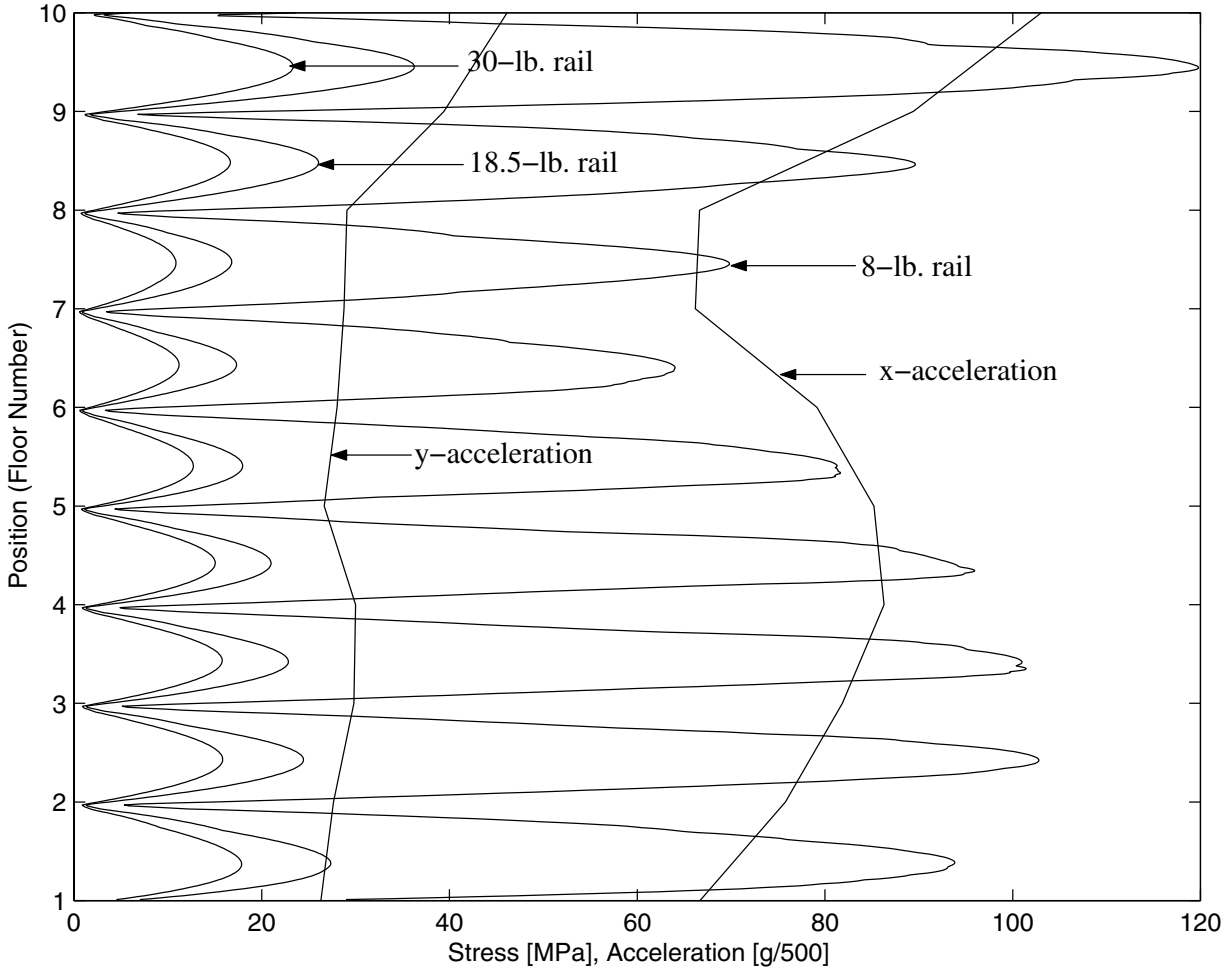

FIGURE 2-19 Maximum Stress in the Rail's Flange for Different Counterweight Positions Along the 10-Story Building for Northridge Earthquake, Compared to Maximum Floor Accelerations

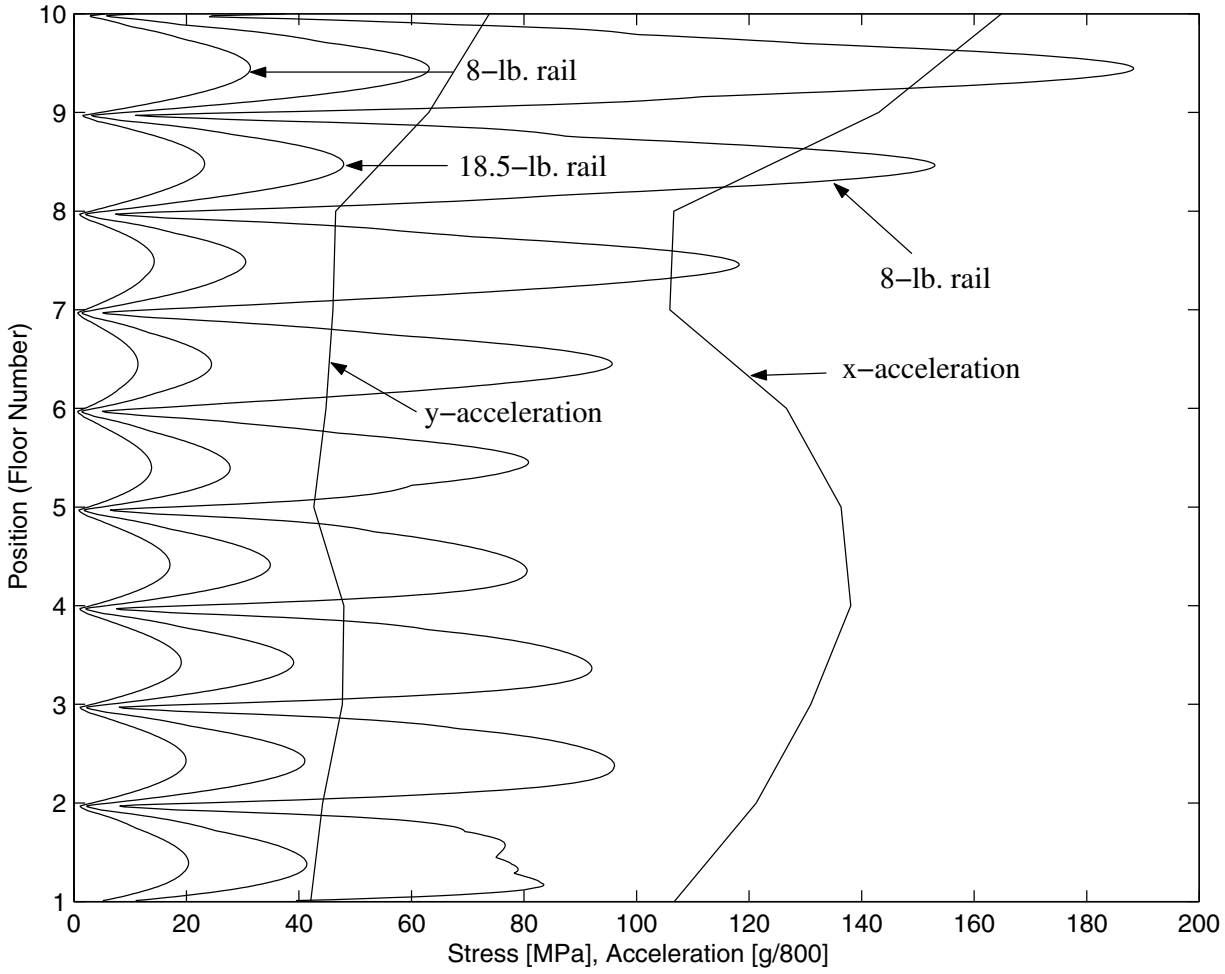

FIGURE 2-20 Maximum Stress in the Rail's Web for Different Counterweight Positions Along the 10-Story Building for Northridge Earthquake, Compared to Maximum Floor Accelerations

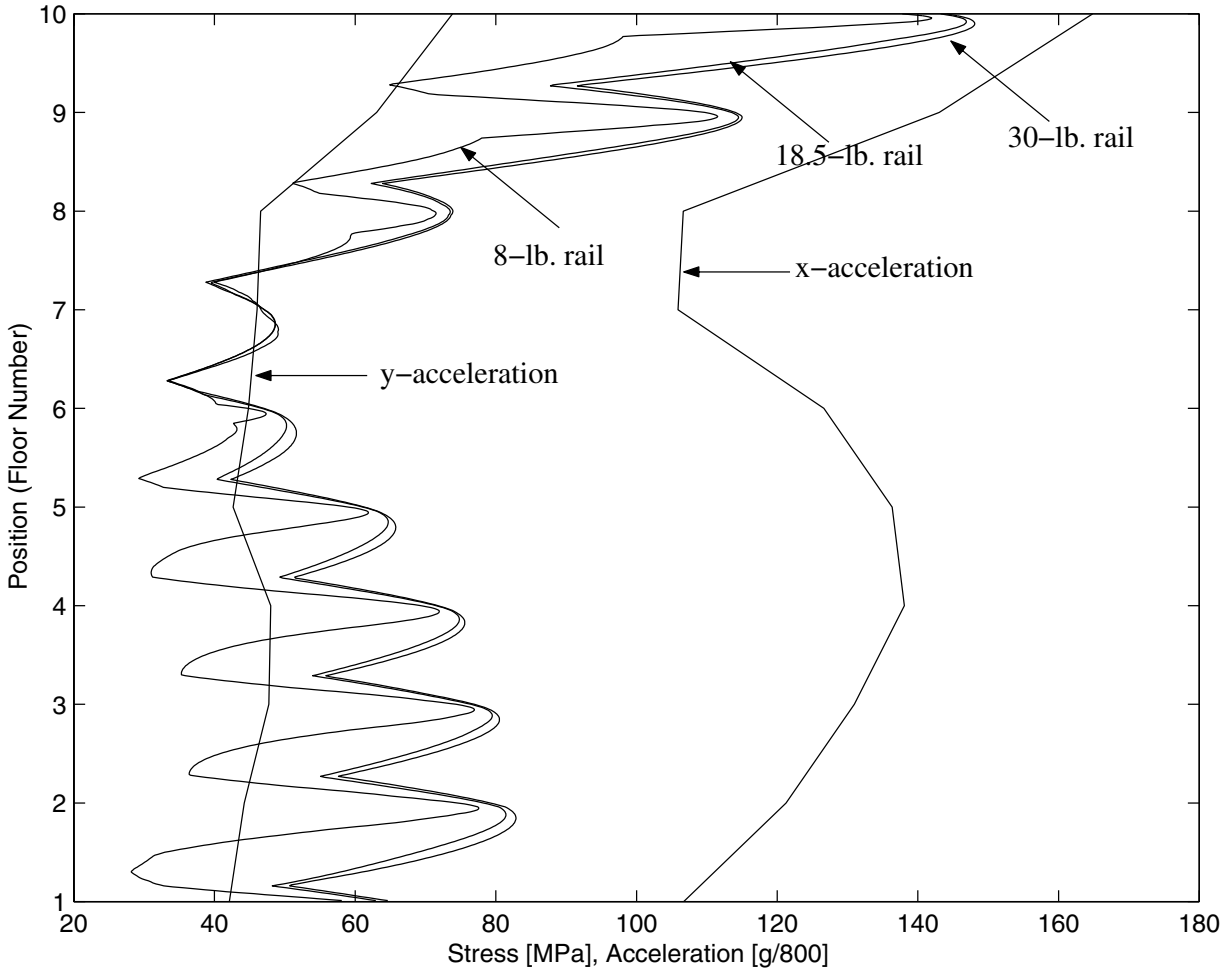

FIGURE 2-21 Maximum Stress in the Bracket for Different Counterweight Positions Along the 10-Story Building for Northridge Earthquake, Compared to Maximum Floor Accelerations

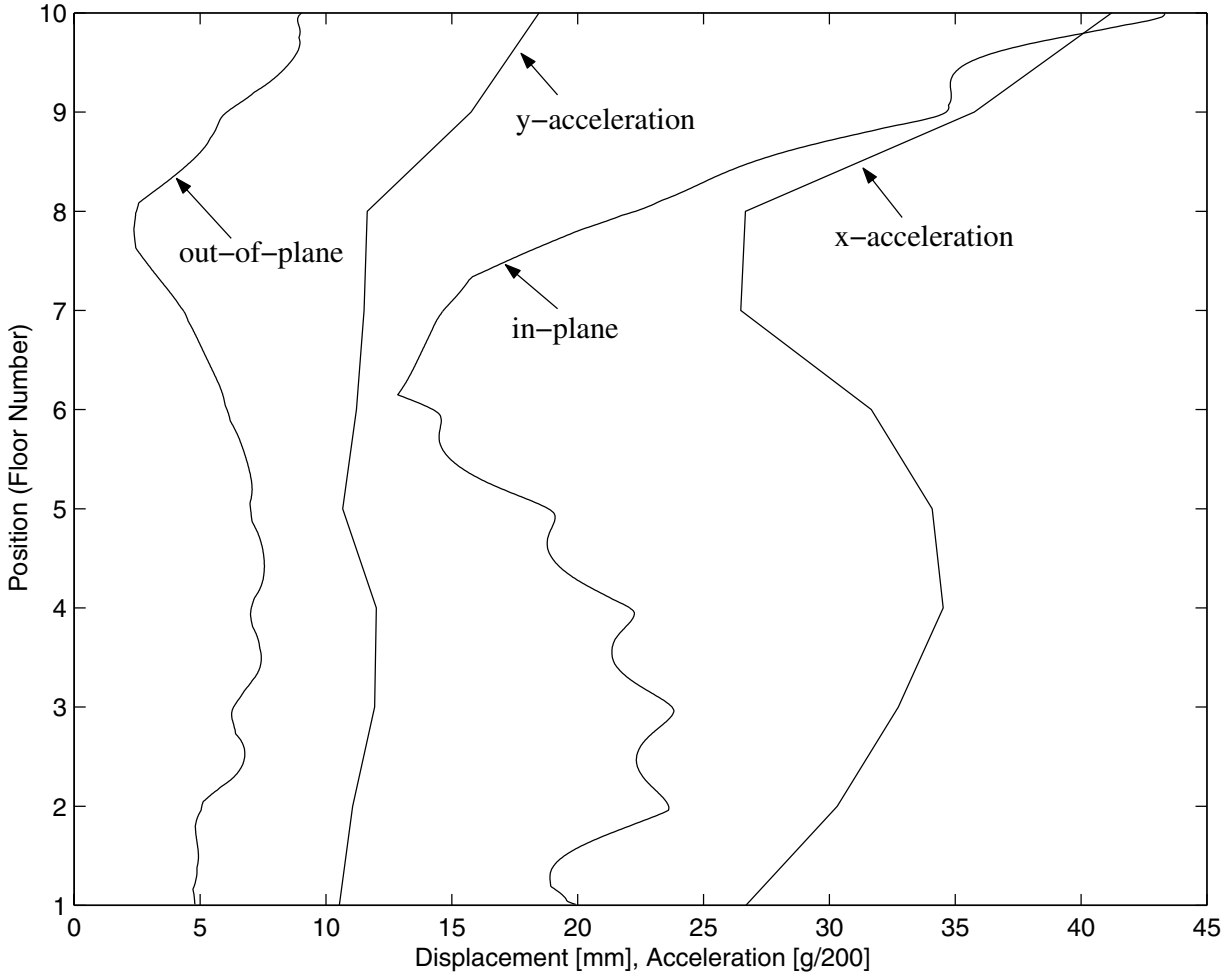

FIGURE 2-22 Maximum Deformation of Roller Guide Assembly for Different Counterweight Positions Along the 10-Story Building for Northridge Earthquake, Compared to Maximum Floor Acceleration

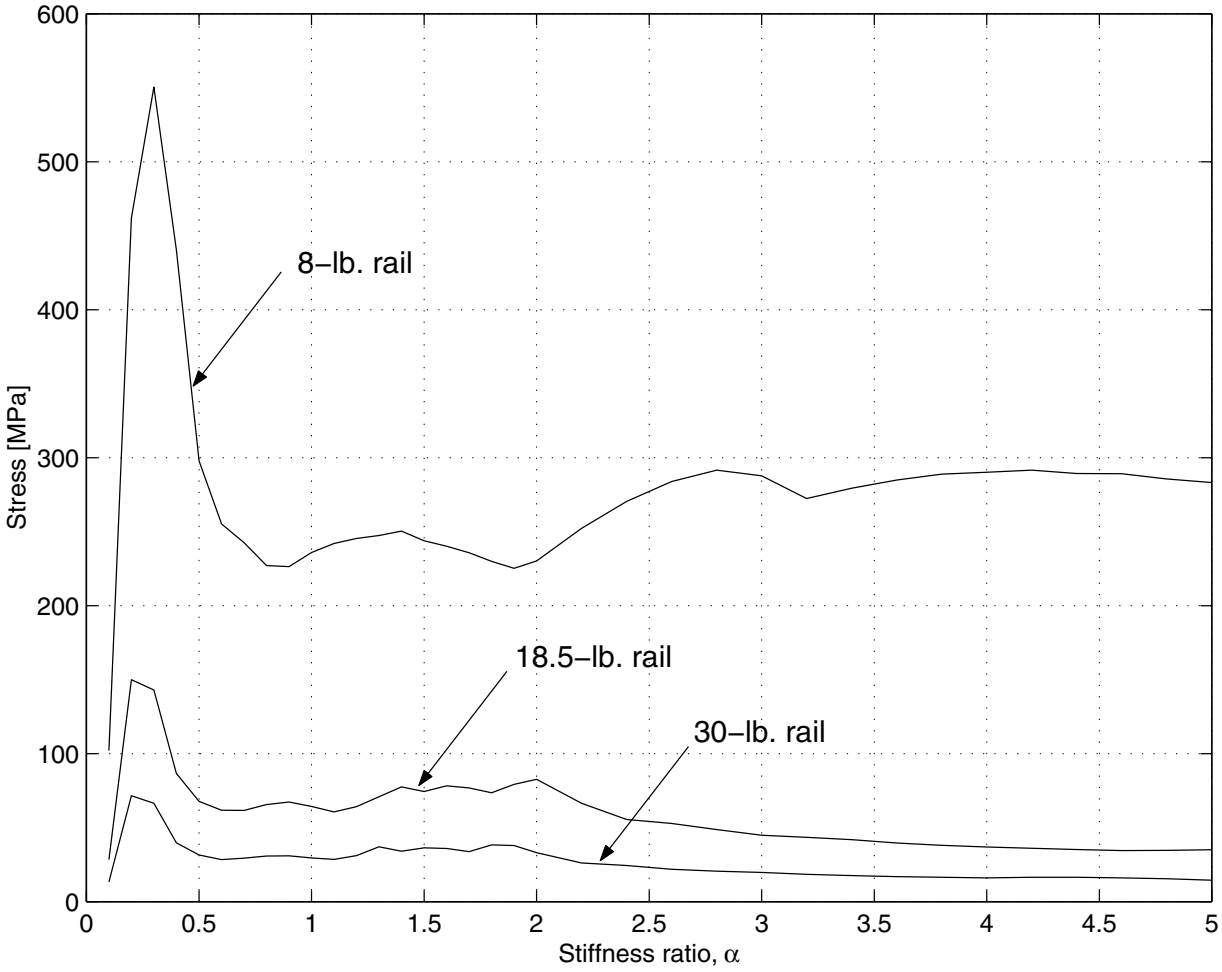

FIGURE 2-23 Maximum Stress in the Rail's Web when the Counterweight is in the Top Story of the 10-Story Building as a Function of Stiffness Ratio α for El Centro Earthquake

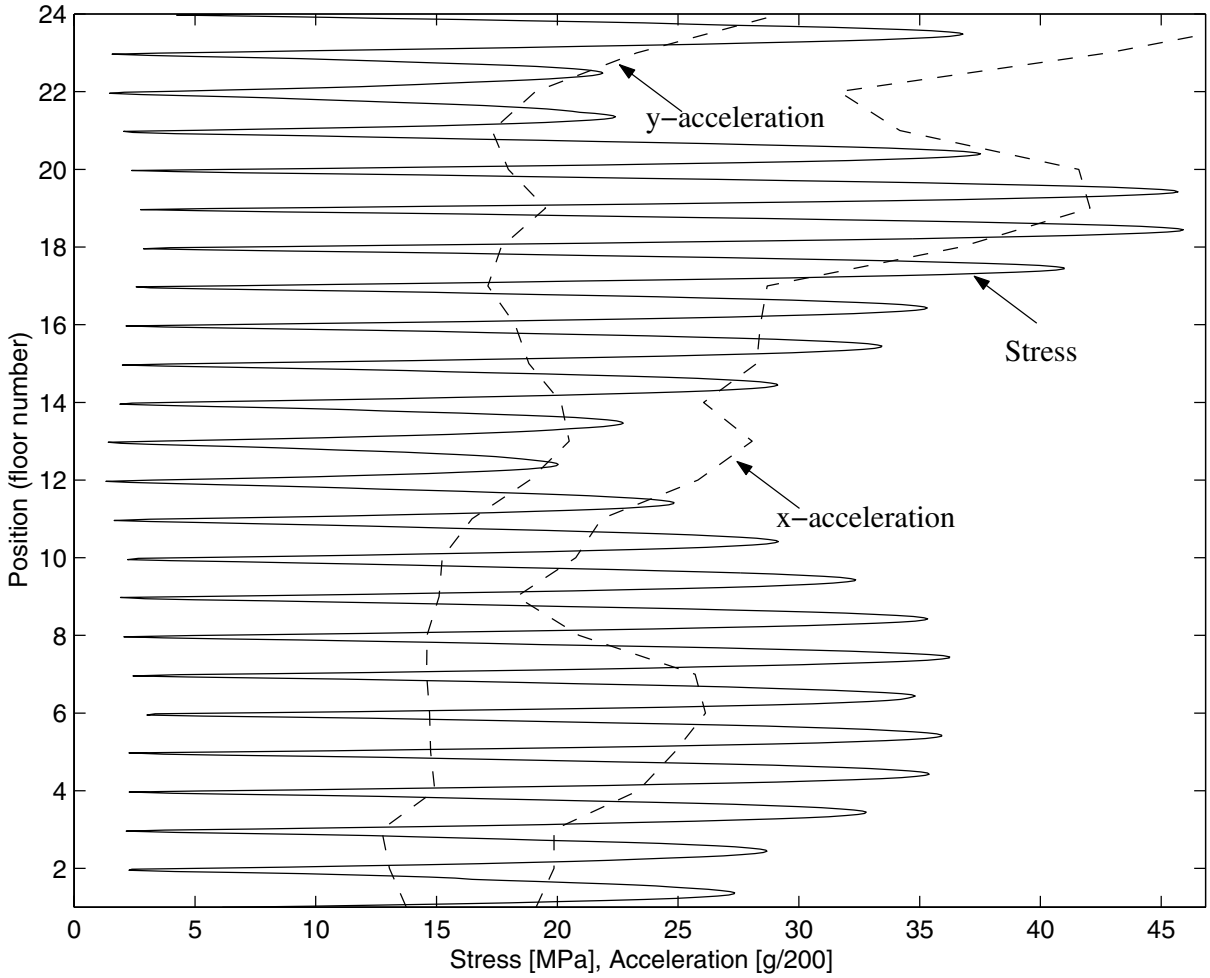

FIGURE 2-24 Maximum Stress in the Rail's Flange for Different Counterweight Positions Along the of the 24-Story Building for Northridge Earthquake, Compared to Maximum Floor Acceleration

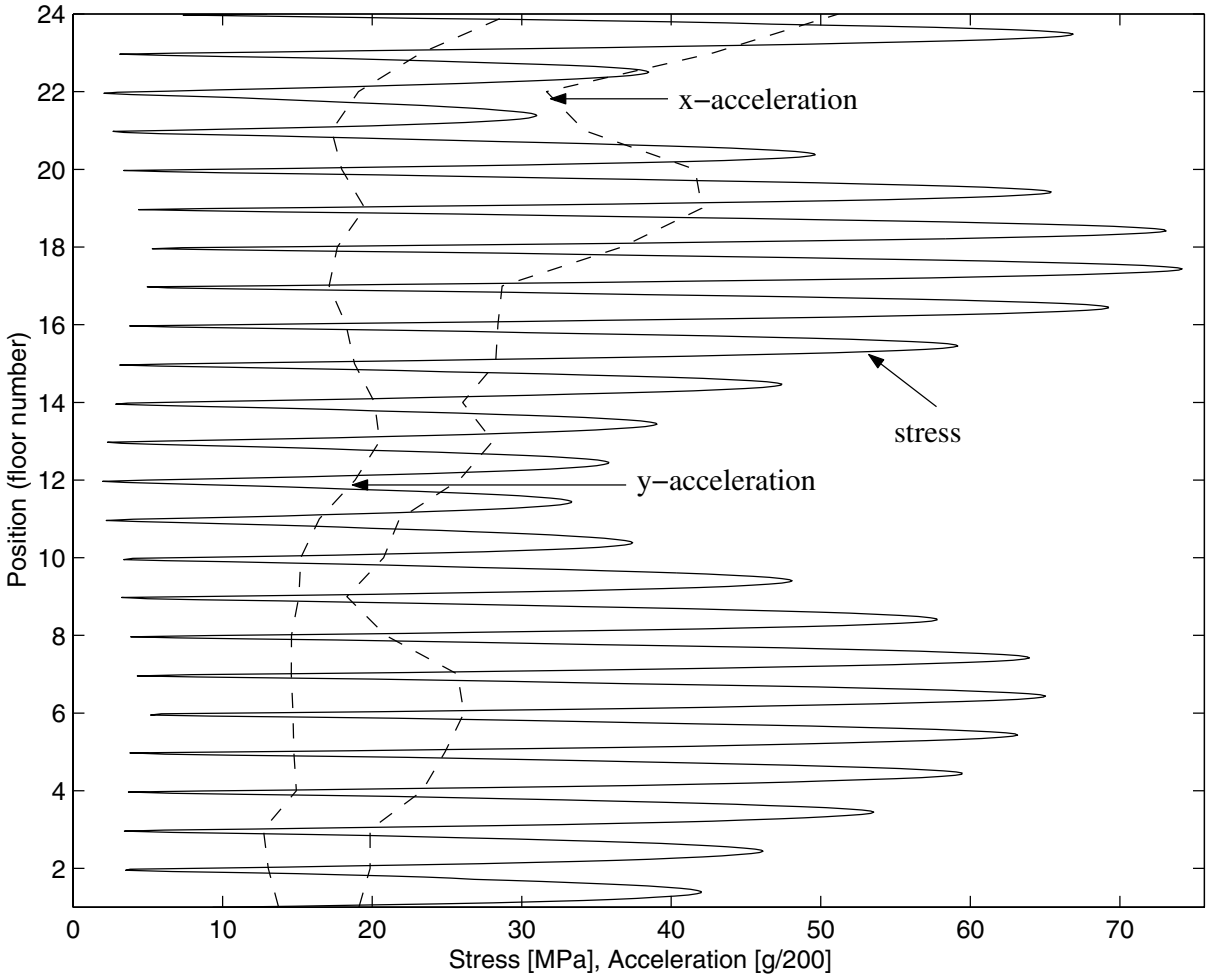

FIGURE 2-25 Maximum Stress in the Rail's Web for Different Counterweight Positions Along the of the 24-Story Building for Northridge Earthquake, Compared to Maximum Floor Acceleration

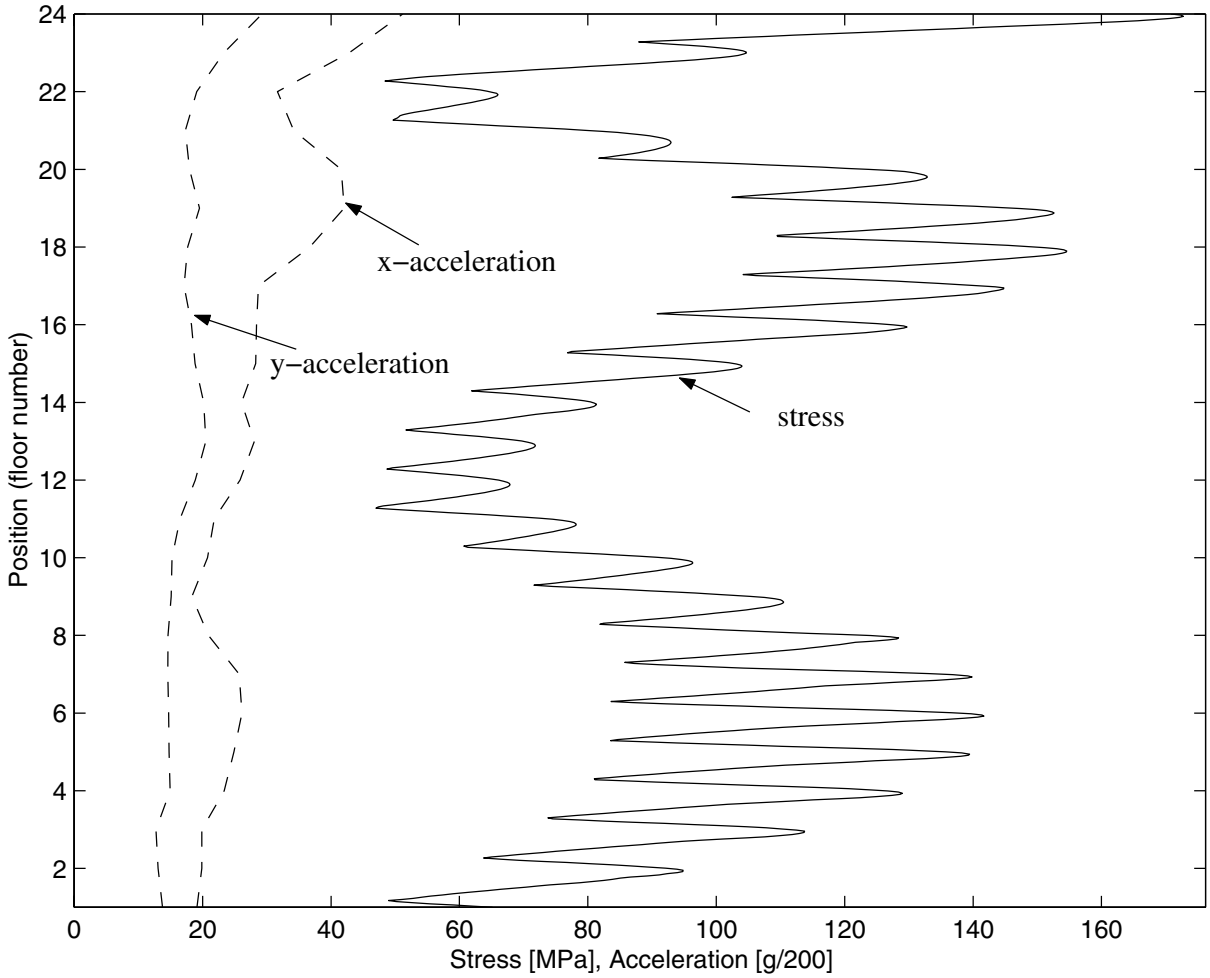

FIGURE 2-26 Maximum Stress in the Bracket for Different Counterweight Positions Along the of the 24-Story Building for Northridge Earthquake, Compared to Maximum Floor Acceleration

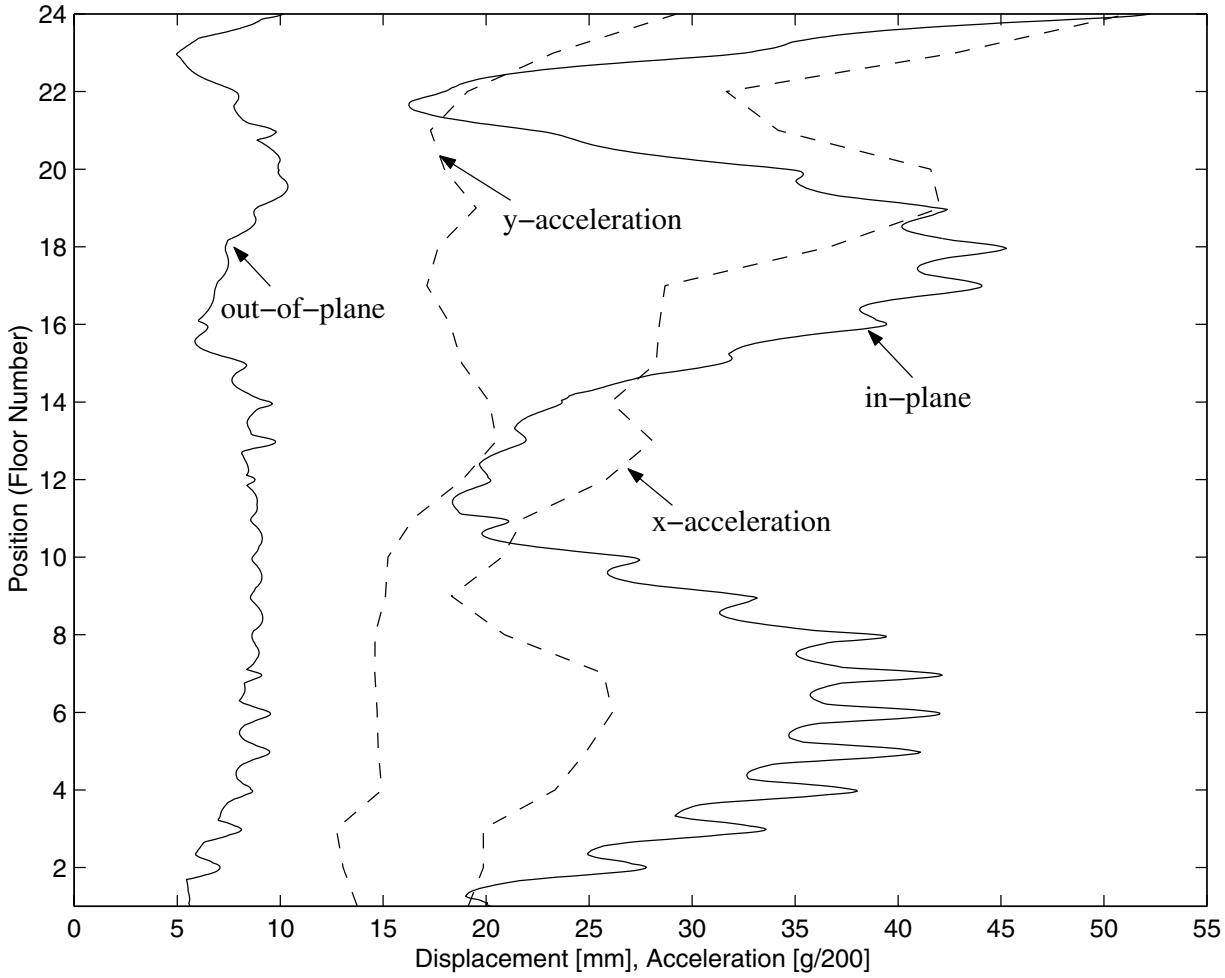

FIGURE 2-27 Maximum Deformation of Roller Guide Assembly for Different Counterweight Positions Along the of the 24-Story Building for Northridge Earthquake, Compared to Maximum Floor Acceleration

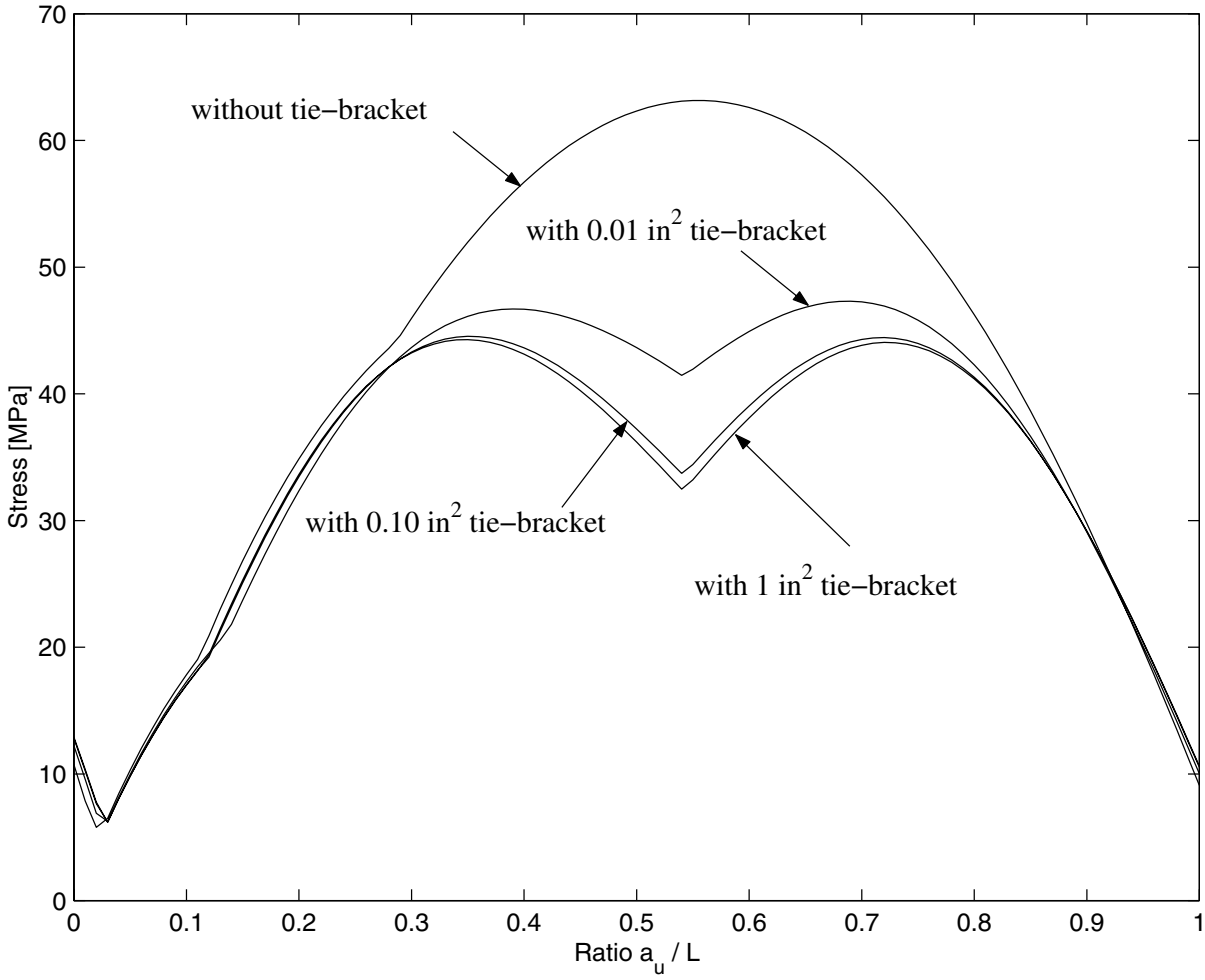

FIGURE 2-28 Maximum Stress in the Rail's Web, with and without Intermediate Tie-Brackets of Different Axial Stiffness, for Different Counterweight Positions Along the Top Story of 10-Story Building for Northridge Earthquake

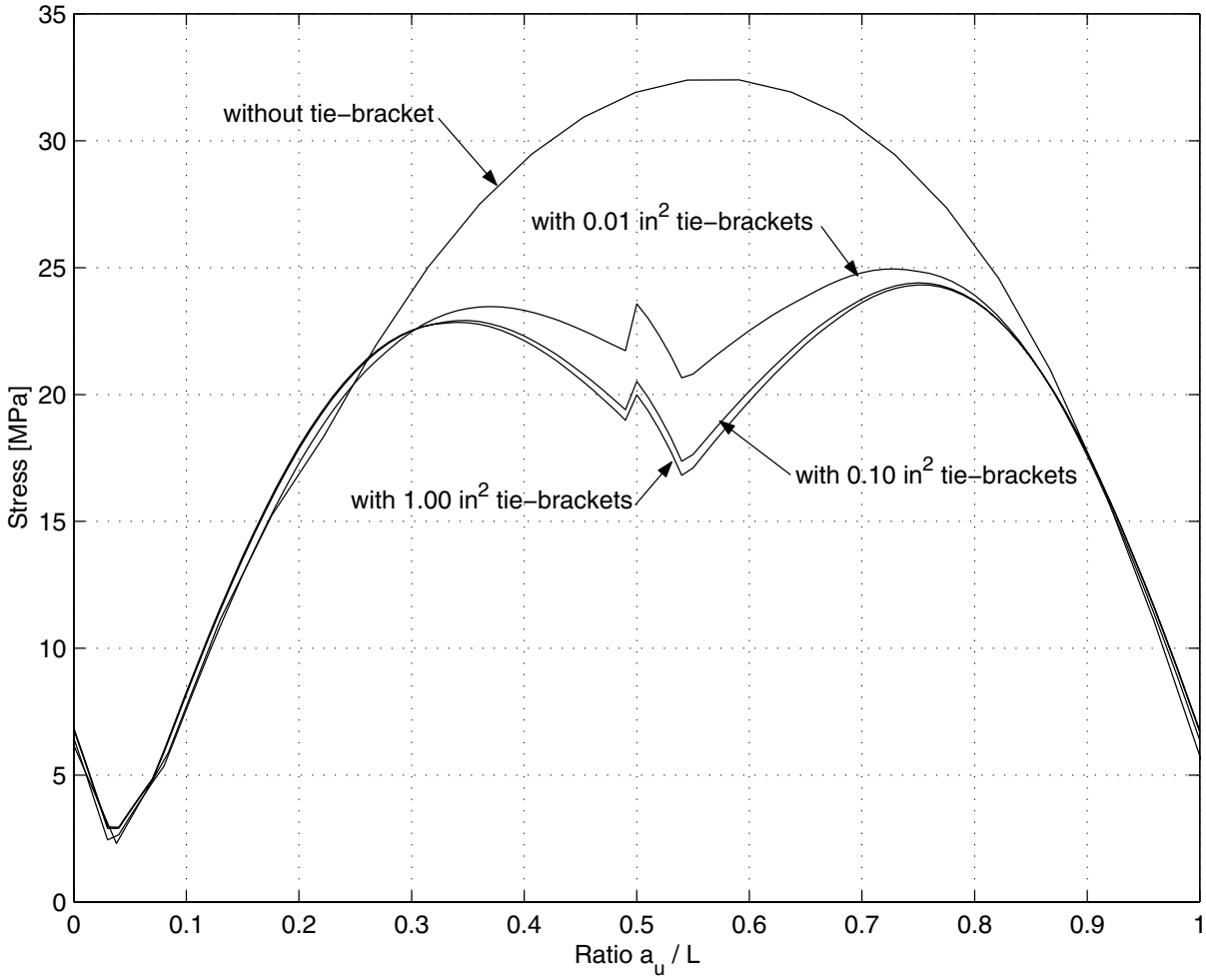

FIGURE 2-29 Maximum Stress in the Rail's Web, with and without Intermediate Tie-Brackets of Different Axial Stiffness, for Different Counterweight Positions in the 18th story for the Whittier earthquake. 24-story building.

SECTION 3
NONLINEAR MODEL AND ANALYSIS

3.1 Introduction

The analysis presented in Section 2 assumed that the rail and counterweight system behaved in a linear fashion. However, depending upon the level of excitation intensity, the system can go in to the nonlinear range. In this section, we will examine the effect of the system nonlinearities on the seismic response of the rail-counterweight system.

The nonlinearity in the system can be introduced primarily due to the following five reasons:

(1) Nonlinear force deformation characteristics of the elastomer tires,
(2) Nonlinearity due to possible yielding of the rails or brackets,
(3) Saturation of helical springs in the roller guide assemblies due to excessive deformations,
(4) Closing of the gap between the restraining plated and the rails at any of the four roller guide assemblies,
(5) Closing of the gap between the counterweight frame and the rails at a bracket support when the roller guides are on either side of the support in the in-plane motion.

The nonlinear behavior of the roller tires can be established in a reliable manner only through experiments. However, as shown by Diaz [1999], within the range of deformation of the elastomer tire the force deformation relationship can be assumed to be linear.

The second source of nonlinearity can occur due to possible yielding of the rails or the brackets due to excessive forces. This can happen at high levels of excitation intensities or for smaller size rails with softer roller guide assembly, as in this case the rails can experience high bending stresses even at low excitation intensity. However, a study of the post yielding behavior of the rail-counterweight system is not of much practical interest as by then the counterweight derailment is almost inevitable. This condition, thus, ought to be avoided, and should not be a part of the design criterion. This nonlinearity will, therefore, not be the focus of this study.

The third possible source of nonlinearity can occur when the helical spring deforms enough to close the gaps between the helical wire loops. It will be assumed that this can be avoided by proper design of the helical spring to avoid jerking motion. However, this saturation of the helical spring and elastomer tire occurs before the restraining contact with the rail, it can be easily included in the analysis by modifying the force-deformation characteristics associated with the gap at the restraining plate

The fourth cause of nonlinearity is due to the contact of a restraining plate with the rail at any of the four roller guide assemblies. At each roller guide assembly, a restraining plate is provided to avoid roller guide coming off the guide rails during an earthquake. The code prescribes a maximum clearance of 3/16 inch (4.76 mm) between the restraining plate and the rail. In a medium or strong ground shaking it is quite possible that this clearance will be closed. This can happen both in the in-plane motion and/or the out-of-plane motion of the counterweight frame. After a restraining plate comes in contact with the rail, that particular roller guide effectively acts as a rigid element; the flexibility in the system is, then, provided only by the guide rail and their supporting bracket. Because the springs representing the roller guides and rail-brackets are series springs and the guide rails and brackets are much more rigid than the helical springs and

rubber tires, the stiffness of the system will increase significantly after the contact. In this study, we will focus on this source of nonlinearity. We will study the dynamic response of the rail-counterweight systems provided with the code clearance for different earthquakes and different ground level intensities. We will also examine the effect of varying the clearance on the dynamic response.

To avoid excessive deformation of the guide rail, the ASME code also limits the gap between the counterweight and the frame to be not more than 0.5. The last source of nonlinearity is due the closing of this gap between the rail and the counterweight frame. This can happen when the upper and lower roller guide assemblies are on two different sides a bracket support. If the combined deformations of the guide rail and the roller guides at the two ends are large to overcome the gap between the counterweight frame and the rail then a contact between the two occurs at the bracket support. This situation occurs only during the in-plane motion of the counterweight. This condition must be checked at each step of the dynamic analysis as in this case the equations of motion are changed by the new constraint on the frame at the point of contact with the support. The effect of this nonlinearity on the dynamic response of the system is examined in this section. The effect of varying the prescribed clearance on the stresses in the rails and the forces in the brackets is also examined.

3.2 Equations of Motion

The equations of motion in Section 2 were developed using the Lagrange's equations, and were expressed in terms of the stiffness coefficients primarily because our interest was in the behavior of the linear system. Here, however, we will use the Newton's law to write the equations in terms of the forces acting on the counterweight. As done in Section 2, the equations of motion are developed separately for the out-of-plane and the in-plane motions.

3.2.1 Out-of-plane Motion

In the out-of-plane motion there are three degrees of freedom, as shown in figure 2-1. For this case, figure 3-1 shows the free body diagram with four corner forces as well as the effective forces acting at the center of mass. The three equations of motion are obtained by summing up forces in the y-direction perpendicular to the plane of the counterweight, and by balancing the moments about the *z*- and *x*-axes. Summing up the forces in the y-direction provides:

$$f_{u1} + f_{u2} + f_{\ell 1} + f_{\ell 2} = -m_c \left(\ddot{v}_c + \ddot{y}_c \right) \tag{3-1}$$

Similarly, the moment balance equations about the *z* and *x* axes, respectively provide the following two equations, respectively:

$$-\left[-\left(f_{u1} + f_{u2} \right) \left(\ell_c - \ell_m \right) + \left(f_{\ell 1} + f_{\ell 2} \right) \ell_m \right] = J_\theta \left(\ddot{\theta} + \ddot{\beta} \right) \tag{3-2}$$

$$-\left(f_{u1} - f_{u2} + f_{\ell 1} - f_{\ell 2} \right) \frac{d}{2} = J_\phi \left(\ddot{\phi} + \ddot{\alpha} \right) \tag{3-3}$$

where

$$J_\theta = \frac{m_c d^2}{12}\left(1+\frac{e^2}{d^2}\right) \tag{3-4}$$

$$J_\phi = \frac{m_c \ell_m^2}{3}\left(1+\frac{e^2}{4\ell_m^2}\right) \tag{3-5}$$

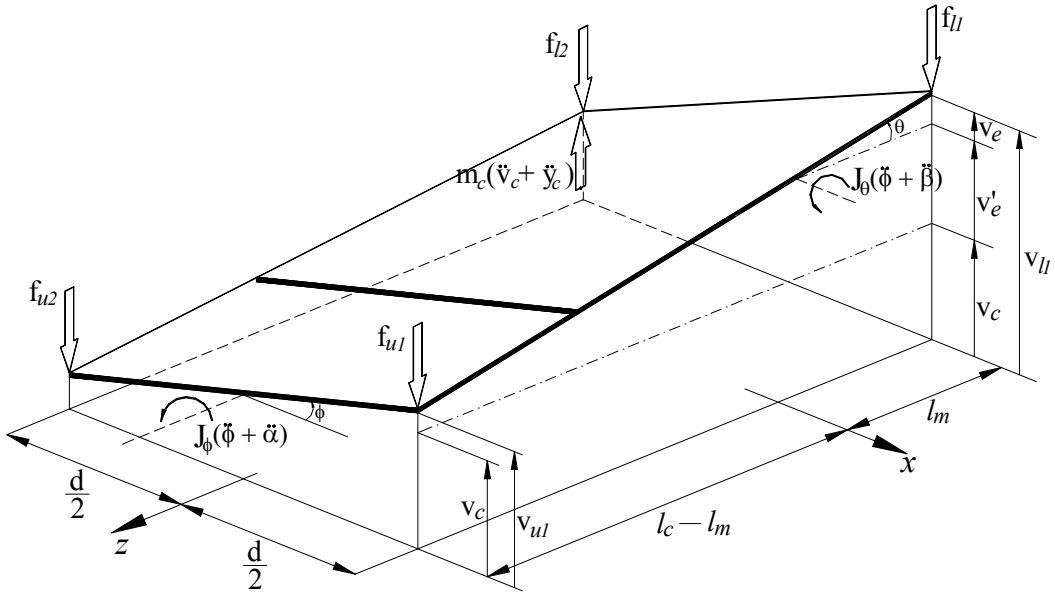

FIGURE 3-1 Free Body and Kinetic Diagram for the Out-of-Plane Motion of the Counterweight

As done in the previous section, we introduce the following response variables

$$v_e = \ell_m \theta \quad ; \quad v_e^{'} = \frac{d}{2}\phi \tag{3-6}$$

$$y_{dif} = \ell_m \beta \quad ; \quad y_{dif}^{'} = \frac{d}{2}\alpha \tag{3-7}$$

and re-write the equations of motion in terms of these variables as

$$\left[M_o\right]\left\{\ddot{q}_o(t)\right\} + \left\{F_o(t)\right\} = -\left[M_o\right]\left\{\ddot{y}(t)\right\} \tag{3-8}$$

where

$$\left[M_o\right] = m_c\begin{bmatrix} 1 & 0 & 0 \\ 0 & \gamma_2 & 0 \\ 0 & 0 & \gamma_1 \end{bmatrix} \quad ; \quad \left\{q_o(t)\right\} = \begin{Bmatrix} v_c \\ v_e \\ v_e^{'} \end{Bmatrix} \tag{3-9}$$

$$\left\{F_o(t)\right\} = \begin{Bmatrix} f_{u1}+f_{u2}+f_{\ell 1}+f_{\ell 2} \\ \left(f_{u1}+f_{u2}\right)\left(1-\dfrac{\ell_c}{\ell_m}\right)+f_{\ell 1}+f_{\ell 2} \\ f_{u1}-f_{u2}+f_{\ell 1}-f_{\ell 2} \end{Bmatrix} \quad ; \quad \left\{\ddot{y}(t)\right\} = \begin{Bmatrix} \ddot{y}_c \\ \ddot{y}_{dif} \\ \ddot{y}_{dif}^{'} \end{Bmatrix} \tag{3-10}$$

In the above equations, the subscripts u and ℓ with the force and other quantities associate them, respectively, with the upper and lower ends of the counterweight; the second subscript on these quantities refers to the values under the left or the right roller guide.

Figure 3-2 shows the force deformation diagram for the forces at the four corners. The initial flat portion of the force deformation diagram occurs before the restraining plate at a roller guide assembly comes in contact with the rail. Associated with this flat portion of the force-deformation diagram, the stiffness coefficients k_u and k_ℓ for the upper and lower springs of the equivalent springs, respectively, are defined in terms of the rail-bracket and roller guide assembly as follows:

$$k_u = \frac{\left(k_{gr}\right)_u k_{rs}}{\left(k_{gr}\right)_u + k_{rs}} \qquad \text{for} \quad \left|\left(v_{rs}\right)_{ui}\right| \le v_m \quad ; \tag{3-11}$$

$$k_\ell = \frac{\left(k_{gr}\right)_\ell k_{rs}}{\left(k_{gr}\right)_\ell + k_{rs}} \qquad \text{for} \quad \left|\left(v_{rs}\right)_{\ell i}\right| \le v_m \tag{3-12}$$

where $\left(v_{rs}\right)_{ui}$ and $\left(v_{rs}\right)_{\ell i}$ are the deformations of the upper and lower roller guide assemblies. These equations are valid whenever, these deformations are less than the clearance v_m between the restraining plate and the rail. $(k_{gr})_u$ and $(k_{gr})_\ell$ are the stiffness coefficients of the guide rail-bracket system at the upper and lower roller locations, respectively. It is noted that these stiffness coefficients will be different for different positions of the rollers. k_{rs} is the stiffness coefficient of the roller guide assembly; this coefficient will be assumed to be the same for all roller guide assemblies.

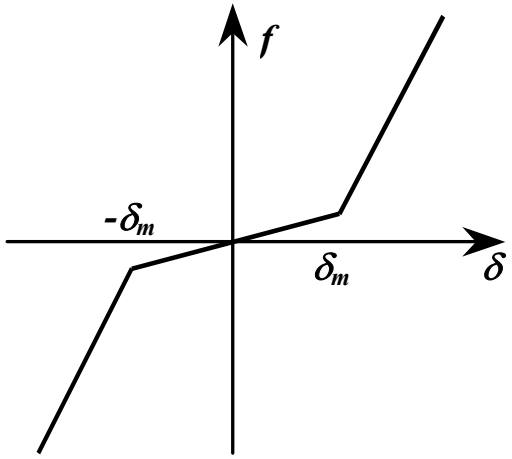

FIGURE 3-2 The Bilinear Restoring Force of the Upper Spring

The steep portion of the force-deformation diagram occurs whenever a roller guide assembly deforms more than the clearance v_m. In this situation, the restraining plate contacts the rail, and the total flexibility is then provided by the rail-bracket system. The upper and lower stiffness coefficients k'_u and k'_ℓ associated with this condition are then given by the combined stiffness of the guide rail and bracket as follows:

$$k_u^{'} = \left(k_{gr}\right)_u \qquad \text{for} \quad \left|\left(v_{rs}\right)_{ui}\right| \geq v_m \tag{3-13}$$

$$k_\ell^{'} = \left(k_{gr}\right)_\ell \qquad \text{for} \quad \left|\left(v_{rs}\right)_{\ell i}\right| \geq v_m \tag{3-14}$$

In terms of these stiffness coefficients, the force in the upper and lower equivalent springs can be written as follows:

$$f_{ui} = k_{ui}\, v_{ui} - \Delta k_{ui}\, \text{sgn}\left(v_{ui}\right) v_m \qquad ;\, i = 1,2 \tag{3-15}$$

$$f_{\ell i} = k_{\ell i}\, v_{\ell i} - \Delta k_{\ell i}\, \text{sgn}\left(v_{\ell i}\right) v_m \qquad ;\, i = 1,2 \tag{3-16}$$

where sgn(v_{ui}) is the sign function of v_{ui} which takes a value of 1 if $v_{ui} > 0$, -1 if $v_{ui} < 0$ and 0 if $v_{ui} = 0$. k_{ui} and $k_{\ell i}$ are the stiffness coefficients of the equivalent springs at the upper and lower roller guide locations. They also depend upon the deformation of the roller guide assembly and are defined as follows:

$$k_{ui} = \begin{cases} k_u & \text{if} \quad \left|\left(v_{rs}\right)_{ui}\right| \leq v_m \\ k_u^{'} & \text{if} \quad \left|\left(v_{rs}\right)_{ui}\right| > v_m \end{cases} \quad ; \quad i = 1,2 \tag{3-17}$$

$$k_{\ell i} = \begin{cases} k_\ell & \text{if} \quad \left|\left(v_{rs}\right)_{\ell i}\right| \leq v_m \\ k_\ell^{'} & \text{if} \quad \left|\left(v_{rs}\right)_{\ell i}\right| > v_m \end{cases} \quad ; \quad i = 1,2 \tag{3-18}$$

Also,

$$\begin{aligned} \Delta k_{ui} &= k_{ui} - k_u \\ \Delta k_{\ell i} &= k_{\ell i} - k_\ell \end{aligned} \quad ; \quad i = 1,2 \tag{3-19}$$

In order to solve the equations of motion (3-8) using a step-by-step integration scheme, it will be convenient to express the force term $\{F_s(t)\}$ in terms of a tangent or instantaneous stiffness matrix. Examining (3-15) and (3-16), the elastic forces f_{u1}, f_{u2}, etc. can be written as:

$$\begin{Bmatrix} f_{u1} \\ f_{u2} \\ f_{\ell 1} \\ f_{\ell 2} \end{Bmatrix} = \begin{bmatrix} k_{u1} & 0 & 0 & 0 \\ 0 & k_{u2} & 0 & 0 \\ 0 & 0 & k_{\ell 1} & 0 \\ 0 & 0 & 0 & k_{\ell 2} \end{bmatrix} \begin{Bmatrix} v_{u1} \\ v_{u2} \\ v_{\ell 1} \\ v_{\ell 2} \end{Bmatrix} - v_m \begin{Bmatrix} \Delta k_{u1}\, \text{sgn}\left(v_{u1}\right) \\ \Delta k_{u2}\, \text{sgn}\left(v_{u2}\right) \\ \Delta k_{\ell 1}\, \text{sgn}\left(v_{\ell 1}\right) \\ \Delta k_{\ell 2}\, \text{sgn}\left(v_{\ell 2}\right) \end{Bmatrix} \tag{3-20}$$

Furthermore, the deformations of the equivalent springs at the four corners and the coordinates in the equations of motion in (3-8) are related as follows:

$$\begin{Bmatrix} v_{u1} \\ v_{u2} \\ v_{\ell 1} \\ v_{\ell 2} \end{Bmatrix} = \begin{bmatrix} 1 & 1-\dfrac{\ell_c}{\ell_m} & 1 \\ 1 & 1-\dfrac{\ell_c}{\ell_m} & -1 \\ 1 & 1 & 1 \\ 1 & 1 & -1 \end{bmatrix} \begin{Bmatrix} v_c \\ v_e \\ v_e \end{Bmatrix} = [C_o]\{q_o(t)\} \tag{3-21}$$

Eqs. (3-20) and (3-21) can now be used to express the force vector $\{F_o(t)\}$ in (3-10) as follows:

$$\{F_o(t)\} = [K_{ot}]\{q_o(t)\} - \{f_o(t)\} \tag{3-22}$$

where $[K_{ot}]$ is the tangent stiffness matrix for the out-of-plane motion

$$[K_{ot}] = [C_o]^T \begin{bmatrix} k_{u1} & 0 & 0 & 0 \\ 0 & k_{u2} & 0 & 0 \\ 0 & 0 & k_{\ell 1} & 0 \\ 0 & 0 & 0 & k_{\ell 2} \end{bmatrix} [C_o] \tag{3-23}$$

and $\{f(t)\}$ is the nonlinear part of force vector defined as

$$\{f_o(t)\} = v_m [C_o]^T \begin{Bmatrix} \Delta k_{u1} \operatorname{sgn}(v_{u1}) \\ \Delta k_{u2} \operatorname{sgn}(v_{u2}) \\ \Delta k_{\ell 1} \operatorname{sgn}(v_{\ell 1}) \\ \Delta k_{\ell 2} \operatorname{sgn}(v_{\ell 2}) \end{Bmatrix} \tag{3-24}$$

Using (3-22), the equations of motion (3-8) can then be written as

$$[M_o]\{\ddot{q}_o(t)\} + [K_{ot}]\{q_o(t)\} = -[M_o]\{\ddot{y}(t)\} + \{f_o(t)\} \tag{3-25}$$

3.2.2 In-Plane Motion

The in-plane motion has two degrees of freedom, also shown in figure 2-1. At any time of the motion, one of the two rollers will always be in contact at the upper and lower roller guides giving the forces f_u and f_ℓ. Another resisting force, f_s, occurs when the frame of the counterweight comes into contact with the rail at the bracket support. This could happen when the upper and lower roller guides on either sides of a bracket support. In this position, the distance that defined the location of the counterweight will be such that

$$a_u > L - \ell_c \tag{3-26}$$

Let the distance of the bracket support from the upper roller guide be denoted ℓ_s. This distance can be written as,

$$\ell_s = L - a_u \tag{3-27}$$

If at this distance the displacement of the frame with respect to the rail exceeds the original clearance u_{sm} between the frame and the rail, the contact between the two will occur. The code

limits this clearance to a maximum value of 0.5 inch. The total displacement of the counterweight at this bracket level can be determined from the displacements of the upper and lower corner of the counterweight:

$$u_s = u_u + \left(u_\ell - u_u\right)\frac{\ell_s}{\ell_c} \tag{3-28}$$

and the force f_s can be calculated from:

$$f_s = k_{br}\left(u_s - u_{sm}\,\mathrm{sgn}\left(u_s\right)\right) \tag{3-29}$$

where

$$k_{br} = \begin{cases} k_{br-inplane} & \text{if } a_u > L - \ell_c \text{ and } \left|\left(u_s\right)\right| > u_{sm} \\ 0 & \text{otherwise} \end{cases} \tag{3-30}$$

Figure 3-3 shows the force-deformation diagram for the contact force f_s.

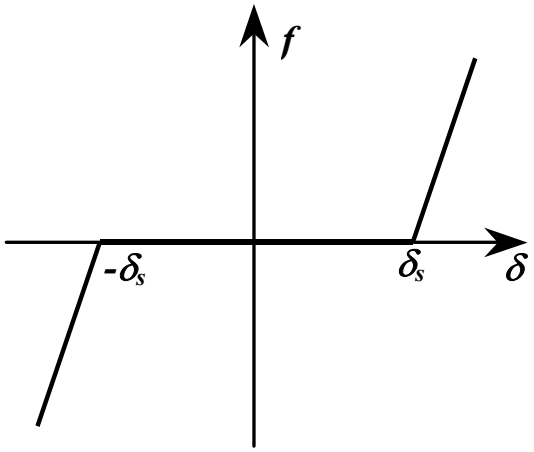

FIGURE 3-3 The Bilinear Restoring Force for Contact Between Rail and Counterweight Frame

Figure 3-4 shows the free body diagram, in which the roller contact only on the left hand side rail is shown. In the figure are also shown the forces at the upper and lower roller contacts and the force at the contact with the bracket support. Using the force balance equation along the *x*-axis we obtain:

$$-\left(f_u + f_\ell + f_s\right) = m_c\left(\ddot{u}_c + \ddot{x}_c\right) \tag{3-31}$$

Similarly, writing the moment balance equation about the *y*-axis, we obtain:

$$-f_u\left(\ell_c - \ell_m\right) - f_s\left(\ell_c - \ell_m - \ell_s\right) + f_\ell\,\ell_m = J_\psi\left(\ddot{\psi} + \ddot{\delta}\right) \tag{3-32}$$

where

$$J_\psi = \frac{m_c \ell_m^2}{3}\left(1 + \frac{d^2}{4\ell_m^2}\right) \tag{3-33}$$

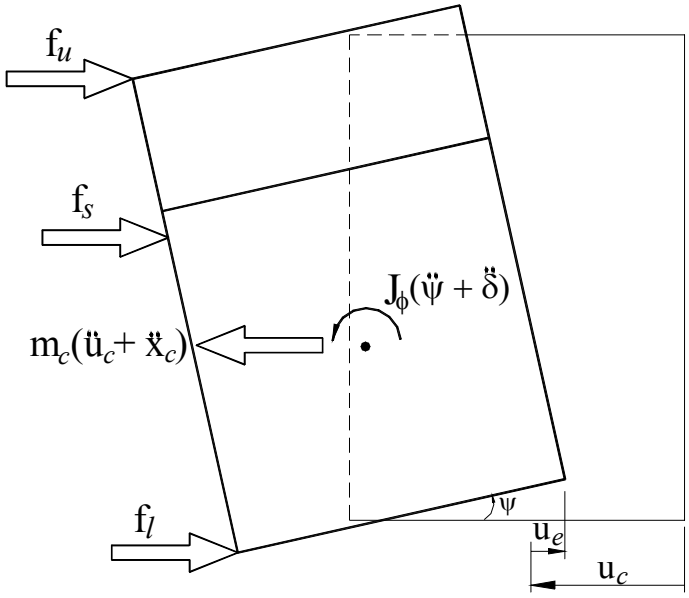

FIGURE 3-4 Free Body and Kinetic Diagram for the In-Plane Motion of the Counterweight

Introducing new variables:

$$u_e = \ell_m \psi \tag{3-34}$$

$$\ddot{x}_{dif} = \ell_m \ddot{\delta} = \frac{\ell_m}{\ell_c}\left(\ddot{x}_u - \ddot{x}_\ell\right) \tag{3-35}$$

and rearranging (3-31) and (3-32), we get

$$m_c \begin{bmatrix} 1 & 0 \\ 0 & \gamma_3 \end{bmatrix} \begin{Bmatrix} \ddot{u}_c \\ \ddot{u}_e \end{Bmatrix} + \left\{F_i(t)\right\} = -m_c \begin{bmatrix} 1 & 0 \\ 0 & \gamma_3 \end{bmatrix} \begin{Bmatrix} \ddot{x}_c \\ \ddot{x}_{dif} \end{Bmatrix} \tag{3-36}$$

where

$$\left\{F_i(t)\right\} = \begin{bmatrix} 1 & 1 & 1 \\ \frac{\ell_c}{\ell_m} - 1 & -1 & \frac{\ell_c}{\ell_m} - 1 - \frac{\ell_s}{\ell_m} \end{bmatrix} \begin{Bmatrix} f_u \\ f_\ell \\ f_s \end{Bmatrix} = \left[C_i\right]^T \begin{Bmatrix} f_u \\ f_\ell \end{Bmatrix} \tag{3-37}$$

$$\gamma_3 = \frac{1}{3}\left(1 + \frac{d^2}{4\ell_m^2}\right) \tag{3-38}$$

Following the procedure used for the development of the out-of-plane equations we define the force vector in terms of the displacement as follows:

$$\begin{Bmatrix} f_u \\ f_\ell \\ f_s \end{Bmatrix} = \begin{bmatrix} s_u & 0 & 0 \\ 0 & s_\ell & 0 \\ 0 & 0 & k_{br} \end{bmatrix} \begin{Bmatrix} u_u \\ u_\ell \\ u_s \end{Bmatrix} - \begin{Bmatrix} u_m \Delta s_u \ \mathrm{sgn}(u_u) \\ u_m \Delta s_\ell \ \mathrm{sgn}(u_\ell) \\ u_{sm} k_{br} \ \mathrm{sgn}(u_s) \end{Bmatrix} \tag{3-39}$$

Also, the displacement vector can also be related to the displacement degrees of freedom of the system as follows:

$$\begin{Bmatrix} u_u \\ u_\ell \\ u_s \end{Bmatrix} = \begin{bmatrix} 1 & \frac{\ell_c}{\ell_m} - 1 \\ 1 & -1 \\ 1 & \frac{\ell_c}{\ell_m} - 1 - \frac{\ell_s}{\ell_m} \end{bmatrix} \begin{Bmatrix} u_c \\ u_e \end{Bmatrix} \tag{3-40}$$

Substituting (3-39) and (3-40) into (3-37), we can express the static force in terms of the tangent stiffness matrix and the nonlinear force component as follows:

$$\{F_i(t)\} = [K_{it}] \begin{Bmatrix} u_c \\ u_e \end{Bmatrix} - \{f_i(t)\} \tag{3-41}$$

where

$$\begin{aligned} [K_{it}] &= [C_i]^T \begin{bmatrix} s_u & 0 & 0 \\ 0 & s_\ell & 0 \\ 0 & 0 & k_{br} \end{bmatrix} [C_i] \\ &= \begin{bmatrix} s_u + s_\ell + k_{br} & s_u\left(\frac{\ell_c}{\ell_m} - 1\right) - s_\ell + k_{br}\left(\frac{\ell_c}{\ell_m} - 1 - \frac{\ell_s}{\ell_m}\right) \\ s_u\left(\frac{\ell_c}{\ell_m} - 1\right) - s_\ell + k_{br}\left(\frac{\ell_c}{\ell_m} - 1 - \frac{\ell_s}{\ell_m}\right) & s_u\left(\frac{\ell_c}{\ell_m} - 1\right)^2 + s_\ell + k_{br}\left(\frac{\ell_c}{\ell_m} - 1 - \frac{\ell_s}{\ell_m}\right)^2 \end{bmatrix} \end{aligned} \tag{3-42}$$

$$\{f_i(t)\} = [C_i]^T \begin{Bmatrix} u_m \Delta s_u \ \mathrm{sgn}(u_u) \\ u_m \Delta s_\ell \ \mathrm{sgn}(u_\ell) \\ u_{sm} k_{br} \ \mathrm{sgn}(u_s) \end{Bmatrix} \tag{3-43}$$

The equations of motion for in-plane motion of the counterweight can now be written as:

$$[M_i] \begin{Bmatrix} \ddot{u}_c \\ \ddot{u}_e \end{Bmatrix} + [K_{it}] \begin{Bmatrix} u_c \\ u_e \end{Bmatrix} = -[M_i] \begin{Bmatrix} \ddot{x}_c \\ \ddot{x}_{dif} \end{Bmatrix} + \{f_i(t)\} \tag{3-44}$$

where

$$[M_i] = m_c \begin{bmatrix} 1 & 0 \\ 0 & \gamma_3 \end{bmatrix} \tag{3-45}$$

In the numerical integration, the equations of motion (3-25) for the out-of-plane motion and (3-44) for in-plane motion are combined into the following equation as:

$$[M]\{\ddot{q}\}+[K_t]\{q\}=-[M]\{\ddot{Y}\}+\{f(t)\} \tag{3-46}$$

where

$$[M]=\begin{bmatrix}[M_i] & 0\\ 0 & [M_o]\end{bmatrix} \;;\; [K_t]=\begin{bmatrix}[K_{it}] & 0\\ 0 & [K_{ot}]\end{bmatrix} \tag{3-47}$$

$$\{q\}=\begin{Bmatrix}\{q_i\}\\ \{q_o\}\end{Bmatrix} \;;\; \{f\}=\begin{Bmatrix}\{f_i\}\\ \{f_o\}\end{Bmatrix} \tag{3-48}$$

$$\{\ddot{Y}\}=\begin{pmatrix}\ddot{x}_c & \ddot{x}_{dif} & \ddot{y}_c & \ddot{y}_{dif} & \ddot{y}_{dif}\end{pmatrix}^T \tag{3-49}$$

3.2.3 Damping Mechanism

The equations of motion (3-46) were derived without any damping mechanism in the system. However, to incorporate some inevitable energy dissipation in the system, here a viscous damping matrix is introduced. This damping matrix is defined in terms of constant modal damping ratios as follows:

$$[C_d]=2\xi[M][\Phi][\omega_j][\Phi]^T[M] \tag{3-50}$$

where ξ = the modal damping ratio, [Φ]= eigenvector matrix, and $[\omega_j]$ = the diagonal matrix of the system frequencies. Since the eigenproperties of the system change whenever an equivalent stiffness element deforms more than v_m, or a contact of the frame with the bracket occurs, this damping matrix also changes to provide a constant damping ratio. The final form of the equations of motion with the damping matrix included becomes

$$[M]\{\ddot{q}\}+[C_d]\{\dot{q}\}+[K_t]\{q\}=-[M]\{\ddot{Y}\}+\{f(t)\} \tag{3-51}$$

3.3 Numerical Results

In the numerical analysis of a nonlinear problem with force-deformation characteristics shown in figures 3-2 and 3-3, proper selection of the time step Δt is very crucial for accurate calculation of the forces and deformations. This is, of course, true for any step-by-step algorithm, but it is especially important for the rail and counterweight system because the stiffness characteristics of the system change from a relatively soft to a very rigid one any time the deformation of the roller guide $v_c(t) > v_m$ or whenever the frame contacts the rail. When this happens, not only the period of oscillation decreases dramatically but the amplitude of the oscillations above and below v_m become very small because of the sudden increase in the stiffness. This can be clearly observed from figure 3-5 where the displacement time histories of equivalent springs for the in-plane motion are shown. The time histories for the spring deformations were obtained for the Northridge earthquake normalized to a maximum ground acceleration level of 0.1g. The 18.5 lb guide rails were used for these results, and the clearance between the rail and the restraining plate was set at 3/16 in. It is seen that there are several excursions of the deformation response above the saturation limit, and that these excursions last only for a very small period of time.

Similar excursions are also observed in the out-of-plane motion. The time step of integration should be small enough to capture the peaks of these oscillations above the clearance limit, as these peaks are associated with the maximum stresses in the rails and brackets. In the initial study, the popular Newmark-β was used with a reasonably small time step. However, further study found this method to be quite unsuitable for the numerical calculations needed in this investigation. Appendix A provides a more detailed account of this study. Based on this study, the fourth order Runge-Kutta method with adaptive time step was selected for its numerical efficiency and accuracy. All the results presented in this section are obtained with this method.

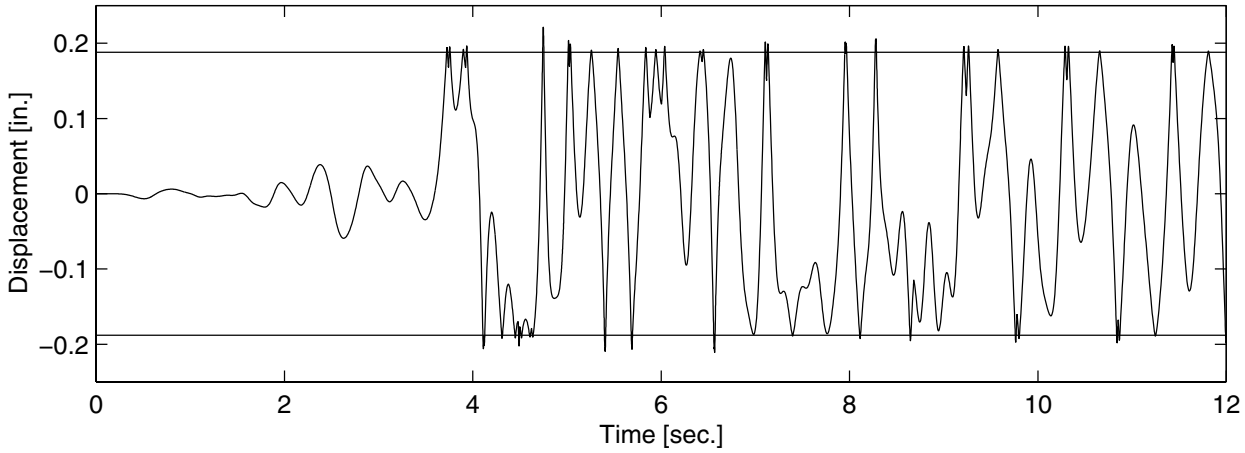

FIGURE 3-5 In-plane Displacement Time History at the Lower Left Roller Guide for $a_u/L = 0$, Northridge Earthquake 0.1g

A 4300-pound counterweight on 18.5-lb guide rails with no intermediate tie brackets is used as a basic system to obtain the numerical results in this section. As per ASME Code A17.1, 18.5-lb rails are quite acceptable for a 4300-pound counterweight with a good margin for bracket supports at 12 ft center-to-center spacing. For this bracket spacing, Table 4-1 shows the maximum weight of the counterweights that can be used with various rail sizes in seismic Zone 3 or higher as per the code. Figure 3-6 shows the dimensions and cross sectional properties of the bracket support used with the guide rails. The code specified clearances of 3/16 inch between the restraining plates and the guide rails, and ½ inch between the counterweight frame and the rails are also assumed. For this basic counterweight-rail system, several sets of numerical results are obtained to examine the effect of various problem parameters. Although several different recorded and synthetically generated input motions have been used in this study, the majority of numerical results presented are for the normalized 1994 Northridge and 1941 El Centro earthquake motions.

Table 3-1 Maximum Weight of Counterweight for Different Rail Size

Rail Size [lb/ft]	W_{max} [kips]		Stress [ksi] for W = 4300 lb.
	No tie	With 1 tie	
8	4.325	5.737	48.122
11	8.976	11.906	23.187
12	9.245	12.263	22.512
15	9.398	12.466	22.146
18.5	16.197	21.485	12.850
22.5	20.529	27.232	10.138
30	34.772	46.124	5.985

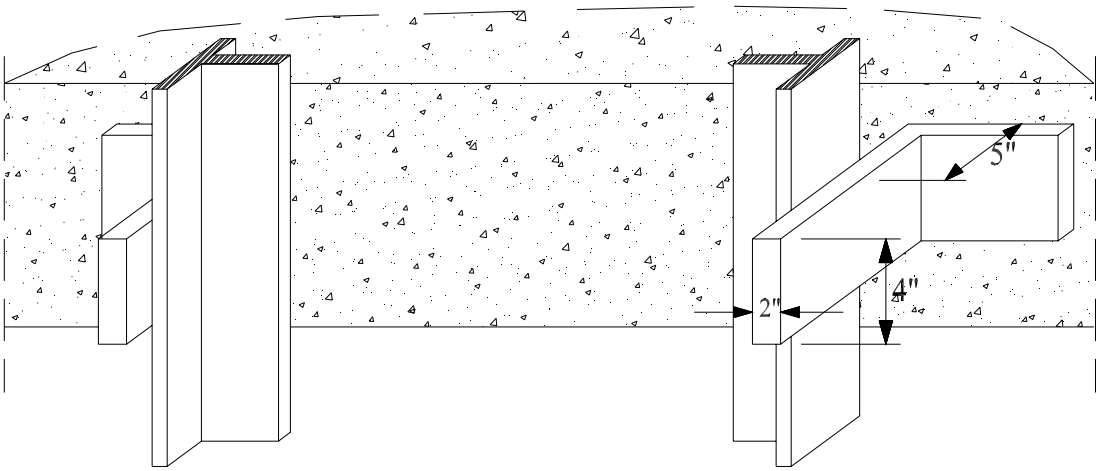

FIGURE 3-6 Cross-sectional properties of the Bracket

Figures 3-7 and 3-8 show the maximum stresses in the rails and bracket for the different positions of the counterweight along the building height a 10-story for the Northridge and El Centro earthquakes. Since this 10-story building is assume to be torsionally coupled, the response is calculated for two horizontal component applied simultaneously as the base motions. The maximum stresses in the flange and the web are shown. It is observed that the pattern of stress in different stories of the building in the two earthquakes motions are qualitatively similar, except that global maximum response in different earthquake can occur in different stories; also the maximum stresses in the rails and the brackets need not occur in the top story, even though the floor acceleration may be higher there. Similar pattern of the results is also seen from the results for a 24-story shear building in Figures 3-9 and 3-10. These results are for the actually recorded ground motion in the Northridge earthquake with maximum ground acceleration of 0.843g. Since there are no torsional effects in this building, the results are only shown for the in-plane motion. The stresses are high for this full intensity earthquake. It is noted that the pattern of stresses and the forces in the brackets in the two buildings is qualitatively similar.

In the following we further explore the response characteristics of this counterweight-rail system by conducting a comprehensive parametric study. The following results are only for the ten story torsional building. Since the stress and force responses in different building stories have

similar trend, here we will focus on the details of the responses as the counterweight moves down the 10th story. The position of the counterweight is defined by the location of the upper roller guides in terms of the position parameter a_u/L. The main parameters of interest in this study are: (1) clearance between the restraining plate and the guide rail, (2) ground motion intensity, (3) bracket stiffness, (4) guide rail size, (5) variability in the ground motion, (6) clearance between the frame and the rail, and (7) the use of tie brackets. The parameter values are varied one at a time, keeping the other parameter fixed at their normal values.

The Effect of Clearance Between the Rail and the Restraining Plate

Figures 3-11 and 3-12, respectively, show the maximum stresses in the rail and in the brackets as a function of the counterweight position in the 10th story for several values of the clearance at the restraining plates. The input used is the 1941 El Centro Earthquake normalized to a maximum ground acceleration of 0.1g. The web of the rail experienced higher stress than the flange indicating the predominance of the in-plane motion. For the rail, the stress is higher when the top roller guides are located around the middle of the story. The stress in the brackets is higher when the top roller guides are located near or on top of the bracket supports. The results show very high stresses in the brackets for some clearances. They indicate that restraining plate is impacting the support through the rails, causing high impacting forces. The high stresses shown are obviously not possible, as the brackets will yield before these stress levels are reached. Also, perhaps, the strength design criterion may not be relevant in such cases of impact. In Figure 3-13 and hereafter, we thus show the maximum force in the bracket for different clearances. These high stresses and forces, however, do indicate that special attention is necessary for the design of bracket supports.

Figures 3-14 show the maximum stress at different points in the rails as a function of the clearance at the restraining plates for El Centro earthquake. The maximum stress irrespective of the location is also shown. The Figure 3-15 shows the maximum bracket force as a function of the clearance. This is maximum of forces in several adjacent brackets, and not in any particular bracket. Both the in-plane and out-of-plane forces are shown. These figures show that the maximum stresses in the rail and forces in bracket increase with increasing clearance up to an optimal point, which is 0.75 inch for the El Centro motion. The maximum values start to decrease with increasing clearance, as for very large clearances there is no contact of the restraining plate with the rails and the system behaves linearly. The code prescribes a maximum clearance of 3/16 inch, which is smaller than the clearance corresponding to the maximum effects (0.75 in). It is noted that maximum force and stress effects can be further reduced by decreasing this clearance. For very low clearances, however, there will be many more excursions of the response beyond the clearance value accompanied by a noisy ride during an earthquake motion. It is also shown that the maximum stresses in the rail do not necessarily occur in the middle of the rail span or right on top of the bracket support. It could be under one of the roller guides, depending upon their positions.

The Effect of Ground Acceleration Intensity

Next we show the stress and force responses for three clearances as function of the intensity of the input motion acceleration. Figures 3-16, 3-17, and 3-18 are for the El Centro ground motion,

and figures 3-19, 3-20, and 3-21 are for the Northridge motion, both normalized to a maximum ground acceleration value of 0.1g. Figures 3-16 and 3-19 are for the maximum stress in the rail which occurs in the web. Figures 3-17 and 3-120 are for the maximum in-plane force and Figures 3-18 and 3-21 for the maximum out-of-plane forces in the brackets. Each figure shows three curves; one corresponding to the code specified clearance of 3/16 inch and the other for 1/8 and ½ inch clearance values. Clearly, the maximum stresses increase with an increase in the level of ground motion acceleration. The trend for the values is similar for two the earthquake motions used. Also the increase in the force and stress response when we change the clearance form 3/16 in to ½ in is large than the increase when the clearance is changed from 1/8 in to 3/16 in. Thus, for the clearances in the range of ½ in, the impacting forces between the restraining plates and the rails can be large even though there may be fewer number of incursions or contact between the two at these higher clearances. Thus keeping the clearance smaller than 3/16 may be desirable even if there are more rail contacts at the restraining plates.

Effect of Bracket Rigidity

Next we show the effect of increasing bracket stiffness on the stresses in the rail and the forces in the bracket. For the previous results the bracket cross section and dimensions shown in Figure 3-6 were used to calculate the spring constant for the brackets. This stiffness is now increased to investigate its effect on the stresses in the rails and forces on the brackets. Figure 3-22 shows the maximum stress in the rails and Figure 2-23 the maximum in-plane and out-of-plane forces as a function of the brackets stiffness ratio(this is the ratio of the bracket stiffness to that of the original bracket in figure 3-6.) It is noted that the stresses in the rail are slightly decreased but, as one would expect, the forces in the bracket increase with increasing bracket stiffness. The stiffer brackets attract more forces, but this increase is not directly proportional to the stiffness. Thus a larger bracket cross section can be used to have lower stresses.

Effect of Rail Size

In the elevator industry several different rail sizes, as given in Table 1-1, are used. The 8 lb rails are not permitted to be used in the seismic areas. In Figures 3-24 through 3-26, we show the stresses in the rails and forces in the brackets, but now for three different rail cross sections. Figure 3-24 shows the stresses, and Figure 3-25 and 3-26 show the forces in the brackets. These results are for the El Centro record normalized to 0.1g. The large rails, of course, experience smaller stresses. In Figure 3-27 and 3-28 we show the rail stresses caused by the actual recorded El Centro (0.348g) and Northridge (0.843g) motions. It is noticed that even though the 12 lb rail is acceptable according to the code for the chosen bracket spacing, it gets overstressed in these the Northridge earthquake event.

Variability of the Input Motion Characteristics

In this section we include more recorded earthquake motions, as well as an ensemble of synthetically generated motions, to examine the effect of input motion variability. In Figures 3-29 through 3-36 we show the results for the input motions recorded in six different earthquake events all normalized to 0.1g. Figure 3-29 shows the maximum stress in the rail, and Figure 3-30 shows the maximum in-plane force in the brackets for different earthquakes. Figure 3-31 and 3-

32 show the plot of the average, minimum and maximum values for these two response quantities for different counterweight positions. The trends of stress and force variations are similar for different earthquakes, but the magnitudes of the maximum stresses for different motions can be quite different for the same position of the counterweight. This point to the need of considering an ensemble of ground motions in evaluating the performance of an elevator system in a seismic environment. Figure 3-33 to 3-36 show results similar to those in Figures 3-29 to 3-32, but now for increased ground motion intensities normalized to a higher level of 0.5g. It is interesting to note that in this case the counterweight frame comes in contact with the support when the top rollers are in the middle of the span, causing a sudden increase in the bracket force shown in Figures 3-34 and 3-36. Again a significant difference in the maximum and minimum values of the stresses and the bracket forces is noted. Comparing Figures 3-31 and 3-35, we observe that the average stress in the rails do increase with increased intensity of the ground motion, but not proportionately.

In tables 3-2 and 3-3, respectively, we show the global maximum stress in the flange and the web for different earthquakes. All earthquake motions are normalized to 0.1g. The last four columns also shows the average values, minimum, maximum, and the allowable stresses. It is noted that the stresses in the web, primarily caused by the in-plane motion are generally larger than the stresses in the flange, primarily caused by the out-of-plane motion. This shows the dominance of the in-plane motion.. It is again noted that there is wide variability in the maximum stress values caused by different earthquakes.

Table 3-2 Maximum Stress in the Rail's Flange [MPa]

Rail Size	North-ridge	El Centro	Loma Prieta	Parkfield	San Fernando	Whittier	Max.	Avg.	Min.
8-lb	199.83	212.72	146.93	164.44	181.25	162.43	212.72	177.93	146.93
11-lb	89.21	93.50	76.91	125.70	129.40	123.51	129.40	106.37	76.91
12-lb	78.85	76.46	94.49	98.93	97.00	141.88	141.88	97.93	76.46
15-lb	62.64	59.29	79.27	71.99	81.91	83.87	83.87	73.16	59.29
18.5-lb	46.96	53.94	57.07	61.70	66.92	66.23	66.92	58.80	46.96
22.5-lb	45.07	50.81	49.31	57.99	63.74	62.43	63.74	54.89	45.07
30-lb	38.53	44.19	32.94	50.87	64.37	53.29	64.37	47.37	32.94

Table 3-3 Maximum Stress in the Rail's Web [MPa]

Rail Size	North-ridge	El Centro	Loma Prieta	Parkfield	San Fernando	Whittier	Max.	Avg.	Min.
8-lb	355.53	304.95	215.58	244.24	230.81	223.05	355.53	262.36	215.58
11-lb	174.05	134.80	137.14	190.55	158.16	157.06	190.55	158.63	134.80
12-lb	165.70	130.28	129.34	170.85	158.76	152.82	170.85	151.29	129.34
15-lb	165.82	127.59	124.71	173.37	153.79	140.05	173.37	147.55	124.71
18.5-lb	104.96	102.81	84.19	88.08	96.67	87.06	104.96	93.96	84.19
22.5-lb	83.23	84.83	70.21	71.73	79.56	68.86	84.83	76.40	68.86
30-lb	70.06	58.49	58.87	50.63	66.50	45.61	70.06	58.36	45.61

The recorded ground motions used in the preceding results had different frequency characteristics as they were recorded in different events and at different sites. In the following we present some results of the stresses in the 18.5 lb rail for an ensemble of earthquake motions all having similar frequency characteristics. The ensemble consists of 50 synthetically generated earthquake motions corresponding to a broadband spectral density function. In Figure 3-37 we show the average and mean plus one standard deviation acceleration spectra for the 50 input motions. In Figures 3-38 and 3-39 we show the mean and coefficient of variation of the maximum stress as a function of the counterweight location. Each figure shows the results for the motions normalized to 0.1g and 0.5g. The trend of the stress variation at different counterweight positions is somewhat different for the two acceleration levels. The coefficient of variation of the stresses calculated for the two intensity levels are about the same and also in the same range as that of the input motions. In Figure 3-40 is shown the variation of the global maximum of the stress in the rail with acceleration level of the input motions. It is noted that the average stress does not increase proportionately with the excitation intensity, clearly indicating the effect of the nonlinearity in the system.

Effect of Clearance Between the Counterweight Frame and Rail

As mentioned earlier, the ASME code specifies that the clearance between the frame and the rail should not be more than ½ inch. The primary objective of the specification is to limit the deformation of the rail when the upper and lower roller guides are in two adjacent spans during a strong ground shaking. In such situations, if the rail tends to deform too much then the bracket support would come in contact with the counterweight frame to transfer the inertial force directly to the support. It is of interest to examine the beneficial effect of this clearance on the stresses in the rails. In Figures 3-41 and 3-42 we show this effect of changing this clearance. Figure 3-41 shows the maximum stress in the rail and Figure 3-42 shows the maximum in-plane force in the bracket. The results only for the actual recorded Northridge earthquake with maximum ground acceleration of 0.843g are shown as at the lower intensity considered earlier (0.1g) there was no contact of the counterweight frame with the support. The result show that the maximum stress in the web, which usually occurs when the upper roller guide is in the middle of the span, can be reduced significantly by using smaller clearances. However, the smaller clearances may also cause an increase in the stresses for some other locations, thereby lessening the overall benefit of the reduced frame-rail clearance. Figure 3-41, showing the in-plane forces in the bracket support, confirm that there is indeed a transfer of force to the bracket due to contact with the frame when the top roller guides are in the middle of the span. For smaller clearances, the contact would occur for many different locations of the roller guide. For larger clearance, the contact is primarily confined to the roller guide locations near the middle of the span. It is noted that the maximum contact force could be higher than the force without any contact which occur when the roller guide is near one of the bracket supports.

Figures 3-43 and 3-44 show the effect of clearance on the rail stress and bracket force, respectively. The response values shown in the figures are the peak of the maximum response values obtained at different counterweight positions in the span. The actual recorded motions in the Northridge and El Centro events are considered. For the Northridge earthquake, as observed from Figure 3-43, the stress in the web is smaller for smaller clearances. There is, however, no significant effect on this quantity for the El Centro ground motion with maximum acceleration of 0.348g as at this level of acceleration the contact between the fame and the rail develops only at

very low clearances. The in-plane force in the bracket is also affected by the clearance, with a general tendency to decrease with increasing clearance. Some clearance value may also give higher forces than the other smaller values (e.g., 0.25 inch for the Northridge Earthquake). Limiting the clearance between the frame and the rail has a tradeoff; it does seem to help the rail at the higher levels of excitation but with a correspondingly higher demand on the bracket support. Since it is simpler to strengthen the brackets, this code provision might be beneficial to the system in an overall sense.

Effect of Intermediate Tie Brackets

The ASME code permits a larger spacing between the bracket support if intermediate tie brackets are used to tie up the two rails. The next sets of results are obtained to examine this effect. Figures 3-45 through 3-46 show the effect of using an intermediate tie-bracket on the maximum stresses in the rails. Figure 3-45 shows the maximum stress with and without a tie bracket for 0.1g Northridge earthquake time history. Figure 4-46 shows similar results but for the actual recorded ground motion with the maximum acceleration of 0.843 g. In both cases, the peak stress, which occurs when the upper rollers are in the middle of the span, is reduced significantly. Similar results, shown in Figures 3-47 and 3-48 are obtained for the El Centro ground motion. The decrease in the peak stress is usually accompanied by an increase in the stresses for the roller positions near the supports. In fact, in the case of the Northridge earthquake (normalized to 0.1g) this even increases the stress higher than the maximum obtained with no tie brackets.

In the next set of results we further examine this effect for an ensemble of 50 sets synthetically generated input motions considered earlier. Figure 3-49 shows the variation in the mean of the 50 maximum stress calculated for 50 input motions for different counterweight positions. All input motions were normalized to 0.1g. Similar results are shown in Figure 3-50 but for input acceleration normalized to 0.5g. Also shown in the figures are the average values of the maximum stress obtained with no tie brackets. As observed earlier for the Northridge earthquake results, the maximum stresses for the input normalized to 0.1g (Figure 3-49) are significantly decreased for the positions near the middle, but increased for the position of near the upper support. For the higher levels of excitation input (Figure 3-50), however, there is a decrease in the peak stress. This is more clearly seen from the results in Figure 3-51 where we plot the peak values (global maximum) of the average stress as a function of the increasing input motion intensity. In figure 3-52 we show the coefficient of variation of the maximum stresses for different counterweight positions. As observed for the results shown in figure 3-39, there is no trend in the coefficient of variation values of these stresses with the position of the counterweight. In general, the tie bracket are seen to be helpful in reducing the stresses in the in the rails for higher levels of excitation.

Nonlinear Versus Linear Response

It is of interest to compare the response of a nonlinear counterweight-rail system with code prescribed constraints on the clearances, with the response of an assumed linear system with no constraints on the clearances. We compare the peak stresses in the rails in Figure 3-53 and the in-plane and out-of-plane forces in the brackets in Figure 3-54 for the assumed linear and nonlinear cases at different levels of excitation intensities for El Centro earthquake. A similar

comparison is shown in Figures 3-55 and 3-56 for the Northridge earthquake. Both sets of figures show that for lower levels of intensities the stresses in the rails in the nonlinear case are higher than those for the linear case. As the excitation intensities increase, the nonlinearities due to the constraints tend to reduce the stresses. The bracket forces on the other hand are increased significantly in the nonlinear case, primarily due to the frequent impact of the restraining plates or the counterweight frame. However, since it is easier to accommodate higher forces in the brackets than the higher stresses in the rails, the nonlinearities caused by the constraints imposed on the system clearances seem to help the counterweight-rail system, especially at higher excitation levels.

3.4 Concluding Remarks

In this section a nonlinear analytical model of the rail-counterweight system of an elevator is developed. The nonlinearity can come from different components of the system. For the elevator systems, the nonlinearity in the force-deformation characteristics due to contact between the restraining plates and the rail and between counterweight frame and the rail is of special interest. The nonlinearity can also be caused by the yielding of the rails and bracket material, but post yielding analysis of the system is rarely of any interest as by then the elevator function would have been already compromised.

Here the nonlinearity caused by the gap closures are included by utilizing a simple bilinear model to represent the force-deformation characteristics of the equivalent springs at the four corners of the counterweight. In this model, the initial stiffness is represented by combined stiffness coefficient of the brackets, rails, and the roller guide assembly. However, when the deformation of the roller guide assembly exceeds the clearance between the restraining plate and the rail, the system stiffness increases significantly. This increased stiffness is primarily provided by the rail and bracket support system. A similar bilinear model is used to represent the contact force at the point where the counterweight frame comes in contact with the frame. Before the contact this force is, of course, zero, but it increases linearly proportional to the stiffness of the bracket support.

To integrate the equations of motion with such nonlinear characteristic, the selection of an appropriate numerical integration scheme is of utmost importance. This selection is described in more details in Appendix A. Herein, the Newmark-β approach, commonly used for seismic analysis of nonlinear structural system, was found to be impractical. The fourth-order Runge-Kutta scheme with adaptive time step was most efficient and accurate.

A comprehensive parametric study is conducted to investigate the effect of each problem parameters. The general conclusions of this study are:

1. The stresses in the rails are higher when one of the roller guides is in the middle of a rail span. The forces in the support brackets are higher when one of the roller guides is on or near a support.
2. The code specifies a clearance of no more than 3/16 inch at the restraining plates required to be installed at each roller guide assembly. Depending upon the clearance, there can be frequent impacting contacts between the restraining plates and guide rails. The stresses in the rails and forces in the bracket can be lowered by reducing this clearance. This will, however, cause more frequent metal contacts during an earthquake but, perhaps, these

annoying noises due to metal contact can be tolerated for a few seconds of earthquake duration.

3. The code also specifies a maximum clearance of ½ inch between the counterweight frame and the rails. Again, depending upon the intensity of the motion and the clearance used, there can be several impacting contacts between the frame and the rails. For higher intensities of ground motion, a smaller clearance can help reduce the stress in the rails, but not without frequent impacting contacts and increased forces in the bracket supports.
4. As one would expect, the heavier rails would experience lower stresses than the lighter rails, and thus would perform better during earthquakes.
5. Although the general trend of stresses in the rails and forces in the bracket remains same qualitatively for different input motion, the detailed response characteristics can be quite different with large variability in the values. This suggests that for a realistic performance assessment of the system in a seismic environment, several different motion that can be expected at the site must be considered.
6. As one would expect, the stresses and forces in the system would increase with increasing intensity of the ground motion. However, because of the nonlinear effects introduced by the clearance restraints, the stress and force do not increase in direct proportion to the input motion intensity. The nonlinearity due to clearance restraints helps the rails by reducing the stresses, especially for higher intensities of the motion, but significantly increase the forces on the brackets.
7. In general, it is quite difficult to predict the magnitude of the maximum stress and the location where it would occur without carrying out a detailed analysis. The earthquake intensity level, clearance limits, location of the counterweight in the building, dynamic characteristics of the input and the system interact in a rather complex manner to affect the response of the system. Thus, explicit consideration of the nonlinearities with different earthquake motions and different system parameters is essential to evaluate the performance of an elevator system in a seismic environment.

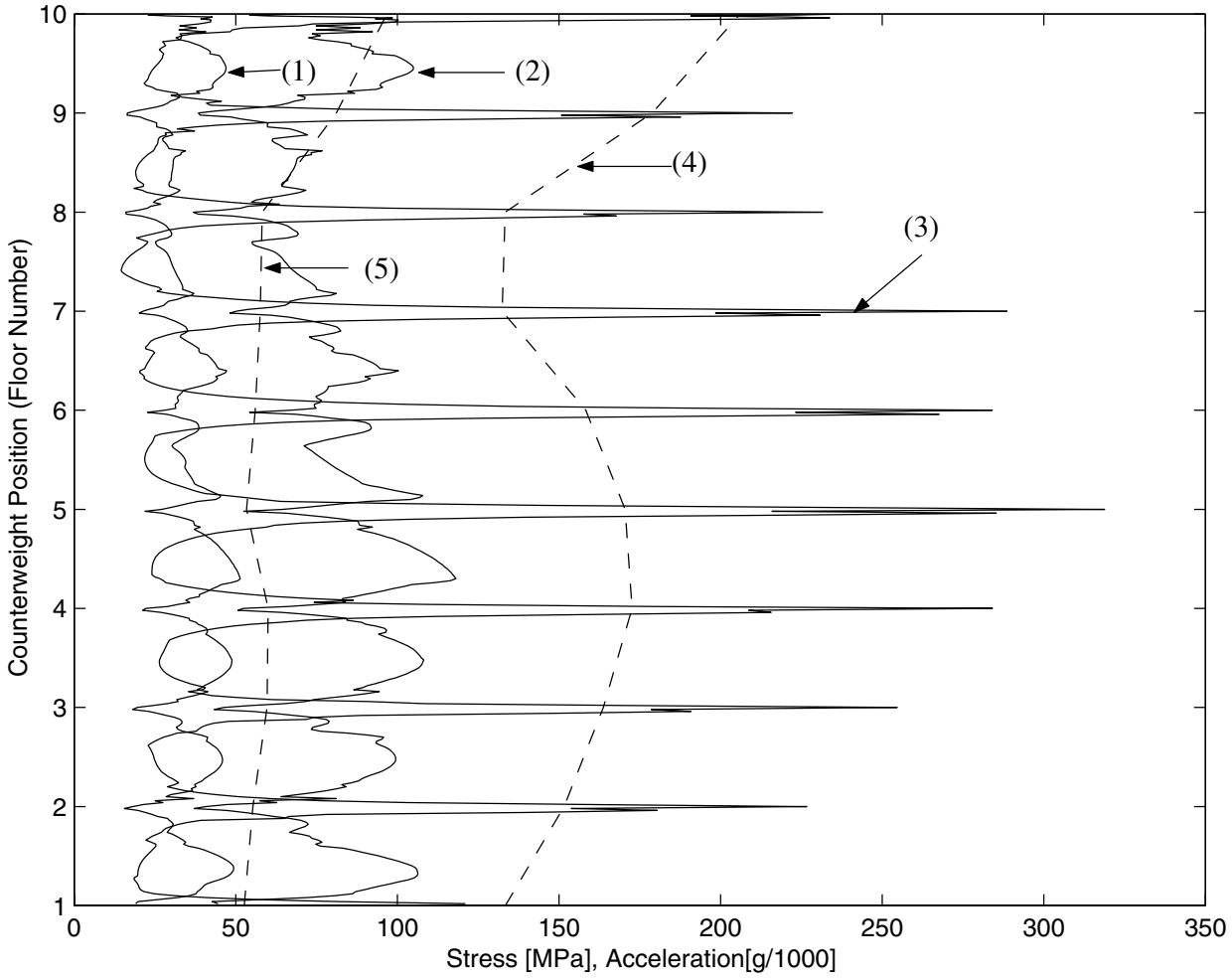

FIGURE 3-7 Maximum (1) Stress in the Rail Flange, (2) Rail Web, and (3) Brackets, (4) Floor Acceleration X-Direction, and (5) Floor Acceleration Y-Direction As A Function of Counterweight Position Along the Building Height 10-Story Building; Northridge Earthquake 0.1g

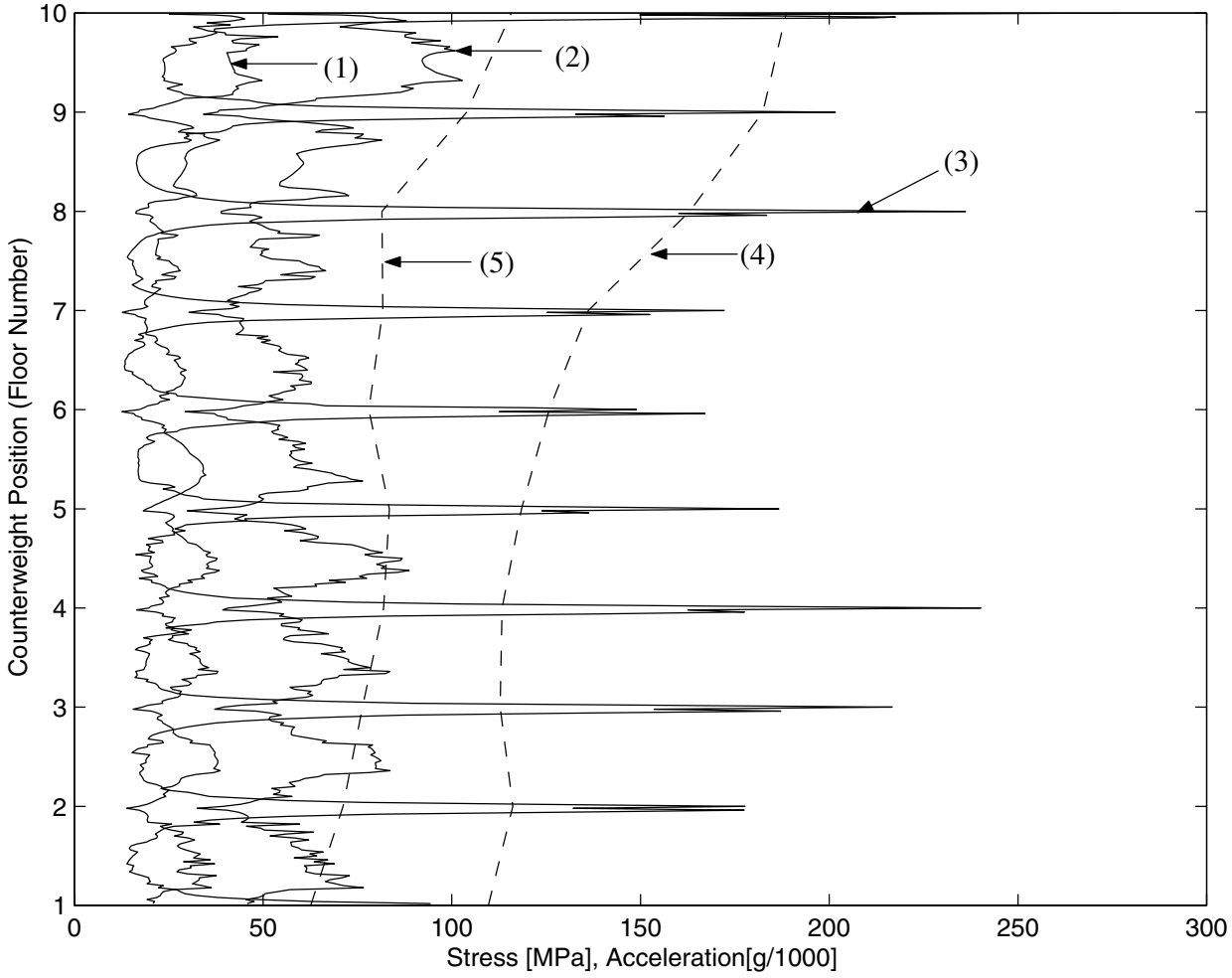

FIGURE 3-8 Maximum (1) Stress in the Rail Flange, (2) Rail Web, and (3) Brackets, (4) Floor Acceleration X-Direction, and (5) Floor Acceleration Y-Direction As A Function of Counterweight Position Along the Building Height 10-Story Building; El Centro Earthquake: 0.1g

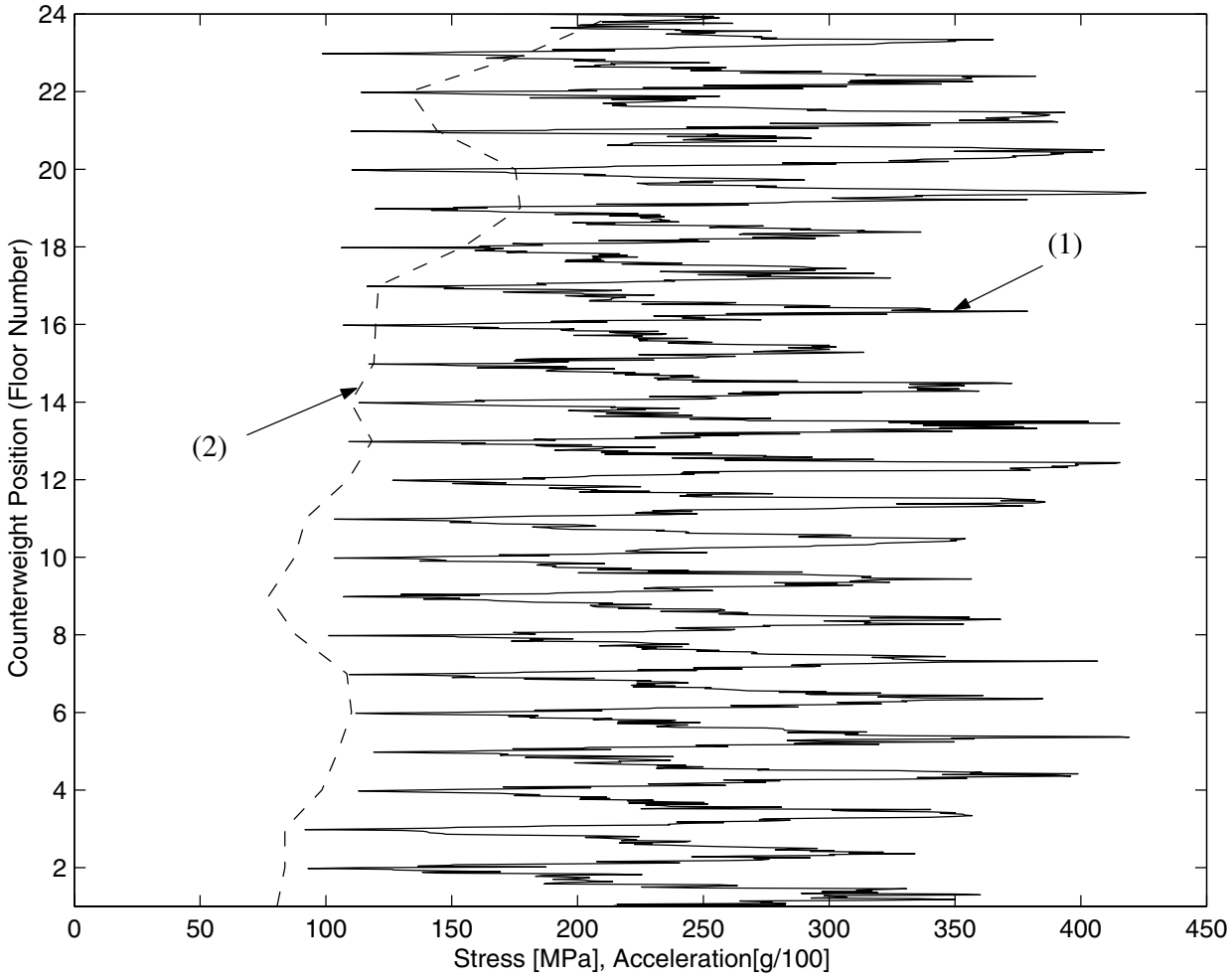

FIGURE 3-9 Maximum (1) Stress in the Rail Web and (2) Floor Acceleration X-Direction As A Function of Counterweight Position Along the Building Height 24-Story Building; Northridge Earthquake 0.843g

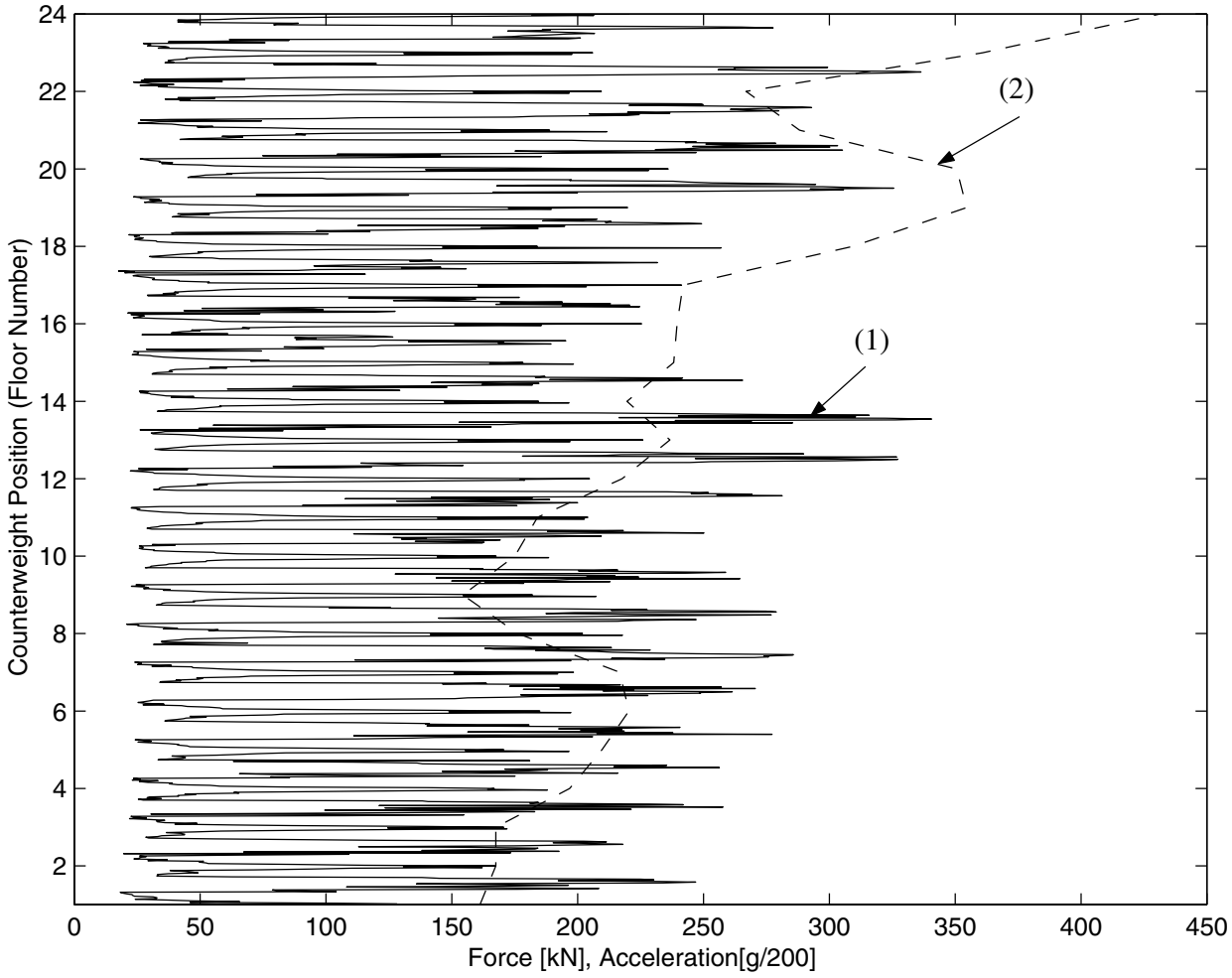

FIGURE 3-10 Maximum (1) In-Plane Force in the Brackets and (2) Floor Acceleration X-Direction As A Function of Counterweight Position Along the Building Height
24-Story Building; Northridge Earthquake 0.843g

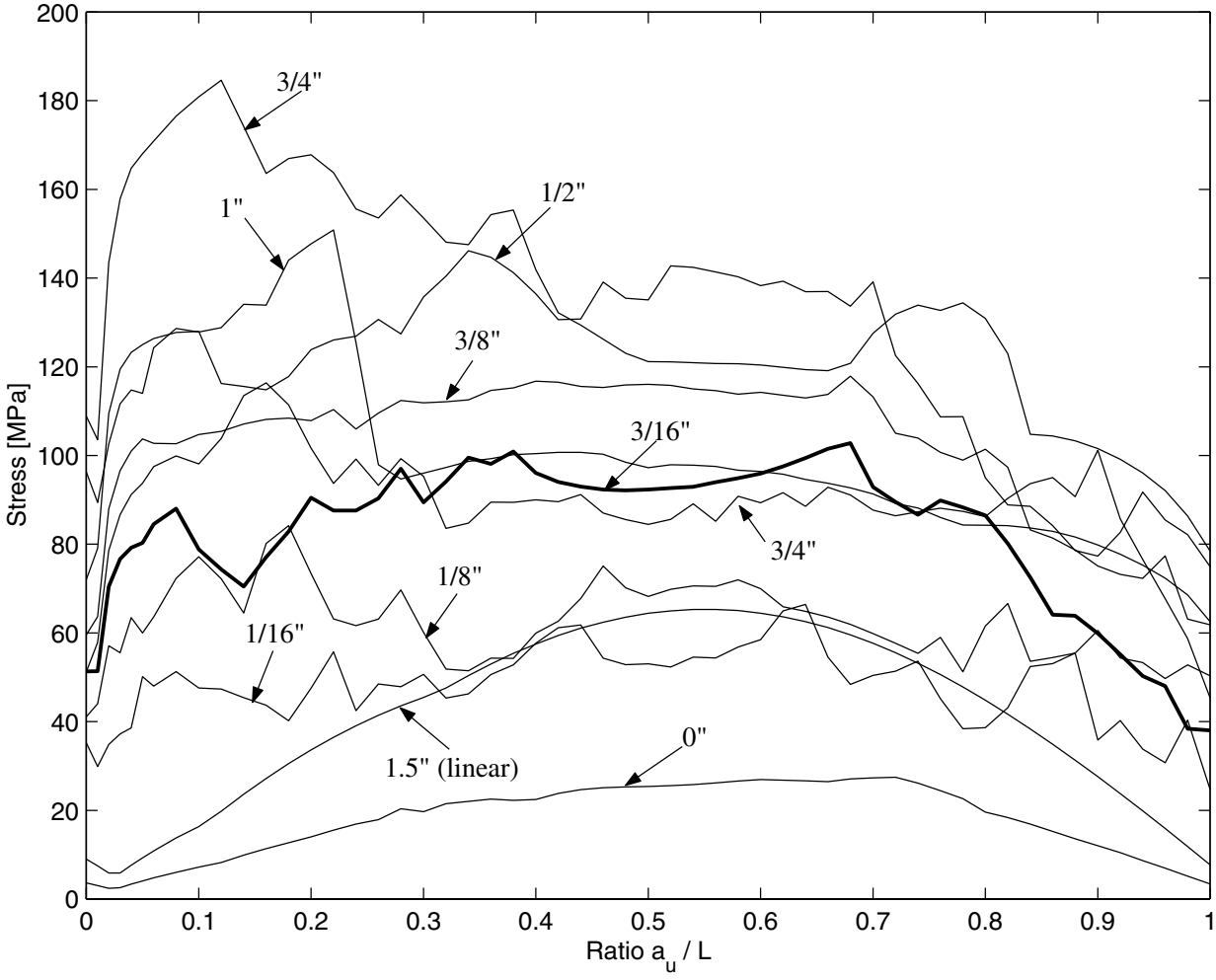

FIGURE 3-11 Maximum Stress in the Rail As A Function of Counterweight Position for Different Values of the Clearance at Restraining Plates El Centro Earthquake 0.1g

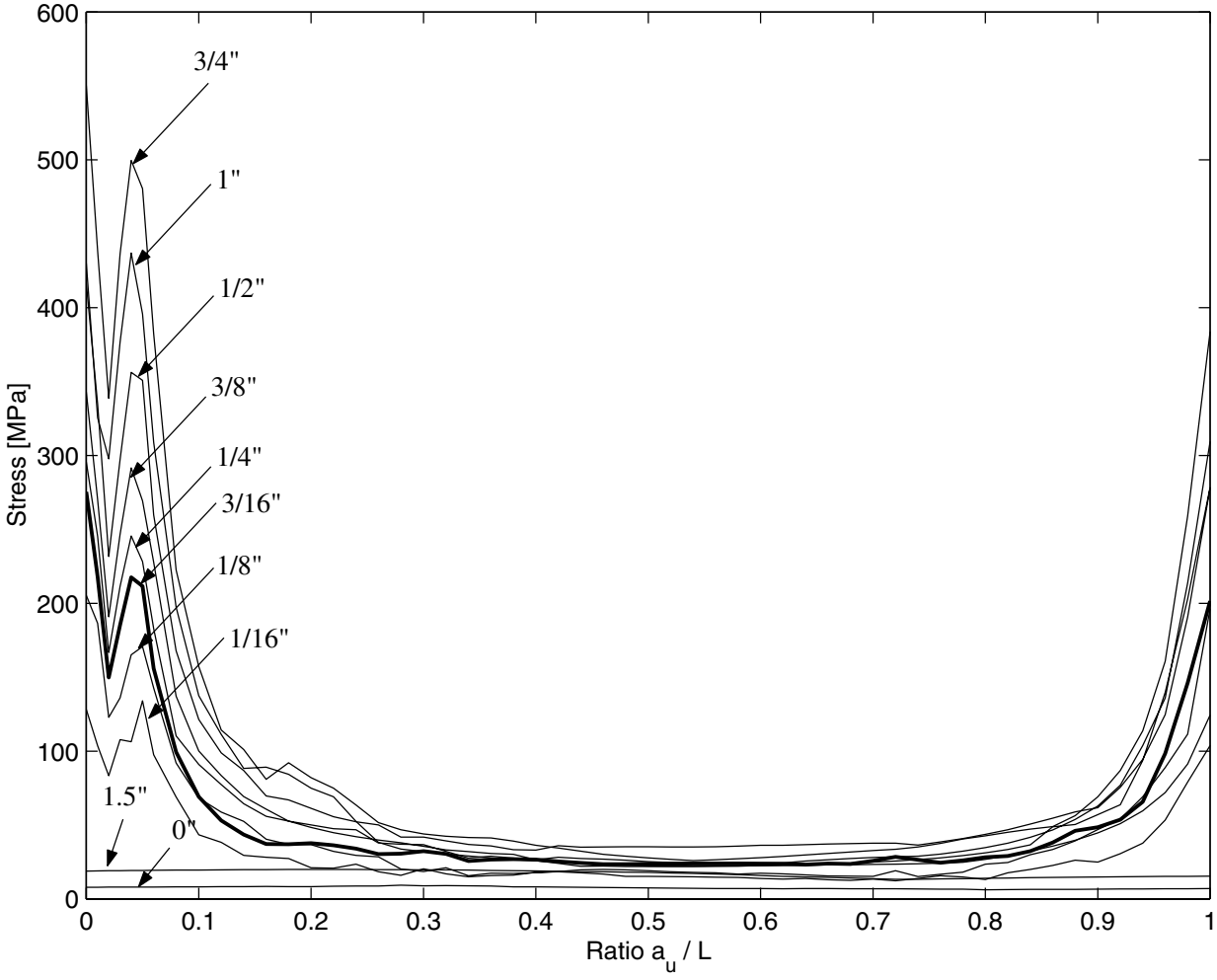

FIGURE 3-12 Maximum Stress in the Brackets As A Function of Counterweight Position for Different Values of Clearances at the Restraining Plate El Centro 0.1g

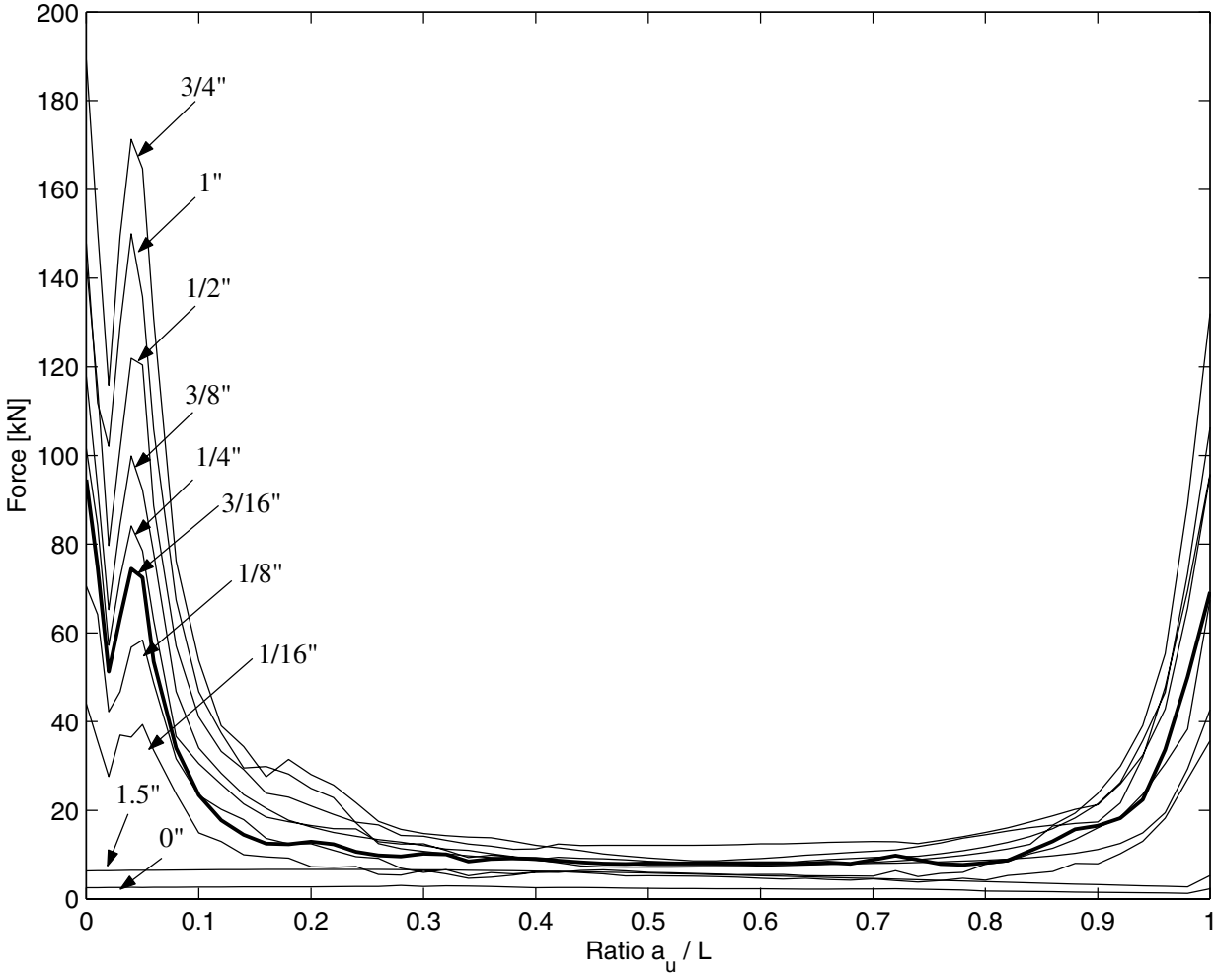

FIGURE 3-13 Maximum In-Plane Force in the Brackets As A Function of the Counterweight Position for Different Values of Clearances at the Restraining Plates El Centro 0.1g

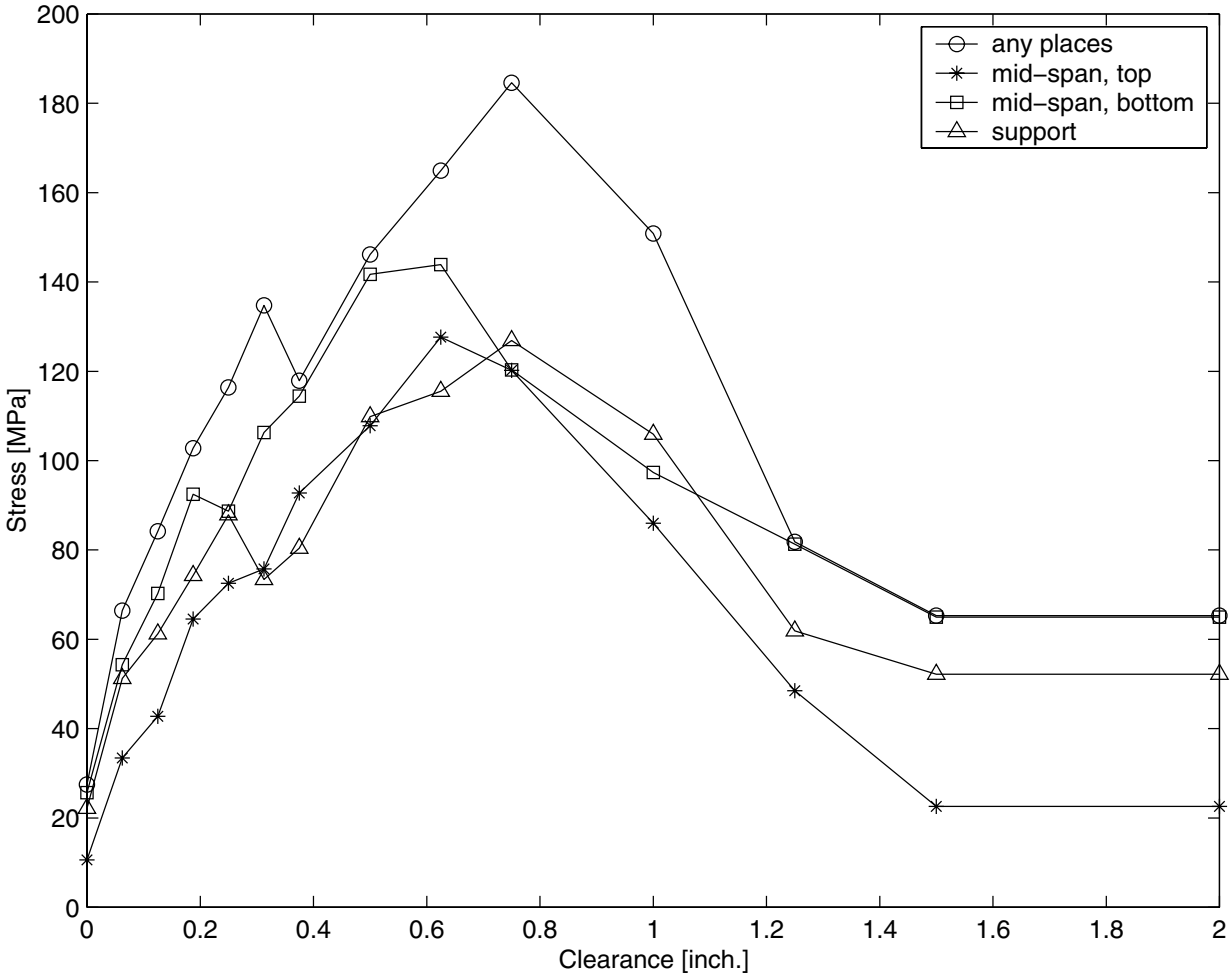

FIGURE 3-14 Maximum Stress in the Rail As A Function of Clearance at the Restraining Plates
El Centro Earthquake 0.1g

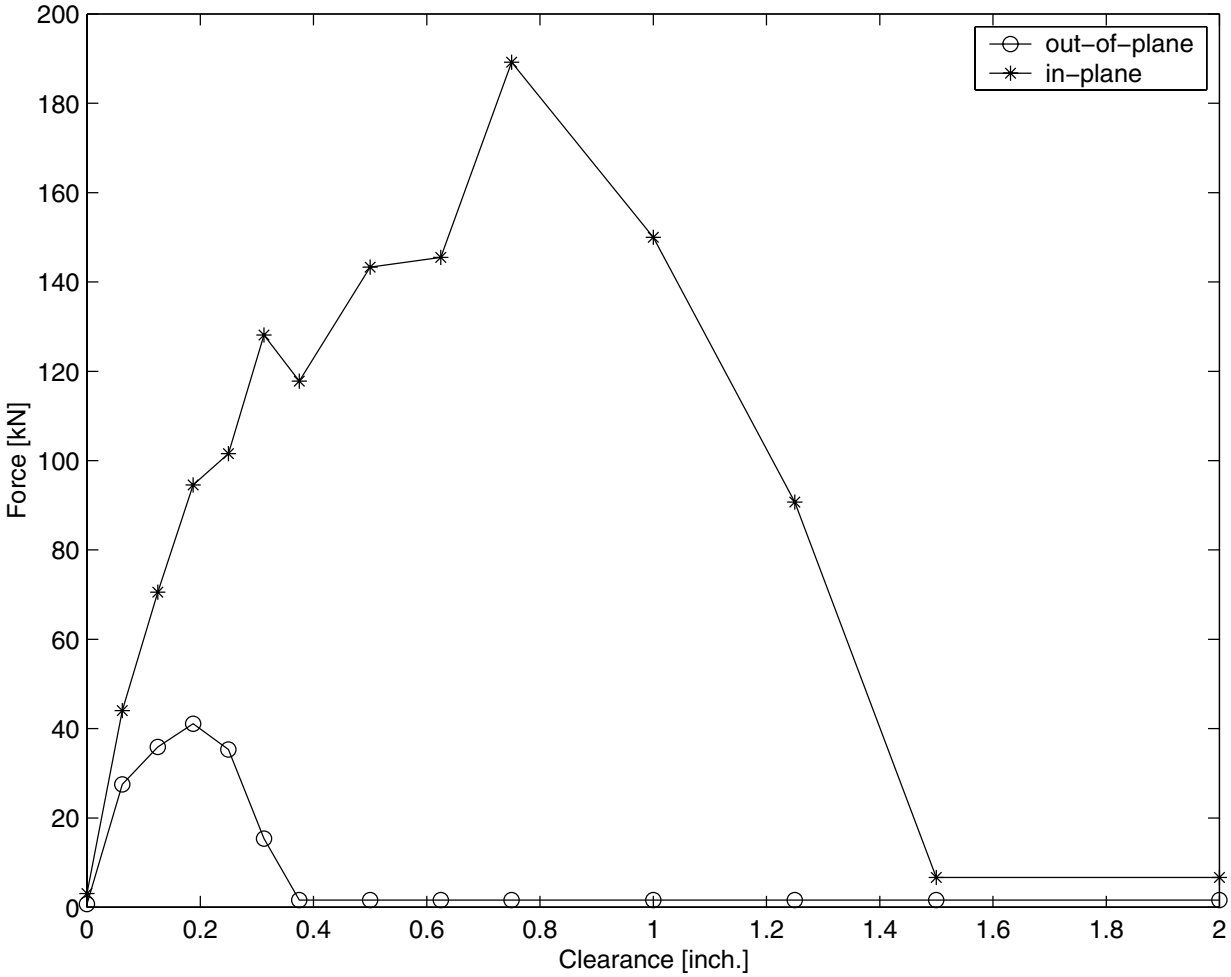

FIGURE 3-15 Maximum Force in the Brackets As A Function of Clearance at the Restraining Plates
El Centro Earthquake 0.1g

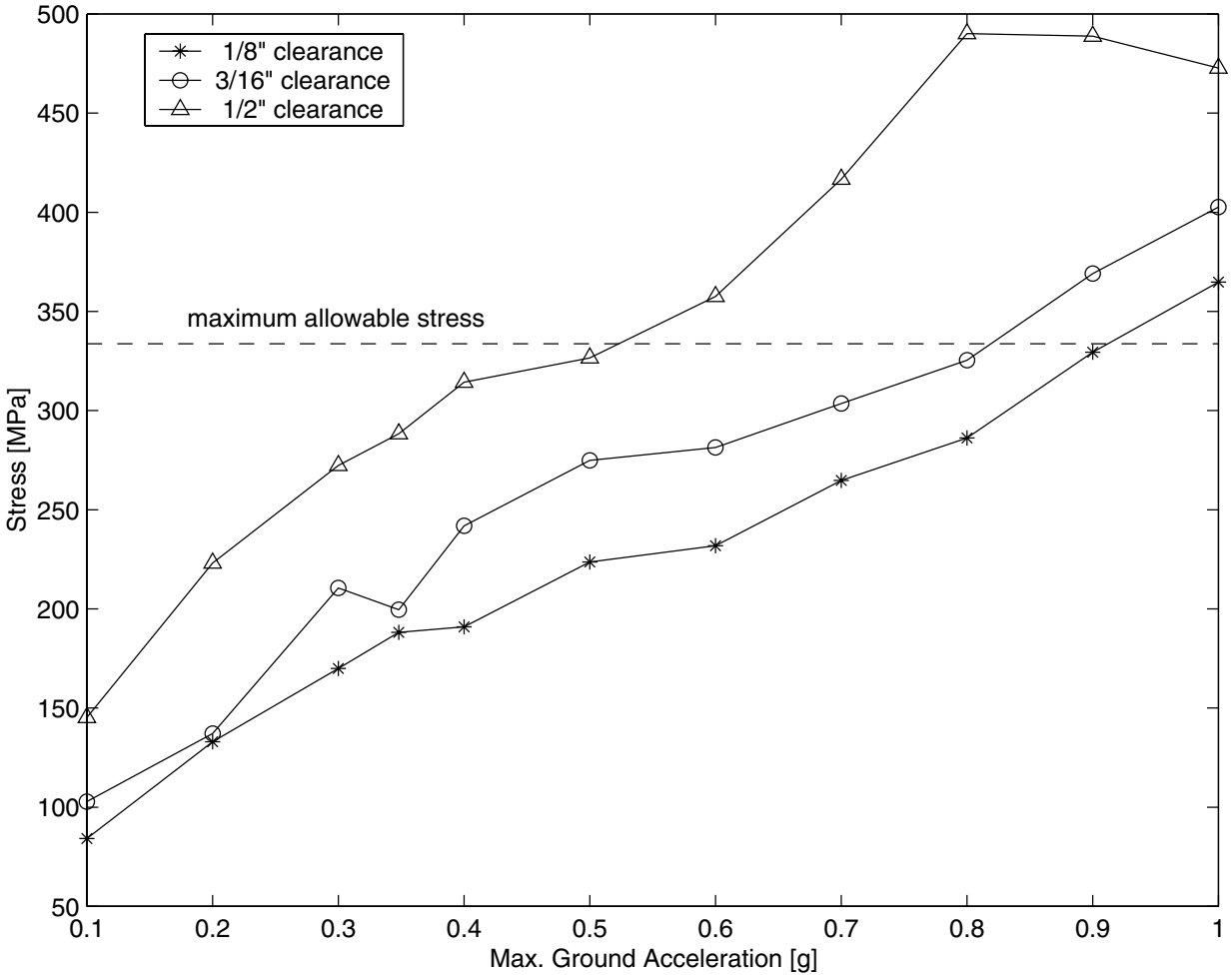

FIGURE 3-16 Maximum Stress in the Rail As A Function of Maximum Ground Acceleration for Different Clearance Values El Centro Earthquake

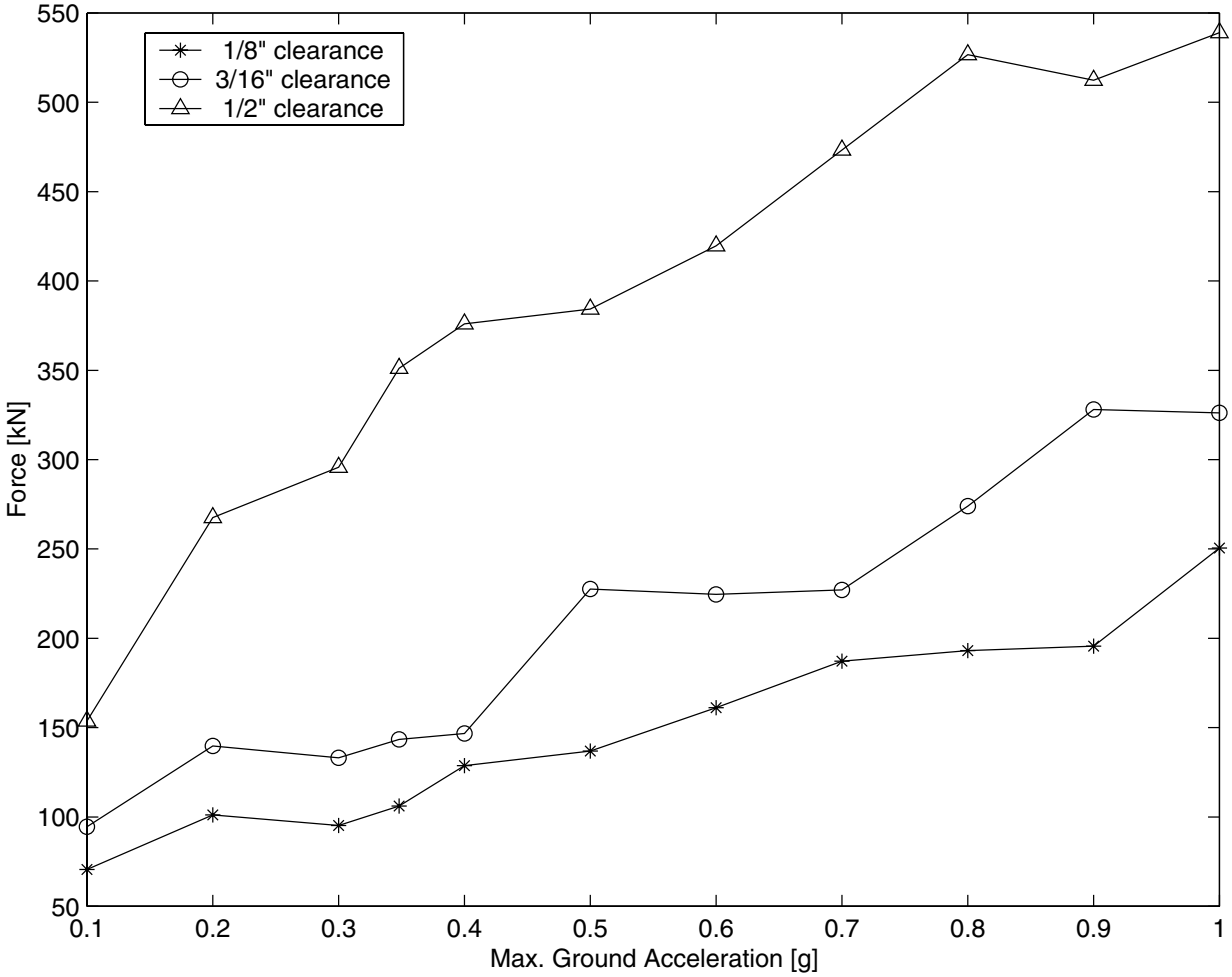

FIGURE 3-17 Maximum Inplane Forces in the Brackets As A Function of Maximum Ground Acceleration for Different Clearance Values El Centro Earthquake

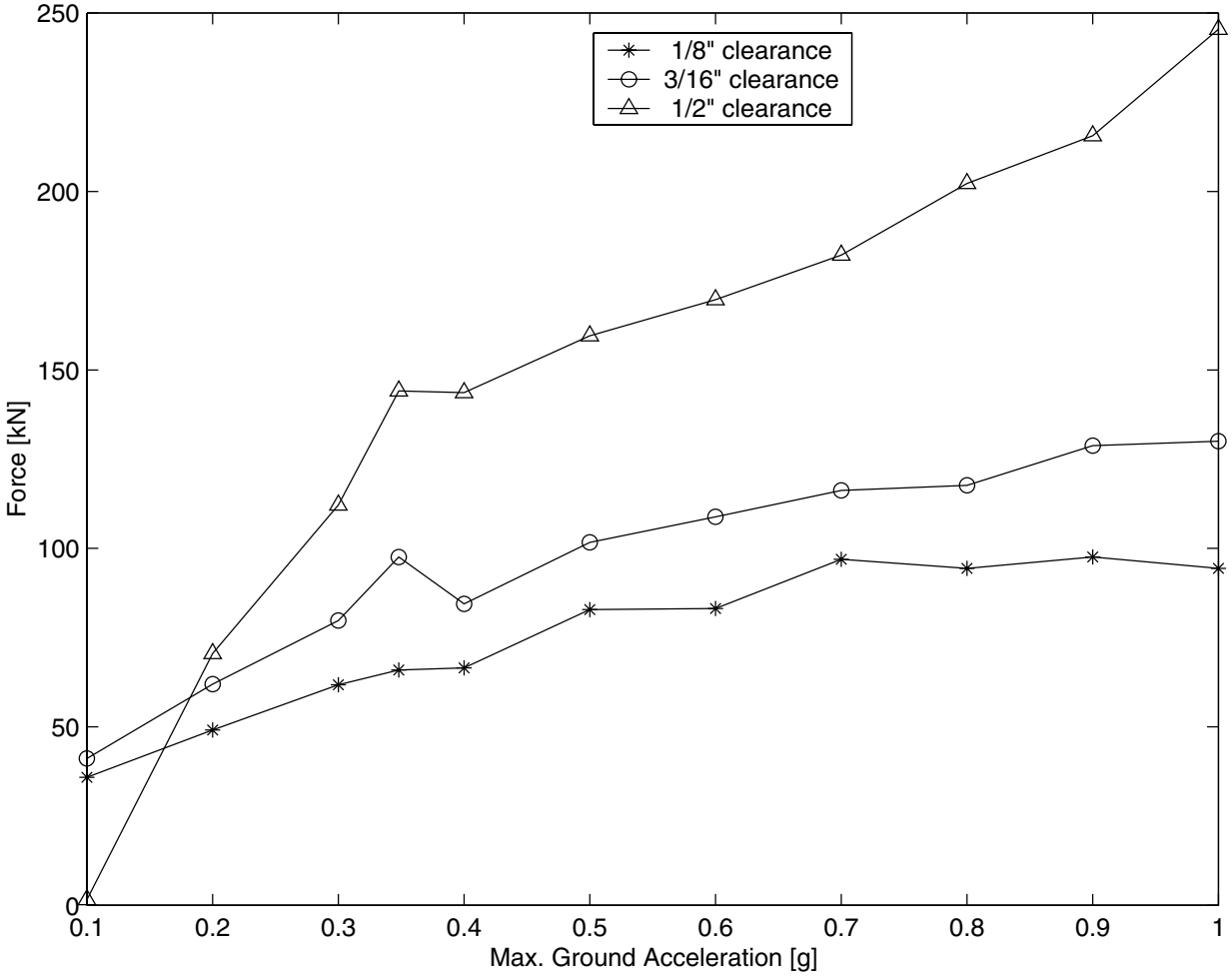

FIGURE 3-18 Maximum Out-of-Plane Forces in the Brackets As A Function of Maximum Ground Acceleration for Difference Clearance Values El Centro Earthquake

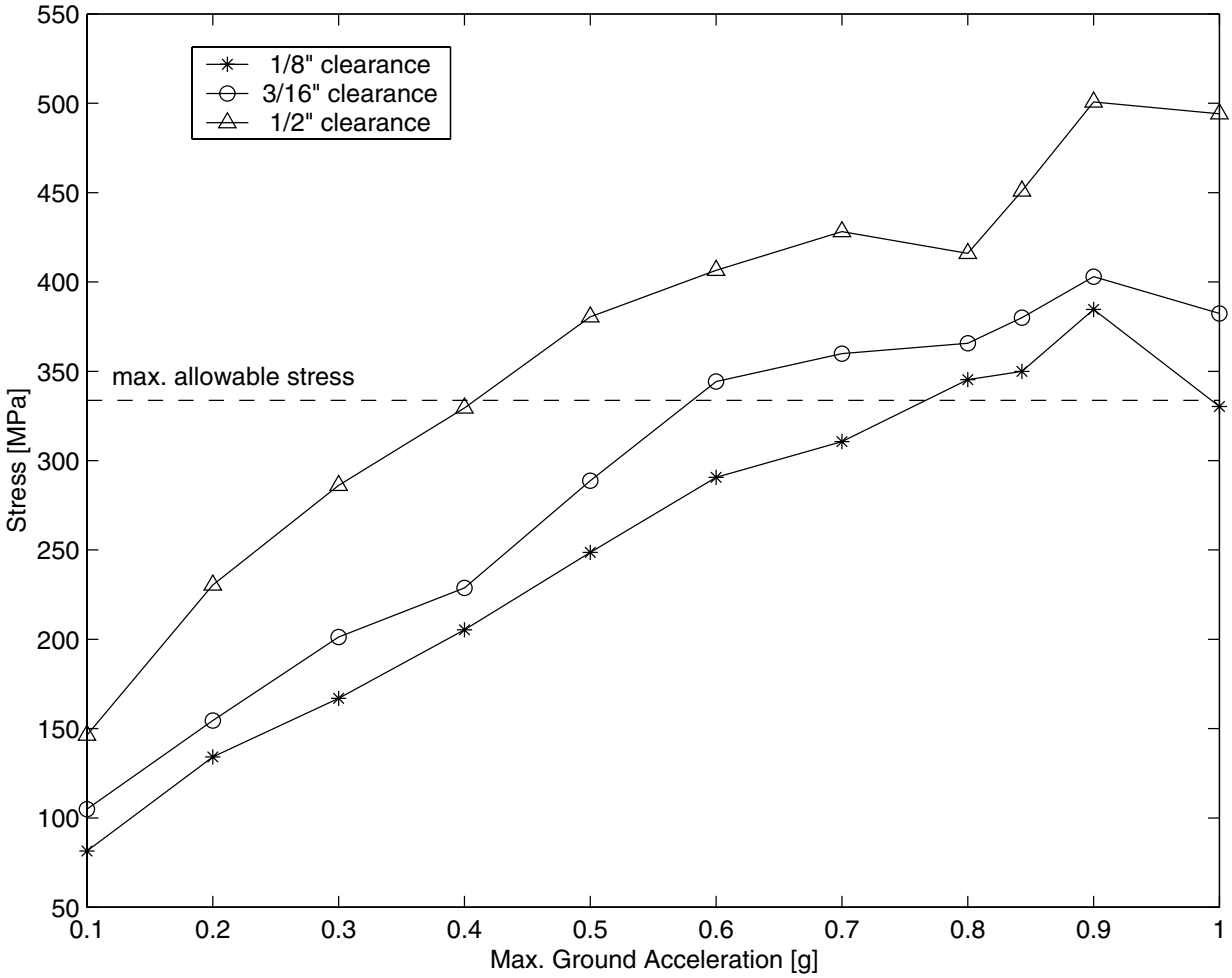

FIGURE 3-19 Maximum Stress in the Rail As A Function of Maximum Ground Acceleration for Different Clearance Values Northridge Earthquake

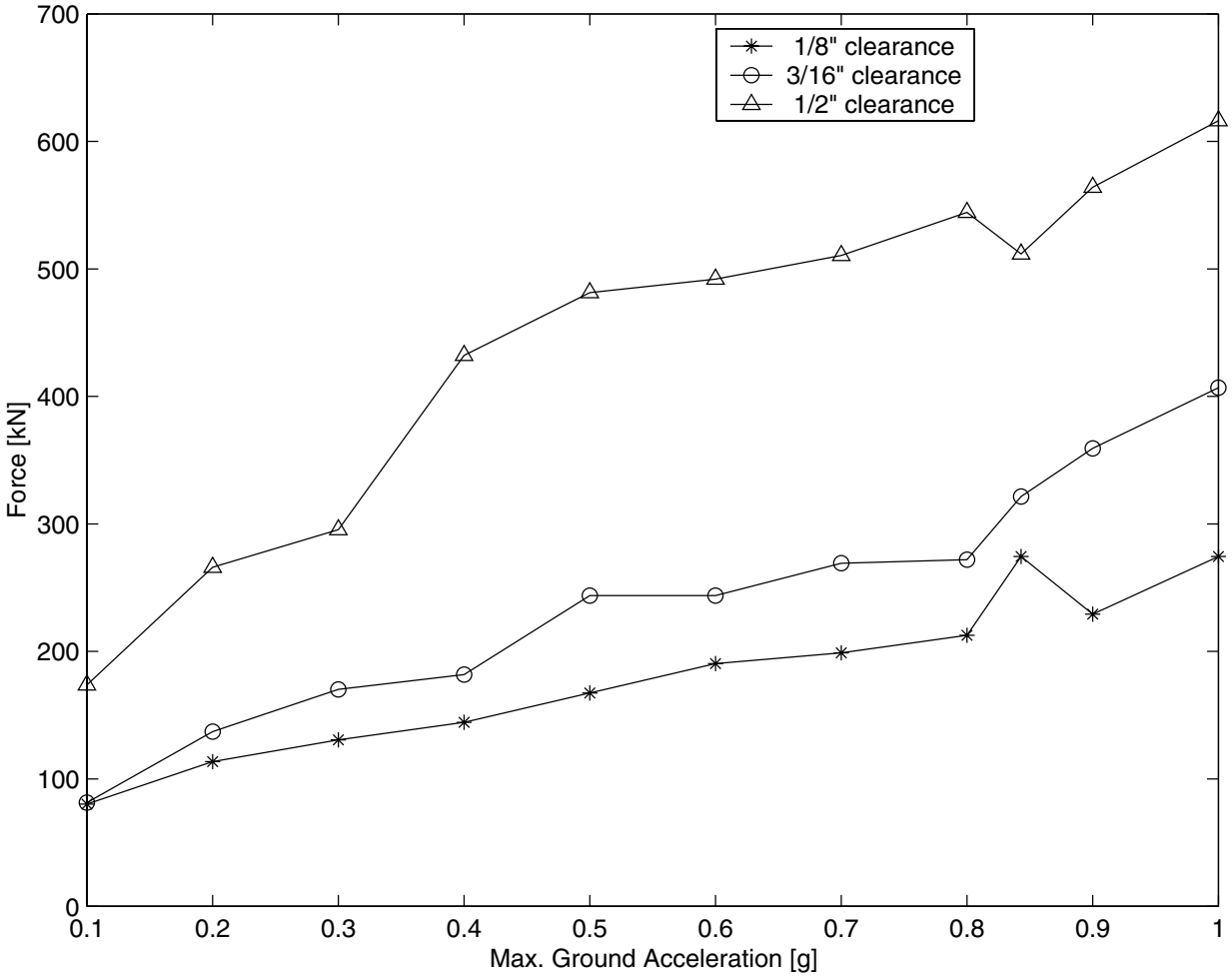

FIGURE 3-20 Maximum Inplane Forces in the Brackets As A Function of Maximum Ground Acceleration for Different Clearance Values Northridge Earthquake

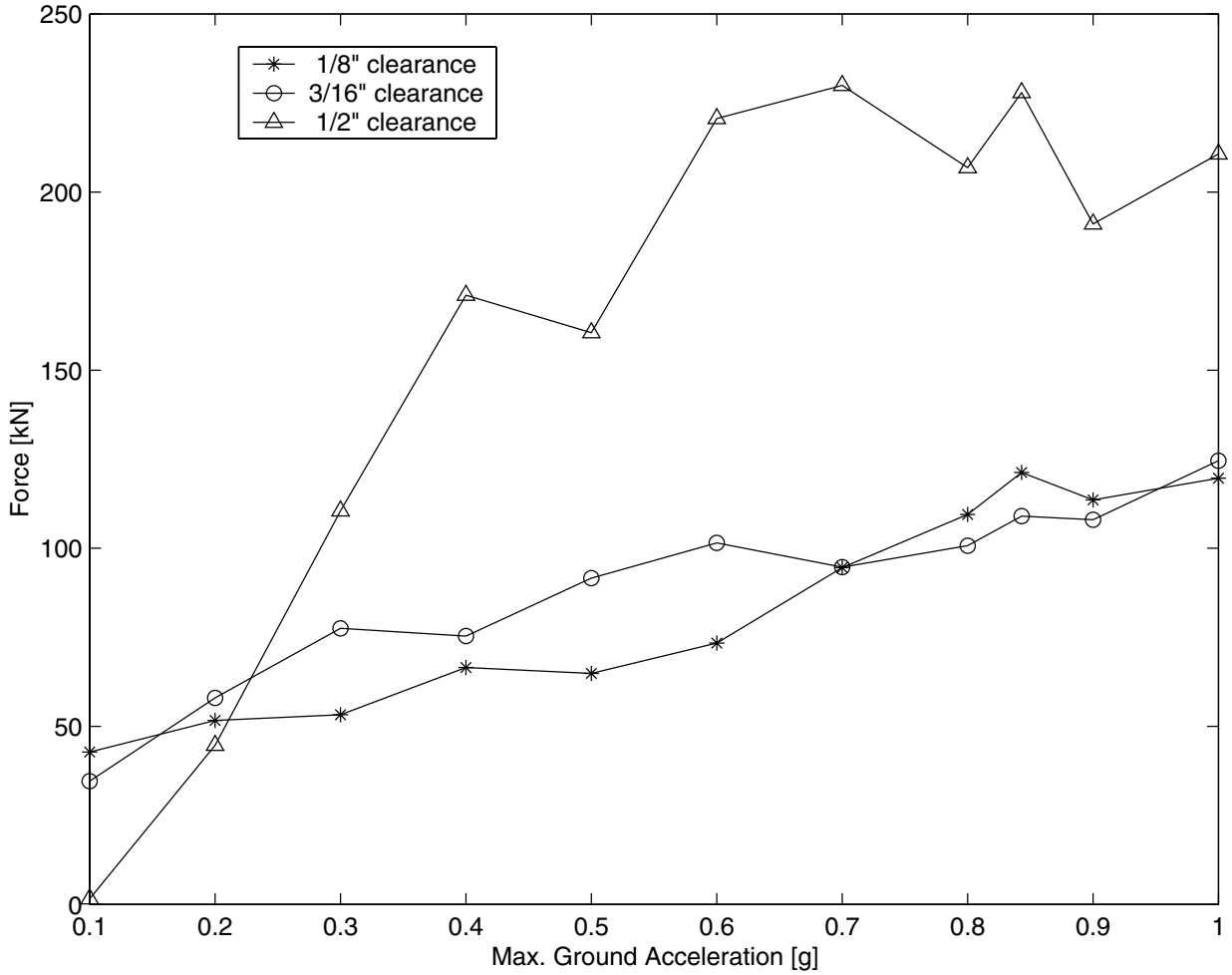

FIGURE 3-21 Maximum Out-of-Plane Forces in the Brackets As A Function of Maximum Ground Acceleration for Different Clearance Values Northridge Earthquake

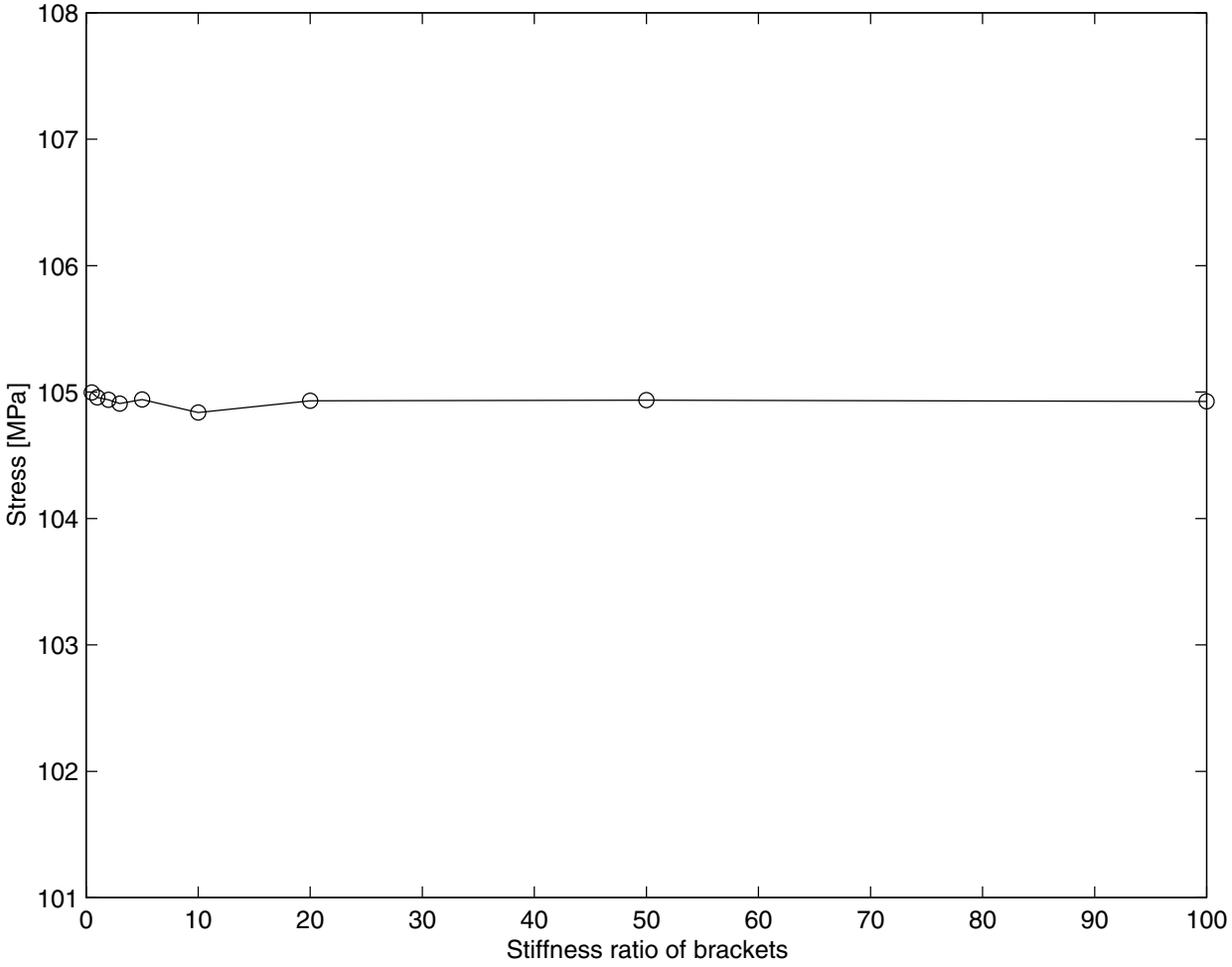

FIGURE 3-22 Maximum Stress in the Rail As A Function of the Bracket Stiffness Ratio, Northridge 0.1g

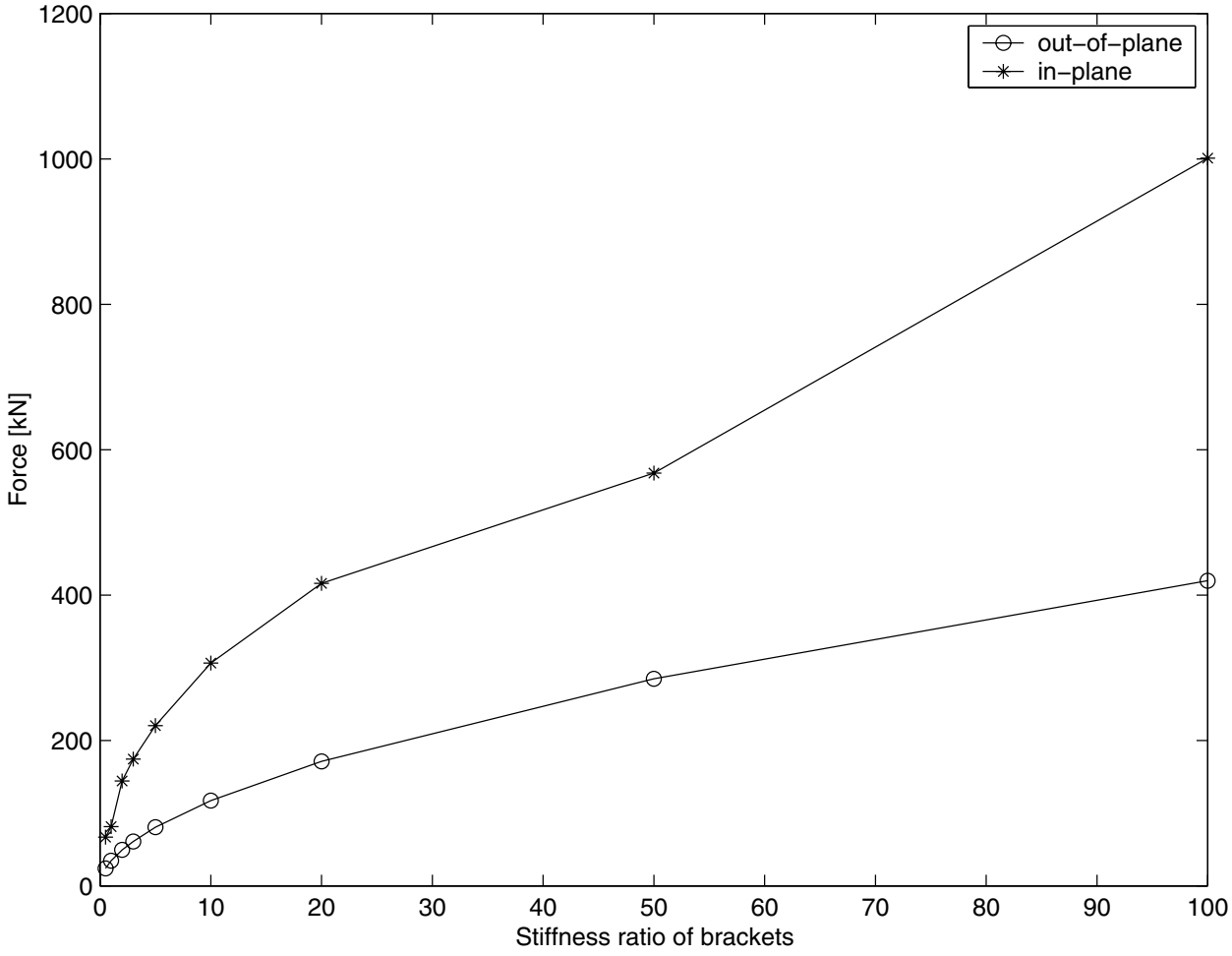

FIGURE 3-23 Maximum Forces in the Brackets As A Function of the Bracket Stiffness Ratio, Northridge Earthquake 0.1g

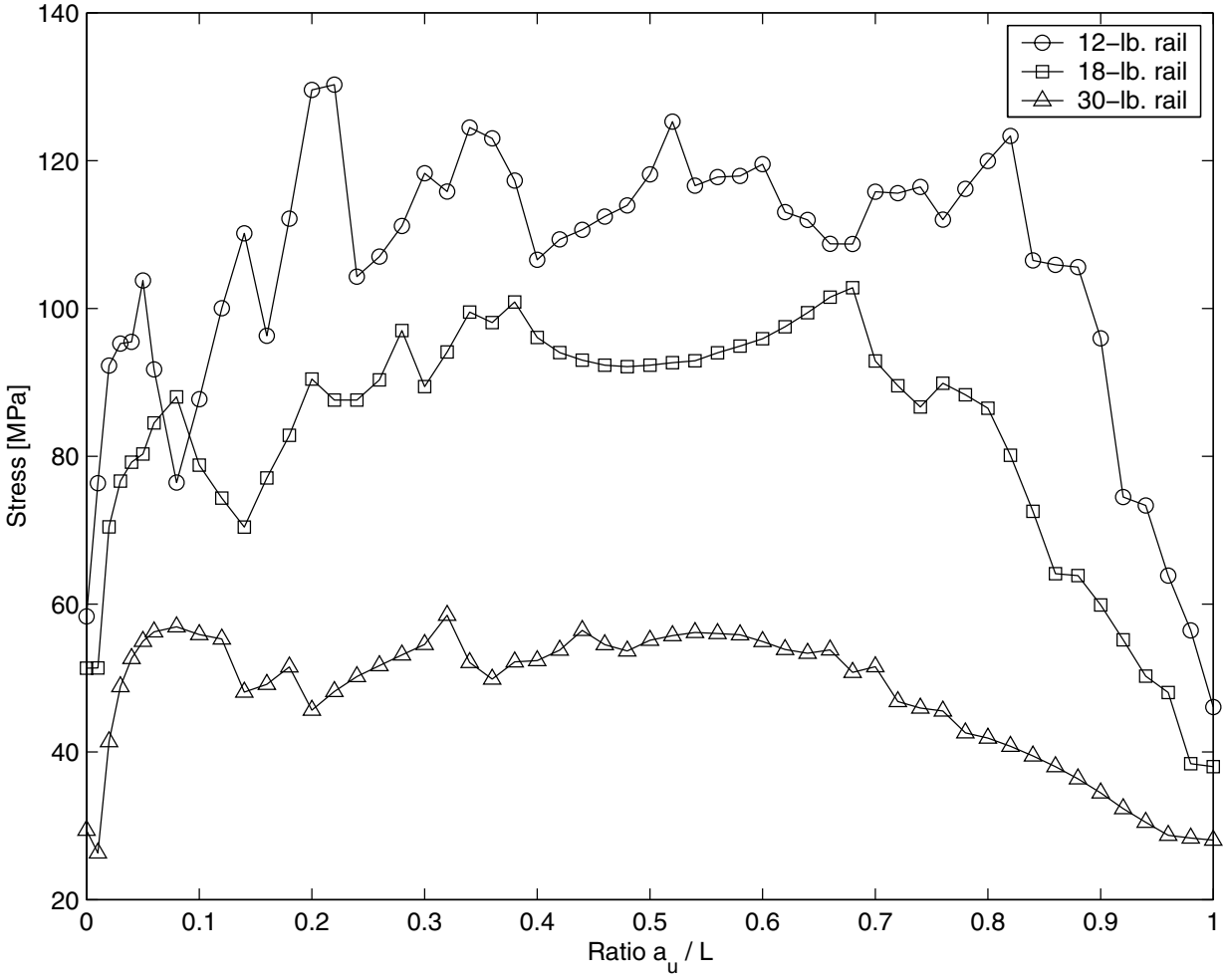

FIGURE 3-24 Maximum Stress in Different Rails As A Function of Counterweight Position, El Centro Earthquake 0.1g

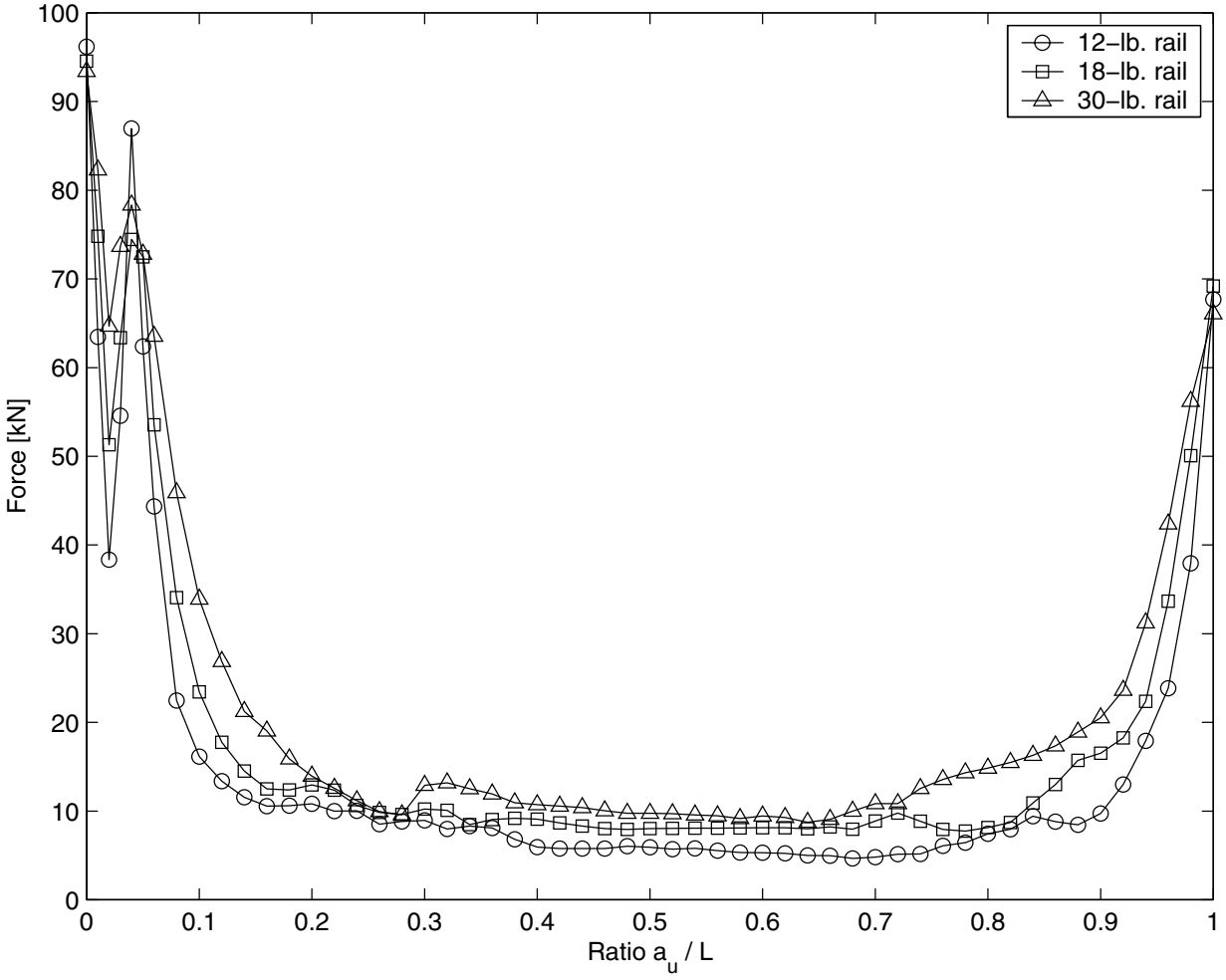

FIGURE 3-25 Maximum Inplane Force in the Brackets for Different Rails As A Function of Counterweight Position
El Centro Earthquake 0.1g

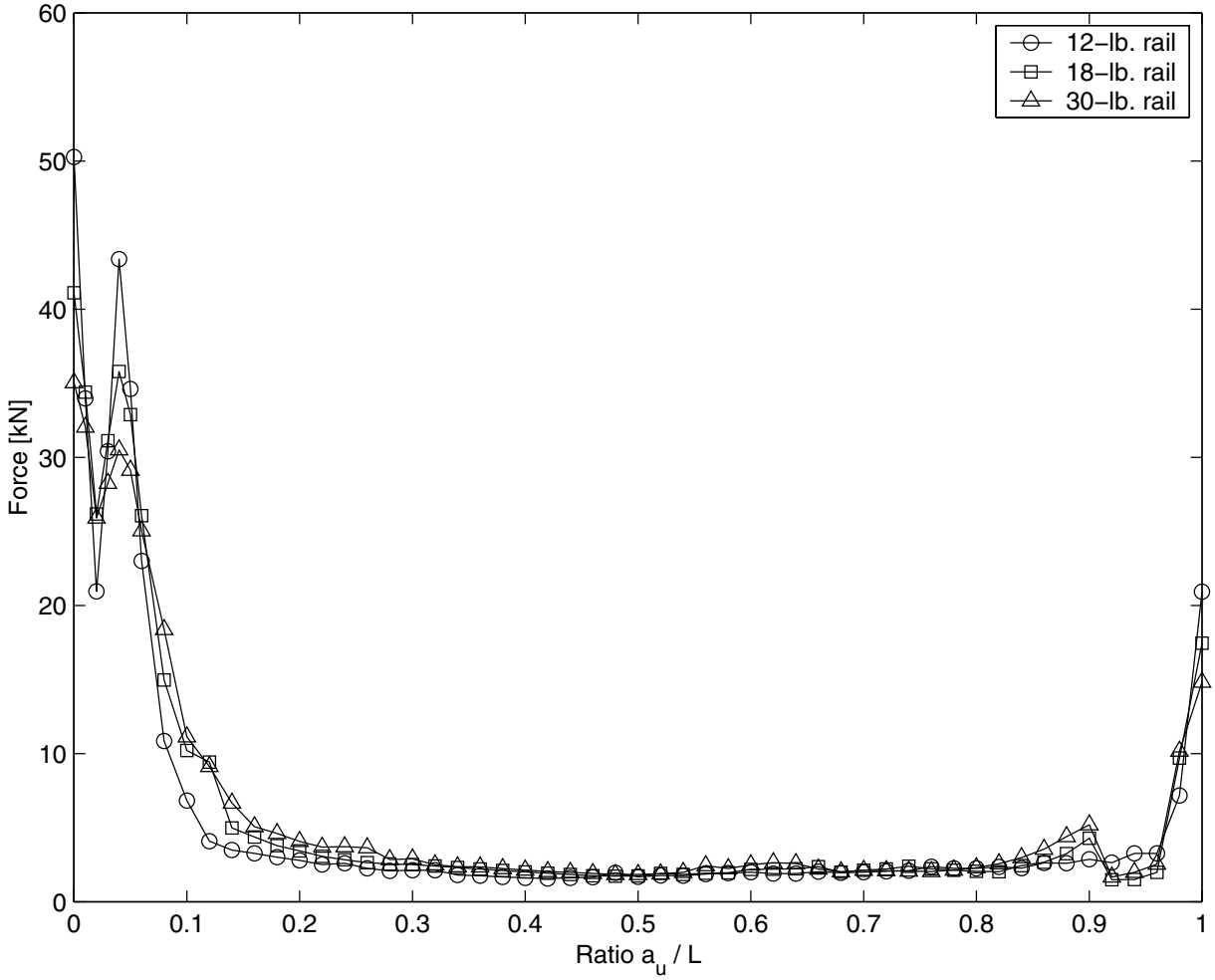

FIGURE 3-26 Maximum Out-of-Plane Force in the Bracket for Different Rail Sizes As A Function of Counterweight Position El Centro Earthquake 0.1g

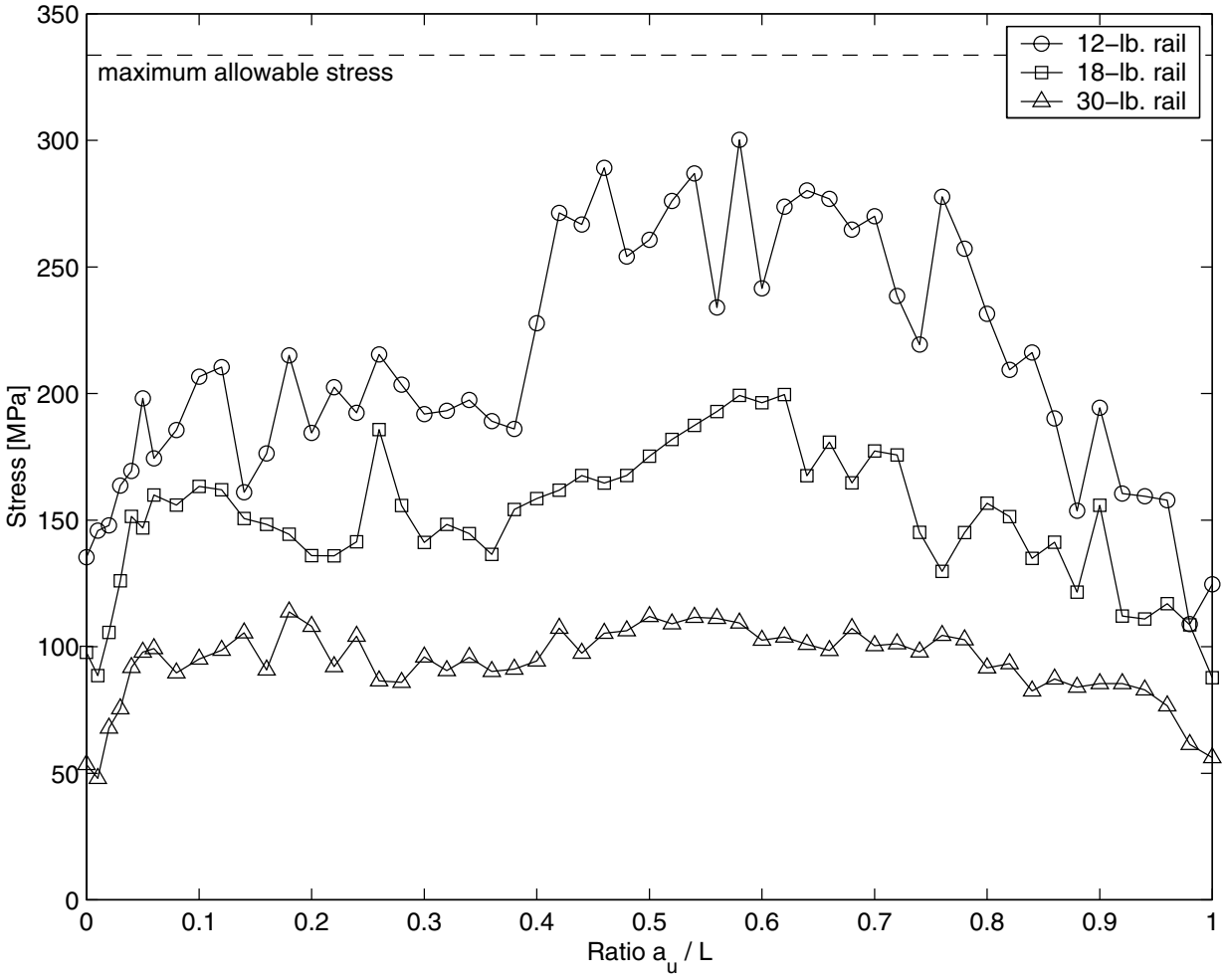

FIGURE 3-27 Maximum Stress in Different Rails As A Function of Counterweight Position
As Recorded El Centro (0.348g)

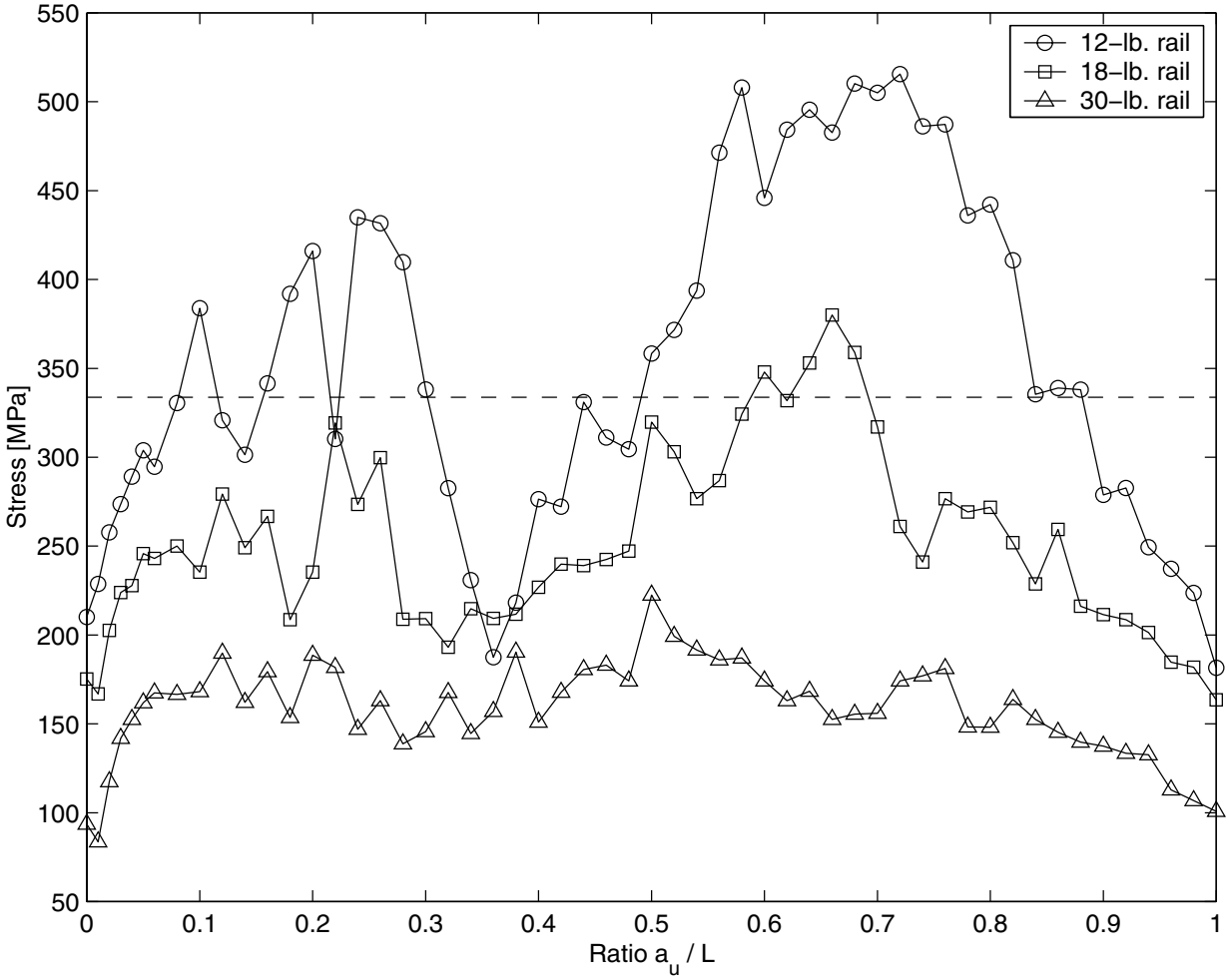

FIGURE 3-28 Maximum Stress in Different Rails As A Function of Counterweight Position
As Recorded Northridge Earthquake 0.843g

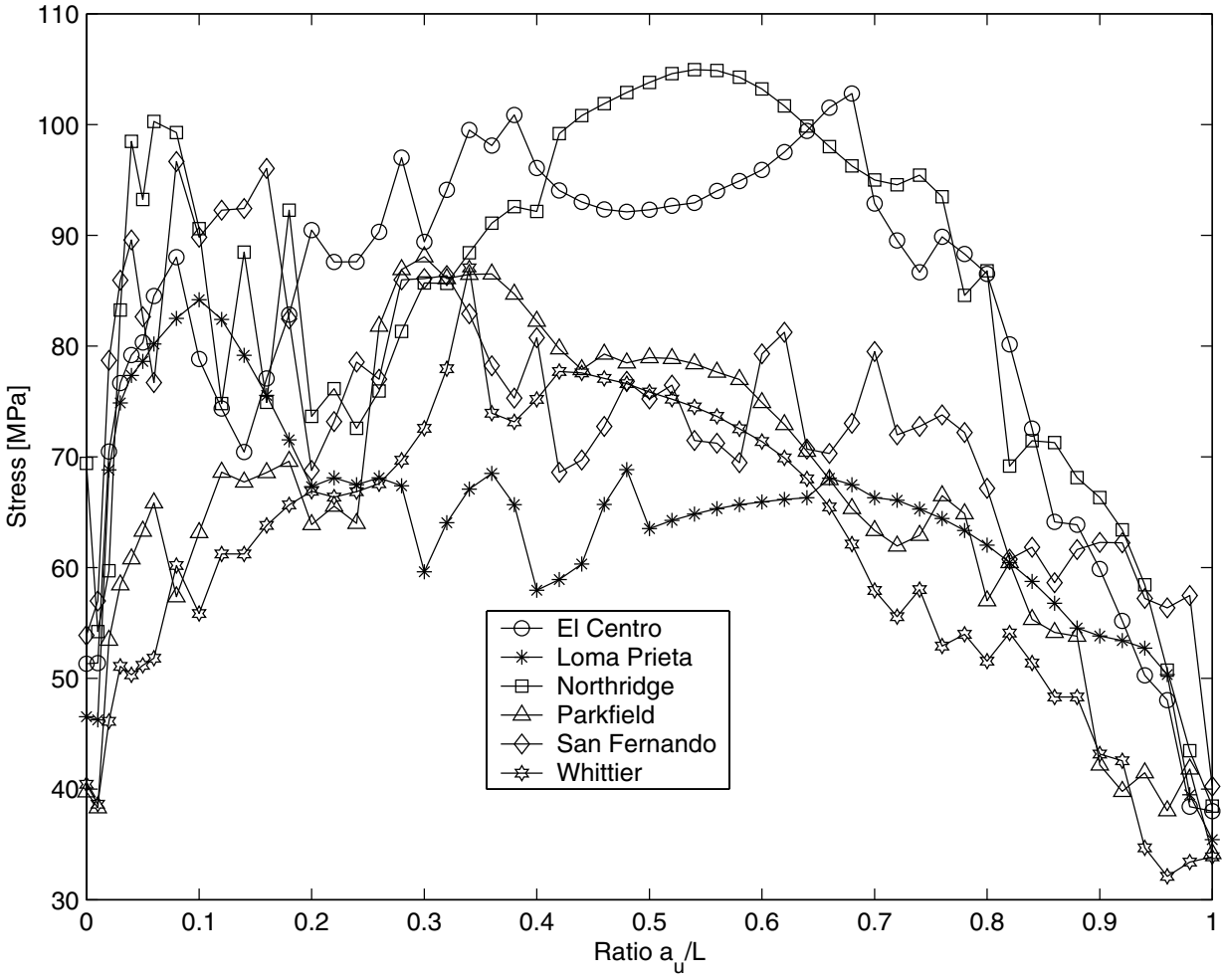

FIGURE 3-29 Maximum Stress in the Rails for Different Base Inputs As A Function of Counterweight Position
All Motion Normalized To 0.1g

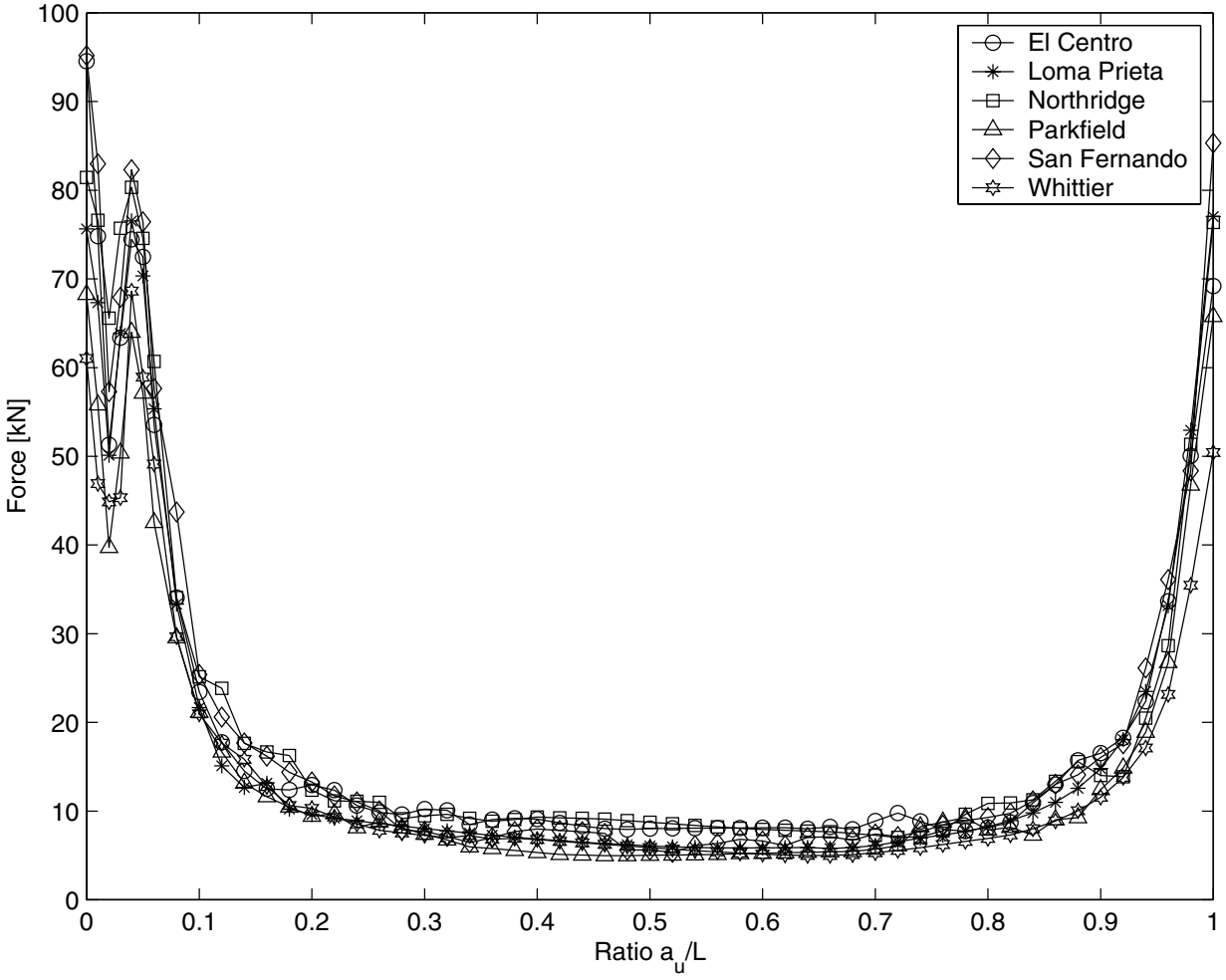

FIGURE 3-30 Maximum Inplane Force in Brackets for Different Inputs As A Function of Counterweight Position All Motions Normalized To 0.1g

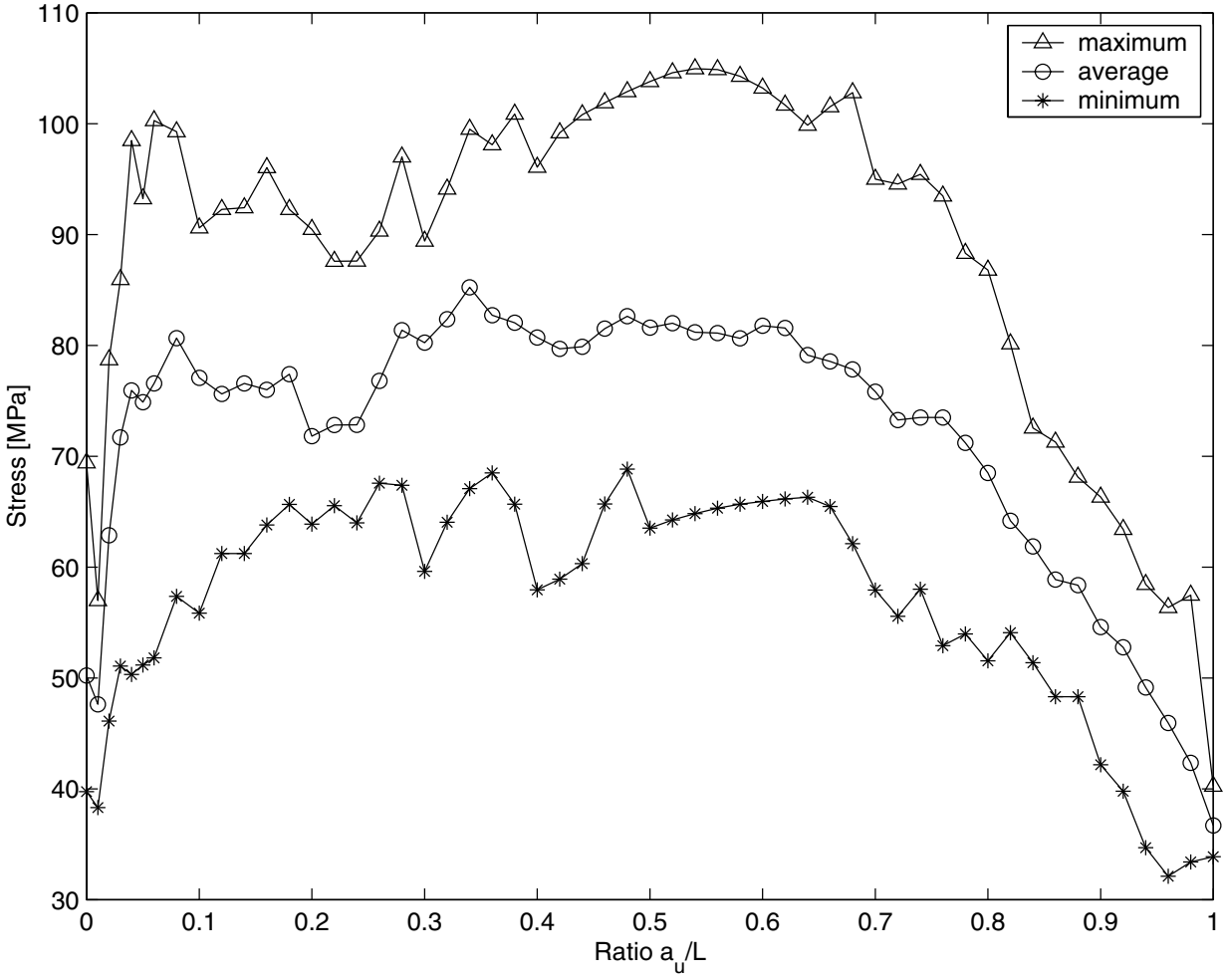

FIGURE 3-31 Mean, Maximum And Minimum Values of the Stress Shown in Figure 3-29 for Different Inputs As A Function of Counterweight Position All Motions Normalized To 0.1g

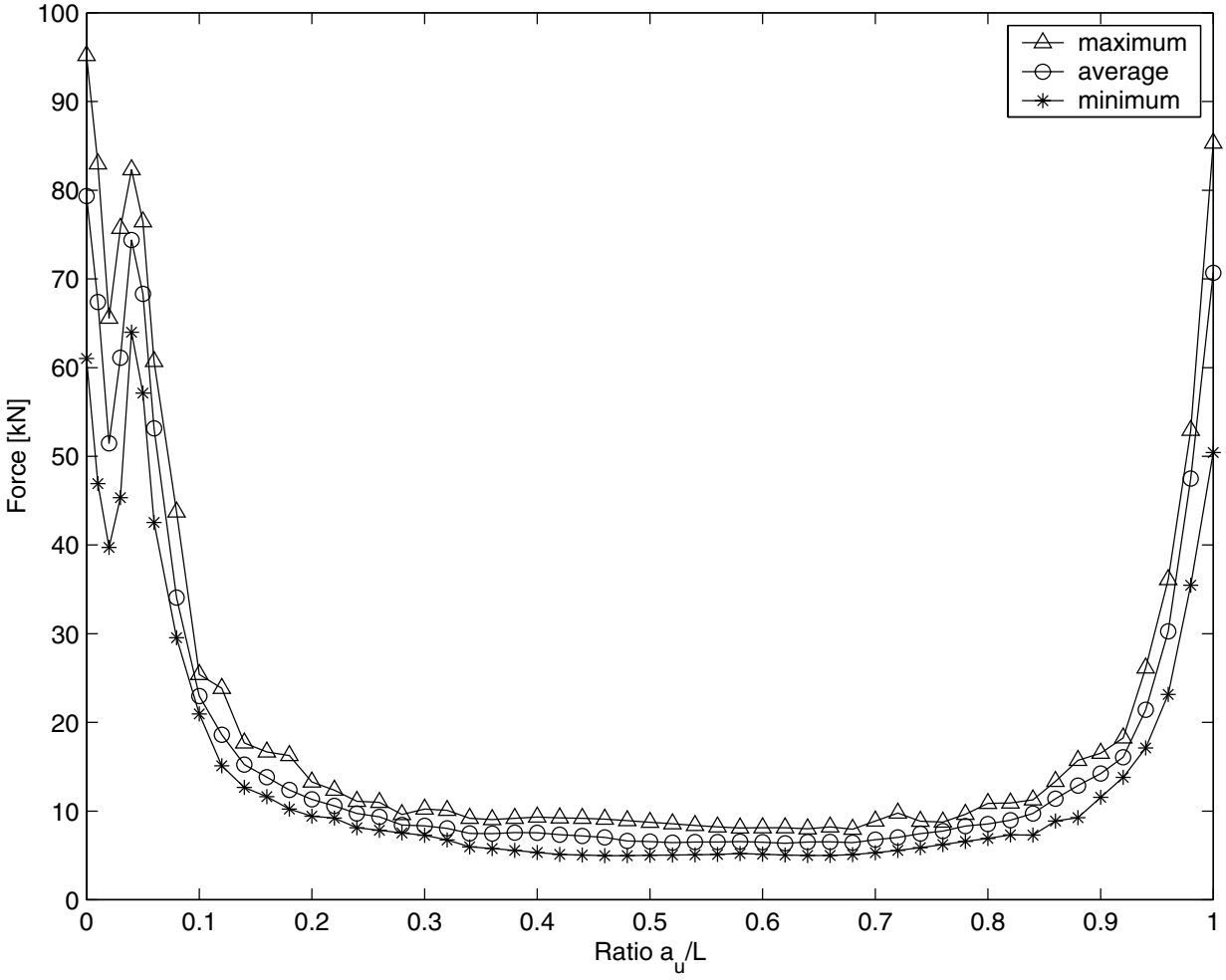

FIGURE 3-32 Mean, Maximum And Minimum Values of the Inplane Force Shown in Figure 3-30 for Different Inputs As A Function of Counterweight Position All Motions Normalized To 0.1g

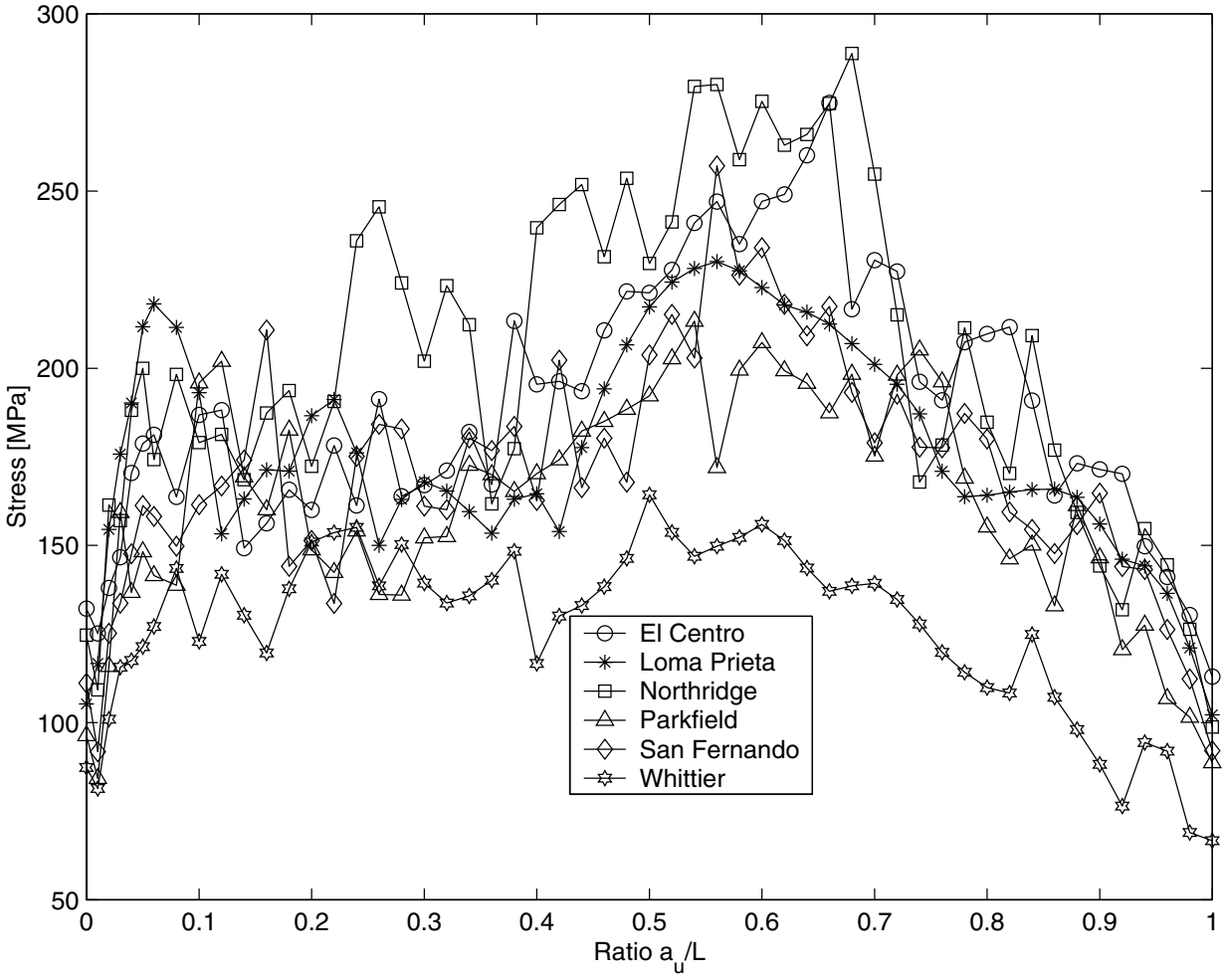

FIGURE 3-33 Maximum Stress in the Rails for Different Base Inputs As A Function of Counterweight Position All Motion Normalized To 0.5g

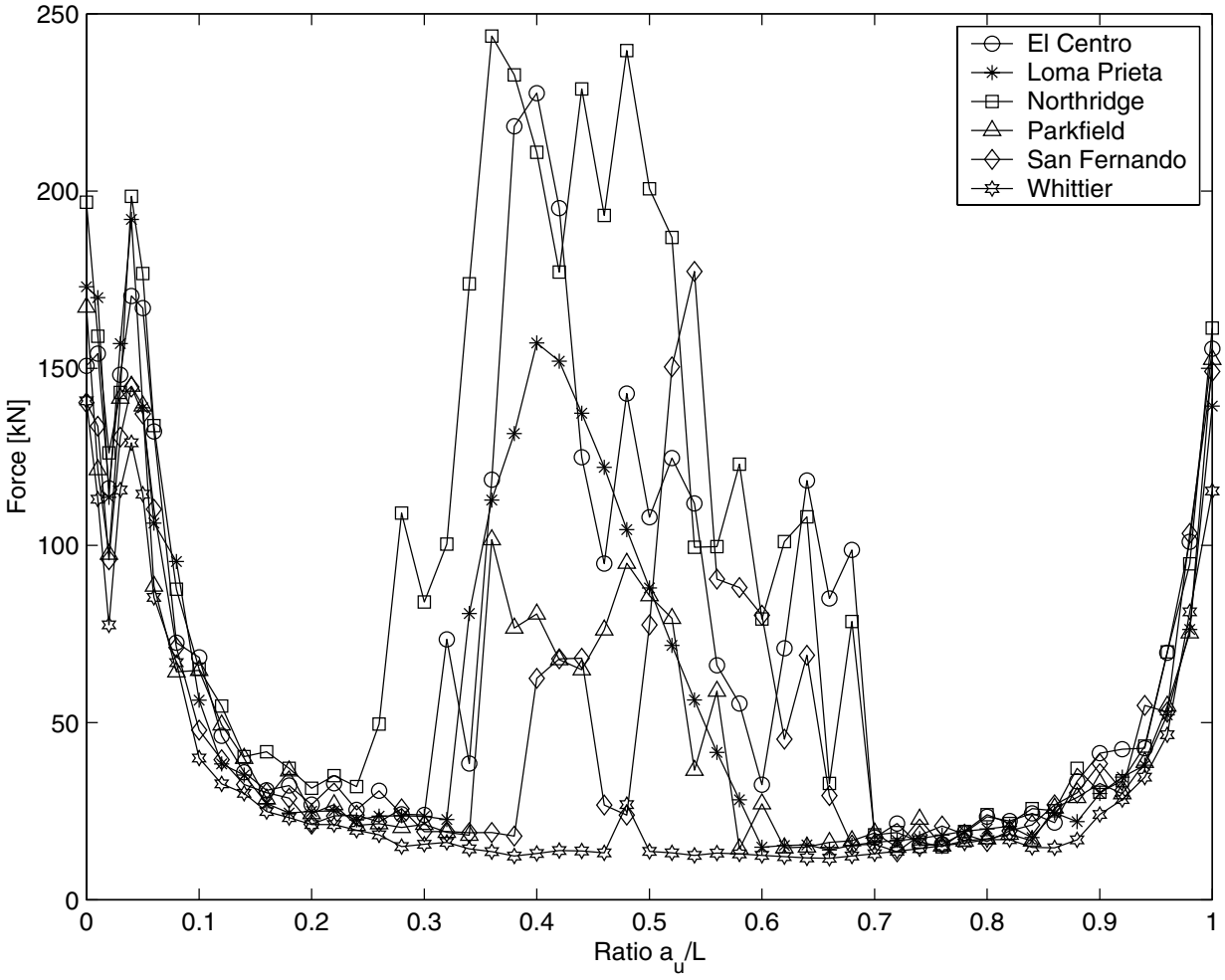

FIGURE 3-34 Maximum Inplane Force in Brackets for Different Inputs As A Function of Counterweight Position All Motions Normalized To 0.5g

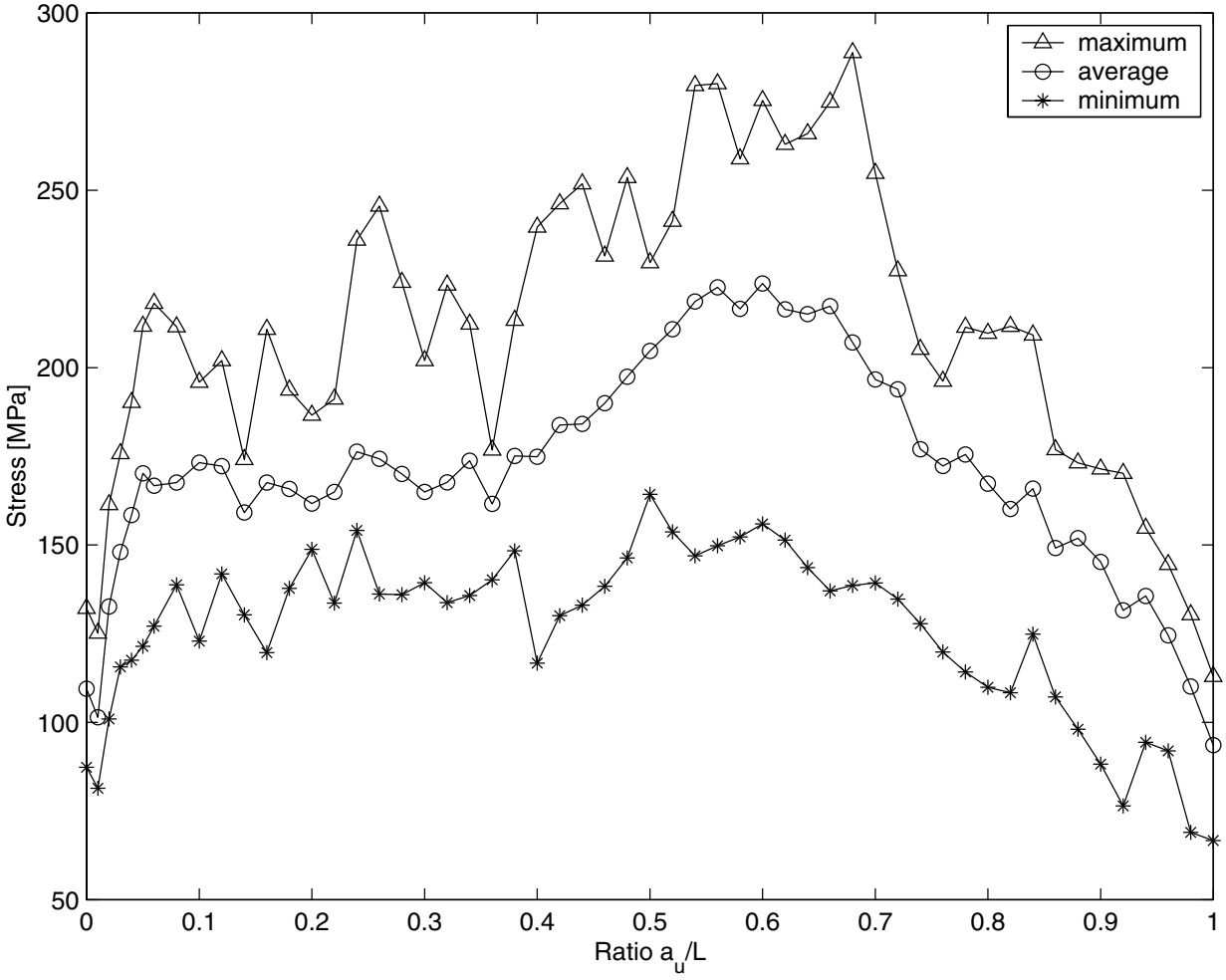

FIGURE 3-35 Mean, Maximum And Minimum Values of the Stress Shown in Figure 3-33 for Different Inputs As A Function of Counterweight Position All Motions Normalized To 0.5g

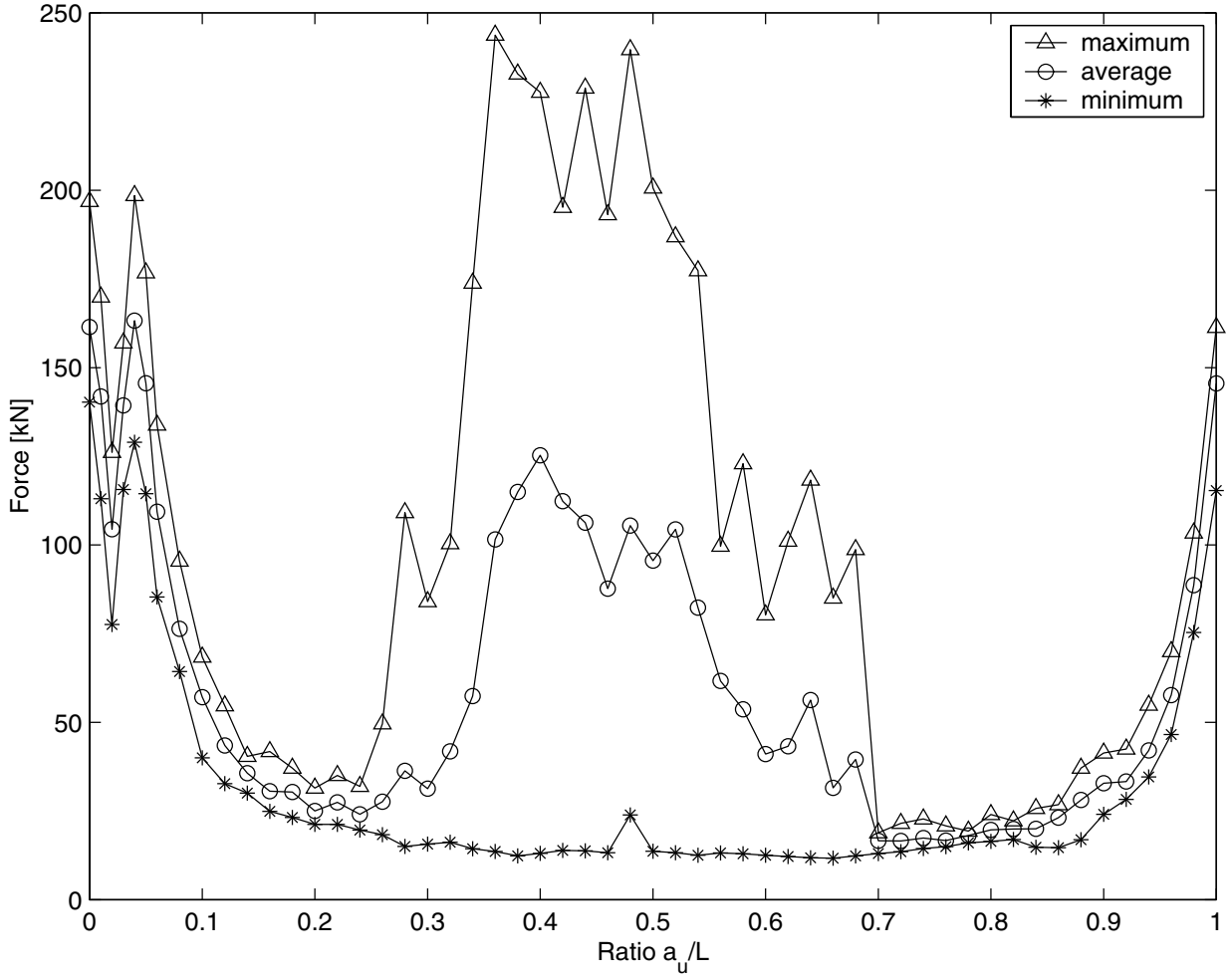

FIGURE 3-36 Mean, Maximum And Minimum Values of the Inplane Force Shown in Figure 3-34 for Different Inputs As A Function of Counterweight Position All Motions Normalized To 0.5g

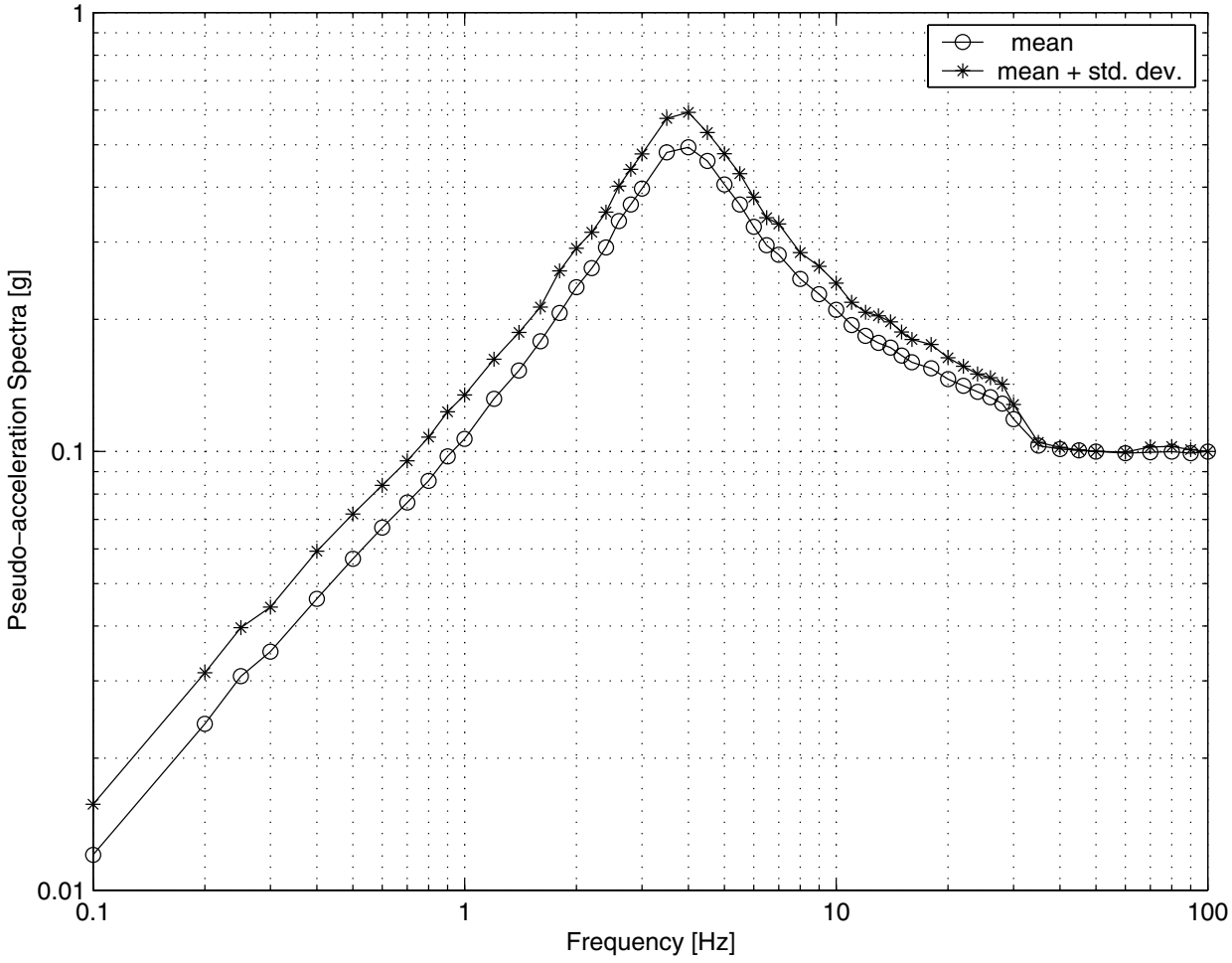

FIGURE 3-37 Mean And Mean-Plus-One-Standard Deviation of Pseudo Acceleration Spectra of 50 Sets of Synthetic Earthquakes Normalized To 0.1g

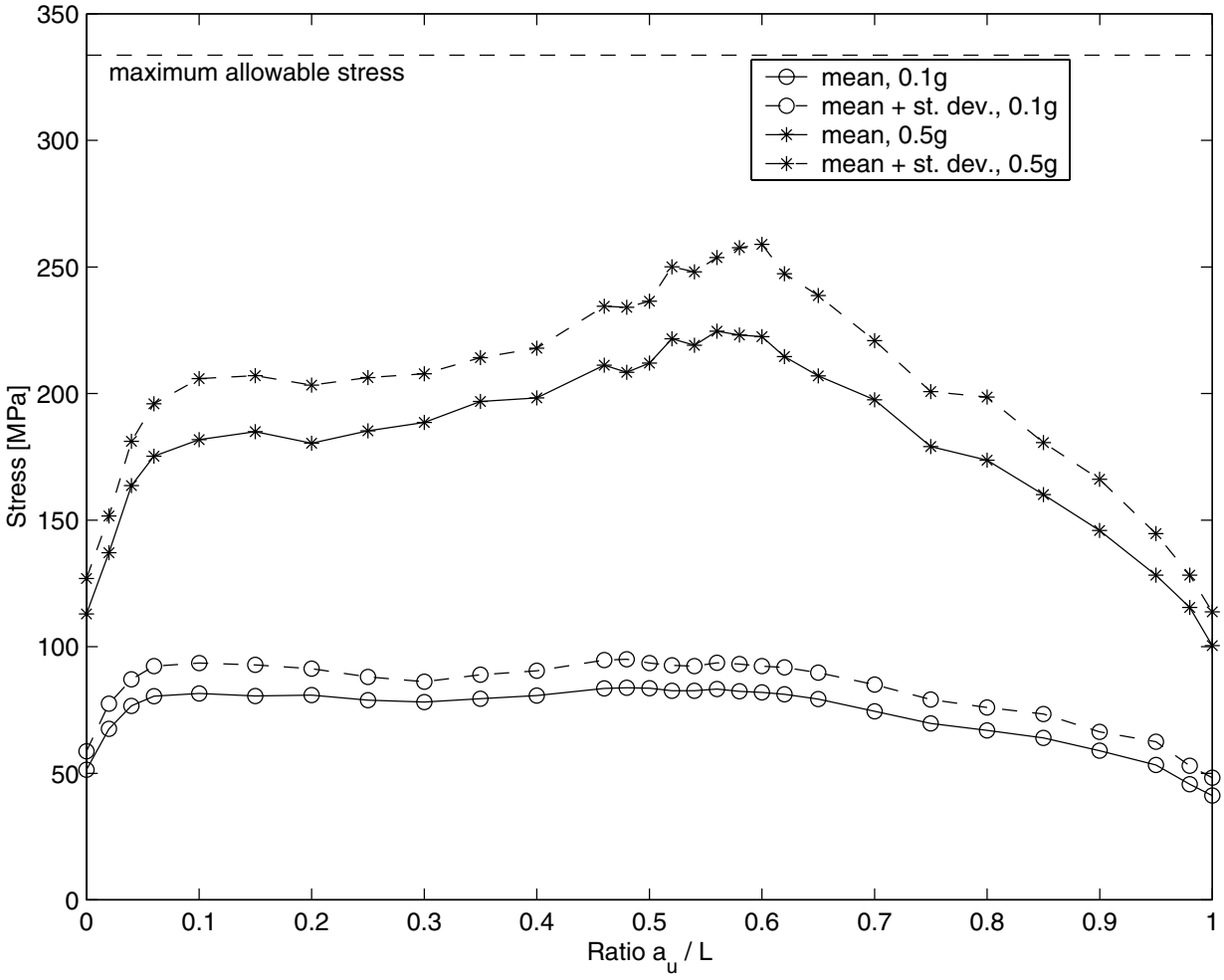

FIGURE 3-38 Mean And Mean-Plus-One-Standard Deviation of the Maximum Stress in the Rails for 50 Synthetic Earthquakes Normalized To 0.1g And 0.5g

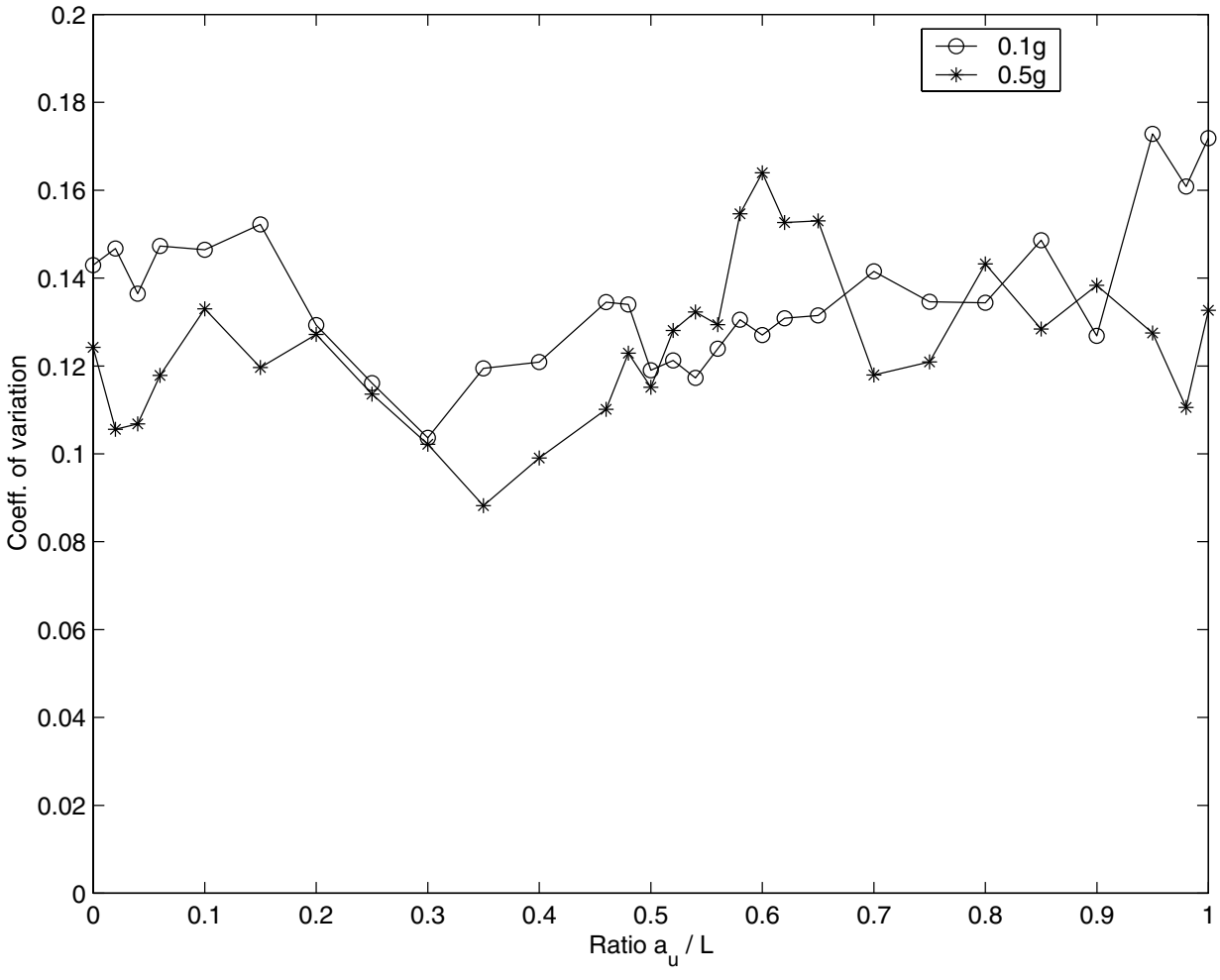

FIGURE 3-39 The Coefficients of Variations of the Maximum Stress in the Rails for 50 Synthetic Earthquakes Normalized To 0.1g And 0.5g

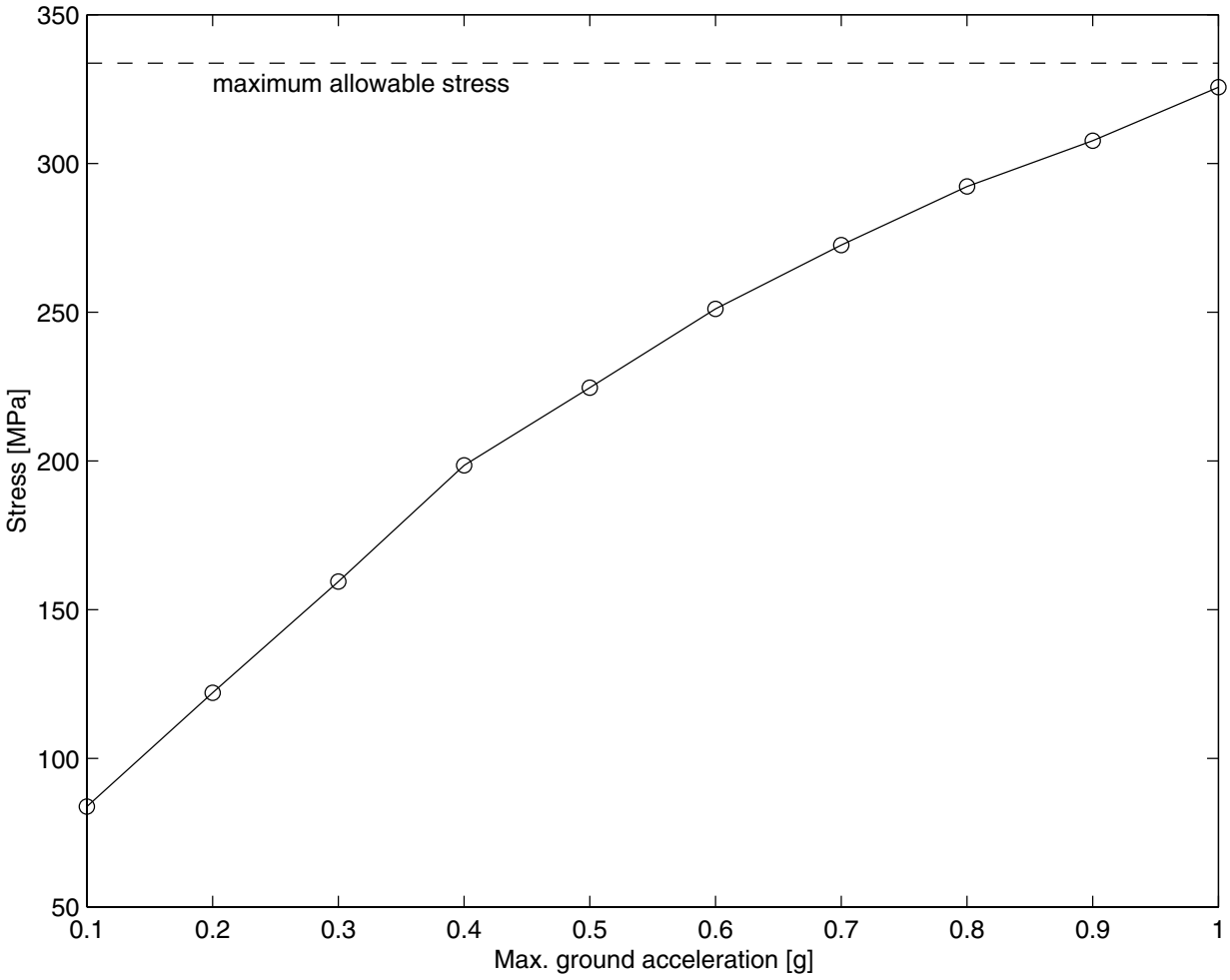

FIGURE 3-40 Average of the Peak Stress in the Rails for 50 Synthetic Motions As A Function of Input Motion Intensity

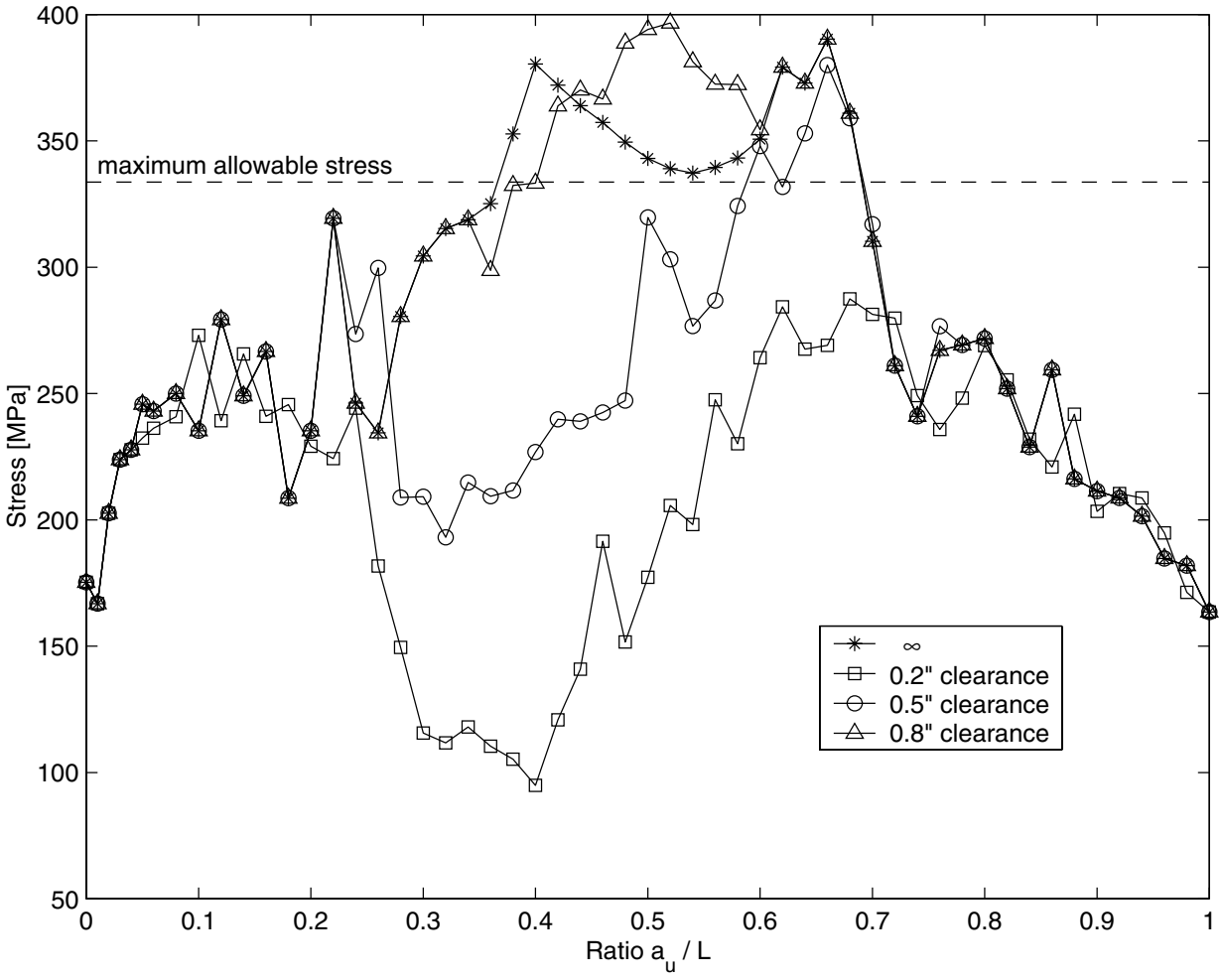

FIGURE 3-41 Maximum Stress in the Rail for Different Frame Clearances As A Function of Counterweight Position for As Recorded Northridge Earthquake (0.834g)

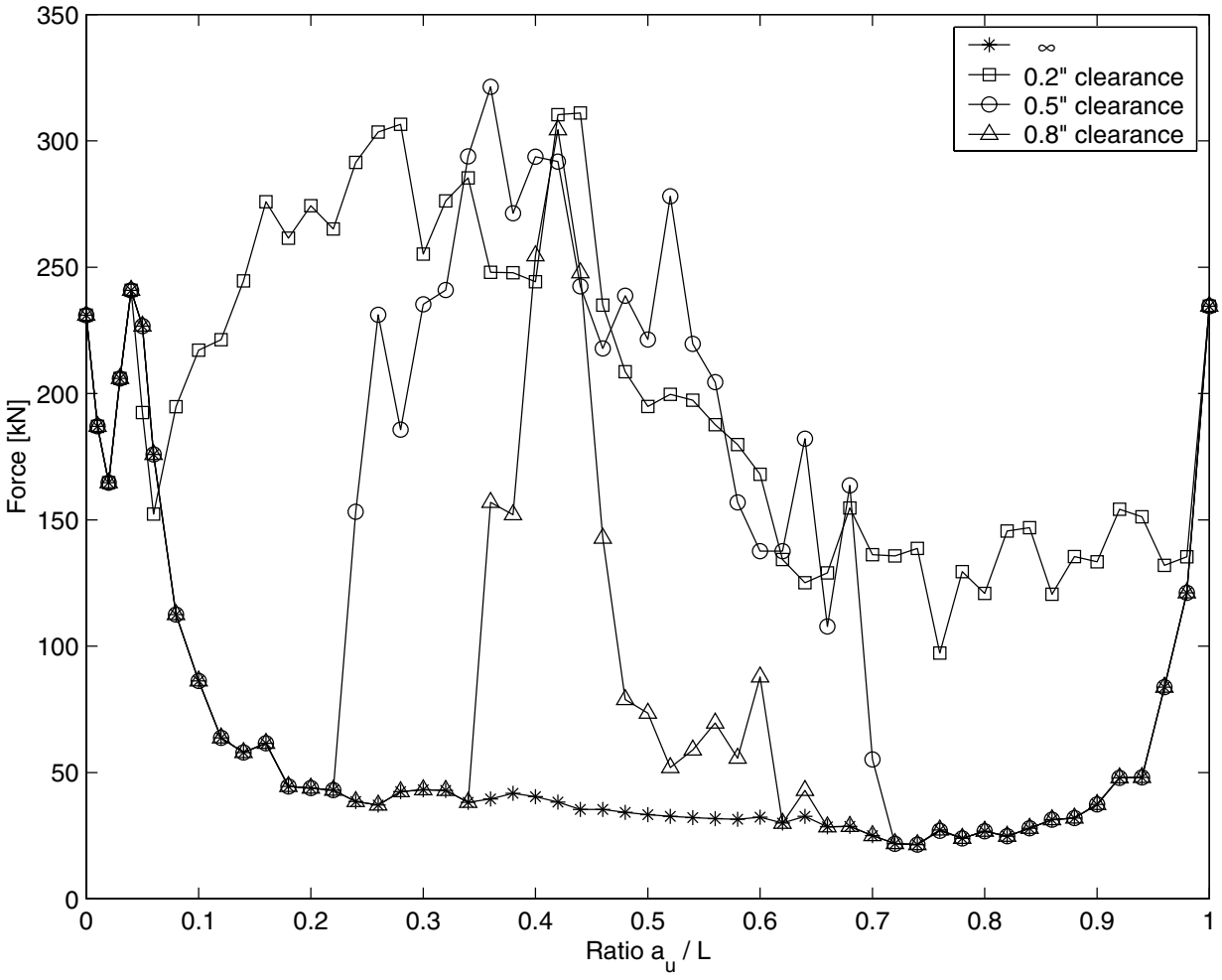

FIGURE 3-42 Maximum In-Plane Force in the Brackets for Different Frame Clearances As A Function of Counterweight Position For As Recorded Northridge Earthquake (0.834g)

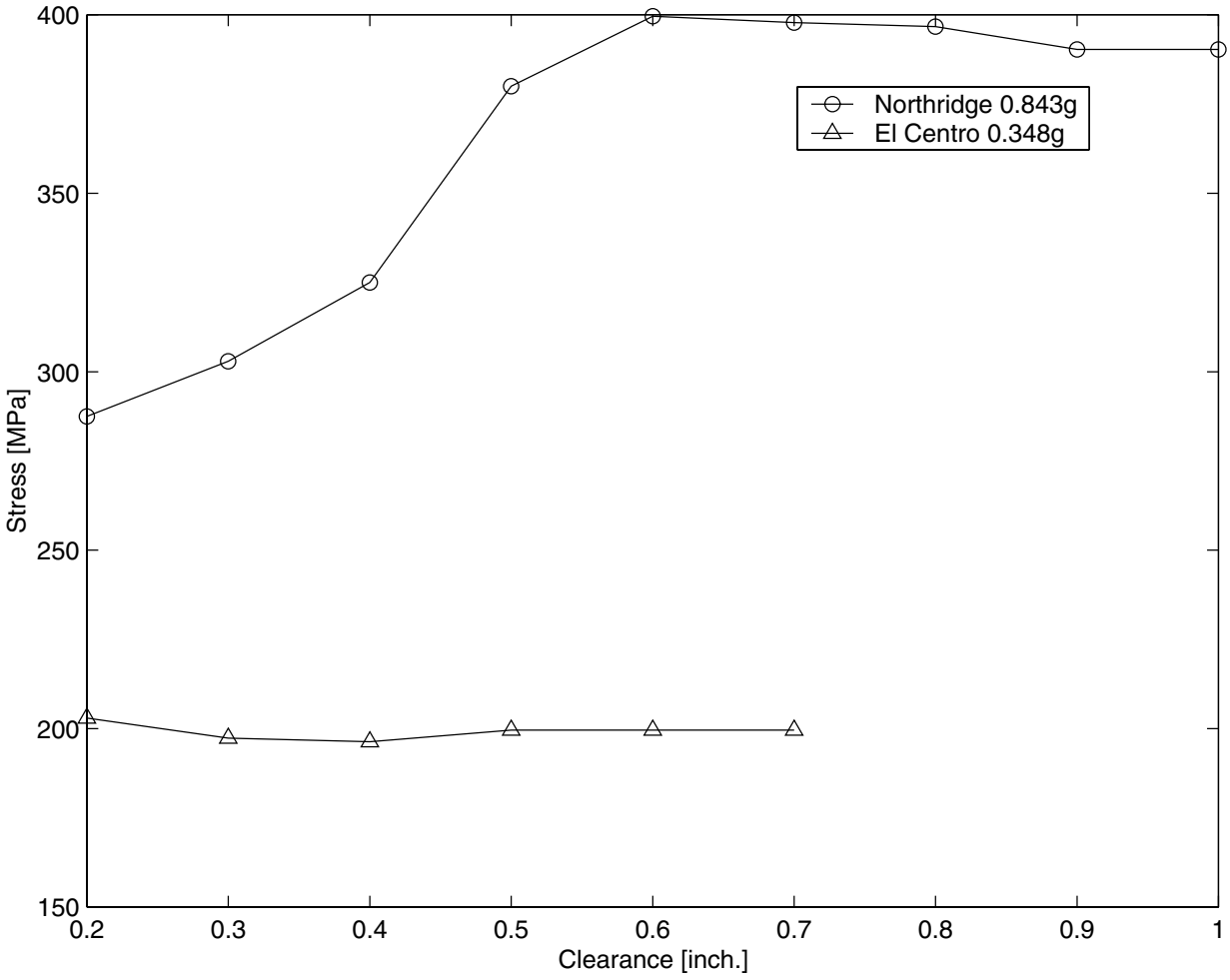

FIGURE 3-43 Maximum Stress in the Rail As A Function of the Frame Clearance for Actual Northridge (0.843g) And El Centro (0.348) Earthquakes

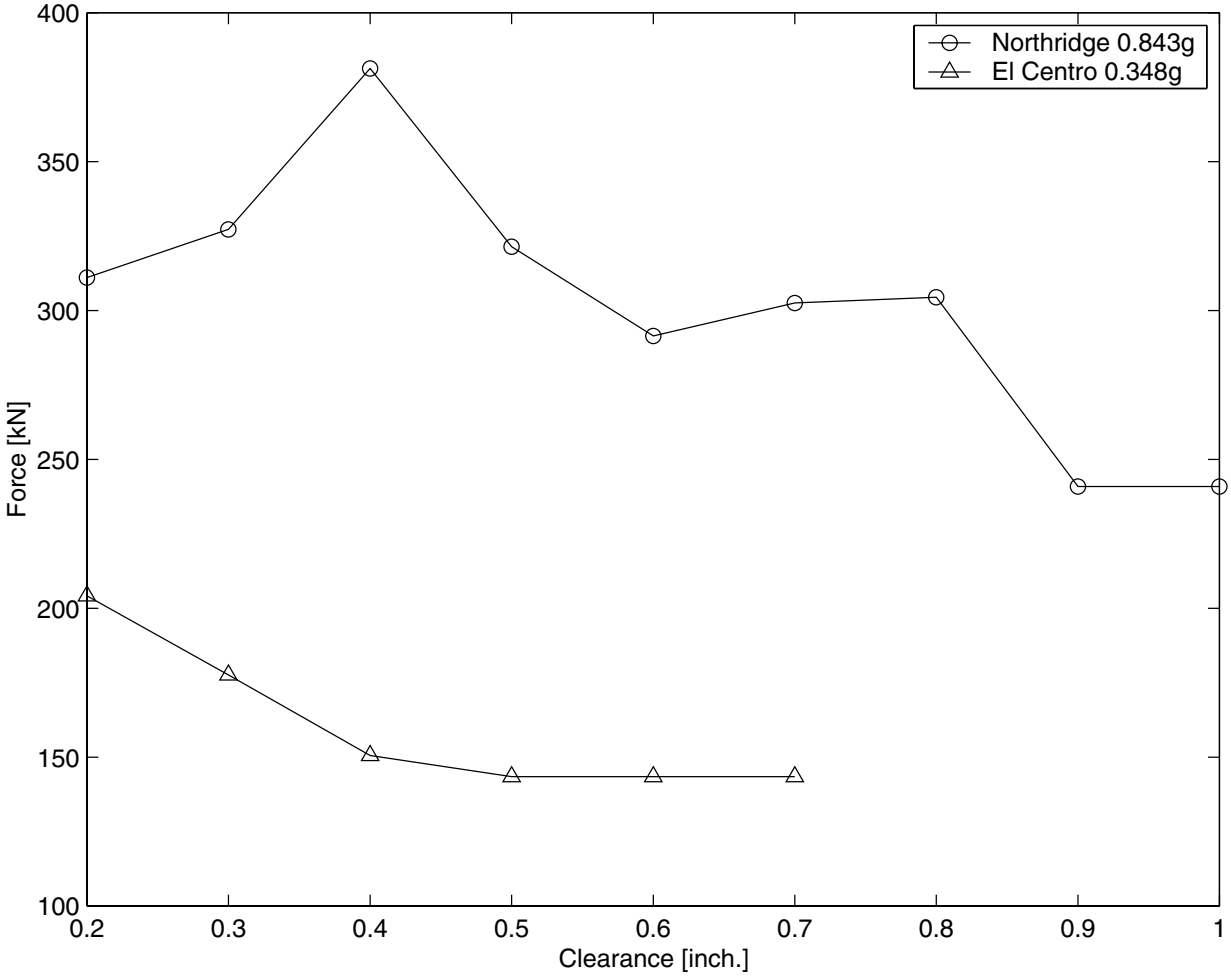

FIGURE 3-44 Maximum In-Plane Force in the Brackets As A Function of the Frame Clearances for Actual Northridge (0.834g) And El Centro (0.348g) Earthquakes

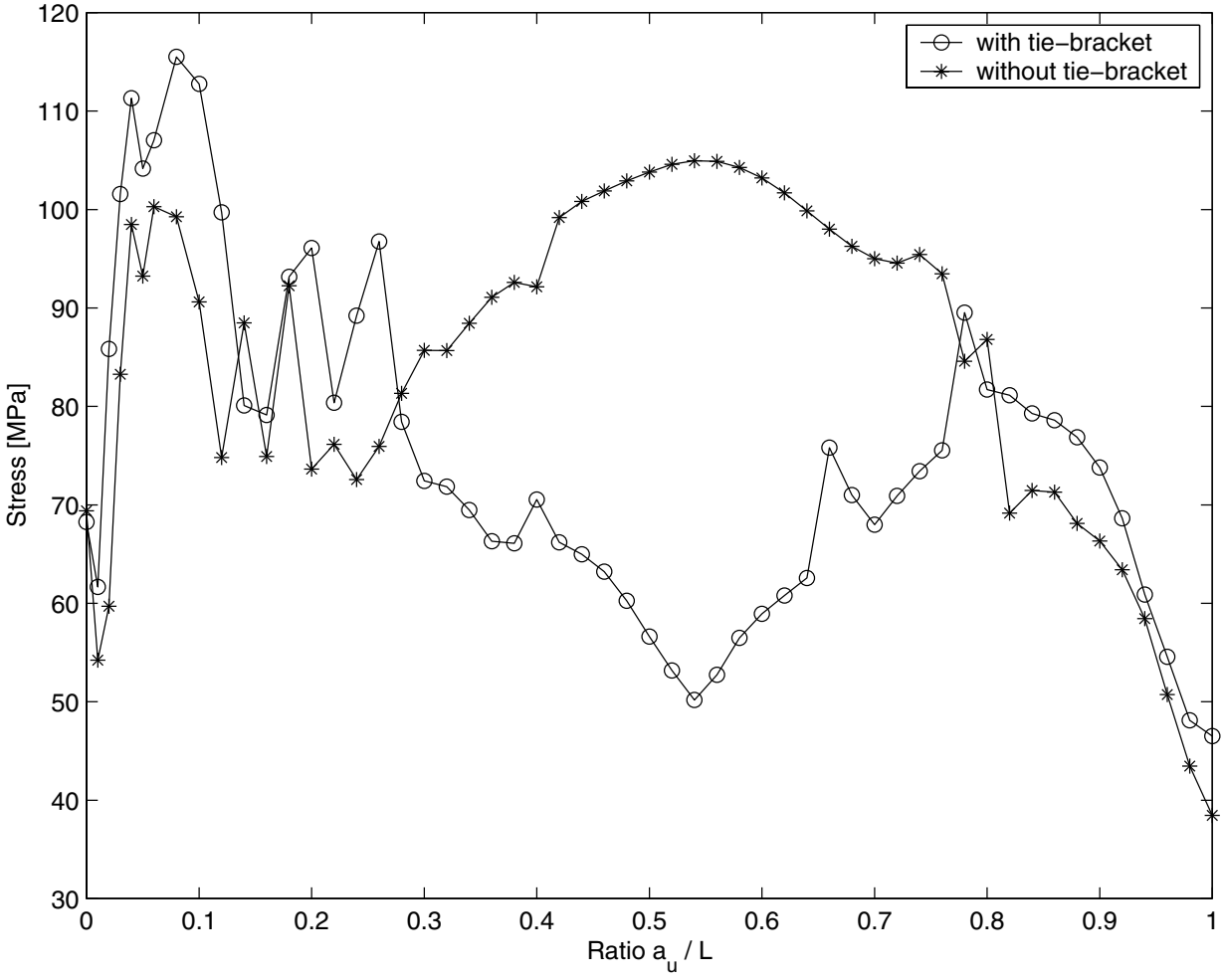

FIGURE 3-45 Maximum Stress in the Rails With And Without An Intermediate Tie-Bracket As A Function of Counterweight Position Northridge Earthquake 0.1g.

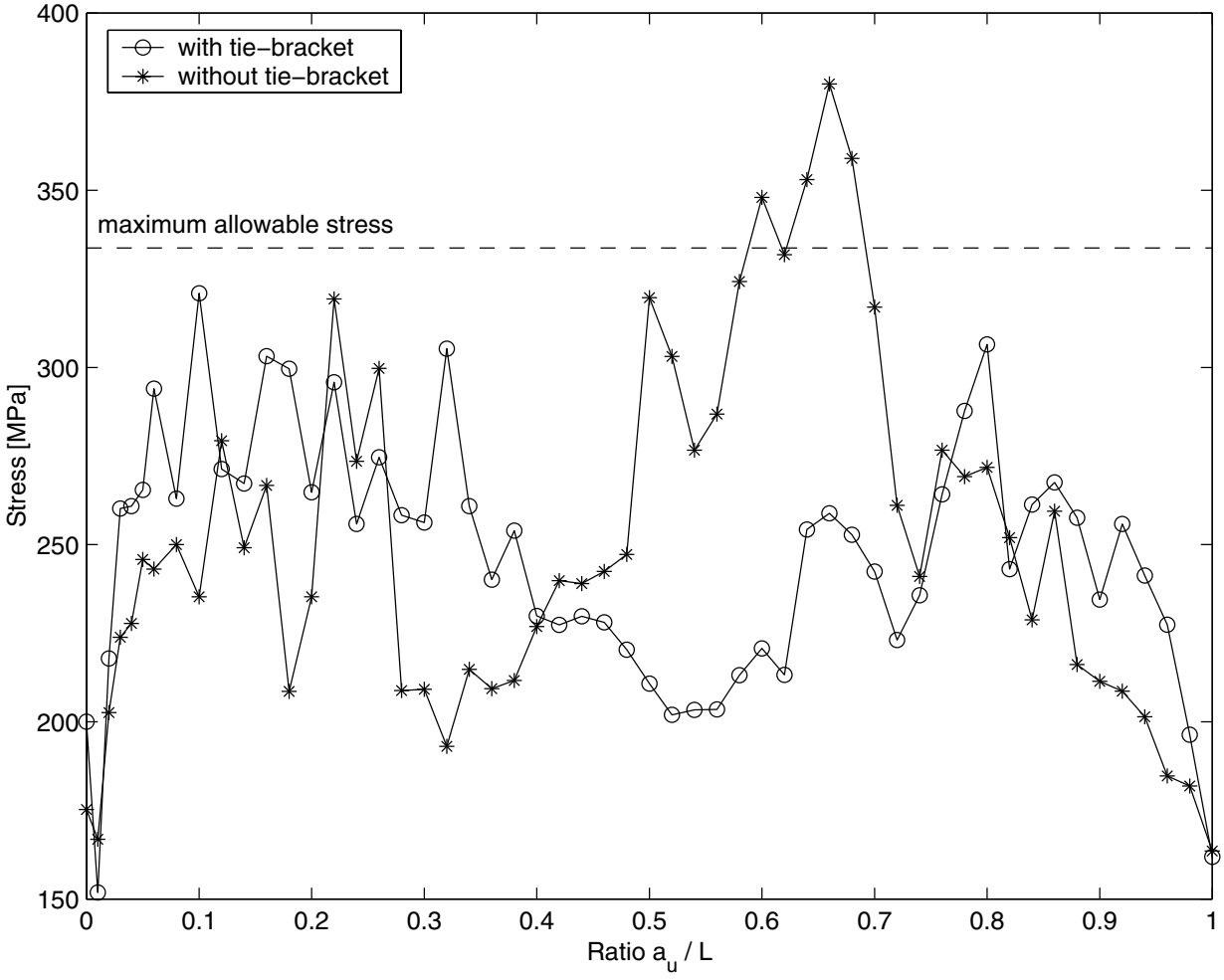

FIGURE 3-46 Maximum Stress in the Rails With and Without An Intermediate Tie-Bracket As A Function of Counterweight Position For As Recorded Northridge Earthquake 0.843g.

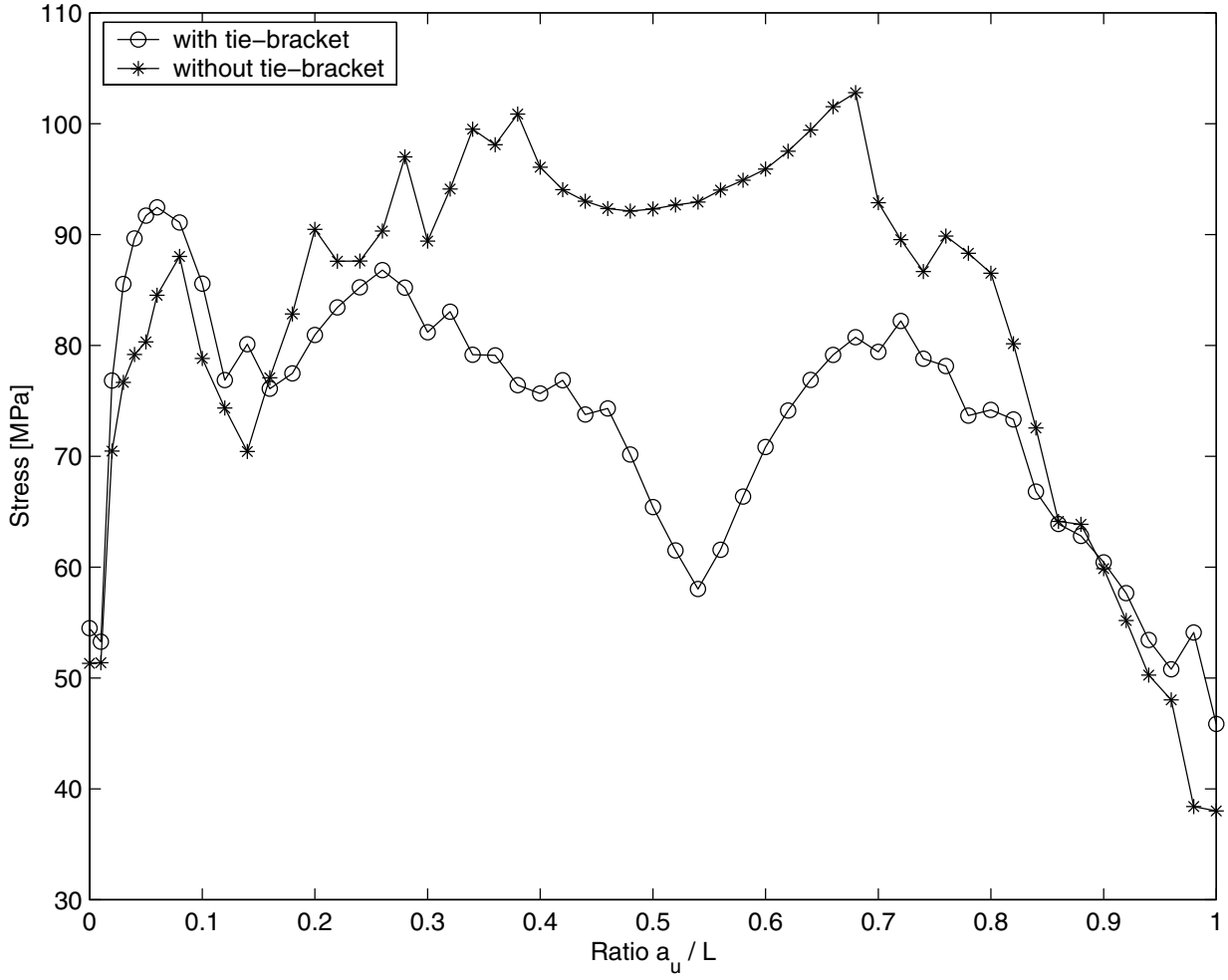

FIGURE 3-47 Maximum Stress in the Rails With and Without An Intermediate Tie-Bracket As A Function of Counterweight Position For El Centro Earthquake 0.1g.

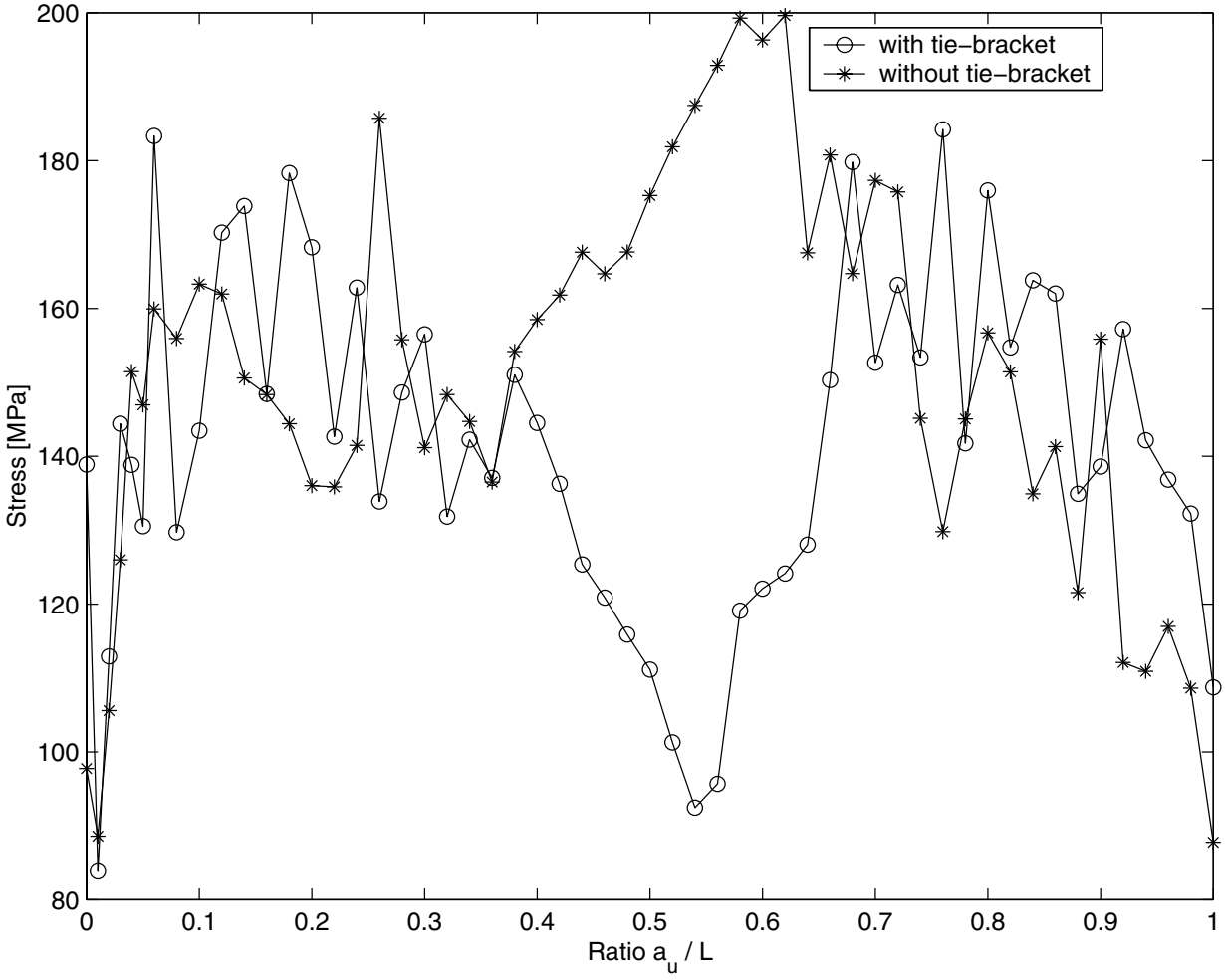

FIGURE 3-48 Maximum Stress in the Rails With and Without An Intermediate Tie-Bracket As A Function of Counterweight Position For As Recorded El Centro Earthquake 0.348g

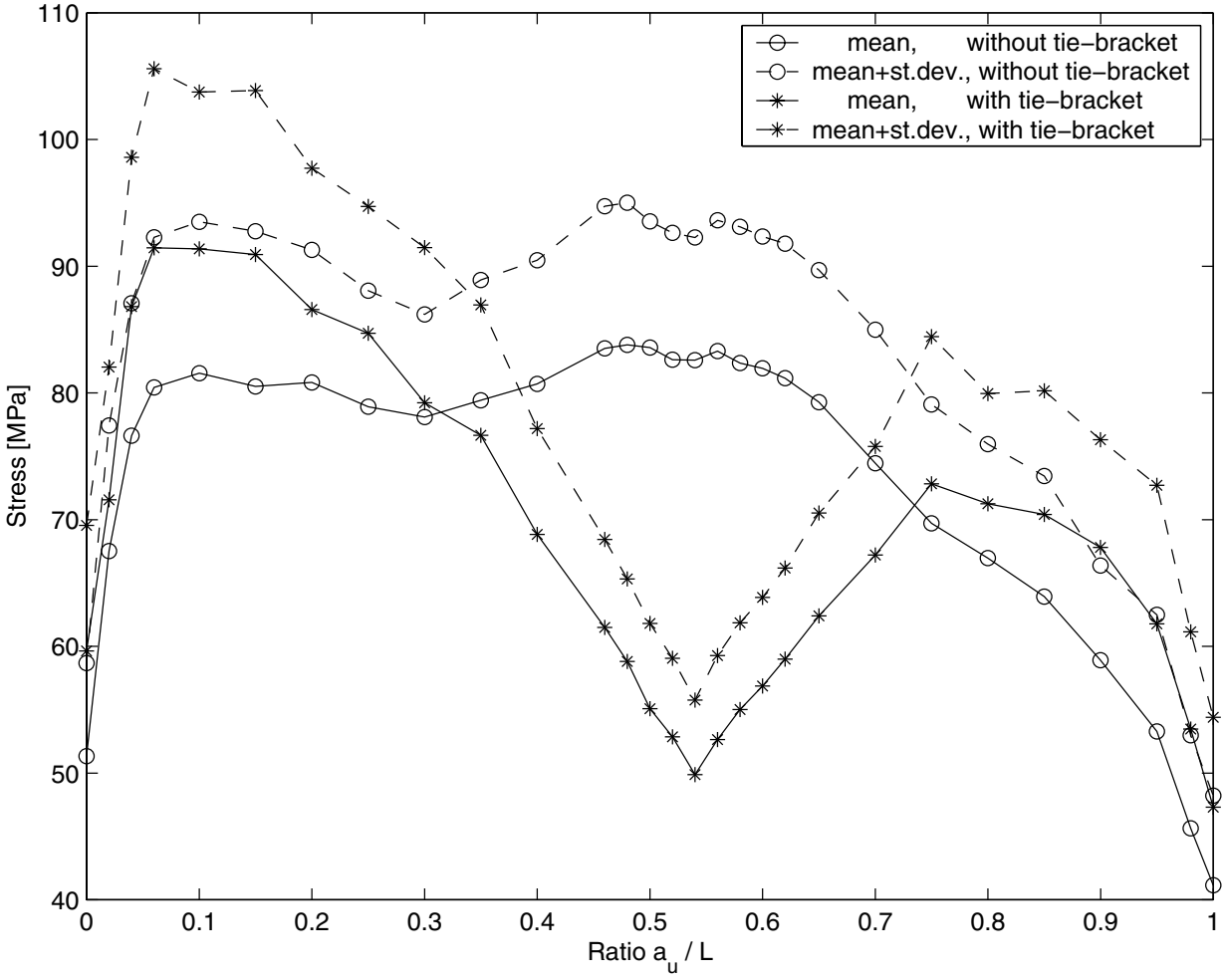

FIGURE 3-49 Mean and Mean-Plus-One-Standard Deviation of the Maximum Stress in the Rail With An Intermediate Tie Bracket 50 Synthetic Motions All Normalized to 0.1g

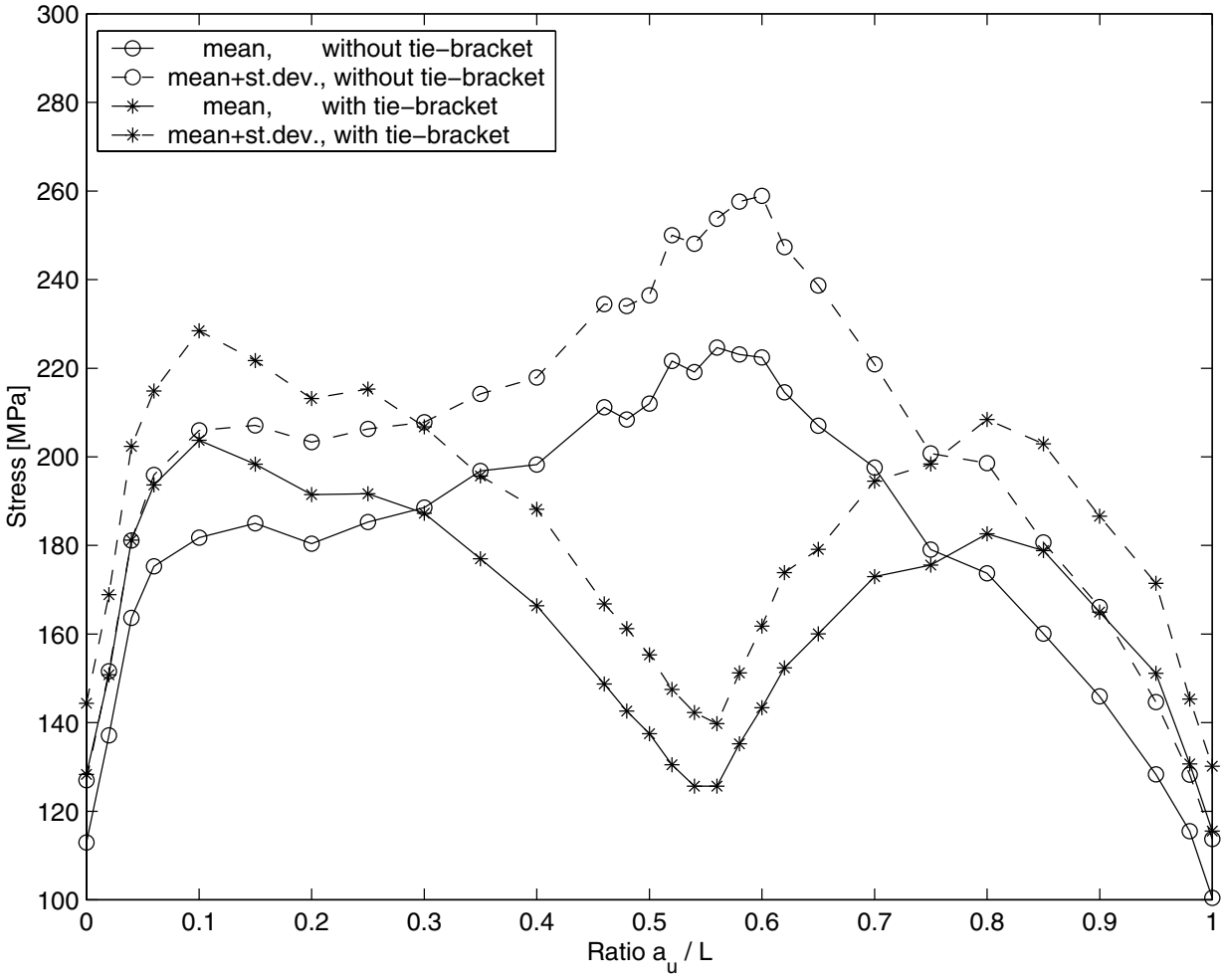

FIGURE 3-50 Mean and Mean-Plus-One-Standard Deviation of the Maximum Stress in the Rail with An Intermediate Tie Bracket 50 Synthetic Motions All Normalized to 0.5g

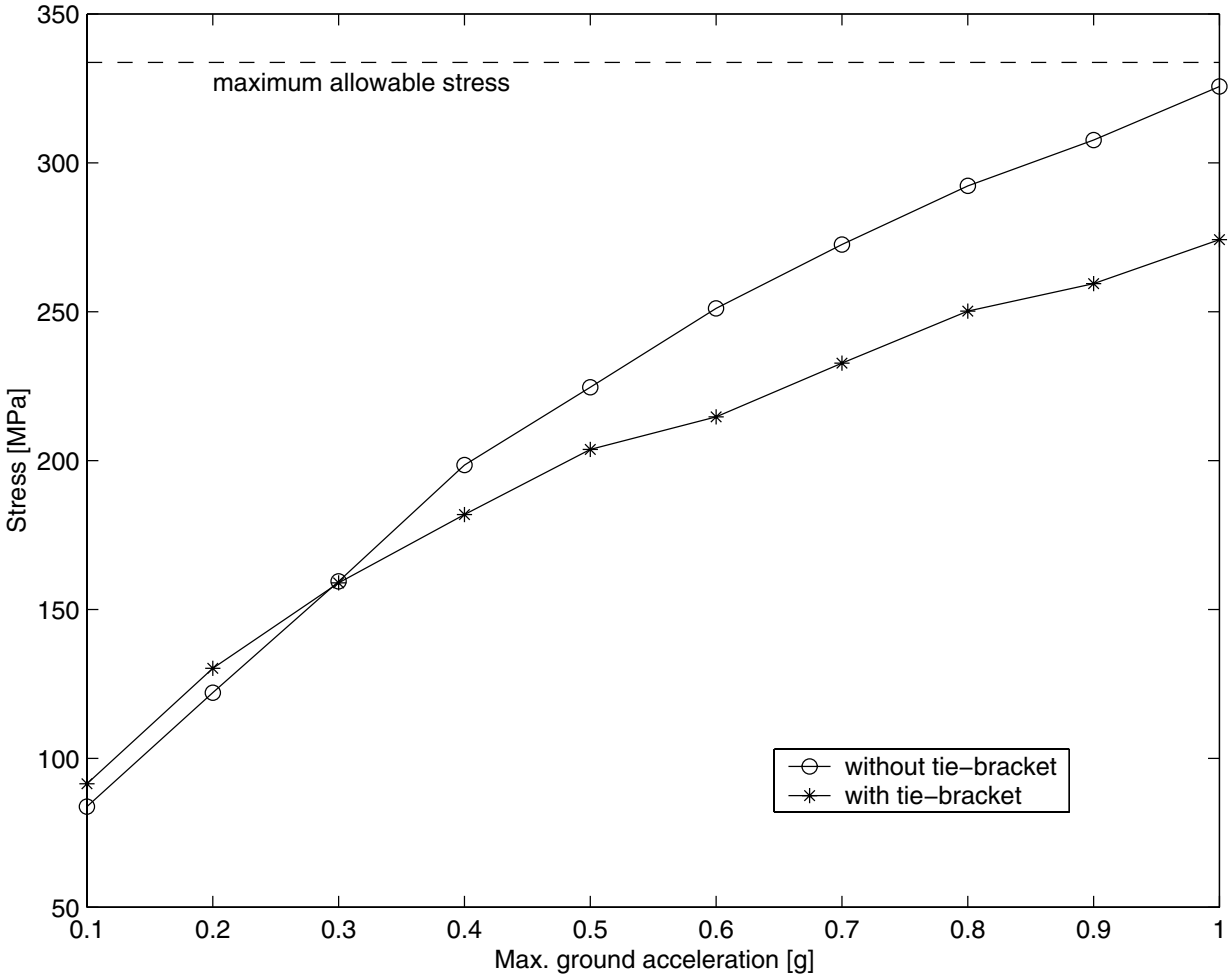

FIGURE 3-51 The Average of the Peak Stresses in the Rails With and Without An Intermediate Tie-Bracket As A Function of Input Motion Intensity. Averaged from 50 Synthetic Earthquakes.

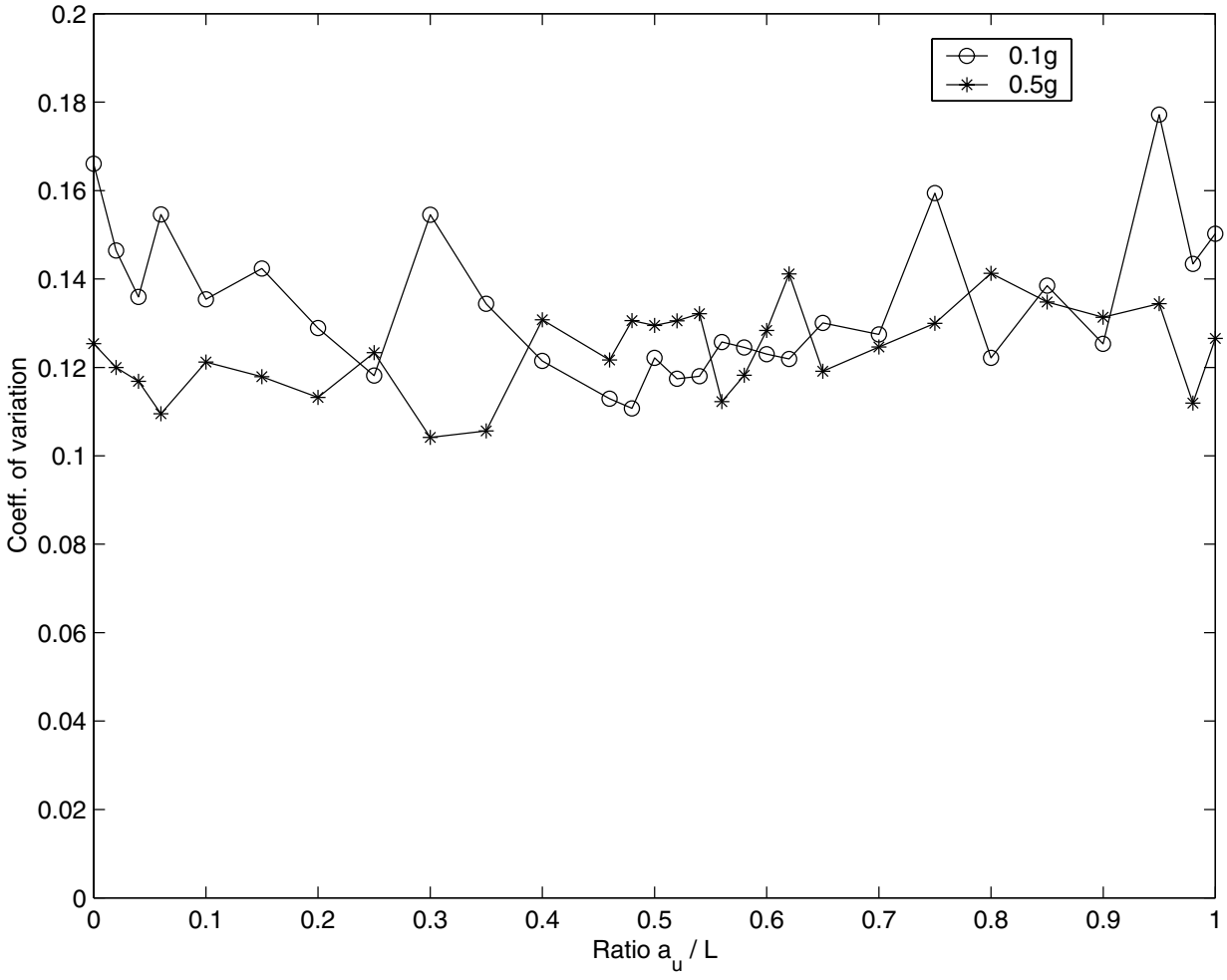

FIGURE 3-52 Coefficient of Variation of Maximum Stress in the Rail with Intermediate Tie-Bracket As A Function of Counterweight Position. 50 Synthetic Earthquakes Normalized to 0.1g and 0.5g.

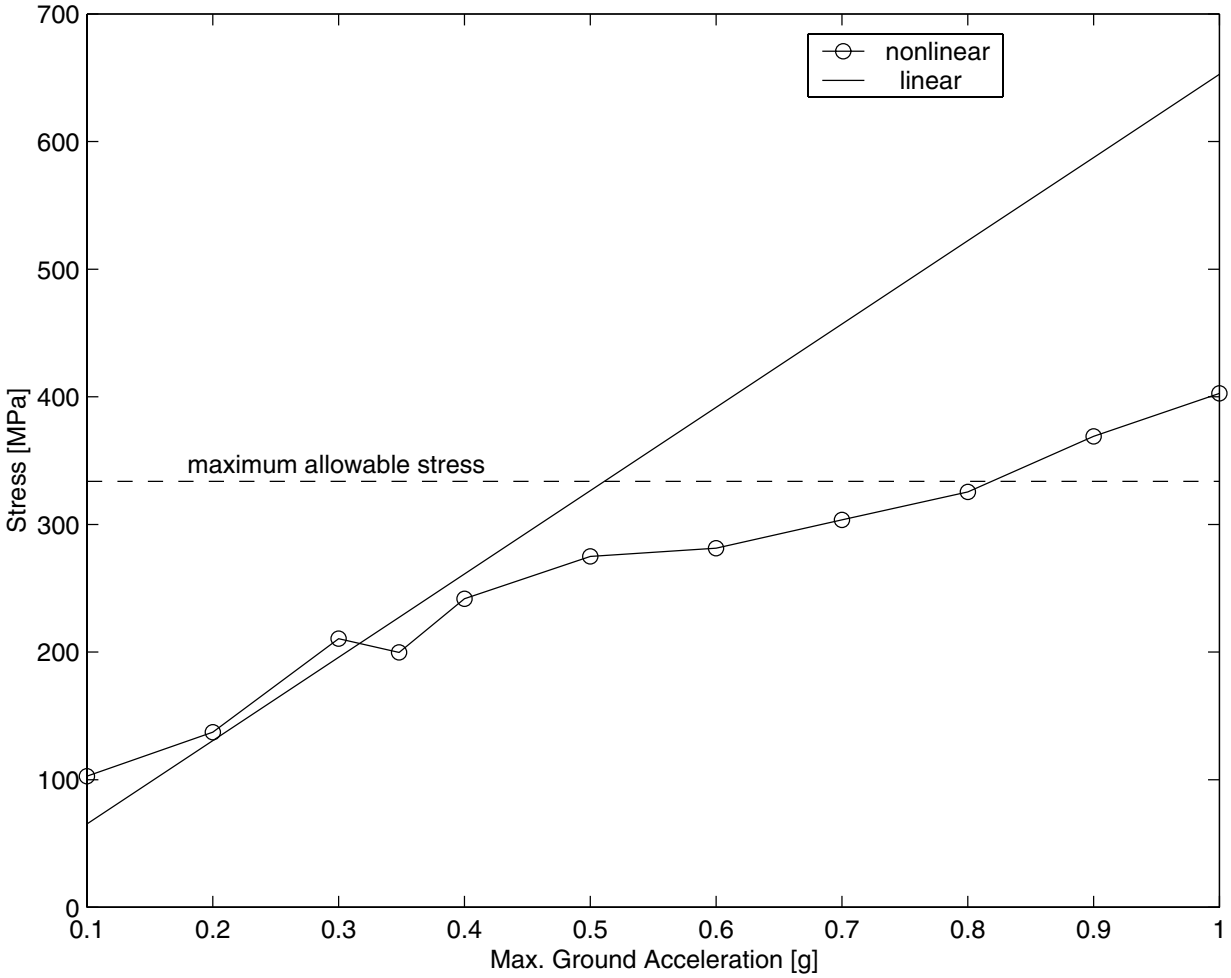

FIGURE 3-53 Maximum Stress in the Rail for Increasing Intensity of El Centro Earthquake

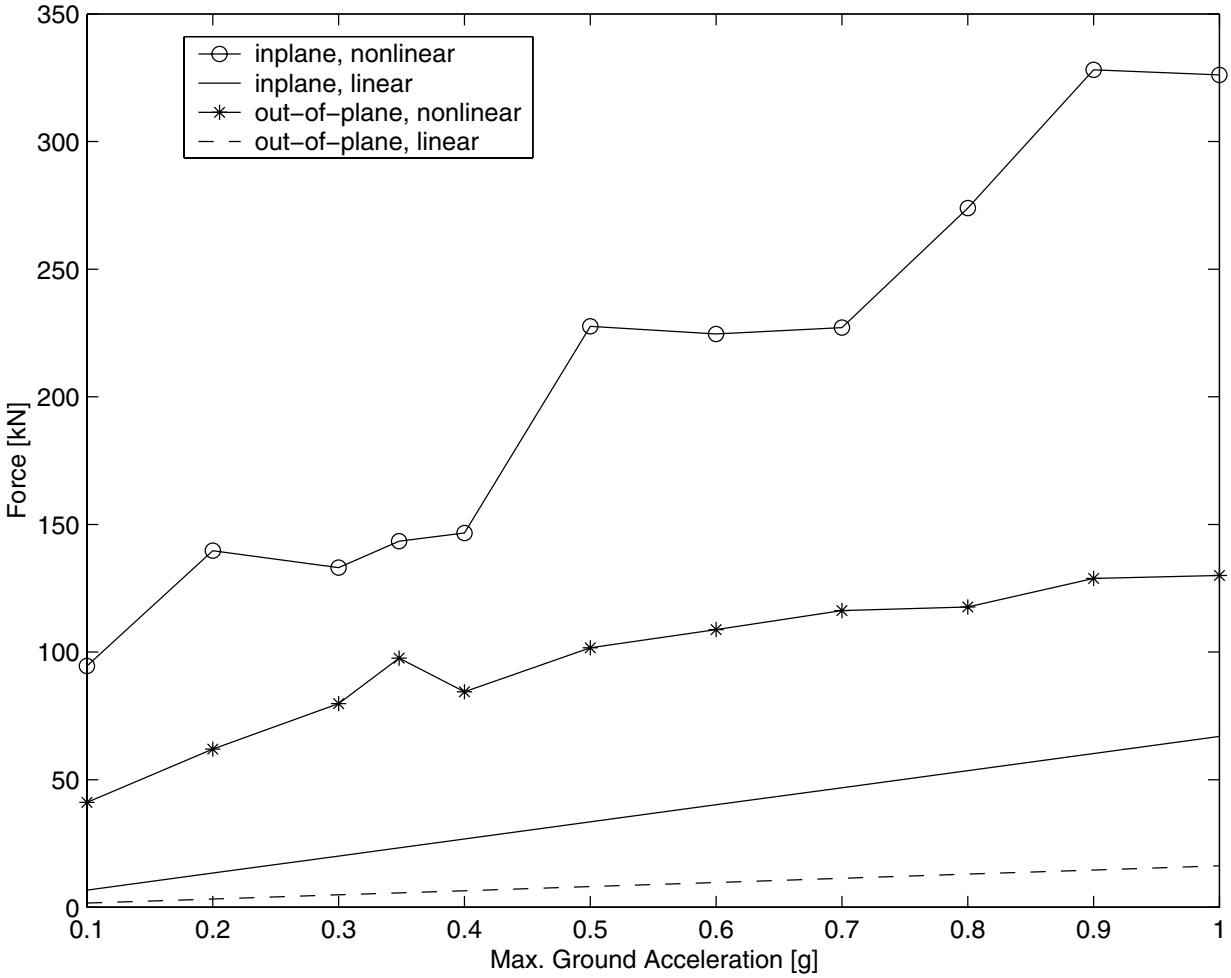

FIGURE 3-54 Maximum Forces in the Bracket for Increasing Intensity of El Centro Earthquake

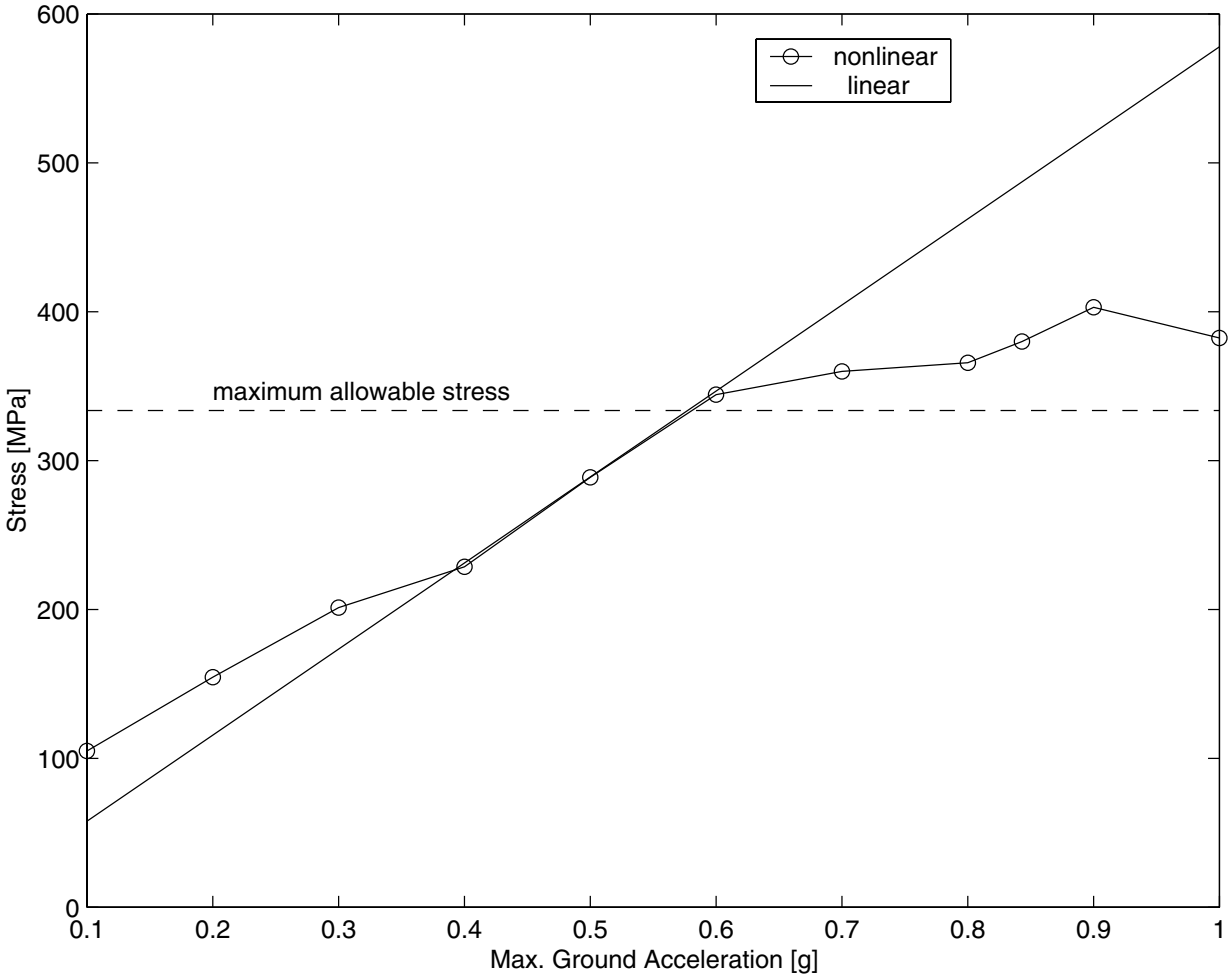

FIGURE 3-55 Maximum Stress in the Rail for Increasing Intensity of Northridge Earthquake

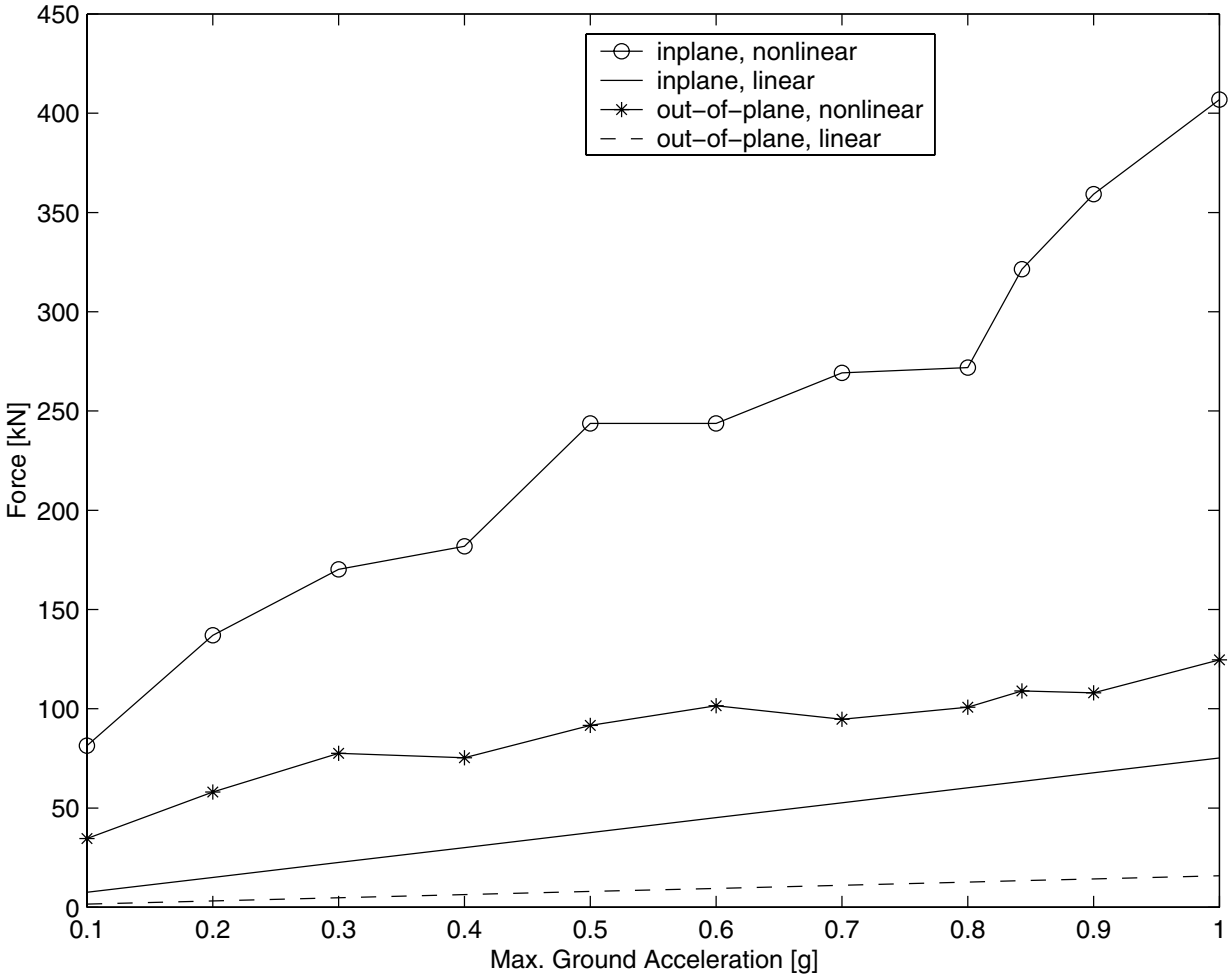

FIGURE 3-56 Maximum Forces in the Bracket for Increasing Intensity of Northridge Earthquake

SECTION 4
SUMMARY AND CONCLUDING REMARKS

Elevators are complex mechanical and electrical systems with several components that are vulnerable to seismic induced ground motions. This study is concerned with seismic response behavior of rail-counterweight systems in elevators in multi-story buildings. This section provides an overview of the study, and general conclusions. Specific conclusions are provided in previous sections.

Section 1 provides an overview of elevator systems used in buildings. Various important components of the system and their functions are identified. From the standpoint of seismic performance, the rail-counterweights are the most susceptible components of the system. A review of the current code procedures used for the design of rail and guidance system is provided. A survey of the literature available on the seismic response and performance evaluation of elevator system is provided. Although several investigators have studied the seismic response behavior of elevators, there has not been a systematic study of the rail-counterweight system with realistic analytical models. Section 2 and 3, therefore, present the developments of realistic analytical models of the rail-counterweight system for their comprehensive seismic response study. The seismic motion is transmitted to a counterweight through its guide rail-bracket support system attached to the building, causing the in-plane and out-of-plane vibrations of the counterweight. It is necessary to consider both the in-plane and out-of-plane seismic inputs and effects in evaluating a counterweight-rail system.

Section 2 deals with the linear model and analysis of a rail-counterweight system. The differential support motions applied by the building through different components of the counterweight guidance system are considered in the analysis. The flexibilities of the components that support and link different structural and mechanical elements such as the support brackets, guide rails, elastomeric rollers, and pre-loaded helical springs are included in the analysis. Numerical results are presented for several earthquake inputs, different building characteristics, different locations of the counterweight in the buildings, different response quantities, different guide rail sizes, and different stiffness characteristics of roller guide assemblies. Linear analysis can provide a valuable insight into the dynamic behavior of the system under earthquake loads. Linear analysis can also be conveniently used to examine different protective options one can use to improve the performance of the elevator systems during earthquakes.

Section 3 presents the development of a more realistic nonlinear vibration model. The nonlinearity in the system can be introduced by several sources. The yielding of rails and support brackets can surely occur during a strong ground motion. However, by then the performance of the system will definitely be compromised. This type of nonlinearity is thus not a part of design criteria of the elevators, and it not considered herein. The main focus of this study is on the nonlinearities that can occur due to the closing of certain gaps and thus cause a sudden change in the stiffness characteristics of the system during its motion. Each roller guide assembly is provided with a restraining plate that prevents the disengagement of the rollers from the rails in the case of a strong ground shaking.

There is, however, a gap between the restraining plates and rail to avoid constant rubbing of the metal surface during normal operation. During strong ground shaking this gap can, however, close. A clearance is also provided between the counterweight frame. However, to protect the rails from deflecting too much during a strong shaking, this clearance is limited to a maximum of ½ inch. During strong ground shaking this gap can also close; the frame then impacts the bracket support and transfers a part of inertial loads directly to the bracket support. For an accurate analysis of the system it is important to consider these possibilities of gap closings. The analytical model developed in Section 3 is primarily focused to include this type of nonlinearities. The bi-linear force deformation diagrams with hardening characteristics are used to represent the contact elements at the gaps. A comprehensive parametric study is conducted to evaluate the effect of various system parameters. Several sets of numerical results are presented for different earthquakes, levels of excitations, gap sizes, positions of the counterweight, rails sizes, and tie brackets. Each case with a selected set of parameter values requires an accurate time history analysis to incorporate the nonlinear effects properly. A detailed discussion of the effect of various parameters on the response characteristics and design of the system is given in Section 3.

REFERENCES

1. American Society of Mechanical Engineers (1981, 1993, 1996), "Safety code for elevators and escalators ASME A17.1," ASME, New York, New York.
2. Avallone, E. A. and Baumeister III, T., Eds. (1986), "Mark's Standard Book for Mechanical Engineers," 9th Edition, McGraw-Hill, New York.
3. Ayres, J. M. and Sun, T. Y. (1973), "Nonstructural damage," in: The San Fernando, California, Earthquake of February 9, 1971, US Department of Commerce, National Ocean and Atmospheric Administration, Vol., 1, Part B, 736-742.
4. Ayres, J. M., Sun, T. Y., and Brown, F. R. (1973), "Nonstructural damage to buildings," in: The Great Alaska Earthquake of 1964: Engineering," Division of Earth Sciences, National Research Council, National Academy of Sciences, Washington, DC, 346-456.
5. Benuska, K. L., Aroni, S., and Schroll, W. (1977), "Elevator earthquake safety control," Proceedings of the Sixth World Conference on Earthquake Engineering, New Delhi, India, Vol. 12, 61-66.
6. Blume, J. A., Newmark, N. M., and Corning, L. H. (1961), "Design of Multistory Reinforced Concrete Buildings for Earthquake Motions," Portland Cement Association.
7. Building Seismic Safety Council (1994), "NEHRP recommended provisions for the development of seismic regulations for new buildings, Part 1 - Provisions," 1994 Edition, Federal Emergency Management Agency, US Government Printing Office, Washington, DC.
8. California Building Standards Commission (1998), "California Elevator Safety Construction Code," Part 7 of the California Code of Regulations - Title 24, International Conference of Building Officials, Whittier, California.
9. Caporale, R. S. (1995), "Great Hanshin (Kobe) earthquake of 1955, Elevator World, Vol. XLIII, No. 6, 55-72.
10. Cash, J. R., and Karp, A. H. (1990). "A variable order Runge-Kutta method for initial value problems with rapidly varying right-hand sides", *ACM Transactions on Mathematical Software*, 16(3), 201-222.
11. Chopra, A. K. (1995). *Dynamics of Structures Theory and Applications to Earthquake Engineering*, Prentice Hall, NJ.
12. Conner, H. W., Harris, J. R., Viest, I. M., and Dillon, R. M. (1987), "Guide to application of the NEHRP recommended provisions in earthquake-resistant building design," Federal Emergency Management Agency, US Government Printing Office, Washington, DC.
13. D'Amato, A. (1997), "The derailment of counterweights in seismic zones," Elevator World, Vol. XLV, No. 5, 134-137.

14. Diaz, O. (1999). "Nonlinear response of a rail and counterweight system using the differential Taylor transform", *MS Thesis*, Dept. of Civil Engineering, University of Puerto Rico, Mayaguez, PR.
15. Ding, D. and Arnold, C., Coordinators (1990), "Architecture, building contents, and building systems", Chapter 9 in Supplement to Volume 6: Loma Prieta Earthquake Reconnaissance Report, Earthquake Spectra, 339-377.
16. Finley, J., Anderson, D., and Kwan, L. (1996), "Report on the Northridge earthquake impacts to hospital elevators," Contract No. 94-5122, Office of Statewide Health Planning and Development, Sacramento, California.
17. Fukuda, T. (1990), "Earthquake Resistive Elevators," in Elevator World Educational Package and Reference Library, Vol. 3, VI.3-VI.5.
18. Gates, W.E. and McGavin, G. (1998), "Lessons learned from the 1994 Northridge earthquake on the vulnerability of nonstructural systems," Proceedings of the Seminar on Seismic Design, Retrofit, and Performance of Nonstructural Components," ATC 29-1, Applied Technology Council, 93-106.
19. Hamming, R. W. (1973). *Numerical Methods for Scientists and Engineers*, 2nd edition, McGraw-Hill, NY.
20. Highlands, D., Oppenheim, I., and Strain, J. (1975), "Hospital design for earthquake performance: vertical circulation," Proceedings of the US National Conference on Earthquake Engineering, Ann Arbor, Michigan, 347-356.
21. Janovsky, L. (1993), "Elevator mechanical design," 2nd Edition, Ellis Horwood Series in Mechanical Engineering, Great Britain.
22. Levy, R., Rutenberg, A., Segal, F., and Marianchik, E. (1996), "Analytical evaluation of elevator safety code seismic provisions in low-rise buildings," Elevator World, Vol. XLIV, No. 6, 110-115.
23. Mathworks Inc. (1992), "MATLAB® Reference Guide," The Mathworks Inc.: Natick, Mass.
24. McGavin, G. L. (1981), "Earthquake protection of essential building equipment: design, engineering, installation, John Wiley & Sons, New York, New York.
25. Meirovitch, L. (1997). *Principles and Techniques of Vibrations*, Prentice Hall, NJ.
26. Miller, L.D. (1990), "Seismic switches: a status report," in Elevator World Educational Package and Reference Library, Vol. 3, VI.6-VI.11.
27. Nazarova, M.K. (1990), "Measured full-scale investigations of lifts seismic stability," Proceedings of the Ninth European Conference on Earthquake Engineering, Moscow, Russia, Vol. 6, 238-242.
28. Office of Statewide Health Planning and Development (1995), "Northridge earthquake: a report to the Hospital Building Safety Board on the performance of hospitals", Technical Report, OSHPD, Facilities Development Division, Sacramento, California.

29. Onoda, Y. and Ikeda, E. (1988), "Development of seismic wave energy sensing - type earthquake detector," Proceedings of the Ninth World Conference on Earthquake Engineering, Tokyo-Kyoto, Japan, Vol. VII, 661-666.

30. Onoda, Y. and Yamatoshi, T. (1990), "Seismic-wave energy-sensing earthquake detector," in Elevator World Educational Package and Reference Library, Vol. 3, VI.12-VI.14.

31. Onoda, Y., Nakazato, M., Nara, T., and Yokoi, I. (1992), "Development of elevator-use, popular-type seismic energy-sensing earthquake detector," Proceedings of the Tenth World Conference on Earthquake Engineering, Madrid, Spain, Vol. 10, 5959-5962.

32. Pavlow, A. V. (1994), Associate Safety Engineer, Elevator, Tramway and Ride Unit, DOSH, State of California, "Personal communication," September 1994.

33. Press, W. H., Teukolsky, S. A., Vetterling, W. T., and Flannery, B. P. (1992). *Numerical Recipes in FORTRAN The Art of Scientific Computing*, 2nd edition, Cambridge University Press.

34. Rutenberg, A., Levy, R., Segal, F., and Marianchik, E. (1996), "Structure-elevator systems under earthquake excitation," Proceedings of the 11th World Conference on Earthquake Engineering, Acapulco, Mexico, CD-ROM, Paper No. 285, Pergamon Press.

35. Schiff, A. J. (1988), "The Whittier Narrows, California earthquake of October 1, 1987-response of elevators," Earthquake Spectra, Vol. 4, No. 2, 367-375.

36. Schiff, A. J. (1990), "Response of elevators to the Whittier Narrows earthquakes of October 1987," in Elevator World Educational Package and Reference Library, Vol. 3, VI.21-VI.25.

37. Schiff, A. J. (1994), Precision Measurement Instruments, "Personal communication," September 1994.

38. Schiff, A.J., Tzou, H.S., and Chu, Y.H. (1980), "Earthquake response of elevator counterweights," Proceedings of the Seventh World Conference on Earthquake Engineering, Istanbul, Turkey, Vol. 8, 483-486.

39. Segal, F., Rutenberg, A. and Levy, R. (1994), "Seismic interaction of elevator-structure systems," Proceedings of the Fifth US National Conference on Earthquake Engineering, Chicago, Illinois, EERI, Vol. IV, 1031-1039.

40. Segal, F., Rutenberg, A., and Levy, R. (1995), "Earthquake response of structure-elevator systems," Proceedings of the 10th European Conference on Earthquake Engineering, Vienna, Austria, A.A. Balkema, Vol. 3, 1545-1549.

41. Segal, F., Rutenberg, A., and Levy, R. (1996), "Earthquake response of structure-elevator system," Journal of Structural Engineering, Vol. 122, No. 6, 607-616.

42. Sturgeon, W., Ed. (1972), "Earthquakes and elevators: Elevator World's 1972 annual study," Elevator World, Mobile, Alabama, October, 75 pp.

43. Suarez, L.E. and Singh, M P. (1996), "Seismic response of rail-counterweight systems of elevators," Proceedings of the 11th World Conference on Earthquake Engineering, Acapulco, Mexico, CD-ROM, Paper No. 1657, Pergamon Press.

44. Suarez, L.E. and Singh, M.P. (1998), "Dynamics and response of rail-counterweight systems under strong seismic motions," Proceedings of the 6th US National Conference on Earthquake Engineering, Seattle, Washington.

45. Suzuki, K. and Kishimoto, F. (1990), "An earthquake-emergency landing device with a primary-wave sensor for elevators," in Elevator World Educational Package and Reference Library, Vol. 3, VI.15-VI.16.

46. Swerrie, D.A. (1990a), "California's 1989 earthquake: attendees at Elevator World seminar discuss earthquakes experiences," Elevator World, Vol. XXXVIII, No. 2, 30-37.

47. Swerrie, D.A. (1990b), "The San Francisco earthquake of 1989 and an inspector's reflections", Elevator World, Vol. XXXVIII, No. 5, 14-22.

48. Swerrie, D.A. (1991), "Enhancing elevator passenger safety and mitigating elevator damage during earthquakes," Proceedings of the Second Conference on Tall Buildings in Seismic Regions, Los Angeles, California, Council on Tall Buildings and Human Habitat, 393-401.

49. Tzou, H.S. (1985), "Dynamic analysis of an elevator counterweight systems," Proceedings of the 3rd International Modal Analysis Conference, Orlando, Florida, Vol. 1, 231-236.

50. Tzou, H.S. and Schiff, A. J. (1984), "Vibration isolation of an elevator system," Proceedings of the 1984 Vibration Damping Workshop, Long Beach, California, LL1-LL5.

51. Tzou, H.S. and Schiff, A. J. (1987), "Development and evaluation of a pseudo-force approximation applied to nonlinear dynamic contacts and viscoelastic damping," Computers and Structures, Vol. 26, No. 3, 481-493.

52. Tzou, H.S. and Schiff, A. J. (1988), "Structural dynamics of elevator counterweight systems and evaluation of passive constraint," Journal of Structural Engineering, Vol. 114, No. 4, 783-803.

53. Tzou, H.S. and Schiff, A. J. (1989), "Dynamics and control of elevators with large gaps and rubber dampers," Journal of Structural Engineering, Vol. 115, No. 11, 2753-2771.

54. Wada, T. and Kitamura, S. (1995), "Report on elevator/escalator damage by the Hyogo-Ken Nanbu earthquake," Elevator World, Vol. XLIII, No. 11, 111-115.

55. Yang, T.Y., Kullegowda, H., Kapania, R.K., and Schiff, A.J. (1983), "Dynamic response analysis of elevator model," Journal of Structural Engineering, Vol. 109, No. 5, 1194-1210.

APPENDIX A

NUMERICAL INTEGRATION METHODS

To solve the nonlinear equations (3-51) for the input motion at the roller guide supports, one must employ a step-by-step time history analysis. Initially in this study the popular Newmark-β method was used. This method is probably the most popular method for the numerical integration of the equations of motion in structural dynamics, especially for nonlinear systems. It was, however, discovered that were some problem with this approach in providing accurate enough results, especially for stiffer brackets. The problem stems from the fact that in the force-deformation relationship shown in Figure 3.2, there is a several orders of magnitude difference in the stiffness values of the two portions. This can cause serious inaccuracy problems if the time step for numerical integration is not chosen properly. The problem is primarily due to the difficulty in locating the point where the change in the stiffness occurs. It was therefore considered necessary to investigate the effectiveness and accuracy of other numerical integration approaches. The methods that were used are: (1) Displacement-based Newmark-β algorithm, (2) Acceleration-based Newmark-β algorithm, (3) Predictor-Corrector methods, (4) Runge-Kutta with fixed time steps, an (5) Runge-Kutta with adaptive time steps. In the following we provide the necessary steps of each numerical algorithm for the nonlinear (bi-linear) spring force model for the sake of the completeness of this study, although finally the Runge-Kutta with adaptive time step was chosen for its accuracy and efficiency.

A.1 Newmark-β

Although the method is discussed in many textbooks in structural dynamics (see, for instance, Chopra, 1995), a brief description of this method specialized for the nonlinear (bilinear) force-deformation model is provided here. Two approaches are presented, displacement-based and acceleration based.

Displacement based

The Newmark-β method is based on the solution of an incremental form of the equations of motion. For the equations of motion (3-51), the incremental equilibrium equation is:

$$[M]\{\Delta\ddot{q}_i\}+\{F_D(\dot{q}_{i+1})\}-\{F_D(\dot{q}_i)\}+\{F_S(q_{i+1})\}-\{F_S(q_i)\}-(\{f_{i+1}\}-\{f_i\})=-[M]\{\Delta\ddot{y}_i\} \quad \text{(A-1)}$$

where

$$\{F_D(\dot{q}_i)\}=[C_d]_i\{\dot{q}_i\} \quad \text{(A-2)}$$

$$\{F_S(q_i)\}=[K_t]_i\{q_i\} \quad \text{(A-3)}$$

Assuming a certain specific variation for the acceleration within the time interval $\Delta t = t_{i+1} - t_i$, the incremental velocity and acceleration can be written as:

$$\{\Delta\dot{q}_i\}=c_1\{\Delta q_i\}-c_2\{\dot{q}_i\}-c_3\{\ddot{q}_i\} \quad \text{(A-4)}$$

$$\{\Delta\ddot{q}_i\}=c_4\{\Delta q_i\}-c_5\{\dot{q}_i\}-c_6\{\ddot{q}_i\} \quad \text{(A-5)}$$

in which c_i, i = 1, … , 6, are constants expressed in terms of the algorithm parameters γ, β, and Δt:

$$c_1 = \frac{\gamma}{\beta \Delta t} \;\; ; \;\; c_2 = \frac{\gamma}{\beta} \;\; ; \;\; c_3 = \Delta t \left(\frac{\gamma}{2\beta} - 1 \right)$$
$$c_4 = \frac{1}{\beta \Delta t^2} \;\; ; \;\; c_5 = \frac{1}{\beta \Delta t} \;\; ; \;\; c_6 = \frac{1}{2\beta} \tag{A-6}$$

where γ = ½, β = ¼ for the average acceleration method and γ = ½, β = 1/6 for the linear acceleration method.

Substituting (A-4) and (A-5) into (A-1) we obtain:

$$\begin{aligned} & c_4 [M] \{\Delta q_i\} + \left\{ F_D \left(c_1 \Delta q_i + \dot{q}_i - c_2 \dot{q}_i - c_3 \ddot{q}_i \right) \right\} - \left\{ F_D \left(\dot{q}_i \right) \right\} \\ & + \left\{ F_S \left(q_i + \Delta q_i \right) \right\} - \left\{ F_S \left(q_i \right) \right\} - \{\Delta f_i\} - \{\Delta P_i\} = 0 \end{aligned} \tag{A-7}$$

where

$$\{\Delta f_i\} = \{f_{i+1}\} - \{f_i\} \tag{A-8}$$
$$\{\Delta P_i\} = -[M]\{\Delta \ddot{y}_i\} + c_5 [M]\{\dot{q}_i\} + c_6 [M]\{\ddot{q}_i\} \tag{A-9}$$

If the tangent stiffness $[K_t]$ and damping matrix $[C_d]$ remain the same during the time step, i.e. each spring at the corners remain in the same region of the bilinear force-deformation relationship, equation (A-7) can be solved for $\{\Delta q_i\}$:

$$\{\Delta q_i\} = \left(c_4 [M] + c_1 [C_d] + [K_t] \right)^{-1} \{\Delta R_i\} \tag{A-10}$$

where

$$\{\Delta R_i\} = \{\Delta P_i\} + [C_d] \left(c_2 \{\dot{q}_i\} + c_3 \{\ddot{q}_i\} \right) \tag{A-11}$$

Once $\{\Delta q_i\}$ is known, the incremental velocity and acceleration can be obtained from (A-4) and (A-5). They, in turn, can be used to obtain the values at the end of the interval:

$$\{q_{i+1}\} = \{q_i\} + \{\Delta q_i\} \tag{A-12}$$
$$\{\dot{q}_{i+1}\} = \{\dot{q}_i\} + \{\Delta \dot{q}_i\} \tag{A-13}$$
$$\{\ddot{q}_{i+1}\} = \{\ddot{q}_i\} + \{\Delta \ddot{q}_i\} \tag{A-14}$$

Usually the acceleration is calculated directly from the equations of motion at time t_{i+1} instead of using (A-14).

Because the tangent stiffness $[K_t]$ and damping matrix $[C_d]$ may not remain the same during the time step, we have to do iteration using Newton-Raphson scheme where the solution of function $g(\Delta q_i) = 0$ as in equation (A-7) is calculated incrementally so that

$$\{\Delta q_i\} = \{\Delta q_i\}^{(n)} = \Delta\{\Delta q_i\}^{(1)} + \Delta\{\Delta q_i\}^{(2)} + \ldots + \Delta\{\Delta q_i\}^{(n)} \tag{A-15}$$

The k-th approximation $\Delta\{\Delta q_i)^{(k)}$ is calculated by:

$$\Delta\{\Delta q_i\}^{(k)} = -\left[\frac{g(\Delta q_i)}{\left(\frac{dg}{d(\Delta q_i)}\right)}\right]_{\{\Delta q_i\}^{(k-1)}} \tag{A-16}$$

For equation (A-7), we have:

$$\Delta\{\Delta q_i\}^{(k)} = \left(c_4[M] + c_1[C_d]^{(k-1)} + [K_t]^{(k-1)}\right)^{-1}\{\Delta R_i\}^{(k)} \tag{A-17}$$

where

$$\{\Delta R_i\}^{(k)} = \{\Delta P_i\} - \begin{Bmatrix} c_4[M]\{\Delta q_i\}^{(k-1)} + [C_d]^{(k-1)}\{\dot{q}_{i+1}\}^{(k-1)} - [C_d]^{(0)}\{\dot{q}_i\} \\ + [K_t]^{(k-1)}\{q_{i+1}\}^{(k-1)} - [K_t]^{(0)}\{q_i\} - \{\Delta f_i\}^{(k-1)} \end{Bmatrix} \tag{A-18}$$

$$[C_d]^{(k)} = \left[C_d\left(\dot{q}_{i+1}^{(k)}\right)\right] \tag{A-19}$$

$$[K_t]^{(k)} = \left[K_t\left(q_{i+1}^{(k)}\right)\right] \tag{A-20}$$

$$\{\Delta f_i\}^{(k)} = \left\{f\left(q_{i+1}^{(k)}\right)\right\} - \{f(q_i)\} \tag{A-21}$$

$$\{q_{i+1}\}^{(k)} = \{q_i\} + \{\Delta q_i\}^{(k)} \tag{A-22}$$

$$\{\dot{q}_{i+1}\}^{(k)} = \{\dot{q}_i\} + \{\Delta\dot{q}_i\}^{(k)} = \{\dot{q}_i\} + c_1\{\Delta q_i\}^{(k)} - c_2\{\dot{q}_i\} - c_3\{\ddot{q}_i\} \tag{A-23}$$

The iteration should stop when the deformation of each spring remains in the same region of the force-deformation diagram at two consecutive iterations. If each spring remains in the same region at the (k-1)-th and k-th iteration, then:

$$[C_d]^{(k)} = [C_d]^{(k-1)} \tag{A-24}$$

$$[K_t]^{(k)} = [K_t]^{(k-1)} \tag{A-25}$$

$$\{\Delta f_i\}^{(k)} = \{\Delta f_i\}^{(k-1)} \tag{A-26}$$

Using these facts, and writing the current displacement as:

$$\{\Delta q_i\}^{(k)} = \{\Delta q_i\}^{(k-1)} + \Delta\{\Delta q_i\}^{(k)} \tag{A-27}$$

the incremental force $\{\Delta R_i\}^{(k+1)}$ for the next step can be written as:

$$\begin{aligned}\{\Delta R_i\}^{(k+1)} &= \{\Delta R_i\}^k - \left(c_4[M] + c_1[C_d]^{(k-1)} + [K_t]^{(k-1)}\right)\Delta\{\Delta q_i\}^{(k)} \\ &= \{\Delta R_i\}^k - \{\Delta R_i\}^k = 0\end{aligned} \tag{A-28}$$

Thus the next correction to the displacement will be zero and the iteration can be stopped.

In the following, the steps of the displacement-based Newmark method for the numerical integration of equations of motion (3-51) are described.

1. Calculate mass matrix [M] and choose time step Δt and parameter γ and β.
2. Calculate the constants c_1 to c_6 from equation (A-6).
3. Initialize the displacement, velocity, and acceleration vectors.
4. Based on displacement vector, record the position of each spring in the force-deformation diagram.
5. Based on the displacement vector, calculate the tangent stiffness matrix [K_t], damping matrix [C_d] and nonlinear force vector $\{f_i\}$.
6. Calculate $\{\Delta P_i\}$ from equation (A-9) and $\{\Delta R_i\}$ from (A-11).
7. Use (A-10), then (A-4), (A-12), and (A-13) to obtain incremental displacement and velocity, and total displacement and velocity at the next time step, respectively.
8. Based on the new displacement vector, calculate the displacement of each spring and record the position of each spring in the force-deformation diagram. Compare the position of each spring to the previous one (step 4). If each spring stays within the same region, the results of step 7 are final and go to step 13, otherwise the results from step 7 are only the first approximation and continue to step 9.

   Steps 9 through 12 are done iteratively until each corner spring stays within the same region of force-displacement diagram in two consecutive iterations.

9. Based on current (k-1)-th displacement vector, recalculate the tangent stiffness $[K_t]^{(k\text{-}1)}$, damping matrix $[C_d]^{(k\text{-}1)}$ and nonlinear force vector $\{\Delta f_i\}^{(k\text{-}1)}$.
10. Calculate $\{\Delta R_i\}^{(k)}$ using (A-18).
11. Use (A-17), (A-15), (A-22), and (A-23) consecutively to obtain the next approximation for displacement and velocity vector.
12. Calculate the displacement of each spring and record the position of each spring in the force-deformation diagram. Compare the positions to the previous ones. If each of them stays in the same region, the results from step 11 are final and continue to step 13. Otherwise, replace the (k-1)-th results with the new approximations and repeat from step 9.
13. Calculate the acceleration for the next time step using the equations of motion.
14. Repeat from step 5 with the next time step.

Acceleration-based

Some of the constants in (A-6) have Δt or Δt^2 in their denominator, and this may create some numerical problems because of the very small time step. Therefore, a numerical scheme based

on the calculation of acceleration first and then the velocity and displacement was formulated. This formulation did not involve division by small numbers associated with Δt^2 but of course this formulation has terms that are multiplied by these small numbers.

In this scheme approach, the incremental equations of motion are solved for incremental acceleration first, and the incremental velocity and displacement are calculated from this incremental acceleration as:

$$\left\{\Delta \dot{q}_i\right\} = a_1 \left\{\Delta \ddot{q}_i\right\} + a_2 \left\{\ddot{q}_i\right\} \tag{A-29}$$

$$\left\{\Delta q_i\right\} = a_3 \left\{\Delta \ddot{q}_i\right\} + a_4 \left\{\ddot{q}_i\right\} + a_2 \left\{\dot{q}_i\right\} \tag{A-30}$$

where

$$a_1 = \frac{\Delta t}{2} \;\; ; \;\; a_2 = \Delta t \;\; ; \;\; a_3 = \beta \Delta t^2 \;\; ; \;\; a_4 = \frac{\Delta t^2}{2} \tag{A-31}$$

The nonlinear function $g(\Delta q_i) = 0$ similar to equation (A-7) for this approach is:

$$\begin{aligned} &\left[M\right]\left\{\Delta \ddot{q}_i\right\} + \left\{F_D\left(\dot{q}_i + a_1 \Delta \ddot{q}_i + a_2 \ddot{q}_i\right)\right\} - \left\{F_D\left(\dot{q}_i\right)\right\} \\ &+ \left\{F_S\left(q_i + a_3 \Delta \ddot{q}_i + a_4 \ddot{q}_i\right)\right\} - \left\{F_S\left(q_i\right)\right\} - \left\{\Delta f_i\right\} - \left\{\Delta \hat{P}_i\right\} = 0 \end{aligned} \tag{A-32}$$

where

$$\left\{\Delta \hat{P}_i\right\} = -\left[M\right]\left\{\Delta \ddot{y}_i\right\} \tag{A-33}$$

The incremental acceleration for the linear case is:

$$\left\{\Delta \ddot{q}_i\right\} = \left(\left[M\right] + a_1\left[C_d\right] + a_3\left[K_t\right]\right)^{-1} \left\{\Delta \hat{R}_i\right\} \tag{A-34}$$

where

$$\left\{\Delta \hat{R}_i\right\} = \left\{\Delta \hat{P}_i\right\} - \left\{\left(a_2\left[C_d\right] + a_4\left[K_t\right]\right)\left\{\ddot{q}_i\right\} + a_2\left[K_t\right]\left\{\dot{q}_i\right\}\right\} \tag{A-35}$$

Using Newton-Raphson iteration, the k-th approximation $\Delta\{\Delta q_i\}^{(k)}$ becomes:

$$\Delta\left\{\Delta \ddot{q}_i\right\}^{(k)} = \left(\left[M\right] + a_1\left[C_d\right]^{(k-1)} + a_3\left[K_t\right]^{k-1}\right)^{-1} \left\{\Delta \hat{R}_i\right\}^{(k)} \tag{A-36}$$

where

$$\left\{\Delta \hat{R}_i\right\}^{(k)} = \left\{\Delta \hat{P}_i\right\} - \begin{Bmatrix} \left[M\right]\left\{\Delta \ddot{q}_i\right\}^{(k-1)} + \left[C_d\right]^{(k-1)}\left\{\dot{q}_{i+1}\right\}^{(k-1)} - \left[C_d\right]^{(0)}\left\{\dot{q}_i\right\} \\ + \left[K_t\right]^{(k-1)}\left\{q_{i+1}\right\}^{(k-1)} - \left[K_t\right]^{(0)}\left\{q_i\right\} - \left\{\Delta f_i\right\}^{(k-1)} \end{Bmatrix} \tag{A-37}$$

$$\left\{\Delta \ddot{q}_i\right\}^{(k)} = \Delta\left\{\Delta \ddot{q}_i\right\}^{(1)} + \Delta\left\{\Delta \ddot{q}_i\right\}^{(2)} + \ldots + \Delta\left\{\Delta \ddot{q}_i\right\}^{(k)} \tag{A-38}$$

$$\{\Delta\dot{q}_i\}^{(k)} = a_1\{\Delta\ddot{q}_i\}^{(k)} + a_2\{\ddot{q}_i\} \tag{A-39}$$

$$\{\Delta q_i\}^{(k)} = a_3\{\Delta\ddot{q}_i\}^{(k)} + a_4\{\ddot{q}_i\} + a_2\{\dot{q}_i\} \tag{A-40}$$

$$\{q_{i+1}\}^{(k)} = \{q_i\} + \{\Delta q_i\}^{(k)} \tag{A-41}$$

$$\{\dot{q}_{i+1}\}^{(k)} = \{\dot{q}_i\} + \{\Delta\dot{q}_i\}^{(k)} \tag{A-42}$$

Again, the final incremental acceleration:

$$\{\Delta\ddot{q}_i\} = \{\Delta\ddot{q}_i\}^{(n)} = \Delta\{\Delta\ddot{q}_i\}^{(1)} + \Delta\{\Delta\ddot{q}_i\}^{(2)} + \ldots + \Delta\{\Delta\ddot{q}_i\}^{(n)} \tag{A-43}$$

is obtained when each spring remains on the same region in two consecutive iterations.

In the following, the steps of the acceleration-based Newmark method for the numerical integration of equations of motion (…..) are described.

1. Calculate mass matrix [M] and choose time step Δt and parameter β.
2. Calculate the constants a_1 to a_4 from equation (A-6).
3. Initialize the displacement, velocity, and acceleration vectors.
4. Based on displacement vector, record the position of each spring in the force-deformation diagram.
5. Based on the displacement vector, calculate the tangent stiffness matrix [K_t], damping matrix [C_d] and nonlinear force vector $\{f_i\}$.
6. Calculate $\left\{\Delta\hat{P}_i\right\}$ from (A-33) and $\left\{\Delta\hat{R}_i\right\}$ from (A-35).
7. Use (A-34), then (A-29), (A-30), (A-12), and (A-13) consecutively to obtain the displacement and velocity at the next time step, respectively.
8. Based on the new displacement vector, calculate the displacement of each spring and record the position of each spring in the force-deformation diagram. Compare the position of each spring to the previous one (step 4). If each spring stays within the same region, the results of step 7 are final and go to step 13, otherwise the results from step 7 are only the first approximation and continue to step 9.
9. Based on current (k-1)-th displacement vector, recalculate the tangent stiffness $[K_t]^{(k\text{-}1)}$, damping matrix $[C_d]^{(k\text{-}1)}$ and nonlinear force vector $\{\Delta f_i\}^{(k\text{-}1)}$.
10. Calculate $\left\{\Delta\hat{R}_i\right\}^{(k)}$ using (A-37).
11. Use (A-36), then (A-38) through (A-42) consecutively to obtain the next approximation for displacement and velocity vector.
12. Calculate the displacement of each spring and record the position of each spring in the force-deformation diagram. Compare the positions to the previous ones. If each of them stays in the same region, the results from step 11 are final and continue to step 13. Otherwise, replace the (k-1)-th results with the new approximations and repeat from step 9.
13. Calculate the acceleration for the next time step using the equations of motion.
14. Repeat from step 5 with the next time step.

A.2 Runge-Kutta Method

In solving ordinary differential equation, the most commonly used Runge-Kutta method is the one classical fourth order scheme. For the state space form of ordinary differential equations:

$$\dot{q} = f\left(t, q\right) \tag{A-44}$$

or, for the combined equations of motion (…..)

$$\left\{\dot{q}\right\} = \left[A\right]\left\{q\right\} + \left\{B\right\} \tag{A-45}$$

where

$$\left\{q\right\} = \begin{bmatrix} u_c & u_e & v_c & v_e & v_e^{'} & \dot{u}_c & \dot{u}_e & \dot{v}_c & \dot{v}_e & \dot{v}_e^{'} \end{bmatrix}^T \tag{A-46}$$

$$\left[A\right] = \begin{bmatrix} \left[O\right]_{5\times5} & \left[I\right]_{5\times5} \\ -\left[M\right]^{-1}\left[K_t\right] & -\left[M\right]^{-1}\left[C_d\right] \end{bmatrix} \tag{A-47}$$

$$\left\{B\right\} = \begin{Bmatrix} \left\{O\right\}_{5\times1} \\ -\left\{\ddot{y}\right\} + \left[M\right]^{-1}\left\{f_i\right\} \end{Bmatrix} \tag{A-48}$$

the fourth order Runge-Kutta formula is:

$$q_{i+1} = q_i + \frac{1}{6}\left(k_1 + 2k_2 + 2k_3 + k_4\right) \tag{A-49}$$

where

$$\begin{aligned} k_1 &= \Delta t\ f\left(t_i, q_i\right) \\ k_2 &= \Delta t\ f\left(t_i + \frac{\Delta t}{2}, q_i + \frac{k_1}{2}\right) \\ k_3 &= \Delta t\ f\left(t_i + \frac{\Delta t}{2}, q_i + \frac{k_2}{2}\right) \\ k_4 &= \Delta t\ f\left(t_i + \Delta t, q_i + k_3\right) \end{aligned} \tag{A-50}$$

The local truncation error is of order $O(\Delta t^5)$. This method is relatively easy to implement and gives good accuracy, but as also happen to other constant time step method, the calculation time may become very large especially in the case where very small time step is needed.

Adaptive step size

To reduce computation time, adaptive step size version of Runge-Kutta method is used. The general formula for adaptive step size method of Runge-Kutta is in the form of:

$$q_{i+1} = q_i + \sum_{n=1}^{6} c_n\, k_n \tag{A-51}$$

where

$$k_1 = \Delta t\ f(t_i, q_i)$$
$$k_n = \Delta t\ f\left(t_i + a_n \Delta t, q_i + \sum_{m=1}^{n-1} b_{nm} k_m\right) \quad , \quad n = 2, \ldots, 6 \tag{A-52}$$

with local truncation error of $O(\Delta t^6)$.

Several sets of coefficients and computer algorithms for implementation of this method are available. In this report, algorithm provided by Press et. al (1992) is used. The algorithm uses coefficients suggested by Cash and Karp (1990):

$$a_2 = \tfrac{1}{5},\ a_3 = \tfrac{3}{10},\ a_4 = \tfrac{3}{5},\ a_5 = 1,\ a_6 = \tfrac{7}{8}$$
$$b_{21} = \tfrac{1}{5}$$
$$b_{31} = \tfrac{3}{40},\ b_{32} = \tfrac{9}{40}$$
$$b_{41} = \tfrac{3}{10},\ b_{42} = \tfrac{-9}{10},\ b_{43} = \tfrac{6}{5}$$
$$b_{51} = \tfrac{-11}{54},\ b_{52} = \tfrac{5}{2},\ b_{53} = \tfrac{-70}{27},\ b_{54} = \tfrac{35}{27}$$
$$b_{61} = \tfrac{1631}{55296},\ b_{62} = \tfrac{175}{512},\ b_{63} = \tfrac{575}{13824},\ b_{64} = \tfrac{44275}{110592},\ b_{65} = \tfrac{253}{4096}$$
$$c_1 = \tfrac{37}{378},\ c_2 = 0,\ c_3 = \tfrac{250}{621},\ c_4 = \tfrac{125}{594},\ c_5 = 0,\ c_6 = \tfrac{512}{1771}$$

which is considered to be more efficient method with better error properties.

With this method, the step size is controlled so that the results would be within the desired accuracy. For instance, if a time step Δt_1 produces an error of Δ_1, the required Δt_0 that would give the desired accuracy Δ_0 is estimated as

$$\Delta t_0 = \Delta t_1 \left| \frac{\Delta_0}{\Delta_1} \right|^{0.2} \tag{A-53}$$

Press et. al (1992) found a step size correction that was more reliable with respect to accumulation of errors as follows

$$\Delta t_0 = \begin{cases} 0.9 \Delta t_1 \left| \dfrac{\Delta_0}{\Delta_1} \right|^{0.2} & \text{for } \Delta_0 \geq \Delta_1 \\ 0.9 \Delta t_1 \left| \dfrac{\Delta_0}{\Delta_1} \right|^{0.25} & \text{for } \Delta_0 \leq \Delta_1 \end{cases} \tag{A-54}$$

with the vector of desired accuracy scaled proportional to the time step:

$$\Delta_0 = \varepsilon \Delta t \times f\left(t_i, q_i\right) \tag{A-55}$$

where ε is a prescribed tolerance.

A.3 Predictor-corrector Method

Some references (for instance, Meirovitch, 1997) consider that predictor-corrector method more accurate results than Runge-Kutta. Press et. al. (1992) indicates that the predictor-corrector is only better if the differential equations contain smooth functions, while Runge-Kutta, especially the adaptive step size versions, is better if the right-hand side of the equations contains non smooth functions or discontinuities, or involves table look-up and interpolation. Here, for comparisons, we also use predictor-corrector method to solve the equations of motion and then compare the results with other methods described above.

Predictor-corrector method is a part of numerical integration techniques for ordinary differential equations, called *multi-step* methods. With these multi-step methods, the information at the next time step is computed using information from more than one previous time step. The method is not self-starting because it needs several starting points so that other self-starting method, such as Runge-Kutta, has to be used to generate the results for these initial points.

In the predictor-corrector method, the predictor is used to obtain approximate solution at the next time step. This solution is, then iteratively corrected by the corrector until the desired level of convergence is satisfied. There are several schemes of predictor-corrector methods available. Here, Hamming's fourth-order method is used (Hamming, 1973). The method uses information from the previous four time steps to compute the result at the next time step. In the following, the calculation process is presented.

First, the predicted solution to the general equation is calculated by:

$$q_{i+1}^{p} = q_{i-3} + \frac{4\Delta t}{3}\left(2\dot{q}_i - \dot{q}_{i-1} + 2\dot{q}_{i-2}\right) \tag{A-56}$$

To speed the convergence, the predicted solution is modified by the truncation errors E_i from the previous time step:

$$q_{i+1}^{0} = q_{i+1}^{p} + \frac{112}{9}E_i \tag{A-57}$$

This prediction is corrected iteratively using the corrector:

$$q_{i+1}^{k+1} = \frac{1}{8}\left[9q_i - q_{i-2} + 3\Delta t\left(\dot{q}_{i+1}^{k} + 2\dot{q}_i - \dot{q}_{i-1}\right)\right] \tag{A-58}$$

The iteration is stopped when the convergence criteria is achieved:

$$\left\| q_{i+1}^{k+1} - q_{i+1}^{k} \right\| \le \varepsilon \tag{A-59}$$

and the final solution for the time step is again modified by the truncation error:

$$q_{i+1} = q_{i+1}^{k+1} - E_{i+1} \tag{A-60}$$

where

$$E_{i+1} = \frac{9}{121}\left(q_{i+1}^{k+1} - q_{i+1}^{p}\right) \tag{A-61}$$

As mentioned before, other method has to be used to generate the first starting points, in this case the first three time step. Here, to be consistent with using predictor-corrector methods, we use lower order predictor-corrector methods, i.e. first-order for the first, second-order for the second, and third-order for the third time step.

The *Euler* method is used as predictor for the first-order at the first time step:

$$q_{i+1}^{0} = q_i + \Delta t\ \dot{q}_i \tag{A-62}$$

and the correction is given by *Modified Euler* method:

$$q_1^{k+1} = q_0 + \frac{\Delta t}{2}\left(\dot{q}_1^{k} + \dot{q}_0\right) \tag{A-63}$$

In the second time step Adams-Bashforth two-step method is used as the predictor:

$$q_2^{0} = q_1 + \frac{\Delta t}{2}\left(3\dot{q}_1 - \dot{q}_0\right) \tag{A-64}$$

and Adams-Moulton two-step method as the corrector:

$$q_2^{k+1} = q_1 + \frac{\Delta t}{12}\left(5\dot{q}_2^{k} + 8\dot{q}_1 - \dot{q}_0\right) \tag{A-65}$$

For the third time step we use Adams-Bashforth three-step method as the predictor:

$$q_3^{0} = q_2 + \frac{\Delta t}{12}\left(23\dot{q}_2 - 16\dot{q}_1 + 5\dot{q}_0\right) \tag{A-66}$$

and Adams-Moulton three-step method as the corrector:

$$q_3^{k+1} = q_2 + \frac{\Delta t}{24}\left(9\dot{q}_3^{k} + 19\dot{q}_2 - 5\dot{q}_1 + \dot{q}_0\right) \tag{A-67}$$

At every time step mentioned above, the iteration for the corrector is stopped when the convergence criteria is satisfied.

A.4 Comparison of Numerical Results

All the methods mentioned above are used to solve the equations of motion of the counterweight for Northridge earthquake with maximum ground acceleration of 0.1g and 0.843g (actual). Higher level of input intensity is used to verify the accuracy of the methods at these levels of excitation as well. The adaptive step size of Runge-Kutta is the only method that uses variable time step. To verify the accuracy of numerical results, several sets of results obtained for different step sizes are compared with each other as no exact solution of a similar problem is available.

With the adaptive step size method, the time steps are varied between the order of 10^{-10} to 10^{-3} seconds. For the constant time step, first we started with a step size of $\Delta t = 10^{-3}$ seconds. For this step size, however, the predictor-corrector method could not converge. In Figures A-1 through

A-4 we compare the results obtained with the Newmark-β and RK4 (fourth-order Runge-Kutta, constant time step) with that of the adaptive Runge-Kutta method. We observe that the Newmark - β and the RK4 both give values close to the values obtained by more accurate adaptive step size method at most counterweight positions in the middle of the span. The response values differe near the end positions, especially so for higher levels of excitation.

We next decreased the size of the time step. With $\Delta t = 10^{-4}$ seconds, the predictor-corrector method did converge for 0.1g but not for the higher excitation intensity =0.843g it again failed to converge. The comparison of the results is now shown in figures A-5 to A-8 for stresses in the rails and the counterweight. The accuracy of the results now further improved as they are closer to the adaptive step size results for most of the counterweight positions but still there are apparent differences when the roller is near the bracket support. The difference in the bracket stress is especially significant when the top roller is on the lower bracket support. Another problem with this smaller step size is, of course, the total time of computation. The computation time for the constant time step methods are much longer than that of the adaptive step size.

Finally we try $\Delta t = 10^{-6}$ seconds and the results are shown in figures A-9 to A-12. The computation time is not practical anymore since each of the constant time step method takes more than 40 hours to produce the results, compare to about 15 minutes taken by with the adaptive step size method on a Pentium 4 machine. All the methods now give results close to each other, especially with Northridge 0.1g. For the higher excitation level, however, some differences still persists when the roller is near the support.

The results above show that the adaptive step size of Runge-Kutta is more reliable and efficient for the analysis. Obviously the computation time is much less with the adaptive time step method. We could also use a variable time step approach with the Newmark-β approach. In fact, we tried the time steps used in the adaptive scheme with the Newmark-β approach, but had numerical problems for the some of smaller time step values used by the adaptive scheme. Since the results of the Newmark-β, predictor corrector, and RK4 tend to approach the values calculated by the adaptive Runge-Kutta scheme with improving accuracy for decreasing values of the time step sizes, this seems to verify the reliability of the latter scheme as claimed by Press. This method has, therefore, been used in thus study to obtain all results in Section3.

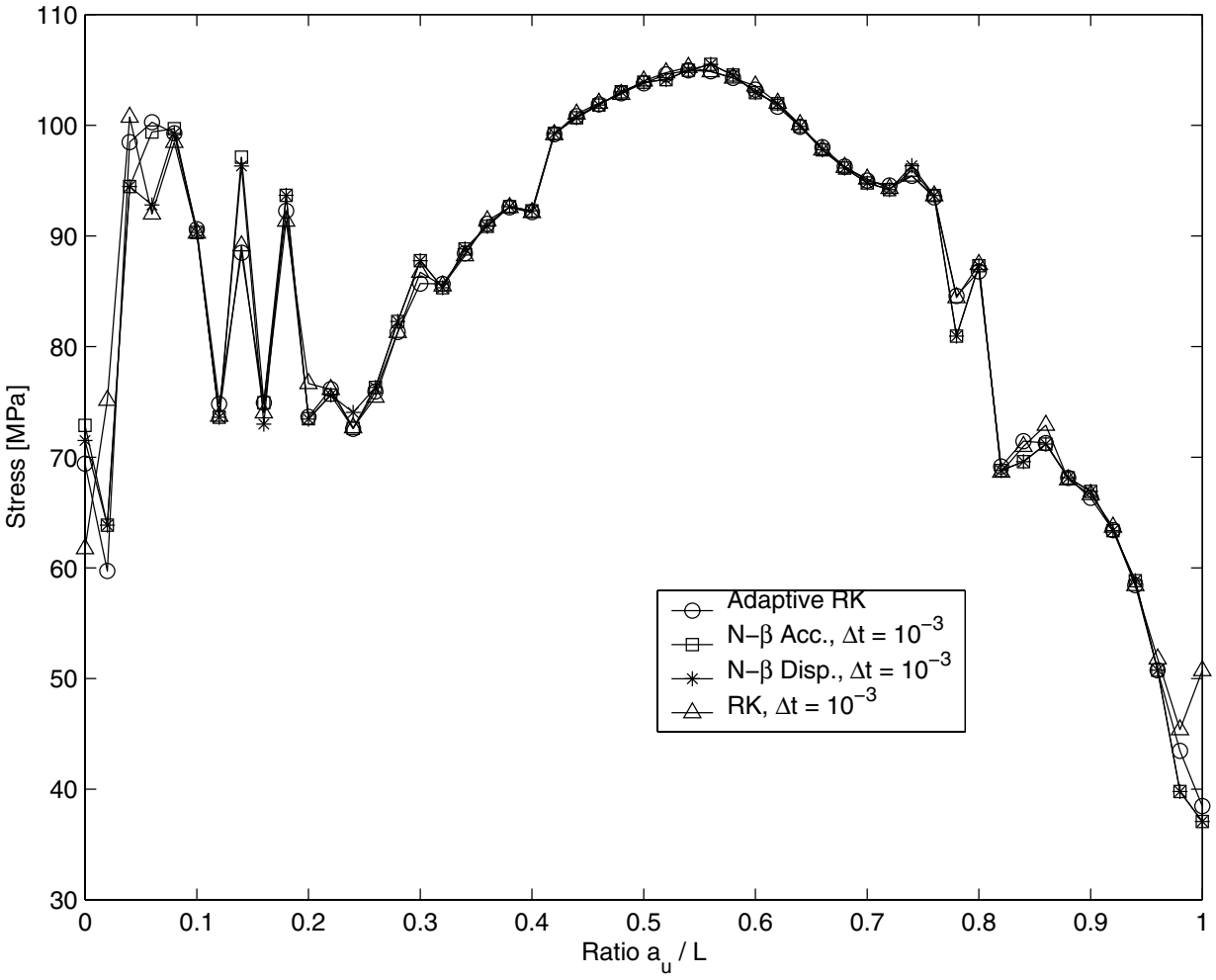

FIGURE A-1 Maximum Stress in the Rail for Counterweight in the Top Story of 10-Story Building, for Northridge 0.1g, Results from Different Numerical Methods

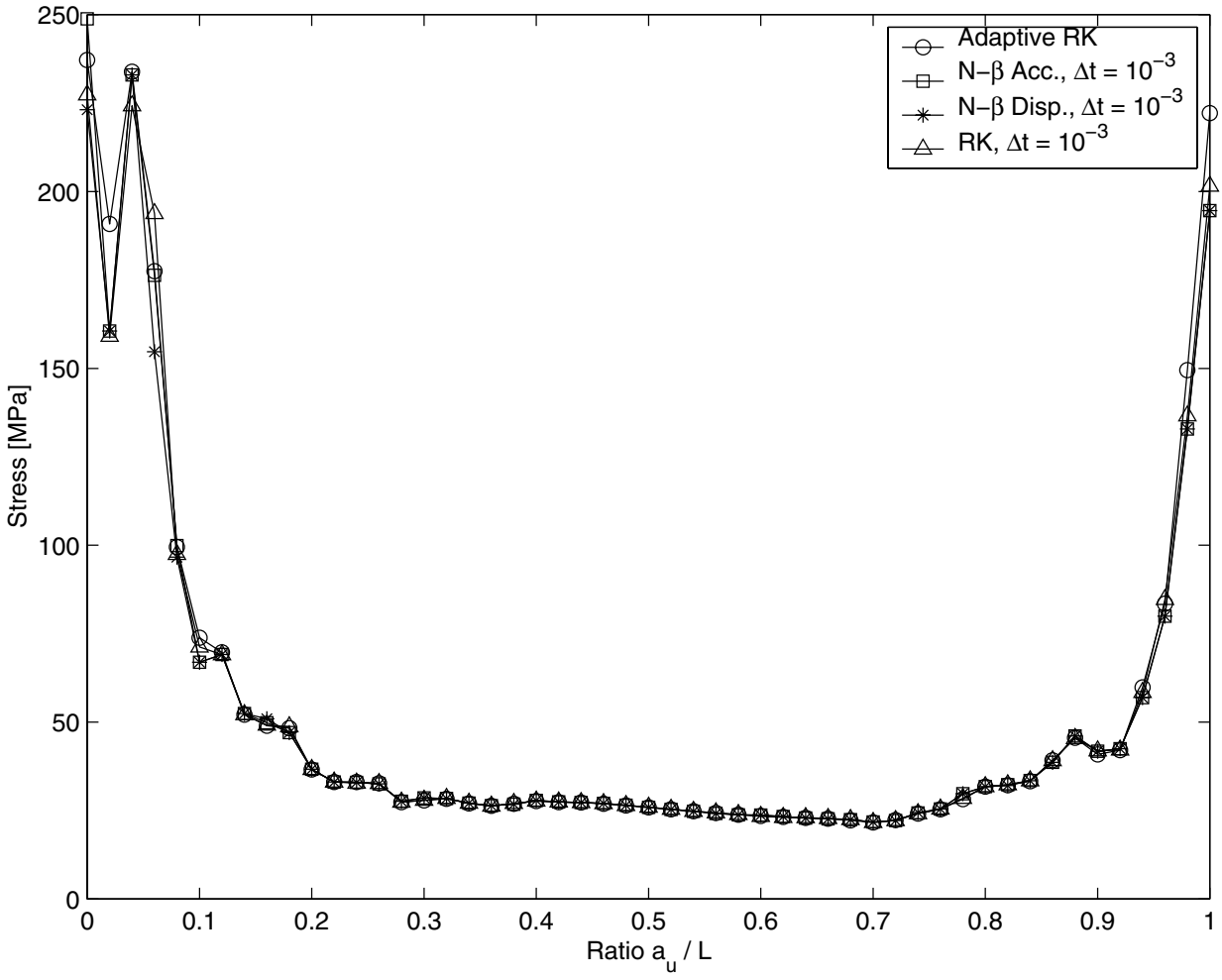

FIGURE A-2 Maximum Stress in the Bracket for Counterweight in the Top Story of 10-Story Building, for Northridge 0.1g, Results from Different Numerical Methods

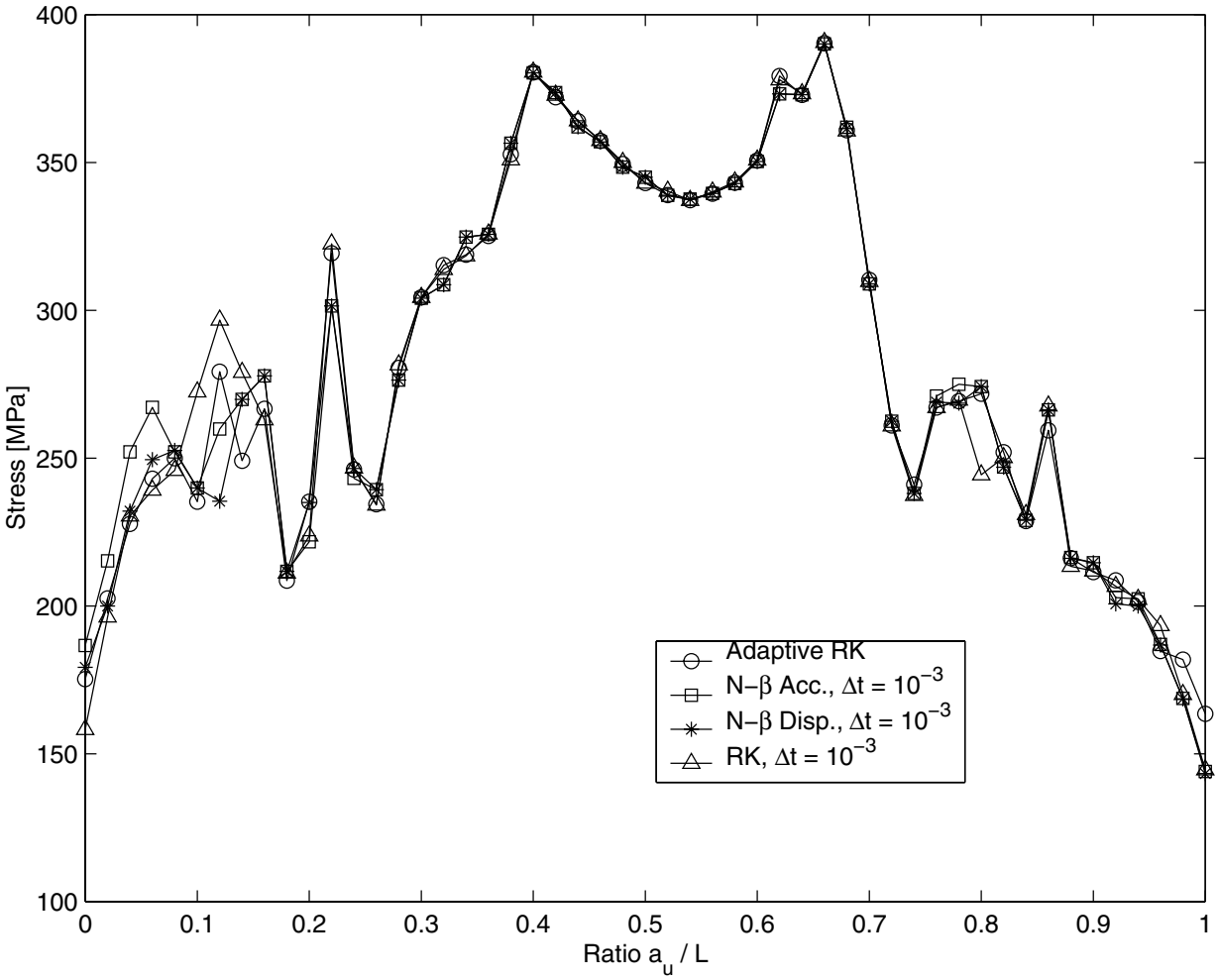

FIGURE A-3 Maximum Stress in the Rail for Counterweight in the Top Story of 10-Story Building, for Actual Northridge Earthquake, Results from Different Numerical Methods

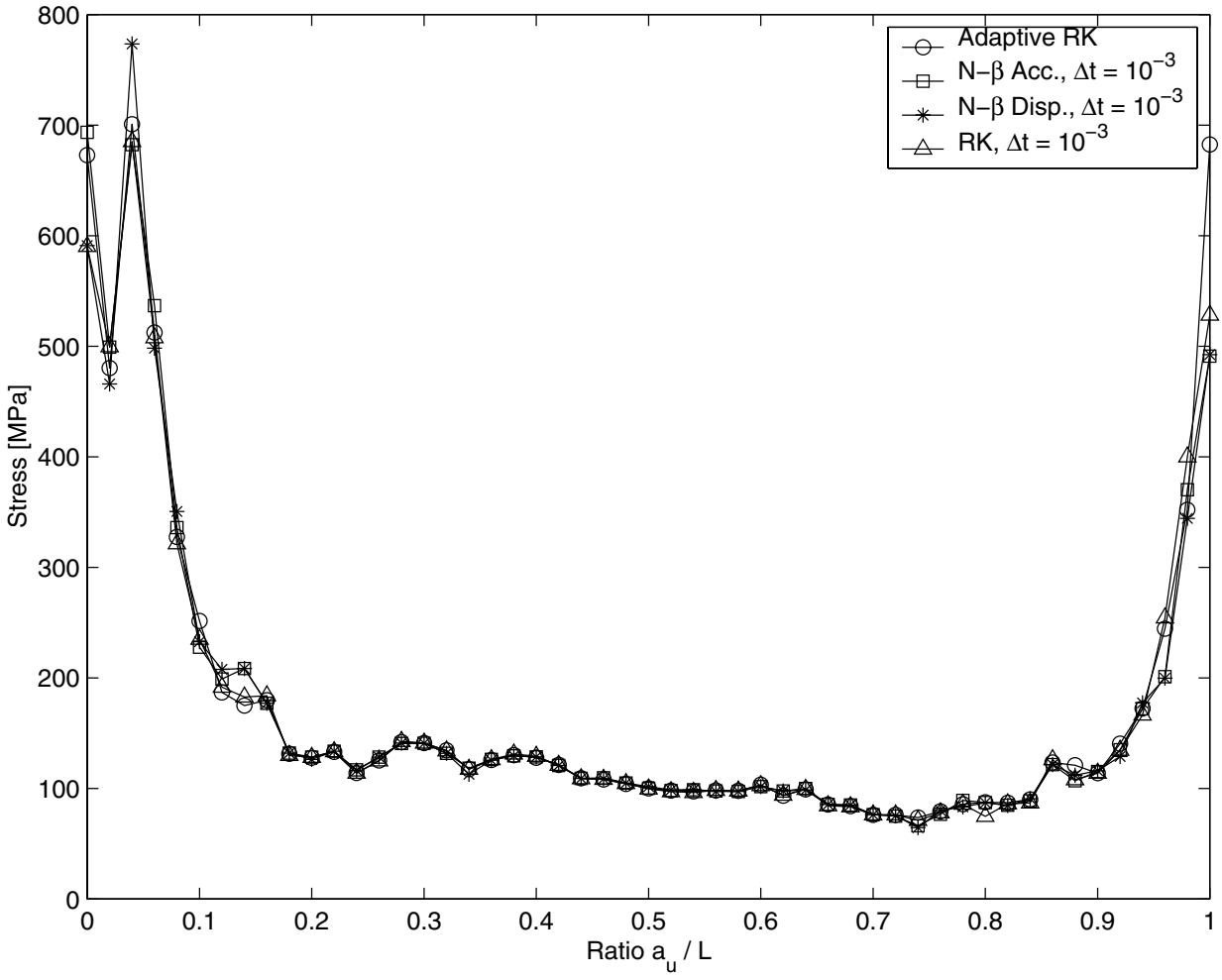

FIGURE A-4 Maximum Stress in the Bracket for Counterweight in the Top Story of 10-Story Building, for Actual Northridge Earthquake, Results from Different Numerical Methods

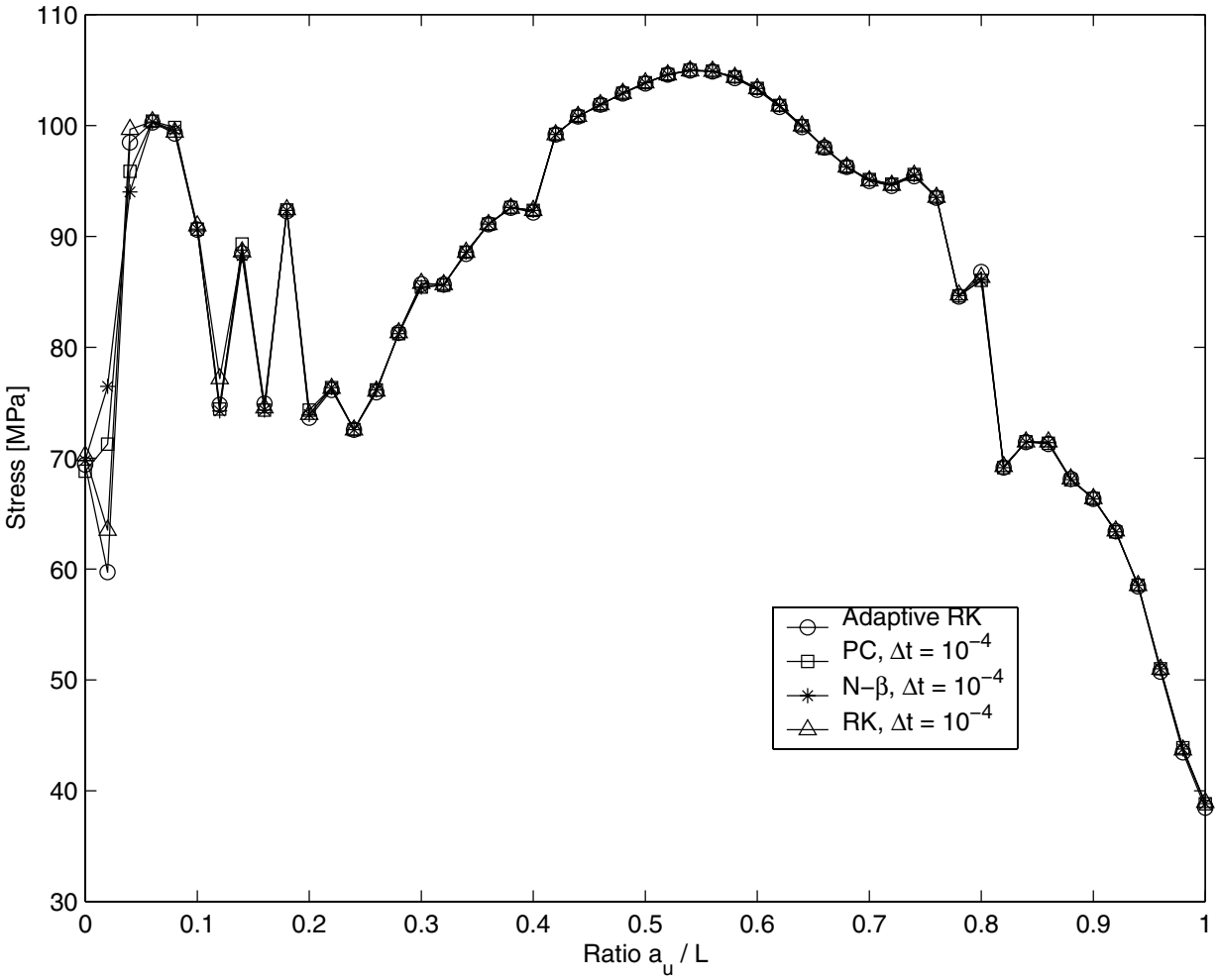

FIGURE A-5 Maximum Stress in the Rail for Counterweight in the Top Story of 10-Story Building, for Northridge 0.1g, Results from Different Numerical Methods

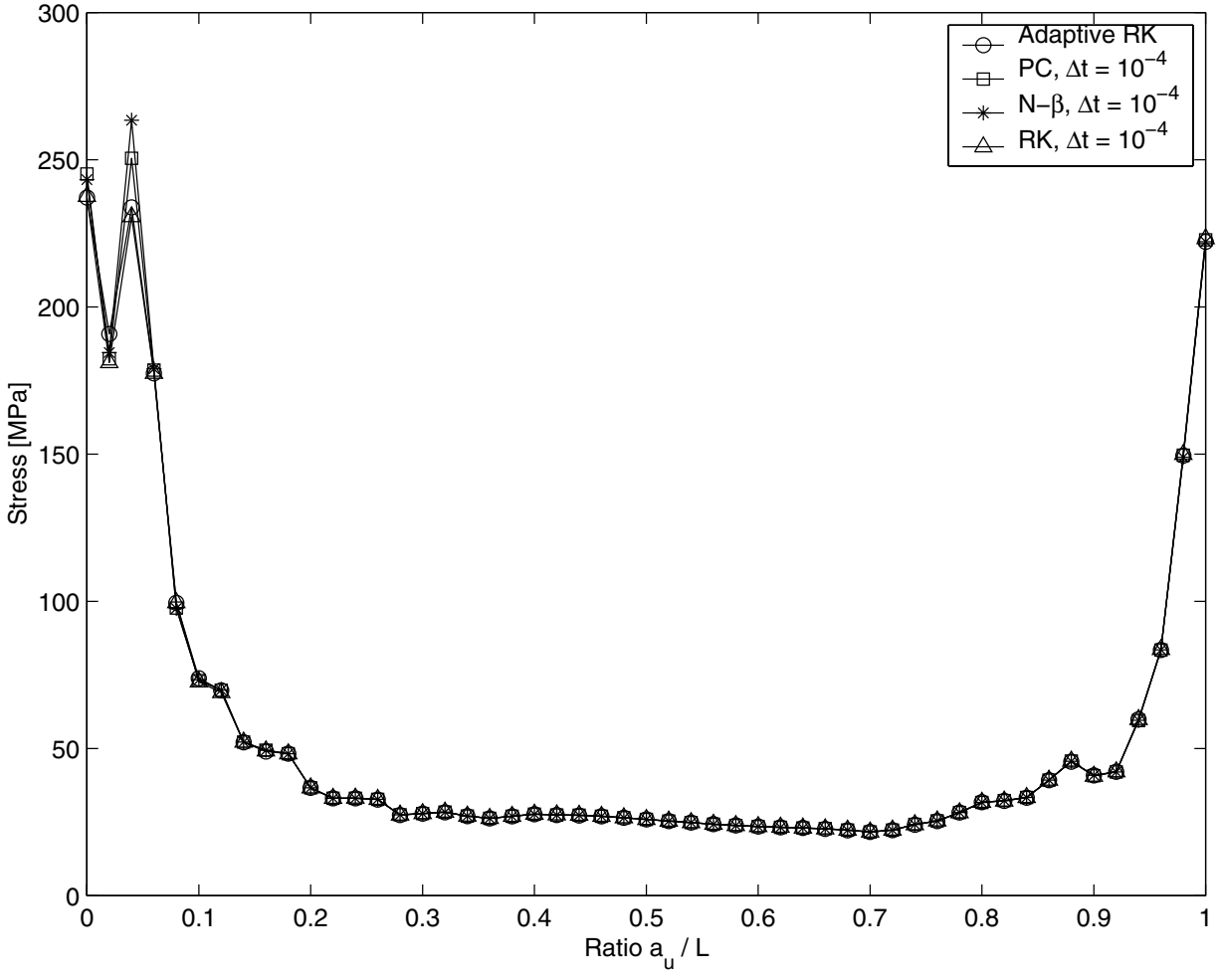

FIGURE A-6 Maximum Stress in the Bracket for Counterweight in the Top Story of 10-Story Building, for Northridge 0.1g, Results from Different Numerical Methods

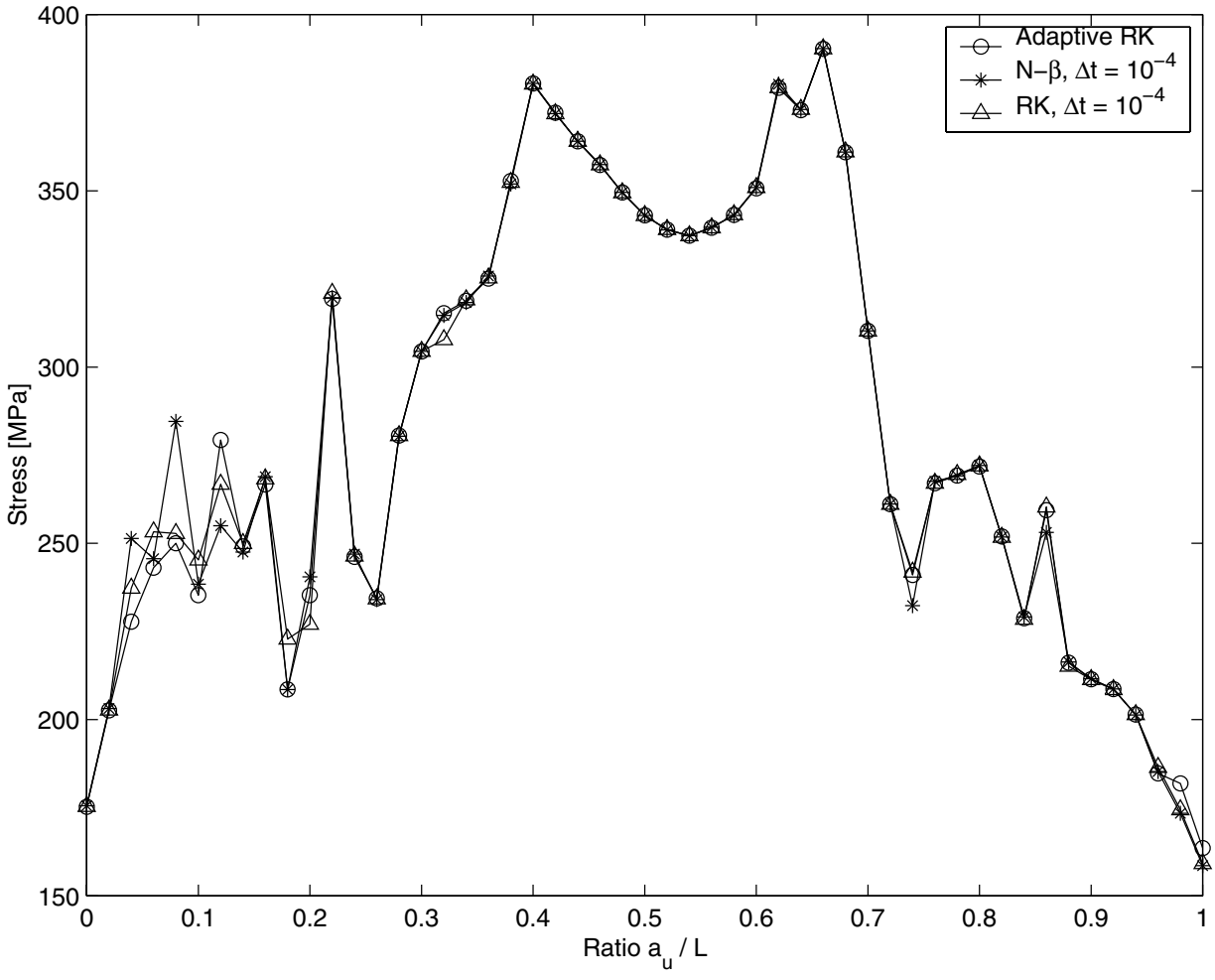

FIGURE A-7 Maximum Stress in the Rail for Counterweight in the Top Story of 10-Story Building, for Actual Northridge Earthquake, Results from Different Numerical Methods

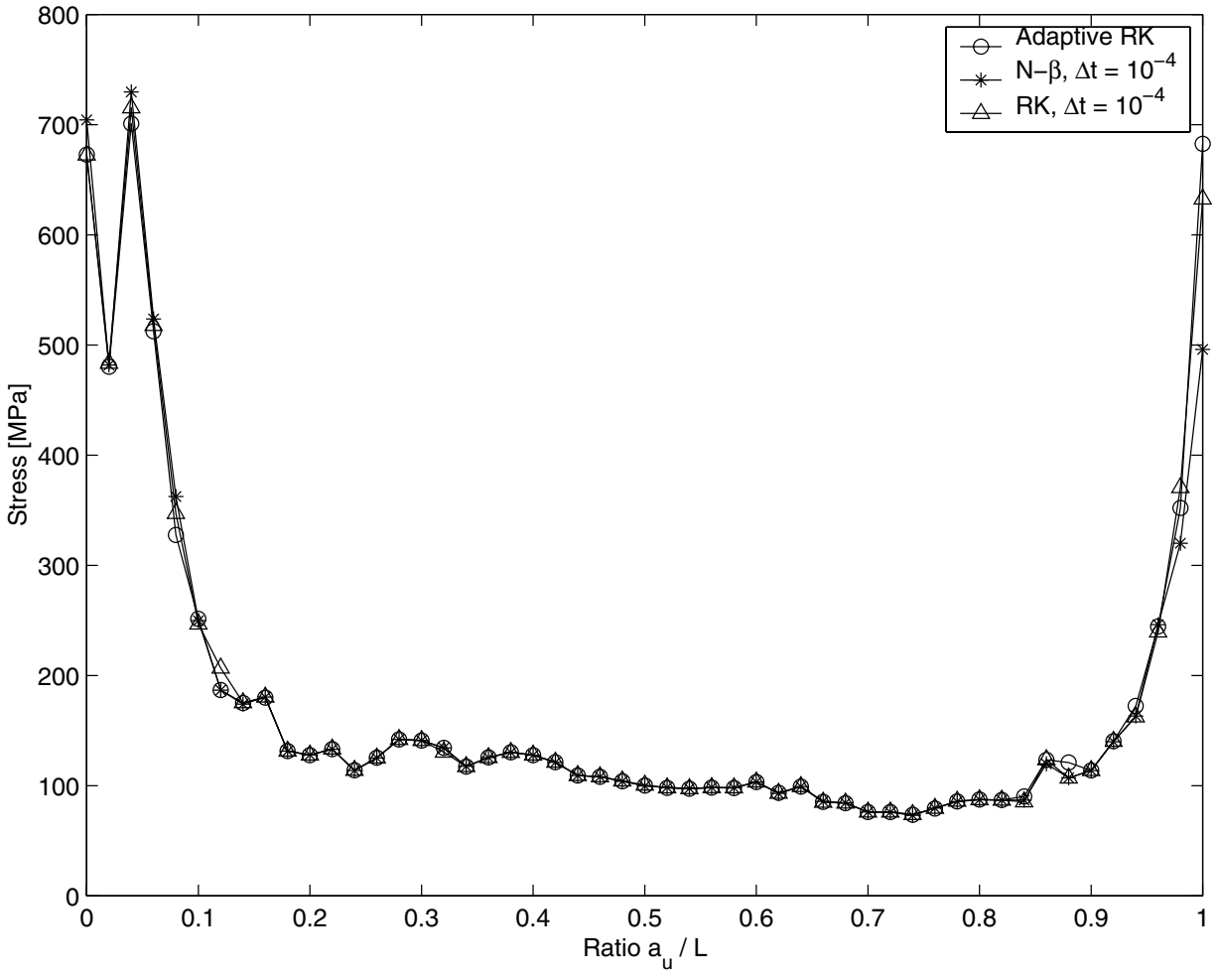

FIGURE A-8 Maximum Stress in the Bracket for Counterweight in the Top Story of 10-Story Building, for Actual Northridge Earthquake, Results from Different Numerical Methods

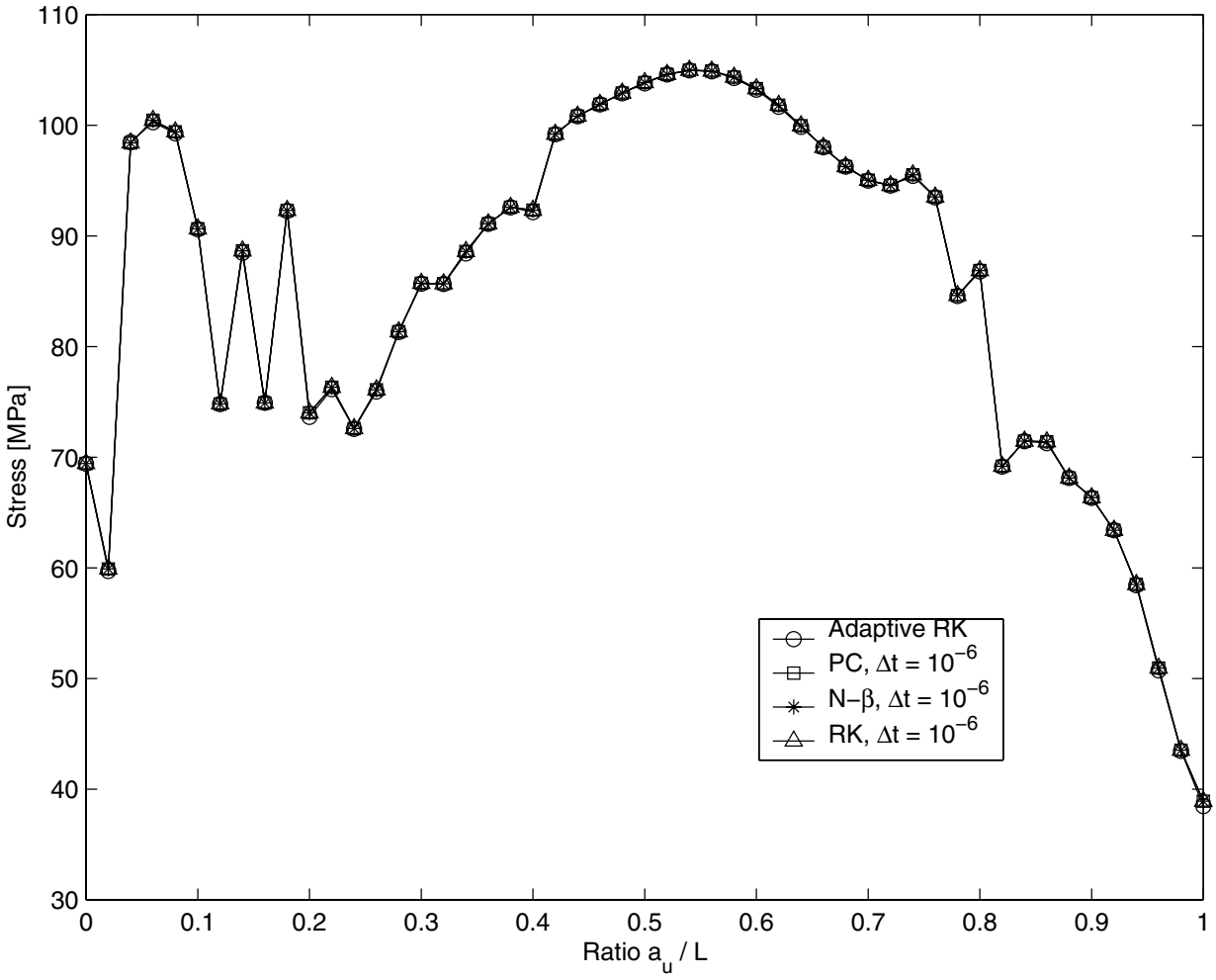

FIGURE A-9 Maximum Stress in the Rail for Counterweight in the Top Story of 10-Story Building, for Northridge 0.1g, Results from Different Numerical Methods

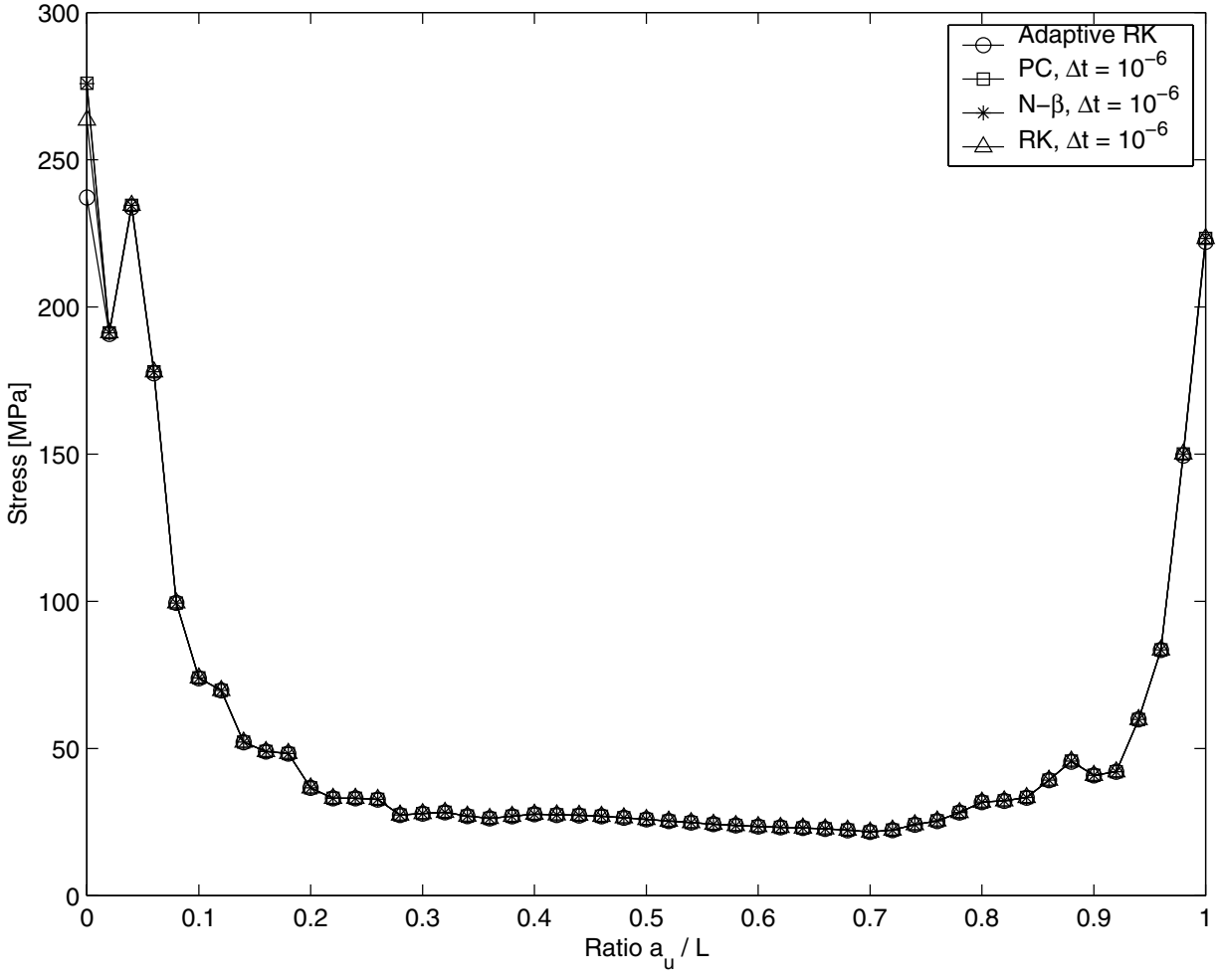

FIGURE A-10 Maximum Stress in the Bracket for Counterweight in the Top Story of 10-Story Building, for Northridge 0.1g, Results from Different Numerical Methods

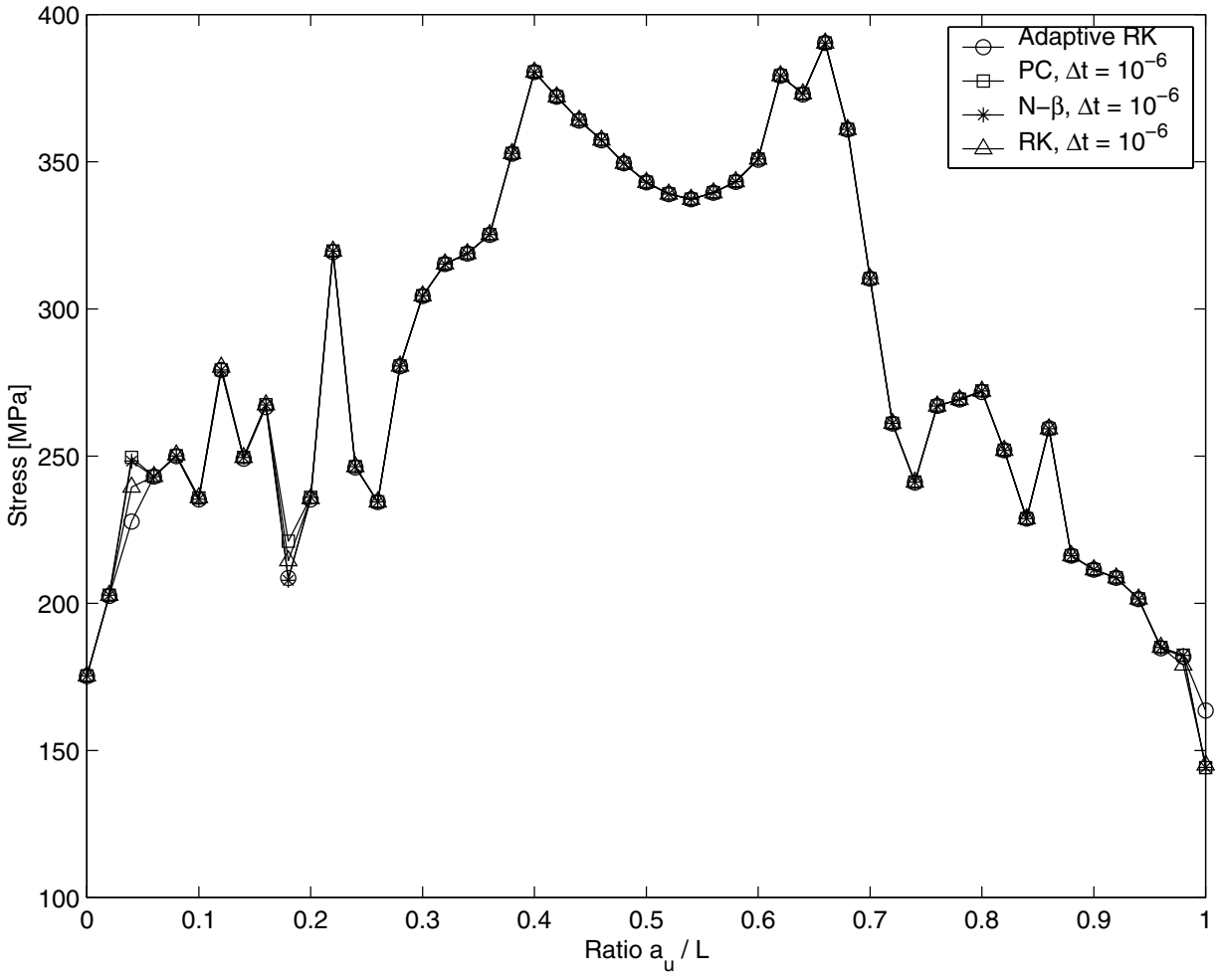

FIGURE A-11 Maximum Stress in the Rail for Counterweight in the Top Story of 10-Story Building, for Actual Northridge Earthquake, Results from Different Numerical Methods

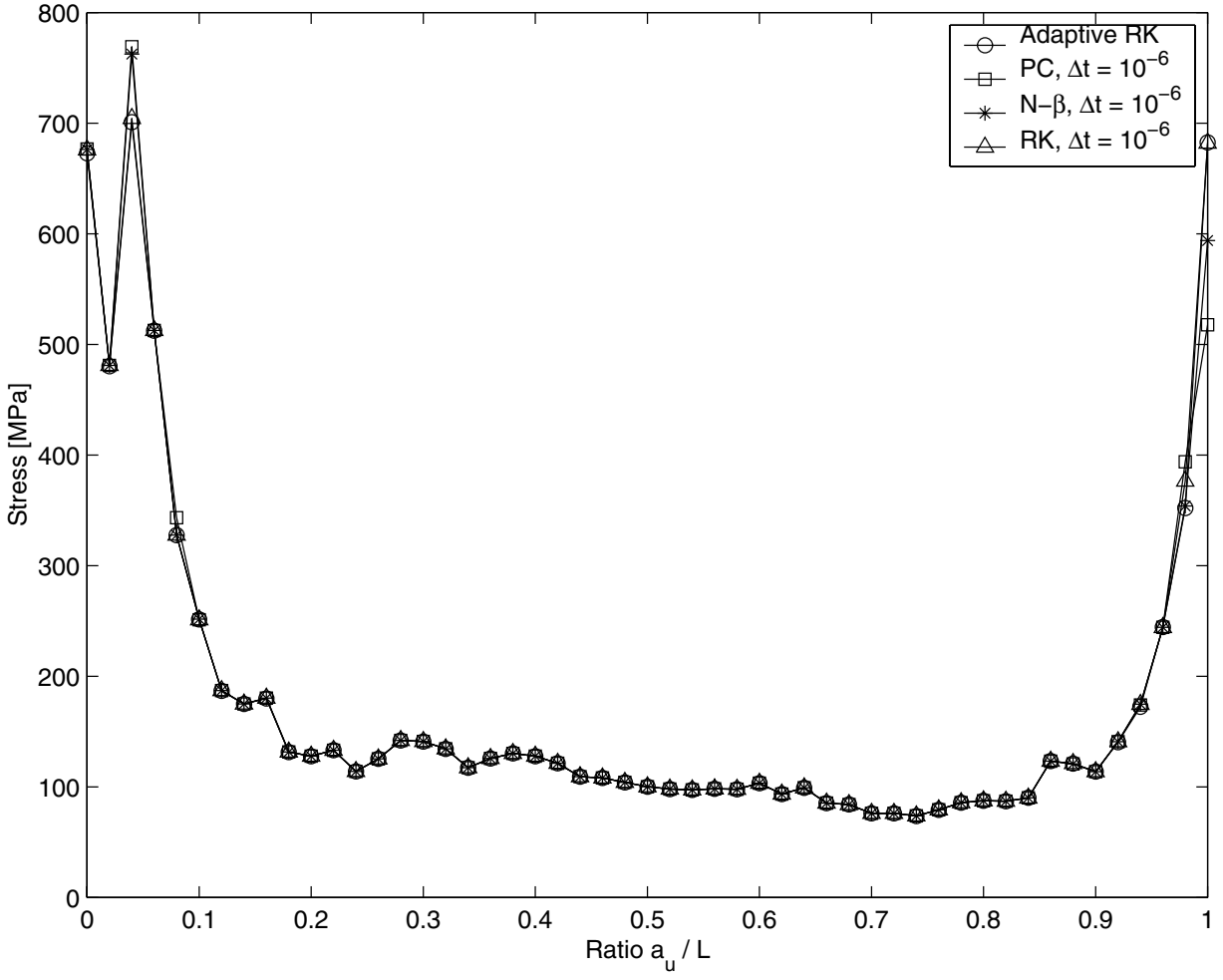

FIGURE A-12 Maximum Stress in the Bracket for Counterweight in the Top Story of 10-Story Building, for Actual Northridge Earthquake, Results from Different Numerical Methods

Multidisciplinary Center for Earthquake Engineering Research
List of Technical Reports

The Multidisciplinary Center for Earthquake Engineering Research (MCEER) publishes technical reports on a variety of subjects related to earthquake engineering written by authors funded through MCEER. These reports are available from both MCEER Publications and the National Technical Information Service (NTIS). Requests for reports should be directed to MCEER Publications, Multidisciplinary Center for Earthquake Engineering Research, State University of New York at Buffalo, Red Jacket Quadrangle, Buffalo, New York 14261. Reports can also be requested through NTIS, 5285 Port Royal Road, Springfield, Virginia 22161. NTIS accession numbers are shown in parenthesis, if available.

NCEER-87-0001 "First-Year Program in Research, Education and Technology Transfer," 3/5/87, (PB88-134275, A04, MF-A01).

NCEER-87-0002 "Experimental Evaluation of Instantaneous Optimal Algorithms for Structural Control," by R.C. Lin, T.T. Soong and A.M. Reinhorn, 4/20/87, (PB88-134341, A04, MF-A01).

NCEER-87-0003 "Experimentation Using the Earthquake Simulation Facilities at University at Buffalo," by A.M. Reinhorn and R.L. Ketter, to be published.

NCEER-87-0004 "The System Characteristics and Performance of a Shaking Table," by J.S. Hwang, K.C. Chang and G.C. Lee, 6/1/87, (PB88-134259, A03, MF-A01). This report is available only through NTIS (see address given above).

NCEER-87-0005 "A Finite Element Formulation for Nonlinear Viscoplastic Material Using a Q Model," by O. Gyebi and G. Dasgupta, 11/2/87, (PB88-213764, A08, MF-A01).

NCEER-87-0006 "Symbolic Manipulation Program (SMP) - Algebraic Codes for Two and Three Dimensional Finite Element Formulations," by X. Lee and G. Dasgupta, 11/9/87, (PB88-218522, A05, MF-A01).

NCEER-87-0007 "Instantaneous Optimal Control Laws for Tall Buildings Under Seismic Excitations," by J.N. Yang, A. Akbarpour and P. Ghaemmaghami, 6/10/87, (PB88-134333, A06, MF-A01). This report is only available through NTIS (see address given above).

NCEER-87-0008 "IDARC: Inelastic Damage Analysis of Reinforced Concrete Frame - Shear-Wall Structures," by Y.J. Park, A.M. Reinhorn and S.K. Kunnath, 7/20/87, (PB88-134325, A09, MF-A01). This report is only available through NTIS (see address given above).

NCEER-87-0009 "Liquefaction Potential for New York State: A Preliminary Report on Sites in Manhattan and Buffalo," by M. Budhu, V. Vijayakumar, R.F. Giese and L. Baumgras, 8/31/87, (PB88-163704, A03, MF-A01). This report is available only through NTIS (see address given above).

NCEER-87-0010 "Vertical and Torsional Vibration of Foundations in Inhomogeneous Media," by A.S. Veletsos and K.W. Dotson, 6/1/87, (PB88-134291, A03, MF-A01). This report is only available through NTIS (see address given above).

NCEER-87-0011 "Seismic Probabilistic Risk Assessment and Seismic Margins Studies for Nuclear Power Plants," by Howard H.M. Hwang, 6/15/87, (PB88-134267, A03, MF-A01). This report is only available through NTIS (see address given above).

NCEER-87-0012 "Parametric Studies of Frequency Response of Secondary Systems Under Ground-Acceleration Excitations," by Y. Yong and Y.K. Lin, 6/10/87, (PB88-134309, A03, MF-A01). This report is only available through NTIS (see address given above).

NCEER-87-0013 "Frequency Response of Secondary Systems Under Seismic Excitation," by J.A. HoLung, J. Cai and Y.K. Lin, 7/31/87, (PB88-134317, A05, MF-A01). This report is only available through NTIS (see address given above).

NCEER-87-0014 "Modelling Earthquake Ground Motions in Seismically Active Regions Using Parametric Time Series Methods," by G.W. Ellis and A.S. Cakmak, 8/25/87, (PB88-134283, A08, MF-A01). This report is only available through NTIS (see address given above).

NCEER-87-0015 "Detection and Assessment of Seismic Structural Damage," by E. DiPasquale and A.S. Cakmak, 8/25/87, (PB88-163712, A05, MF-A01). This report is only available through NTIS (see address given above).

NCEER-87-0016 "Pipeline Experiment at Parkfield, California," by J. Isenberg and E. Richardson, 9/15/87, (PB88-163720, A03, MF-A01). This report is available only through NTIS (see address given above).

NCEER-87-0017 "Digital Simulation of Seismic Ground Motion," by M. Shinozuka, G. Deodatis and T. Harada, 8/31/87, (PB88-155197, A04, MF-A01). This report is available only through NTIS (see address given above).

NCEER-87-0018 "Practical Considerations for Structural Control: System Uncertainty, System Time Delay and Truncation of Small Control Forces," J.N. Yang and A. Akbarpour, 8/10/87, (PB88-163738, A08, MF-A01). This report is only available through NTIS (see address given above).

NCEER-87-0019 "Modal Analysis of Nonclassically Damped Structural Systems Using Canonical Transformation," by J.N. Yang, S. Sarkani and F.X. Long, 9/27/87, (PB88-187851, A04, MF-A01).

NCEER-87-0020 "A Nonstationary Solution in Random Vibration Theory," by J.R. Red-Horse and P.D. Spanos, 11/3/87, (PB88-163746, A03, MF-A01).

NCEER-87-0021 "Horizontal Impedances for Radially Inhomogeneous Viscoelastic Soil Layers," by A.S. Veletsos and K.W. Dotson, 10/15/87, (PB88-150859, A04, MF-A01).

NCEER-87-0022 "Seismic Damage Assessment of Reinforced Concrete Members," by Y.S. Chung, C. Meyer and M. Shinozuka, 10/9/87, (PB88-150867, A05, MF-A01). This report is available only through NTIS (see address given above).

NCEER-87-0023 "Active Structural Control in Civil Engineering," by T.T. Soong, 11/11/87, (PB88-187778, A03, MF-A01).

NCEER-87-0024 "Vertical and Torsional Impedances for Radially Inhomogeneous Viscoelastic Soil Layers," by K.W. Dotson and A.S. Veletsos, 12/87, (PB88-187786, A03, MF-A01).

NCEER-87-0025 "Proceedings from the Symposium on Seismic Hazards, Ground Motions, Soil-Liquefaction and Engineering Practice in Eastern North America," October 20-22, 1987, edited by K.H. Jacob, 12/87, (PB88-188115, A23, MF-A01). This report is available only through NTIS (see address given above).

NCEER-87-0026 "Report on the Whittier-Narrows, California, Earthquake of October 1, 1987," by J. Pantelic and A. Reinhorn, 11/87, (PB88-187752, A03, MF-A01). This report is available only through NTIS (see address given above).

NCEER-87-0027 "Design of a Modular Program for Transient Nonlinear Analysis of Large 3-D Building Structures," by S. Srivastav and J.F. Abel, 12/30/87, (PB88-187950, A05, MF-A01). This report is only available through NTIS (see address given above).

NCEER-87-0028 "Second-Year Program in Research, Education and Technology Transfer," 3/8/88, (PB88-219480, A04, MF-A01).

NCEER-88-0001 "Workshop on Seismic Computer Analysis and Design of Buildings With Interactive Graphics," by W. McGuire, J.F. Abel and C.H. Conley, 1/18/88, (PB88-187760, A03, MF-A01). This report is only available through NTIS (see address given above).

NCEER-88-0002 "Optimal Control of Nonlinear Flexible Structures," by J.N. Yang, F.X. Long and D. Wong, 1/22/88, (PB88-213772, A06, MF-A01).

NCEER-88-0003 "Substructuring Techniques in the Time Domain for Primary-Secondary Structural Systems," by G.D. Manolis and G. Juhn, 2/10/88, (PB88-213780, A04, MF-A01).

NCEER-88-0004 "Iterative Seismic Analysis of Primary-Secondary Systems," by A. Singhal, L.D. Lutes and P.D. Spanos, 2/23/88, (PB88-213798, A04, MF-A01).

NCEER-88-0005 "Stochastic Finite Element Expansion for Random Media," by P.D. Spanos and R. Ghanem, 3/14/88, (PB88-213806, A03, MF-A01).

NCEER-88-0006 "Combining Structural Optimization and Structural Control," by F.Y. Cheng and C.P. Pantelides, 1/10/88, (PB88-213814, A05, MF-A01).

NCEER-88-0007 "Seismic Performance Assessment of Code-Designed Structures," by H.H-M. Hwang, J-W. Jaw and H-J. Shau, 3/20/88, (PB88-219423, A04, MF-A01). This report is only available through NTIS (see address given above).

NCEER-88-0008 "Reliability Analysis of Code-Designed Structures Under Natural Hazards," by H.H-M. Hwang, H. Ushiba and M. Shinozuka, 2/29/88, (PB88-229471, A07, MF-A01). This report is only available through NTIS (see address given above).

NCEER-88-0009 "Seismic Fragility Analysis of Shear Wall Structures," by J-W Jaw and H.H-M. Hwang, 4/30/88, (PB89-102867, A04, MF-A01).

NCEER-88-0010 "Base Isolation of a Multi-Story Building Under a Harmonic Ground Motion - A Comparison of Performances of Various Systems," by F-G Fan, G. Ahmadi and I.G. Tadjbakhsh, 5/18/88, (PB89-122238, A06, MF-A01). This report is only available through NTIS (see address given above).

NCEER-88-0011 "Seismic Floor Response Spectra for a Combined System by Green's Functions," by F.M. Lavelle, L.A. Bergman and P.D. Spanos, 5/1/88, (PB89-102875, A03, MF-A01).

NCEER-88-0012 "A New Solution Technique for Randomly Excited Hysteretic Structures," by G.Q. Cai and Y.K. Lin, 5/16/88, (PB89-102883, A03, MF-A01).

NCEER-88-0013 "A Study of Radiation Damping and Soil-Structure Interaction Effects in the Centrifuge," by K. Weissman, supervised by J.H. Prevost, 5/24/88, (PB89-144703, A06, MF-A01).

NCEER-88-0014 "Parameter Identification and Implementation of a Kinematic Plasticity Model for Frictional Soils," by J.H. Prevost and D.V. Griffiths, to be published.

NCEER-88-0015 "Two- and Three- Dimensional Dynamic Finite Element Analyses of the Long Valley Dam," by D.V. Griffiths and J.H. Prevost, 6/17/88, (PB89-144711, A04, MF-A01).

NCEER-88-0016 "Damage Assessment of Reinforced Concrete Structures in Eastern United States," by A.M. Reinhorn, M.J. Seidel, S.K. Kunnath and Y.J. Park, 6/15/88, (PB89-122220, A04, MF-A01). This report is only available through NTIS (see address given above).

NCEER-88-0017 "Dynamic Compliance of Vertically Loaded Strip Foundations in Multilayered Viscoelastic Soils," by S. Ahmad and A.S.M. Israil, 6/17/88, (PB89-102891, A04, MF-A01).

NCEER-88-0018 "An Experimental Study of Seismic Structural Response With Added Viscoelastic Dampers," by R.C. Lin, Z. Liang, T.T. Soong and R.H. Zhang, 6/30/88, (PB89-122212, A05, MF-A01). This report is available only through NTIS (see address given above).

NCEER-88-0019 "Experimental Investigation of Primary - Secondary System Interaction," by G.D. Manolis, G. Juhn and A.M. Reinhorn, 5/27/88, (PB89-122204, A04, MF-A01).

NCEER-88-0020 "A Response Spectrum Approach For Analysis of Nonclassically Damped Structures," by J.N. Yang, S. Sarkani and F.X. Long, 4/22/88, (PB89-102909, A04, MF-A01).

NCEER-88-0021 "Seismic Interaction of Structures and Soils: Stochastic Approach," by A.S. Veletsos and A.M. Prasad, 7/21/88, (PB89-122196, A04, MF-A01). This report is only available through NTIS (see address given above).

NCEER-88-0022 "Identification of the Serviceability Limit State and Detection of Seismic Structural Damage," by E. DiPasquale and A.S. Cakmak, 6/15/88, (PB89-122188, A05, MF-A01). This report is available only through NTIS (see address given above).

NCEER-88-0023 "Multi-Hazard Risk Analysis: Case of a Simple Offshore Structure," by B.K. Bhartia and E.H. Vanmarcke, 7/21/88, (PB89-145213, A05, MF-A01).

NCEER-88-0024 "Automated Seismic Design of Reinforced Concrete Buildings," by Y.S. Chung, C. Meyer and M. Shinozuka, 7/5/88, (PB89-122170, A06, MF-A01). This report is available only through NTIS (see address given above).

NCEER-88-0025 "Experimental Study of Active Control of MDOF Structures Under Seismic Excitations," by L.L. Chung, R.C. Lin, T.T. Soong and A.M. Reinhorn, 7/10/88, (PB89-122600, A04, MF-A01).

NCEER-88-0026 "Earthquake Simulation Tests of a Low-Rise Metal Structure," by J.S. Hwang, K.C. Chang, G.C. Lee and R.L. Ketter, 8/1/88, (PB89-102917, A04, MF-A01).

NCEER-88-0027 "Systems Study of Urban Response and Reconstruction Due to Catastrophic Earthquakes," by F. Kozin and H.K. Zhou, 9/22/88, (PB90-162348, A04, MF-A01).

NCEER-88-0028 "Seismic Fragility Analysis of Plane Frame Structures," by H.H-M. Hwang and Y.K. Low, 7/31/88, (PB89-131445, A06, MF-A01).

NCEER-88-0029 "Response Analysis of Stochastic Structures," by A. Kardara, C. Bucher and M. Shinozuka, 9/22/88, (PB89-174429, A04, MF-A01).

NCEER-88-0030 "Nonnormal Accelerations Due to Yielding in a Primary Structure," by D.C.K. Chen and L.D. Lutes, 9/19/88, (PB89-131437, A04, MF-A01).

NCEER-88-0031 "Design Approaches for Soil-Structure Interaction," by A.S. Veletsos, A.M. Prasad and Y. Tang, 12/30/88, (PB89-174437, A03, MF-A01). This report is available only through NTIS (see address given above).

NCEER-88-0032 "A Re-evaluation of Design Spectra for Seismic Damage Control," by C.J. Turkstra and A.G. Tallin, 11/7/88, (PB89-145221, A05, MF-A01).

NCEER-88-0033 "The Behavior and Design of Noncontact Lap Splices Subjected to Repeated Inelastic Tensile Loading," by V.E. Sagan, P. Gergely and R.N. White, 12/8/88, (PB89-163737, A08, MF-A01).

NCEER-88-0034 "Seismic Response of Pile Foundations," by S.M. Mamoon, P.K. Banerjee and S. Ahmad, 11/1/88, (PB89-145239, A04, MF-A01).

NCEER-88-0035 "Modeling of R/C Building Structures With Flexible Floor Diaphragms (IDARC2)," by A.M. Reinhorn, S.K. Kunnath and N. Panahshahi, 9/7/88, (PB89-207153, A07, MF-A01).

NCEER-88-0036 "Solution of the Dam-Reservoir Interaction Problem Using a Combination of FEM, BEM with Particular Integrals, Modal Analysis, and Substructuring," by C-S. Tsai, G.C. Lee and R.L. Ketter, 12/31/88, (PB89-207146, A04, MF-A01).

NCEER-88-0037 "Optimal Placement of Actuators for Structural Control," by F.Y. Cheng and C.P. Pantelides, 8/15/88, (PB89-162846, A05, MF-A01).

NCEER-88-0038 "Teflon Bearings in Aseismic Base Isolation: Experimental Studies and Mathematical Modeling," by A. Mokha, M.C. Constantinou and A.M. Reinhorn, 12/5/88, (PB89-218457, A10, MF-A01). This report is available only through NTIS (see address given above).

NCEER-88-0039 "Seismic Behavior of Flat Slab High-Rise Buildings in the New York City Area," by P. Weidlinger and M. Ettouney, 10/15/88, (PB90-145681, A04, MF-A01).

NCEER-88-0040 "Evaluation of the Earthquake Resistance of Existing Buildings in New York City," by P. Weidlinger and M. Ettouney, 10/15/88, to be published.

NCEER-88-0041 "Small-Scale Modeling Techniques for Reinforced Concrete Structures Subjected to Seismic Loads," by W. Kim, A. El-Attar and R.N. White, 11/22/88, (PB89-189625, A05, MF-A01).

NCEER-88-0042 "Modeling Strong Ground Motion from Multiple Event Earthquakes," by G.W. Ellis and A.S. Cakmak, 10/15/88, (PB89-174445, A03, MF-A01).

NCEER-88-0043 "Nonstationary Models of Seismic Ground Acceleration," by M. Grigoriu, S.E. Ruiz and E. Rosenblueth, 7/15/88, (PB89-189617, A04, MF-A01).

NCEER-88-0044 "SARCF User's Guide: Seismic Analysis of Reinforced Concrete Frames," by Y.S. Chung, C. Meyer and M. Shinozuka, 11/9/88, (PB89-174452, A08, MF-A01).

NCEER-88-0045 "First Expert Panel Meeting on Disaster Research and Planning," edited by J. Pantelic and J. Stoyle, 9/15/88, (PB89-174460, A05, MF-A01).

NCEER-88-0046 "Preliminary Studies of the Effect of Degrading Infill Walls on the Nonlinear Seismic Response of Steel Frames," by C.Z. Chrysostomou, P. Gergely and J.F. Abel, 12/19/88, (PB89-208383, A05, MF-A01).

NCEER-88-0047 "Reinforced Concrete Frame Component Testing Facility - Design, Construction, Instrumentation and Operation," by S.P. Pessiki, C. Conley, T. Bond, P. Gergely and R.N. White, 12/16/88, (PB89-174478, A04, MF-A01).

NCEER-89-0001 "Effects of Protective Cushion and Soil Compliancy on the Response of Equipment Within a Seismically Excited Building," by J.A. HoLung, 2/16/89, (PB89-207179, A04, MF-A01).

NCEER-89-0002 "Statistical Evaluation of Response Modification Factors for Reinforced Concrete Structures," by H.H-M. Hwang and J-W. Jaw, 2/17/89, (PB89-207187, A05, MF-A01).

NCEER-89-0003 "Hysteretic Columns Under Random Excitation," by G-Q. Cai and Y.K. Lin, 1/9/89, (PB89-196513, A03, MF-A01).

NCEER-89-0004 "Experimental Study of `Elephant Foot Bulge' Instability of Thin-Walled Metal Tanks," by Z-H. Jia and R.L. Ketter, 2/22/89, (PB89-207195, A03, MF-A01).

NCEER-89-0005 "Experiment on Performance of Buried Pipelines Across San Andreas Fault," by J. Isenberg, E. Richardson and T.D. O'Rourke, 3/10/89, (PB89-218440, A04, MF-A01). This report is available only through NTIS (see address given above).

NCEER-89-0006 "A Knowledge-Based Approach to Structural Design of Earthquake-Resistant Buildings," by M. Subramani, P. Gergely, C.H. Conley, J.F. Abel and A.H. Zaghw, 1/15/89, (PB89-218465, A06, MF-A01).

NCEER-89-0007 "Liquefaction Hazards and Their Effects on Buried Pipelines," by T.D. O'Rourke and P.A. Lane, 2/1/89, (PB89-218481, A09, MF-A01).

NCEER-89-0008 "Fundamentals of System Identification in Structural Dynamics," by H. Imai, C-B. Yun, O. Maruyama and M. Shinozuka, 1/26/89, (PB89-207211, A04, MF-A01).

NCEER-89-0009 "Effects of the 1985 Michoacan Earthquake on Water Systems and Other Buried Lifelines in Mexico," by A.G. Ayala and M.J. O'Rourke, 3/8/89, (PB89-207229, A06, MF-A01).

NCEER-89-R010 "NCEER Bibliography of Earthquake Education Materials," by K.E.K. Ross, Second Revision, 9/1/89, (PB90-125352, A05, MF-A01). This report is replaced by NCEER-92-0018.

NCEER-89-0011 "Inelastic Three-Dimensional Response Analysis of Reinforced Concrete Building Structures (IDARC-3D), Part I - Modeling," by S.K. Kunnath and A.M. Reinhorn, 4/17/89, (PB90-114612, A07, MF-A01). This report is available only through NTIS (see address given above).

NCEER-89-0012 "Recommended Modifications to ATC-14," by C.D. Poland and J.O. Malley, 4/12/89, (PB90-108648, A15, MF-A01).

NCEER-89-0013 "Repair and Strengthening of Beam-to-Column Connections Subjected to Earthquake Loading," by M. Corazao and A.J. Durrani, 2/28/89, (PB90-109885, A06, MF-A01).

NCEER-89-0014 "Program EXKAL2 for Identification of Structural Dynamic Systems," by O. Maruyama, C-B. Yun, M. Hoshiya and M. Shinozuka, 5/19/89, (PB90-109877, A09, MF-A01).

NCEER-89-0015 "Response of Frames With Bolted Semi-Rigid Connections, Part I - Experimental Study and Analytical Predictions," by P.J. DiCorso, A.M. Reinhorn, J.R. Dickerson, J.B. Radziminski and W.L. Harper, 6/1/89, to be published.

NCEER-89-0016 "ARMA Monte Carlo Simulation in Probabilistic Structural Analysis," by P.D. Spanos and M.P. Mignolet, 7/10/89, (PB90-109893, A03, MF-A01).

NCEER-89-P017 "Preliminary Proceedings from the Conference on Disaster Preparedness - The Place of Earthquake Education in Our Schools," Edited by K.E.K. Ross, 6/23/89, (PB90-108606, A03, MF-A01).

NCEER-89-0017 "Proceedings from the Conference on Disaster Preparedness - The Place of Earthquake Education in Our Schools," Edited by K.E.K. Ross, 12/31/89, (PB90-207895, A012, MF-A02). This report is available only through NTIS (see address given above).

NCEER-89-0018 "Multidimensional Models of Hysteretic Material Behavior for Vibration Analysis of Shape Memory Energy Absorbing Devices, by E.J. Graesser and F.A. Cozzarelli, 6/7/89, (PB90-164146, A04, MF-A01).

NCEER-89-0019 "Nonlinear Dynamic Analysis of Three-Dimensional Base Isolated Structures (3D-BASIS)," by S. Nagarajaiah, A.M. Reinhorn and M.C. Constantinou, 8/3/89, (PB90-161936, A06, MF-A01). This report has been replaced by NCEER-93-0011.

NCEER-89-0020 "Structural Control Considering Time-Rate of Control Forces and Control Rate Constraints," by F.Y. Cheng and C.P. Pantelides, 8/3/89, (PB90-120445, A04, MF-A01).

NCEER-89-0021 "Subsurface Conditions of Memphis and Shelby County," by K.W. Ng, T-S. Chang and H-H.M. Hwang, 7/26/89, (PB90-120437, A03, MF-A01).

NCEER-89-0022 "Seismic Wave Propagation Effects on Straight Jointed Buried Pipelines," by K. Elhmadi and M.J. O'Rourke, 8/24/89, (PB90-162322, A10, MF-A02).

NCEER-89-0023 "Workshop on Serviceability Analysis of Water Delivery Systems," edited by M. Grigoriu, 3/6/89, (PB90-127424, A03, MF-A01).

NCEER-89-0024 "Shaking Table Study of a 1/5 Scale Steel Frame Composed of Tapered Members," by K.C. Chang, J.S. Hwang and G.C. Lee, 9/18/89, (PB90-160169, A04, MF-A01).

NCEER-89-0025 "DYNA1D: A Computer Program for Nonlinear Seismic Site Response Analysis - Technical Documentation," by Jean H. Prevost, 9/14/89, (PB90-161944, A07, MF-A01). This report is available only through NTIS (see address given above).

NCEER-89-0026 "1:4 Scale Model Studies of Active Tendon Systems and Active Mass Dampers for Aseismic Protection," by A.M. Reinhorn, T.T. Soong, R.C. Lin, Y.P. Yang, Y. Fukao, H. Abe and M. Nakai, 9/15/89, (PB90-173246, A10, MF-A02). This report is available only through NTIS (see address given above).

NCEER-89-0027 "Scattering of Waves by Inclusions in a Nonhomogeneous Elastic Half Space Solved by Boundary Element Methods," by P.K. Hadley, A. Askar and A.S. Cakmak, 6/15/89, (PB90-145699, A07, MF-A01).

NCEER-89-0028 "Statistical Evaluation of Deflection Amplification Factors for Reinforced Concrete Structures," by H.H.M. Hwang, J-W. Jaw and A.L. Ch'ng, 8/31/89, (PB90-164633, A05, MF-A01).

NCEER-89-0029 "Bedrock Accelerations in Memphis Area Due to Large New Madrid Earthquakes," by H.H.M. Hwang, C.H.S. Chen and G. Yu, 11/7/89, (PB90-162330, A04, MF-A01).

NCEER-89-0030 "Seismic Behavior and Response Sensitivity of Secondary Structural Systems," by Y.Q. Chen and T.T. Soong, 10/23/89, (PB90-164658, A08, MF-A01).

NCEER-89-0031 "Random Vibration and Reliability Analysis of Primary-Secondary Structural Systems," by Y. Ibrahim, M. Grigoriu and T.T. Soong, 11/10/89, (PB90-161951, A04, MF-A01).

NCEER-89-0032 "Proceedings from the Second U.S. - Japan Workshop on Liquefaction, Large Ground Deformation and Their Effects on Lifelines, September 26-29, 1989," Edited by T.D. O'Rourke and M. Hamada, 12/1/89, (PB90-209388, A22, MF-A03).

NCEER-89-0033 "Deterministic Model for Seismic Damage Evaluation of Reinforced Concrete Structures," by J.M. Bracci, A.M. Reinhorn, J.B. Mander and S.K. Kunnath, 9/27/89, (PB91-108803, A06, MF-A01).

NCEER-89-0034 "On the Relation Between Local and Global Damage Indices," by E. DiPasquale and A.S. Cakmak, 8/15/89, (PB90-173865, A05, MF-A01).

NCEER-89-0035 "Cyclic Undrained Behavior of Nonplastic and Low Plasticity Silts," by A.J. Walker and H.E. Stewart, 7/26/89, (PB90-183518, A10, MF-A01).

NCEER-89-0036 "Liquefaction Potential of Surficial Deposits in the City of Buffalo, New York," by M. Budhu, R. Giese and L. Baumgrass, 1/17/89, (PB90-208455, A04, MF-A01).

NCEER-89-0037 "A Deterministic Assessment of Effects of Ground Motion Incoherence," by A.S. Veletsos and Y. Tang, 7/15/89, (PB90-164294, A03, MF-A01).

NCEER-89-0038 "Workshop on Ground Motion Parameters for Seismic Hazard Mapping," July 17-18, 1989, edited by R.V. Whitman, 12/1/89, (PB90-173923, A04, MF-A01).

NCEER-89-0039 "Seismic Effects on Elevated Transit Lines of the New York City Transit Authority," by C.J. Costantino, C.A. Miller and E. Heymsfield, 12/26/89, (PB90-207887, A06, MF-A01).

NCEER-89-0040 "Centrifugal Modeling of Dynamic Soil-Structure Interaction," by K. Weissman, Supervised by J.H. Prevost, 5/10/89, (PB90-207879, A07, MF-A01).

NCEER-89-0041 "Linearized Identification of Buildings With Cores for Seismic Vulnerability Assessment," by I-K. Ho and A.E. Aktan, 11/1/89, (PB90-251943, A07, MF-A01).

NCEER-90-0001 "Geotechnical and Lifeline Aspects of the October 17, 1989 Loma Prieta Earthquake in San Francisco," by T.D. O'Rourke, H.E. Stewart, F.T. Blackburn and T.S. Dickerman, 1/90, (PB90-208596, A05, MF-A01).

NCEER-90-0002 "Nonnormal Secondary Response Due to Yielding in a Primary Structure," by D.C.K. Chen and L.D. Lutes, 2/28/90, (PB90-251976, A07, MF-A01).

NCEER-90-0003 "Earthquake Education Materials for Grades K-12," by K.E.K. Ross, 4/16/90, (PB91-251984, A05, MF-A05). This report has been replaced by NCEER-92-0018.

NCEER-90-0004 "Catalog of Strong Motion Stations in Eastern North America," by R.W. Busby, 4/3/90, (PB90-251984, A05, MF-A01).

NCEER-90-0005 "NCEER Strong-Motion Data Base: A User Manual for the GeoBase Release (Version 1.0 for the Sun3)," by P. Friberg and K. Jacob, 3/31/90 (PB90-258062, A04, MF-A01).

NCEER-90-0006 "Seismic Hazard Along a Crude Oil Pipeline in the Event of an 1811-1812 Type New Madrid Earthquake," by H.H.M. Hwang and C-H.S. Chen, 4/16/90, (PB90-258054, A04, MF-A01).

NCEER-90-0007 "Site-Specific Response Spectra for Memphis Sheahan Pumping Station," by H.H.M. Hwang and C.S. Lee, 5/15/90, (PB91-108811, A05, MF-A01).

NCEER-90-0008 "Pilot Study on Seismic Vulnerability of Crude Oil Transmission Systems," by T. Ariman, R. Dobry, M. Grigoriu, F. Kozin, M. O'Rourke, T. O'Rourke and M. Shinozuka, 5/25/90, (PB91-108837, A06, MF-A01).

NCEER-90-0009 "A Program to Generate Site Dependent Time Histories: EQGEN," by G.W. Ellis, M. Srinivasan and A.S. Cakmak, 1/30/90, (PB91-108829, A04, MF-A01).

NCEER-90-0010 "Active Isolation for Seismic Protection of Operating Rooms," by M.E. Talbott, Supervised by M. Shinozuka, 6/8/9, (PB91-110205, A05, MF-A01).

NCEER-90-0011 "Program LINEARID for Identification of Linear Structural Dynamic Systems," by C-B. Yun and M. Shinozuka, 6/25/90, (PB91-110312, A08, MF-A01).

NCEER-90-0012 "Two-Dimensional Two-Phase Elasto-Plastic Seismic Response of Earth Dams," by A.N. Yiagos, Supervised by J.H. Prevost, 6/20/90, (PB91-110197, A13, MF-A02).

NCEER-90-0013 "Secondary Systems in Base-Isolated Structures: Experimental Investigation, Stochastic Response and Stochastic Sensitivity," by G.D. Manolis, G. Juhn, M.C. Constantinou and A.M. Reinhorn, 7/1/90, (PB91-110320, A08, MF-A01).

NCEER-90-0014 "Seismic Behavior of Lightly-Reinforced Concrete Column and Beam-Column Joint Details," by S.P. Pessiki, C.H. Conley, P. Gergely and R.N. White, 8/22/90, (PB91-108795, A11, MF-A02).

NCEER-90-0015 "Two Hybrid Control Systems for Building Structures Under Strong Earthquakes," by J.N. Yang and A. Danielians, 6/29/90, (PB91-125393, A04, MF-A01).

NCEER-90-0016 "Instantaneous Optimal Control with Acceleration and Velocity Feedback," by J.N. Yang and Z. Li, 6/29/90, (PB91-125401, A03, MF-A01).

NCEER-90-0017 "Reconnaissance Report on the Northern Iran Earthquake of June 21, 1990," by M. Mehrain, 10/4/90, (PB91-125377, A03, MF-A01).

NCEER-90-0018 "Evaluation of Liquefaction Potential in Memphis and Shelby County," by T.S. Chang, P.S. Tang, C.S. Lee and H. Hwang, 8/10/90, (PB91-125427, A09, MF-A01).

NCEER-90-0019 "Experimental and Analytical Study of a Combined Sliding Disc Bearing and Helical Steel Spring Isolation System," by M.C. Constantinou, A.S. Mokha and A.M. Reinhorn, 10/4/90, (PB91-125385, A06, MF-A01). This report is available only through NTIS (see address given above).

NCEER-90-0020 "Experimental Study and Analytical Prediction of Earthquake Response of a Sliding Isolation System with a Spherical Surface," by A.S. Mokha, M.C. Constantinou and A.M. Reinhorn, 10/11/90, (PB91-125419, A05, MF-A01).

NCEER-90-0021 "Dynamic Interaction Factors for Floating Pile Groups," by G. Gazetas, K. Fan, A. Kaynia and E. Kausel, 9/10/90, (PB91-170381, A05, MF-A01).

NCEER-90-0022 "Evaluation of Seismic Damage Indices for Reinforced Concrete Structures," by S. Rodriguez-Gomez and A.S. Cakmak, 9/30/90, PB91-171322, A06, MF-A01).

NCEER-90-0023 "Study of Site Response at a Selected Memphis Site," by H. Desai, S. Ahmad, E.S. Gazetas and M.R. Oh, 10/11/90, (PB91-196857, A03, MF-A01).

NCEER-90-0024 "A User's Guide to Strongmo: Version 1.0 of NCEER's Strong-Motion Data Access Tool for PCs and Terminals," by P.A. Friberg and C.A.T. Susch, 11/15/90, (PB91-171272, A03, MF-A01).

NCEER-90-0025 "A Three-Dimensional Analytical Study of Spatial Variability of Seismic Ground Motions," by L-L. Hong and A.H.-S. Ang, 10/30/90, (PB91-170399, A09, MF-A01).

NCEER-90-0026 "MUMOID User's Guide - A Program for the Identification of Modal Parameters," by S. Rodriguez-Gomez and E. DiPasquale, 9/30/90, (PB91-171298, A04, MF-A01).

NCEER-90-0027 "SARCF-II User's Guide - Seismic Analysis of Reinforced Concrete Frames," by S. Rodriguez-Gomez, Y.S. Chung and C. Meyer, 9/30/90, (PB91-171280, A05, MF-A01).

NCEER-90-0028 "Viscous Dampers: Testing, Modeling and Application in Vibration and Seismic Isolation," by N. Makris and M.C. Constantinou, 12/20/90 (PB91-190561, A06, MF-A01).

NCEER-90-0029 "Soil Effects on Earthquake Ground Motions in the Memphis Area," by H. Hwang, C.S. Lee, K.W. Ng and T.S. Chang, 8/2/90, (PB91-190751, A05, MF-A01).

NCEER-91-0001 "Proceedings from the Third Japan-U.S. Workshop on Earthquake Resistant Design of Lifeline Facilities and Countermeasures for Soil Liquefaction, December 17-19, 1990," edited by T.D. O'Rourke and M. Hamada, 2/1/91, (PB91-179259, A99, MF-A04).

NCEER-91-0002 "Physical Space Solutions of Non-Proportionally Damped Systems," by M. Tong, Z. Liang and G.C. Lee, 1/15/91, (PB91-179242, A04, MF-A01).

NCEER-91-0003 "Seismic Response of Single Piles and Pile Groups," by K. Fan and G. Gazetas, 1/10/91, (PB92-174994, A04, MF-A01).

NCEER-91-0004 "Damping of Structures: Part 1 - Theory of Complex Damping," by Z. Liang and G. Lee, 10/10/91, (PB92-197235, A12, MF-A03).

NCEER-91-0005 "3D-BASIS - Nonlinear Dynamic Analysis of Three Dimensional Base Isolated Structures: Part II," by S. Nagarajaiah, A.M. Reinhorn and M.C. Constantinou, 2/28/91, (PB91-190553, A07, MF-A01). This report has been replaced by NCEER-93-0011.

NCEER-91-0006 "A Multidimensional Hysteretic Model for Plasticity Deforming Metals in Energy Absorbing Devices," by E.J. Graesser and F.A. Cozzarelli, 4/9/91, (PB92-108364, A04, MF-A01).

NCEER-91-0007 "A Framework for Customizable Knowledge-Based Expert Systems with an Application to a KBES for Evaluating the Seismic Resistance of Existing Buildings," by E.G. Ibarra-Anaya and S.J. Fenves, 4/9/91, (PB91-210930, A08, MF-A01).

NCEER-91-0008 "Nonlinear Analysis of Steel Frames with Semi-Rigid Connections Using the Capacity Spectrum Method," by G.G. Deierlein, S-H. Hsieh, Y-J. Shen and J.F. Abel, 7/2/91, (PB92-113828, A05, MF-A01).

NCEER-91-0009 "Earthquake Education Materials for Grades K-12," by K.E.K. Ross, 4/30/91, (PB91-212142, A06, MF-A01). This report has been replaced by NCEER-92-0018.

NCEER-91-0010 "Phase Wave Velocities and Displacement Phase Differences in a Harmonically Oscillating Pile," by N. Makris and G. Gazetas, 7/8/91, (PB92-108356, A04, MF-A01).

NCEER-91-0011 "Dynamic Characteristics of a Full-Size Five-Story Steel Structure and a 2/5 Scale Model," by K.C. Chang, G.C. Yao, G.C. Lee, D.S. Hao and Y.C. Yeh," 7/2/91, (PB93-116648, A06, MF-A02).

NCEER-91-0012 "Seismic Response of a 2/5 Scale Steel Structure with Added Viscoelastic Dampers," by K.C. Chang, T.T. Soong, S-T. Oh and M.L. Lai, 5/17/91, (PB92-110816, A05, MF-A01).

NCEER-91-0013 "Earthquake Response of Retaining Walls; Full-Scale Testing and Computational Modeling," by S. Alampalli and A-W.M. Elgamal, 6/20/91, to be published.

NCEER-91-0014 "3D-BASIS-M: Nonlinear Dynamic Analysis of Multiple Building Base Isolated Structures," by P.C. Tsopelas, S. Nagarajaiah, M.C. Constantinou and A.M. Reinhorn, 5/28/91, (PB92-113885, A09, MF-A02).

NCEER-91-0015 "Evaluation of SEAOC Design Requirements for Sliding Isolated Structures," by D. Theodossiou and M.C. Constantinou, 6/10/91, (PB92-114602, A11, MF-A03).

NCEER-91-0016 "Closed-Loop Modal Testing of a 27-Story Reinforced Concrete Flat Plate-Core Building," by H.R. Somaprasad, T. Toksoy, H. Yoshiyuki and A.E. Aktan, 7/15/91, (PB92-129980, A07, MF-A02).

NCEER-91-0017 "Shake Table Test of a 1/6 Scale Two-Story Lightly Reinforced Concrete Building," by A.G. El-Attar, R.N. White and P. Gergely, 2/28/91, (PB92-222447, A06, MF-A02).

NCEER-91-0018 "Shake Table Test of a 1/8 Scale Three-Story Lightly Reinforced Concrete Building," by A.G. El-Attar, R.N. White and P. Gergely, 2/28/91, (PB93-116630, A08, MF-A02).

NCEER-91-0019 "Transfer Functions for Rigid Rectangular Foundations," by A.S. Veletsos, A.M. Prasad and W.H. Wu, 7/31/91, to be published.

NCEER-91-0020 "Hybrid Control of Seismic-Excited Nonlinear and Inelastic Structural Systems," by J.N. Yang, Z. Li and A. Danielians, 8/1/91, (PB92-143171, A06, MF-A02).

NCEER-91-0021 "The NCEER-91 Earthquake Catalog: Improved Intensity-Based Magnitudes and Recurrence Relations for U.S. Earthquakes East of New Madrid," by L. Seeber and J.G. Armbruster, 8/28/91, (PB92-176742, A06, MF-A02).

NCEER-91-0022 "Proceedings from the Implementation of Earthquake Planning and Education in Schools: The Need for Change - The Roles of the Changemakers," by K.E.K. Ross and F. Winslow, 7/23/91, (PB92-129998, A12, MF-A03).

NCEER-91-0023 "A Study of Reliability-Based Criteria for Seismic Design of Reinforced Concrete Frame Buildings," by H.H.M. Hwang and H-M. Hsu, 8/10/91, (PB92-140235, A09, MF-A02).

NCEER-91-0024 "Experimental Verification of a Number of Structural System Identification Algorithms," by R.G. Ghanem, H. Gavin and M. Shinozuka, 9/18/91, (PB92-176577, A18, MF-A04).

NCEER-91-0025 "Probabilistic Evaluation of Liquefaction Potential," by H.H.M. Hwang and C.S. Lee," 11/25/91, (PB92-143429, A05, MF-A01).

NCEER-91-0026 "Instantaneous Optimal Control for Linear, Nonlinear and Hysteretic Structures - Stable Controllers," by J.N. Yang and Z. Li, 11/15/91, (PB92-163807, A04, MF-A01).

NCEER-91-0027 "Experimental and Theoretical Study of a Sliding Isolation System for Bridges," by M.C. Constantinou, A. Kartoum, A.M. Reinhorn and P. Bradford, 11/15/91, (PB92-176973, A10, MF-A03).

NCEER-92-0001 "Case Studies of Liquefaction and Lifeline Performance During Past Earthquakes, Volume 1: Japanese Case Studies," Edited by M. Hamada and T. O'Rourke, 2/17/92, (PB92-197243, A18, MF-A04).

NCEER-92-0002 "Case Studies of Liquefaction and Lifeline Performance During Past Earthquakes, Volume 2: United States Case Studies," Edited by T. O'Rourke and M. Hamada, 2/17/92, (PB92-197250, A20, MF-A04).

NCEER-92-0003 "Issues in Earthquake Education," Edited by K. Ross, 2/3/92, (PB92-222389, A07, MF-A02).

NCEER-92-0004 "Proceedings from the First U.S. - Japan Workshop on Earthquake Protective Systems for Bridges," Edited by I.G. Buckle, 2/4/92, (PB94-142239, A99, MF-A06).

NCEER-92-0005 "Seismic Ground Motion from a Haskell-Type Source in a Multiple-Layered Half-Space," A.P. Theoharis, G. Deodatis and M. Shinozuka, 1/2/92, to be published.

NCEER-92-0006 "Proceedings from the Site Effects Workshop," Edited by R. Whitman, 2/29/92, (PB92-197201, A04, MF-A01).

NCEER-92-0007 "Engineering Evaluation of Permanent Ground Deformations Due to Seismically-Induced Liquefaction," by M.H. Baziar, R. Dobry and A-W.M. Elgamal, 3/24/92, (PB92-222421, A13, MF-A03).

NCEER-92-0008 "A Procedure for the Seismic Evaluation of Buildings in the Central and Eastern United States," by C.D. Poland and J.O. Malley, 4/2/92, (PB92-222439, A20, MF-A04).

NCEER-92-0009 "Experimental and Analytical Study of a Hybrid Isolation System Using Friction Controllable Sliding Bearings," by M.Q. Feng, S. Fujii and M. Shinozuka, 5/15/92, (PB93-150282, A06, MF-A02).

NCEER-92-0010 "Seismic Resistance of Slab-Column Connections in Existing Non-Ductile Flat-Plate Buildings," by A.J. Durrani and Y. Du, 5/18/92, (PB93-116812, A06, MF-A02).

NCEER-92-0011 "The Hysteretic and Dynamic Behavior of Brick Masonry Walls Upgraded by Ferrocement Coatings Under Cyclic Loading and Strong Simulated Ground Motion," by H. Lee and S.P. Prawel, 5/11/92, to be published.

NCEER-92-0012 "Study of Wire Rope Systems for Seismic Protection of Equipment in Buildings," by G.F. Demetriades, M.C. Constantinou and A.M. Reinhorn, 5/20/92, (PB93-116655, A08, MF-A02).

NCEER-92-0013 "Shape Memory Structural Dampers: Material Properties, Design and Seismic Testing," by P.R. Witting and F.A. Cozzarelli, 5/26/92, (PB93-116663, A05, MF-A01).

NCEER-92-0014 "Longitudinal Permanent Ground Deformation Effects on Buried Continuous Pipelines," by M.J. O'Rourke, and C. Nordberg, 6/15/92, (PB93-116671, A08, MF-A02).

NCEER-92-0015 "A Simulation Method for Stationary Gaussian Random Functions Based on the Sampling Theorem," by M. Grigoriu and S. Balopoulou, 6/11/92, (PB93-127496, A05, MF-A01).

NCEER-92-0016 "Gravity-Load-Designed Reinforced Concrete Buildings: Seismic Evaluation of Existing Construction and Detailing Strategies for Improved Seismic Resistance," by G.W. Hoffmann, S.K. Kunnath, A.M. Reinhorn and J.B. Mander, 7/15/92, (PB94-142007, A08, MF-A02).

NCEER-92-0017 "Observations on Water System and Pipeline Performance in the Limón Area of Costa Rica Due to the April 22, 1991 Earthquake," by M. O'Rourke and D. Ballantyne, 6/30/92, (PB93-126811, A06, MF-A02).

NCEER-92-0018 "Fourth Edition of Earthquake Education Materials for Grades K-12," Edited by K.E.K. Ross, 8/10/92, (PB93-114023, A07, MF-A02).

NCEER-92-0019 "Proceedings from the Fourth Japan-U.S. Workshop on Earthquake Resistant Design of Lifeline Facilities and Countermeasures for Soil Liquefaction," Edited by M. Hamada and T.D. O'Rourke, 8/12/92, (PB93-163939, A99, MF-E11).

NCEER-92-0020 "Active Bracing System: A Full Scale Implementation of Active Control," by A.M. Reinhorn, T.T. Soong, R.C. Lin, M.A. Riley, Y.P. Wang, S. Aizawa and M. Higashino, 8/14/92, (PB93-127512, A06, MF-A02).

NCEER-92-0021 "Empirical Analysis of Horizontal Ground Displacement Generated by Liquefaction-Induced Lateral Spreads," by S.F. Bartlett and T.L. Youd, 8/17/92, (PB93-188241, A06, MF-A02).

NCEER-92-0022 "IDARC Version 3.0: Inelastic Damage Analysis of Reinforced Concrete Structures," by S.K. Kunnath, A.M. Reinhorn and R.F. Lobo, 8/31/92, (PB93-227502, A07, MF-A02).

NCEER-92-0023 "A Semi-Empirical Analysis of Strong-Motion Peaks in Terms of Seismic Source, Propagation Path and Local Site Conditions, by M. Kamiyama, M.J. O'Rourke and R. Flores-Berrones, 9/9/92, (PB93-150266, A08, MF-A02).

NCEER-92-0024 "Seismic Behavior of Reinforced Concrete Frame Structures with Nonductile Details, Part I: Summary of Experimental Findings of Full Scale Beam-Column Joint Tests," by A. Beres, R.N. White and P. Gergely, 9/30/92, (PB93-227783, A05, MF-A01).

NCEER-92-0025 "Experimental Results of Repaired and Retrofitted Beam-Column Joint Tests in Lightly Reinforced Concrete Frame Buildings," by A. Beres, S. El-Borgi, R.N. White and P. Gergely, 10/29/92, (PB93-227791, A05, MF-A01).

NCEER-92-0026 "A Generalization of Optimal Control Theory: Linear and Nonlinear Structures," by J.N. Yang, Z. Li and S. Vongchavalitkul, 11/2/92, (PB93-188621, A05, MF-A01).

NCEER-92-0027 "Seismic Resistance of Reinforced Concrete Frame Structures Designed Only for Gravity Loads: Part I - Design and Properties of a One-Third Scale Model Structure," by J.M. Bracci, A.M. Reinhorn and J.B. Mander, 12/1/92, (PB94-104502, A08, MF-A02).

NCEER-92-0028 "Seismic Resistance of Reinforced Concrete Frame Structures Designed Only for Gravity Loads: Part II - Experimental Performance of Subassemblages," by L.E. Aycardi, J.B. Mander and A.M. Reinhorn, 12/1/92, (PB94-104510, A08, MF-A02).

NCEER-92-0029 "Seismic Resistance of Reinforced Concrete Frame Structures Designed Only for Gravity Loads: Part III - Experimental Performance and Analytical Study of a Structural Model," by J.M. Bracci, A.M. Reinhorn and J.B. Mander, 12/1/92, (PB93-227528, A09, MF-A01).

NCEER-92-0030 "Evaluation of Seismic Retrofit of Reinforced Concrete Frame Structures: Part I - Experimental Performance of Retrofitted Subassemblages," by D. Choudhuri, J.B. Mander and A.M. Reinhorn, 12/8/92, (PB93-198307, A07, MF-A02).

NCEER-92-0031 "Evaluation of Seismic Retrofit of Reinforced Concrete Frame Structures: Part II - Experimental Performance and Analytical Study of a Retrofitted Structural Model," by J.M. Bracci, A.M. Reinhorn and J.B. Mander, 12/8/92, (PB93-198315, A09, MF-A03).

NCEER-92-0032 "Experimental and Analytical Investigation of Seismic Response of Structures with Supplemental Fluid Viscous Dampers," by M.C. Constantinou and M.D. Symans, 12/21/92, (PB93-191435, A10, MF-A03). This report is available only through NTIS (see address given above).

NCEER-92-0033 "Reconnaissance Report on the Cairo, Egypt Earthquake of October 12, 1992," by M. Khater, 12/23/92, (PB93-188621, A03, MF-A01).

NCEER-92-0034 "Low-Level Dynamic Characteristics of Four Tall Flat-Plate Buildings in New York City," by H. Gavin, S. Yuan, J. Grossman, E. Pekelis and K. Jacob, 12/28/92, (PB93-188217, A07, MF-A02).

NCEER-93-0001 "An Experimental Study on the Seismic Performance of Brick-Infilled Steel Frames With and Without Retrofit," by J.B. Mander, B. Nair, K. Wojtkowski and J. Ma, 1/29/93, (PB93-227510, A07, MF-A02).

NCEER-93-0002 "Social Accounting for Disaster Preparedness and Recovery Planning," by S. Cole, E. Pantoja and V. Razak, 2/22/93, (PB94-142114, A12, MF-A03).

NCEER-93-0003 "Assessment of 1991 NEHRP Provisions for Nonstructural Components and Recommended Revisions," by T.T. Soong, G. Chen, Z. Wu, R-H. Zhang and M. Grigoriu, 3/1/93, (PB93-188639, A06, MF-A02).

NCEER-93-0004 "Evaluation of Static and Response Spectrum Analysis Procedures of SEAOC/UBC for Seismic Isolated Structures," by C.W. Winters and M.C. Constantinou, 3/23/93, (PB93-198299, A10, MF-A03).

NCEER-93-0005 "Earthquakes in the Northeast - Are We Ignoring the Hazard? A Workshop on Earthquake Science and Safety for Educators," edited by K.E.K. Ross, 4/2/93, (PB94-103066, A09, MF-A02).

NCEER-93-0006 "Inelastic Response of Reinforced Concrete Structures with Viscoelastic Braces," by R.F. Lobo, J.M. Bracci, K.L. Shen, A.M. Reinhorn and T.T. Soong, 4/5/93, (PB93-227486, A05, MF-A02).

NCEER-93-0007 "Seismic Testing of Installation Methods for Computers and Data Processing Equipment," by K. Kosar, T.T. Soong, K.L. Shen, J.A. HoLung and Y.K. Lin, 4/12/93, (PB93-198299, A07, MF-A02).

NCEER-93-0008 "Retrofit of Reinforced Concrete Frames Using Added Dampers," by A. Reinhorn, M. Constantinou and C. Li, to be published.

NCEER-93-0009 "Seismic Behavior and Design Guidelines for Steel Frame Structures with Added Viscoelastic Dampers," by K.C. Chang, M.L. Lai, T.T. Soong, D.S. Hao and Y.C. Yeh, 5/1/93, (PB94-141959, A07, MF-A02).

NCEER-93-0010 "Seismic Performance of Shear-Critical Reinforced Concrete Bridge Piers," by J.B. Mander, S.M. Waheed, M.T.A. Chaudhary and S.S. Chen, 5/12/93, (PB93-227494, A08, MF-A02).

NCEER-93-0011 "3D-BASIS-TABS: Computer Program for Nonlinear Dynamic Analysis of Three Dimensional Base Isolated Structures," by S. Nagarajaiah, C. Li, A.M. Reinhorn and M.C. Constantinou, 8/2/93, (PB94-141819, A09, MF-A02).

NCEER-93-0012 "Effects of Hydrocarbon Spills from an Oil Pipeline Break on Ground Water," by O.J. Helweg and H.H.M. Hwang, 8/3/93, (PB94-141942, A06, MF-A02).

NCEER-93-0013 "Simplified Procedures for Seismic Design of Nonstructural Components and Assessment of Current Code Provisions," by M.P. Singh, L.E. Suarez, E.E. Matheu and G.O. Maldonado, 8/4/93, (PB94-141827, A09, MF-A02).

NCEER-93-0014 "An Energy Approach to Seismic Analysis and Design of Secondary Systems," by G. Chen and T.T. Soong, 8/6/93, (PB94-142767, A11, MF-A03).

NCEER-93-0015 "Proceedings from School Sites: Becoming Prepared for Earthquakes - Commemorating the Third Anniversary of the Loma Prieta Earthquake," Edited by F.E. Winslow and K.E.K. Ross, 8/16/93, (PB94-154275, A16, MF-A02).

NCEER-93-0016 "Reconnaissance Report of Damage to Historic Monuments in Cairo, Egypt Following the October 12, 1992 Dahshur Earthquake," by D. Sykora, D. Look, G. Croci, E. Karaesmen and E. Karaesmen, 8/19/93, (PB94-142221, A08, MF-A02).

NCEER-93-0017 "The Island of Guam Earthquake of August 8, 1993," by S.W. Swan and S.K. Harris, 9/30/93, (PB94-141843, A04, MF-A01).

NCEER-93-0018 "Engineering Aspects of the October 12, 1992 Egyptian Earthquake," by A.W. Elgamal, M. Amer, K. Adalier and A. Abul-Fadl, 10/7/93, (PB94-141983, A05, MF-A01).

NCEER-93-0019 "Development of an Earthquake Motion Simulator and its Application in Dynamic Centrifuge Testing," by I. Krstelj, Supervised by J.H. Prevost, 10/23/93, (PB94-181773, A-10, MF-A03).

NCEER-93-0020 "NCEER-Taisei Corporation Research Program on Sliding Seismic Isolation Systems for Bridges: Experimental and Analytical Study of a Friction Pendulum System (FPS)," by M.C. Constantinou, P. Tsopelas, Y-S. Kim and S. Okamoto, 11/1/93, (PB94-142775, A08, MF-A02).

NCEER-93-0021 "Finite Element Modeling of Elastomeric Seismic Isolation Bearings," by L.J. Billings, Supervised by R. Shepherd, 11/8/93, to be published.

NCEER-93-0022 "Seismic Vulnerability of Equipment in Critical Facilities: Life-Safety and Operational Consequences," by K. Porter, G.S. Johnson, M.M. Zadeh, C. Scawthorn and S. Eder, 11/24/93, (PB94-181765, A16, MF-A03).

NCEER-93-0023 "Hokkaido Nansei-oki, Japan Earthquake of July 12, 1993, by P.I. Yanev and C.R. Scawthorn, 12/23/93, (PB94-181500, A07, MF-A01).

NCEER-94-0001 "An Evaluation of Seismic Serviceability of Water Supply Networks with Application to the San Francisco Auxiliary Water Supply System," by I. Markov, Supervised by M. Grigoriu and T. O'Rourke, 1/21/94, (PB94-204013, A07, MF-A02).

NCEER-94-0002 "NCEER-Taisei Corporation Research Program on Sliding Seismic Isolation Systems for Bridges: Experimental and Analytical Study of Systems Consisting of Sliding Bearings, Rubber Restoring Force Devices and Fluid Dampers," Volumes I and II, by P. Tsopelas, S. Okamoto, M.C. Constantinou, D. Ozaki and S. Fujii, 2/4/94, (PB94-181740, A09, MF-A02 and PB94-181757, A12, MF-A03).

NCEER-94-0003 "A Markov Model for Local and Global Damage Indices in Seismic Analysis," by S. Rahman and M. Grigoriu, 2/18/94, (PB94-206000, A12, MF-A03).

NCEER-94-0004 "Proceedings from the NCEER Workshop on Seismic Response of Masonry Infills," edited by D.P. Abrams, 3/1/94, (PB94-180783, A07, MF-A02).

NCEER-94-0005 "The Northridge, California Earthquake of January 17, 1994: General Reconnaissance Report," edited by J.D. Goltz, 3/11/94, (PB94-193943, A10, MF-A03).

NCEER-94-0006 "Seismic Energy Based Fatigue Damage Analysis of Bridge Columns: Part I - Evaluation of Seismic Capacity," by G.A. Chang and J.B. Mander, 3/14/94, (PB94-219185, A11, MF-A03).

NCEER-94-0007 "Seismic Isolation of Multi-Story Frame Structures Using Spherical Sliding Isolation Systems," by T.M. Al-Hussaini, V.A. Zayas and M.C. Constantinou, 3/17/94, (PB94-193745, A09, MF-A02).

NCEER-94-0008 "The Northridge, California Earthquake of January 17, 1994: Performance of Highway Bridges," edited by I.G. Buckle, 3/24/94, (PB94-193851, A06, MF-A02).

NCEER-94-0009 "Proceedings of the Third U.S.-Japan Workshop on Earthquake Protective Systems for Bridges," edited by I.G. Buckle and I. Friedland, 3/31/94, (PB94-195815, A99, MF-A06).

NCEER-94-0010 "3D-BASIS-ME: Computer Program for Nonlinear Dynamic Analysis of Seismically Isolated Single and Multiple Structures and Liquid Storage Tanks," by P.C. Tsopelas, M.C. Constantinou and A.M. Reinhorn, 4/12/94, (PB94-204922, A09, MF-A02).

NCEER-94-0011 "The Northridge, California Earthquake of January 17, 1994: Performance of Gas Transmission Pipelines," by T.D. O'Rourke and M.C. Palmer, 5/16/94, (PB94-204989, A05, MF-A01).

NCEER-94-0012 "Feasibility Study of Replacement Procedures and Earthquake Performance Related to Gas Transmission Pipelines," by T.D. O'Rourke and M.C. Palmer, 5/25/94, (PB94-206638, A09, MF-A02).

NCEER-94-0013 "Seismic Energy Based Fatigue Damage Analysis of Bridge Columns: Part II - Evaluation of Seismic Demand," by G.A. Chang and J.B. Mander, 6/1/94, (PB95-18106, A08, MF-A02).

NCEER-94-0014 "NCEER-Taisei Corporation Research Program on Sliding Seismic Isolation Systems for Bridges: Experimental and Analytical Study of a System Consisting of Sliding Bearings and Fluid Restoring Force/Damping Devices," by P. Tsopelas and M.C. Constantinou, 6/13/94, (PB94-219144, A10, MF-A03).

NCEER-94-0015 "Generation of Hazard-Consistent Fragility Curves for Seismic Loss Estimation Studies," by H. Hwang and J-R. Huo, 6/14/94, (PB95-181996, A09, MF-A02).

NCEER-94-0016 "Seismic Study of Building Frames with Added Energy-Absorbing Devices," by W.S. Pong, C.S. Tsai and G.C. Lee, 6/20/94, (PB94-219136, A10, A03).

NCEER-94-0017 "Sliding Mode Control for Seismic-Excited Linear and Nonlinear Civil Engineering Structures," by J. Yang, J. Wu, A. Agrawal and Z. Li, 6/21/94, (PB95-138483, A06, MF-A02).

NCEER-94-0018 "3D-BASIS-TABS Version 2.0: Computer Program for Nonlinear Dynamic Analysis of Three Dimensional Base Isolated Structures," by A.M. Reinhorn, S. Nagarajaiah, M.C. Constantinou, P. Tsopelas and R. Li, 6/22/94, (PB95-182176, A08, MF-A02).

NCEER-94-0019 "Proceedings of the International Workshop on Civil Infrastructure Systems: Application of Intelligent Systems and Advanced Materials on Bridge Systems," Edited by G.C. Lee and K.C. Chang, 7/18/94, (PB95-252474, A20, MF-A04).

NCEER-94-0020 "Study of Seismic Isolation Systems for Computer Floors," by V. Lambrou and M.C. Constantinou, 7/19/94, (PB95-138533, A10, MF-A03).

NCEER-94-0021 "Proceedings of the U.S.-Italian Workshop on Guidelines for Seismic Evaluation and Rehabilitation of Unreinforced Masonry Buildings," Edited by D.P. Abrams and G.M. Calvi, 7/20/94, (PB95-138749, A13, MF-A03).

NCEER-94-0022 "NCEER-Taisei Corporation Research Program on Sliding Seismic Isolation Systems for Bridges: Experimental and Analytical Study of a System Consisting of Lubricated PTFE Sliding Bearings and Mild Steel Dampers," by P. Tsopelas and M.C. Constantinou, 7/22/94, (PB95-182184, A08, MF-A02).

NCEER-94-0023 “Development of Reliability-Based Design Criteria for Buildings Under Seismic Load,” by Y.K. Wen, H. Hwang and M. Shinozuka, 8/1/94, (PB95-211934, A08, MF-A02).

NCEER-94-0024 “Experimental Verification of Acceleration Feedback Control Strategies for an Active Tendon System,” by S.J. Dyke, B.F. Spencer, Jr., P. Quast, M.K. Sain, D.C. Kaspari, Jr. and T.T. Soong, 8/29/94, (PB95-212320, A05, MF-A01).

NCEER-94-0025 “Seismic Retrofitting Manual for Highway Bridges,” Edited by I.G. Buckle and I.F. Friedland, published by the Federal Highway Administration (PB95-212676, A15, MF-A03).

NCEER-94-0026 “Proceedings from the Fifth U.S.-Japan Workshop on Earthquake Resistant Design of Lifeline Facilities and Countermeasures Against Soil Liquefaction,” Edited by T.D. O’Rourke and M. Hamada, 11/7/94, (PB95-220802, A99, MF-E08).

NCEER-95-0001 "Experimental and Analytical Investigation of Seismic Retrofit of Structures with Supplemental Damping: Part 1 - Fluid Viscous Damping Devices," by A.M. Reinhorn, C. Li and M.C. Constantinou, 1/3/95, (PB95-266599, A09, MF-A02).

NCEER-95-0002 "Experimental and Analytical Study of Low-Cycle Fatigue Behavior of Semi-Rigid Top-And-Seat Angle Connections," by G. Pekcan, J.B. Mander and S.S. Chen, 1/5/95, (PB95-220042, A07, MF-A02).

NCEER-95-0003 "NCEER-ATC Joint Study on Fragility of Buildings," by T. Anagnos, C. Rojahn and A.S. Kiremidjian, 1/20/95, (PB95-220026, A06, MF-A02).

NCEER-95-0004 "Nonlinear Control Algorithms for Peak Response Reduction," by Z. Wu, T.T. Soong, V. Gattulli and R.C. Lin, 2/16/95, (PB95-220349, A05, MF-A01).

NCEER-95-0005 "Pipeline Replacement Feasibility Study: A Methodology for Minimizing Seismic and Corrosion Risks to Underground Natural Gas Pipelines," by R.T. Eguchi, H.A. Seligson and D.G. Honegger, 3/2/95, (PB95-252326, A06, MF-A02).

NCEER-95-0006 "Evaluation of Seismic Performance of an 11-Story Frame Building During the 1994 Northridge Earthquake," by F. Naeim, R. DiSulio, K. Benuska, A. Reinhorn and C. Li, to be published.

NCEER-95-0007 "Prioritization of Bridges for Seismic Retrofitting," by N. Basöz and A.S. Kiremidjian, 4/24/95, (PB95-252300, A08, MF-A02).

NCEER-95-0008 "Method for Developing Motion Damage Relationships for Reinforced Concrete Frames," by A. Singhal and A.S. Kiremidjian, 5/11/95, (PB95-266607, A06, MF-A02).

NCEER-95-0009 "Experimental and Analytical Investigation of Seismic Retrofit of Structures with Supplemental Damping: Part II - Friction Devices," by C. Li and A.M. Reinhorn, 7/6/95, (PB96-128087, A11, MF-A03).

NCEER-95-0010 "Experimental Performance and Analytical Study of a Non-Ductile Reinforced Concrete Frame Structure Retrofitted with Elastomeric Spring Dampers," by G. Pekcan, J.B. Mander and S.S. Chen, 7/14/95, (PB96-137161, A08, MF-A02).

NCEER-95-0011 "Development and Experimental Study of Semi-Active Fluid Damping Devices for Seismic Protection of Structures," by M.D. Symans and M.C. Constantinou, 8/3/95, (PB96-136940, A23, MF-A04).

NCEER-95-0012 "Real-Time Structural Parameter Modification (RSPM): Development of Innervated Structures," by Z. Liang, M. Tong and G.C. Lee, 4/11/95, (PB96-137153, A06, MF-A01).

NCEER-95-0013 "Experimental and Analytical Investigation of Seismic Retrofit of Structures with Supplemental Damping: Part III - Viscous Damping Walls," by A.M. Reinhorn and C. Li, 10/1/95, (PB96-176409, A11, MF-A03).

NCEER-95-0014 "Seismic Fragility Analysis of Equipment and Structures in a Memphis Electric Substation," by J-R. Huo and H.H.M. Hwang, 8/10/95, (PB96-128087, A09, MF-A02).

NCEER-95-0015 "The Hanshin-Awaji Earthquake of January 17, 1995: Performance of Lifelines," Edited by M. Shinozuka, 11/3/95, (PB96-176383, A15, MF-A03).

NCEER-95-0016 "Highway Culvert Performance During Earthquakes," by T.L. Youd and C.J. Beckman, available as NCEER-96-0015.

NCEER-95-0017 "The Hanshin-Awaji Earthquake of January 17, 1995: Performance of Highway Bridges," Edited by I.G. Buckle, 12/1/95, to be published.

NCEER-95-0018 "Modeling of Masonry Infill Panels for Structural Analysis," by A.M. Reinhorn, A. Madan, R.E. Valles, Y. Reichmann and J.B. Mander, 12/8/95, (PB97-110886, MF-A01, A06).

NCEER-95-0019 "Optimal Polynomial Control for Linear and Nonlinear Structures," by A.K. Agrawal and J.N. Yang, 12/11/95, (PB96-168737, A07, MF-A02).

NCEER-95-0020 "Retrofit of Non-Ductile Reinforced Concrete Frames Using Friction Dampers," by R.S. Rao, P. Gergely and R.N. White, 12/22/95, (PB97-133508, A10, MF-A02).

NCEER-95-0021 "Parametric Results for Seismic Response of Pile-Supported Bridge Bents," by G. Mylonakis, A. Nikolaou and G. Gazetas, 12/22/95, (PB97-100242, A12, MF-A03).

NCEER-95-0022 "Kinematic Bending Moments in Seismically Stressed Piles," by A. Nikolaou, G. Mylonakis and G. Gazetas, 12/23/95, (PB97-113914, MF-A03, A13).

NCEER-96-0001 "Dynamic Response of Unreinforced Masonry Buildings with Flexible Diaphragms," by A.C. Costley and D.P. Abrams," 10/10/96, (PB97-133573, MF-A03, A15).

NCEER-96-0002 "State of the Art Review: Foundations and Retaining Structures," by I. Po Lam, to be published.

NCEER-96-0003 "Ductility of Rectangular Reinforced Concrete Bridge Columns with Moderate Confinement," by N. Wehbe, M. Saiidi, D. Sanders and B. Douglas, 11/7/96, (PB97-133557, A06, MF-A02).

NCEER-96-0004 "Proceedings of the Long-Span Bridge Seismic Research Workshop," edited by I.G. Buckle and I.M. Friedland, to be published.

NCEER-96-0005 "Establish Representative Pier Types for Comprehensive Study: Eastern United States," by J. Kulicki and Z. Prucz, 5/28/96, (PB98-119217, A07, MF-A02).

NCEER-96-0006 "Establish Representative Pier Types for Comprehensive Study: Western United States," by R. Imbsen, R.A. Schamber and T.A. Osterkamp, 5/28/96, (PB98-118607, A07, MF-A02).

NCEER-96-0007 "Nonlinear Control Techniques for Dynamical Systems with Uncertain Parameters," by R.G. Ghanem and M.I. Bujakov, 5/27/96, (PB97-100259, A17, MF-A03).

NCEER-96-0008 "Seismic Evaluation of a 30-Year Old Non-Ductile Highway Bridge Pier and Its Retrofit," by J.B. Mander, B. Mahmoodzadegan, S. Bhadra and S.S. Chen, 5/31/96, (PB97-110902, MF-A03, A10).

NCEER-96-0009 "Seismic Performance of a Model Reinforced Concrete Bridge Pier Before and After Retrofit," by J.B. Mander, J.H. Kim and C.A. Ligozio, 5/31/96, (PB97-110910, MF-A02, A10).

NCEER-96-0010 "IDARC2D Version 4.0: A Computer Program for the Inelastic Damage Analysis of Buildings," by R.E. Valles, A.M. Reinhorn, S.K. Kunnath, C. Li and A. Madan, 6/3/96, (PB97-100234, A17, MF-A03).

NCEER-96-0011 "Estimation of the Economic Impact of Multiple Lifeline Disruption: Memphis Light, Gas and Water Division Case Study," by S.E. Chang, H.A. Seligson and R.T. Eguchi, 8/16/96, (PB97-133490, A11, MF-A03).

NCEER-96-0012 "Proceedings from the Sixth Japan-U.S. Workshop on Earthquake Resistant Design of Lifeline Facilities and Countermeasures Against Soil Liquefaction, Edited by M. Hamada and T. O'Rourke, 9/11/96, (PB97-133581, A99, MF-A06).

NCEER-96-0013 "Chemical Hazards, Mitigation and Preparedness in Areas of High Seismic Risk: A Methodology for Estimating the Risk of Post-Earthquake Hazardous Materials Release," by H.A. Seligson, R.T. Eguchi, K.J. Tierney and K. Richmond, 11/7/96, (PB97-133565, MF-A02, A08).

NCEER-96-0014 "Response of Steel Bridge Bearings to Reversed Cyclic Loading," by J.B. Mander, D-K. Kim, S.S. Chen and G.J. Premus, 11/13/96, (PB97-140735, A12, MF-A03).

NCEER-96-0015 "Highway Culvert Performance During Past Earthquakes," by T.L. Youd and C.J. Beckman, 11/25/96, (PB97-133532, A06, MF-A01).

NCEER-97-0001 "Evaluation, Prevention and Mitigation of Pounding Effects in Building Structures," by R.E. Valles and A.M. Reinhorn, 2/20/97, (PB97-159552, A14, MF-A03).

NCEER-97-0002 "Seismic Design Criteria for Bridges and Other Highway Structures," by C. Rojahn, R. Mayes, D.G. Anderson, J. Clark, J.H. Hom, R.V. Nutt and M.J. O'Rourke, 4/30/97, (PB97-194658, A06, MF-A03).

NCEER-97-0003 “Proceedings of the U.S.-Italian Workshop on Seismic Evaluation and Retrofit,” Edited by D.P. Abrams and G.M. Calvi, 3/19/97, (PB97-194666, A13, MF-A03).

NCEER-97-0004 "Investigation of Seismic Response of Buildings with Linear and Nonlinear Fluid Viscous Dampers," by A.A. Seleemah and M.C. Constantinou, 5/21/97, (PB98-109002, A15, MF-A03).

NCEER-97-0005 "Proceedings of the Workshop on Earthquake Engineering Frontiers in Transportation Facilities," edited by G.C. Lee and I.M. Friedland, 8/29/97, (PB98-128911, A25, MR-A04).

NCEER-97-0006 "Cumulative Seismic Damage of Reinforced Concrete Bridge Piers," by S.K. Kunnath, A. El-Bahy, A. Taylor and W. Stone, 9/2/97, (PB98-108814, A11, MF-A03).

NCEER-97-0007 "Structural Details to Accommodate Seismic Movements of Highway Bridges and Retaining Walls," by R.A. Imbsen, R.A. Schamber, E. Thorkildsen, A. Kartoum, B.T. Martin, T.N. Rosser and J.M. Kulicki, 9/3/97, (PB98-108996, A09, MF-A02).

NCEER-97-0008 "A Method for Earthquake Motion-Damage Relationships with Application to Reinforced Concrete Frames," by A. Singhal and A.S. Kiremidjian, 9/10/97, (PB98-108988, A13, MF-A03).

NCEER-97-0009 "Seismic Analysis and Design of Bridge Abutments Considering Sliding and Rotation," by K. Fishman and R. Richards, Jr., 9/15/97, (PB98-108897, A06, MF-A02).

NCEER-97-0010 "Proceedings of the FHWA/NCEER Workshop on the National Representation of Seismic Ground Motion for New and Existing Highway Facilities," edited by I.M. Friedland, M.S. Power and R.L. Mayes, 9/22/97, (PB98-128903, A21, MF-A04).

NCEER-97-0011 "Seismic Analysis for Design or Retrofit of Gravity Bridge Abutments," by K.L. Fishman, R. Richards, Jr. and R.C. Divito, 10/2/97, (PB98-128937, A08, MF-A02).

NCEER-97-0012 "Evaluation of Simplified Methods of Analysis for Yielding Structures," by P. Tsopelas, M.C. Constantinou, C.A. Kircher and A.S. Whittaker, 10/31/97, (PB98-128929, A10, MF-A03).

NCEER-97-0013 "Seismic Design of Bridge Columns Based on Control and Repairability of Damage," by C-T. Cheng and J.B. Mander, 12/8/97, (PB98-144249, A11, MF-A03).

NCEER-97-0014 "Seismic Resistance of Bridge Piers Based on Damage Avoidance Design," by J.B. Mander and C-T. Cheng, 12/10/97, (PB98-144223, A09, MF-A02).

NCEER-97-0015 “Seismic Response of Nominally Symmetric Systems with Strength Uncertainty,” by S. Balopoulou and M. Grigoriu, 12/23/97, (PB98-153422, A11, MF-A03).

NCEER-97-0016 “Evaluation of Seismic Retrofit Methods for Reinforced Concrete Bridge Columns,” by T.J. Wipf, F.W. Klaiber and F.M. Russo, 12/28/97, (PB98-144215, A12, MF-A03).

NCEER-97-0017 “Seismic Fragility of Existing Conventional Reinforced Concrete Highway Bridges,” by C.L. Mullen and A.S. Cakmak, 12/30/97, (PB98-153406, A08, MF-A02).

NCEER-97-0018 “Loss Asssessment of Memphis Buildings,” edited by D.P. Abrams and M. Shinozuka, 12/31/97, (PB98-144231, A13, MF-A03).

NCEER-97-0019 “Seismic Evaluation of Frames with Infill Walls Using Quasi-static Experiments,” by K.M. Mosalam, R.N. White and P. Gergely, 12/31/97, (PB98-153455, A07, MF-A02).

NCEER-97-0020 “Seismic Evaluation of Frames with Infill Walls Using Pseudo-dynamic Experiments,” by K.M. Mosalam, R.N. White and P. Gergely, 12/31/97, (PB98-153430, A07, MF-A02).

NCEER-97-0021 “Computational Strategies for Frames with Infill Walls: Discrete and Smeared Crack Analyses and Seismic Fragility,” by K.M. Mosalam, R.N. White and P. Gergely, 12/31/97, (PB98-153414, A10, MF-A02).

NCEER-97-0022 "Proceedings of the NCEER Workshop on Evaluation of Liquefaction Resistance of Soils," edited by T.L. Youd and I.M. Idriss, 12/31/97, (PB98-155617, A15, MF-A03).

MCEER-98-0001 "Extraction of Nonlinear Hysteretic Properties of Seismically Isolated Bridges from Quick-Release Field Tests," by Q. Chen, B.M. Douglas, E.M. Maragakis and I.G. Buckle, 5/26/98, (PB99-118838, A06, MF-A01).

MCEER-98-0002 "Methodologies for Evaluating the Importance of Highway Bridges," by A. Thomas, S. Eshenaur and J. Kulicki, 5/29/98, (PB99-118846, A10, MF-A02).

MCEER-98-0003 "Capacity Design of Bridge Piers and the Analysis of Overstrength," by J.B. Mander, A. Dutta and P. Goel, 6/1/98, (PB99-118853, A09, MF-A02).

MCEER-98-0004 "Evaluation of Bridge Damage Data from the Loma Prieta and Northridge, California Earthquakes," by N. Basoz and A. Kiremidjian, 6/2/98, (PB99-118861, A15, MF-A03).

MCEER-98-0005 "Screening Guide for Rapid Assessment of Liquefaction Hazard at Highway Bridge Sites," by T. L. Youd, 6/16/98, (PB99-118879, A06, not available on microfiche).

MCEER-98-0006 "Structural Steel and Steel/Concrete Interface Details for Bridges," by P. Ritchie, N. Kauhl and J. Kulicki, 7/13/98, (PB99-118945, A06, MF-A01).

MCEER-98-0007 "Capacity Design and Fatigue Analysis of Confined Concrete Columns," by A. Dutta and J.B. Mander, 7/14/98, (PB99-118960, A14, MF-A03).

MCEER-98-0008 "Proceedings of the Workshop on Performance Criteria for Telecommunication Services Under Earthquake Conditions," edited by A.J. Schiff, 7/15/98, (PB99-118952, A08, MF-A02).

MCEER-98-0009 "Fatigue Analysis of Unconfined Concrete Columns," by J.B. Mander, A. Dutta and J.H. Kim, 9/12/98, (PB99-123655, A10, MF-A02).

MCEER-98-0010 "Centrifuge Modeling of Cyclic Lateral Response of Pile-Cap Systems and Seat-Type Abutments in Dry Sands," by A.D. Gadre and R. Dobry, 10/2/98, (PB99-123606, A13, MF-A03).

MCEER-98-0011 "IDARC-BRIDGE: A Computational Platform for Seismic Damage Assessment of Bridge Structures," by A.M. Reinhorn, V. Simeonov, G. Mylonakis and Y. Reichman, 10/2/98, (PB99-162919, A15, MF-A03).

MCEER-98-0012 "Experimental Investigation of the Dynamic Response of Two Bridges Before and After Retrofitting with Elastomeric Bearings," by D.A. Wendichansky, S.S. Chen and J.B. Mander, 10/2/98, (PB99-162927, A15, MF-A03).

MCEER-98-0013 "Design Procedures for Hinge Restrainers and Hinge Sear Width for Multiple-Frame Bridges," by R. Des Roches and G.L. Fenves, 11/3/98, (PB99-140477, A13, MF-A03).

MCEER-98-0014 "Response Modification Factors for Seismically Isolated Bridges," by M.C. Constantinou and J.K. Quarshie, 11/3/98, (PB99-140485, A14, MF-A03).

MCEER-98-0015 "Proceedings of the U.S.-Italy Workshop on Seismic Protective Systems for Bridges," edited by I.M. Friedland and M.C. Constantinou, 11/3/98, (PB2000-101711, A22, MF-A04).

MCEER-98-0016 "Appropriate Seismic Reliability for Critical Equipment Systems: Recommendations Based on Regional Analysis of Financial and Life Loss," by K. Porter, C. Scawthorn, C. Taylor and N. Blais, 11/10/98, (PB99-157265, A08, MF-A02).

MCEER-98-0017 "Proceedings of the U.S. Japan Joint Seminar on Civil Infrastructure Systems Research," edited by M. Shinozuka and A. Rose, 11/12/98, (PB99-156713, A16, MF-A03).

MCEER-98-0018 "Modeling of Pile Footings and Drilled Shafts for Seismic Design," by I. PoLam, M. Kapuskar and D. Chaudhuri, 12/21/98, (PB99-157257, A09, MF-A02).

MCEER-99-0001 "Seismic Evaluation of a Masonry Infilled Reinforced Concrete Frame by Pseudodynamic Testing," by S.G. Buonopane and R.N. White, 2/16/99, (PB99-162851, A09, MF-A02).

MCEER-99-0002 "Response History Analysis of Structures with Seismic Isolation and Energy Dissipation Systems: Verification Examples for Program SAP2000," by J. Scheller and M.C. Constantinou, 2/22/99, (PB99-162869, A08, MF-A02).

MCEER-99-0003 "Experimental Study on the Seismic Design and Retrofit of Bridge Columns Including Axial Load Effects," by A. Dutta, T. Kokorina and J.B. Mander, 2/22/99, (PB99-162877, A09, MF-A02).

MCEER-99-0004 "Experimental Study of Bridge Elastomeric and Other Isolation and Energy Dissipation Systems with Emphasis on Uplift Prevention and High Velocity Near-source Seismic Excitation," by A. Kasalanati and M. C. Constantinou, 2/26/99, (PB99-162885, A12, MF-A03).

MCEER-99-0005 "Truss Modeling of Reinforced Concrete Shear-flexure Behavior," by J.H. Kim and J.B. Mander, 3/8/99, (PB99-163693, A12, MF-A03).

MCEER-99-0006 "Experimental Investigation and Computational Modeling of Seismic Response of a 1:4 Scale Model Steel Structure with a Load Balancing Supplemental Damping System," by G. Pekcan, J.B. Mander and S.S. Chen, 4/2/99, (PB99-162893, A11, MF-A03).

MCEER-99-0007 "Effect of Vertical Ground Motions on the Structural Response of Highway Bridges," by M.R. Button, C.J. Cronin and R.L. Mayes, 4/10/99, (PB2000-101411, A10, MF-A03).

MCEER-99-0008 "Seismic Reliability Assessment of Critical Facilities: A Handbook, Supporting Documentation, and Model Code Provisions," by G.S. Johnson, R.E. Sheppard, M.D. Quilici, S.J. Eder and C.R. Scawthorn, 4/12/99, (PB2000-101701, A18, MF-A04).

MCEER-99-0009 "Impact Assessment of Selected MCEER Highway Project Research on the Seismic Design of Highway Structures," by C. Rojahn, R. Mayes, D.G. Anderson, J.H. Clark, D'Appolonia Engineering, S. Gloyd and R.V. Nutt, 4/14/99, (PB99-162901, A10, MF-A02).

MCEER-99-0010 "Site Factors and Site Categories in Seismic Codes," by R. Dobry, R. Ramos and M.S. Power, 7/19/99, (PB2000-101705, A08, MF-A02).

MCEER-99-0011 "Restrainer Design Procedures for Multi-Span Simply-Supported Bridges," by M.J. Randall, M. Saiidi, E. Maragakis and T. Isakovic, 7/20/99, (PB2000-101702, A10, MF-A02).

MCEER-99-0012 "Property Modification Factors for Seismic Isolation Bearings," by M.C. Constantinou, P. Tsopelas, A. Kasalanati and E. Wolff, 7/20/99, (PB2000-103387, A11, MF-A03).

MCEER-99-0013 "Critical Seismic Issues for Existing Steel Bridges," by P. Ritchie, N. Kauhl and J. Kulicki, 7/20/99, (PB2000-101697, A09, MF-A02).

MCEER-99-0014 "Nonstructural Damage Database," by A. Kao, T.T. Soong and A. Vender, 7/24/99, (PB2000-101407, A06, MF-A01).

MCEER-99-0015 "Guide to Remedial Measures for Liquefaction Mitigation at Existing Highway Bridge Sites," by H.G. Cooke and J. K. Mitchell, 7/26/99, (PB2000-101703, A11, MF-A03).

MCEER-99-0016 "Proceedings of the MCEER Workshop on Ground Motion Methodologies for the Eastern United States," edited by N. Abrahamson and A. Becker, 8/11/99, (PB2000-103385, A07, MF-A02).

MCEER-99-0017 "Quindío, Colombia Earthquake of January 25, 1999: Reconnaissance Report," by A.P. Asfura and P.J. Flores, 10/4/99, (PB2000-106893, A06, MF-A01).

MCEER-99-0018 "Hysteretic Models for Cyclic Behavior of Deteriorating Inelastic Structures," by M.V. Sivaselvan and A.M. Reinhorn, 11/5/99, (PB2000-103386, A08, MF-A02).

MCEER-99-0019 "Proceedings of the 7th U.S.- Japan Workshop on Earthquake Resistant Design of Lifeline Facilities and Countermeasures Against Soil Liquefaction," edited by T.D. O'Rourke, J.P. Bardet and M. Hamada, 11/19/99, (PB2000-103354, A99, MF-A06).

MCEER-99-0020 "Development of Measurement Capability for Micro-Vibration Evaluations with Application to Chip Fabrication Facilities," by G.C. Lee, Z. Liang, J.W. Song, J.D. Shen and W.C. Liu, 12/1/99, (PB2000-105993, A08, MF-A02).

MCEER-99-0021 "Design and Retrofit Methodology for Building Structures with Supplemental Energy Dissipating Systems," by G. Pekcan, J.B. Mander and S.S. Chen, 12/31/99, (PB2000-105994, A11, MF-A03).

MCEER-00-0001 "The Marmara, Turkey Earthquake of August 17, 1999: Reconnaissance Report," edited by C. Scawthorn; with major contributions by M. Bruneau, R. Eguchi, T. Holzer, G. Johnson, J. Mander, J. Mitchell, W. Mitchell, A. Papageorgiou, C. Scaethorn, and G. Webb, 3/23/00, (PB2000-106200, A11, MF-A03).

MCEER-00-0002 "Proceedings of the MCEER Workshop for Seismic Hazard Mitigation of Health Care Facilities," edited by G.C. Lee, M. Ettouney, M. Grigoriu, J. Hauer and J. Nigg, 3/29/00, (PB2000-106892, A08, MF-A02).

MCEER-00-0003 "The Chi-Chi, Taiwan Earthquake of September 21, 1999: Reconnaissance Report," edited by G.C. Lee and C.H. Loh, with major contributions by G.C. Lee, M. Bruneau, I.G. Buckle, S.E. Chang, P.J. Flores, T.D. O'Rourke, M. Shinozuka, T.T. Soong, C-H. Loh, K-C. Chang, Z-J. Chen, J-S. Hwang, M-L. Lin, G-Y. Liu, K-C. Tsai, G.C. Yao and C-L. Yen, 4/30/00, (PB2001-100980, A10, MF-A02).

MCEER-00-0004 "Seismic Retrofit of End-Sway Frames of Steel Deck-Truss Bridges with a Supplemental Tendon System: Experimental and Analytical Investigation," by G. Pekcan, J.B. Mander and S.S. Chen, 7/1/00, (PB2001-100982, A10, MF-A02).

MCEER-00-0005 "Sliding Fragility of Unrestrained Equipment in Critical Facilities," by W.H. Chong and T.T. Soong, 7/5/00, (PB2001-100983, A08, MF-A02).

MCEER-00-0006 "Seismic Response of Reinforced Concrete Bridge Pier Walls in the Weak Direction," by N. Abo-Shadi, M. Saiidi and D. Sanders, 7/17/00, (PB2001-100981, A17, MF-A03).

MCEER-00-0007 "Low-Cycle Fatigue Behavior of Longitudinal Reinforcement in Reinforced Concrete Bridge Columns," by J. Brown and S.K. Kunnath, 7/23/00, (PB2001-104392, A08, MF-A02).

MCEER-00-0008 "Soil Structure Interaction of Bridges for Seismic Analysis," I. PoLam and H. Law, 9/25/00, (PB2001-105397, A08, MF-A02).

MCEER-00-0009 "Proceedings of the First MCEER Workshop on Mitigation of Earthquake Disaster by Advanced Technologies (MEDAT-1), edited by M. Shinozuka, D.J. Inman and T.D. O'Rourke, 11/10/00, (PB2001-105399, A14, MF-A03).

MCEER-00-0010 "Development and Evaluation of Simplified Procedures for Analysis and Design of Buildings with Passive Energy Dissipation Systems," by O.M. Ramirez, M.C. Constantinou, C.A. Kircher, A.S. Whittaker, M.W. Johnson, J.D. Gomez and C. Chrysostomou, 11/16/01, (PB2001-105523, A23, MF-A04).

MCEER-00-0011 "Dynamic Soil-Foundation-Structure Interaction Analyses of Large Caissons," by C-Y. Chang, C-M. Mok, Z-L. Wang, R. Settgast, F. Waggoner, M.A. Ketchum, H.M. Gonnermann and C-C. Chin, 12/30/00, (PB2001-104373, A07, MF-A02).

MCEER-00-0012 "Experimental Evaluation of Seismic Performance of Bridge Restrainers," by A.G. Vlassis, E.M. Maragakis and M. Saiid Saiidi, 12/30/00, (PB2001-104354, A09, MF-A02).

MCEER-00-0013 "Effect of Spatial Variation of Ground Motion on Highway Structures," by M. Shinozuka, V. Saxena and G. Deodatis, 12/31/00, (PB2001-108755, A13, MF-A03).

MCEER-00-0014 "A Risk-Based Methodology for Assessing the Seismic Performance of Highway Systems," by S.D. Werner, C.E. Taylor, J.E. Moore, II, J.S. Walton and S. Cho, 12/31/00, (PB2001-108756, A14, MF-A03).

MCEER-01-0001 "Experimental Investigation of P-Delta Effects to Collapse During Earthquakes," by D. Vian and M. Bruneau, 6/25/01, (PB2002-100534, A17, MF-A03).

MCEER-01-0002 "Proceedings of the Second MCEER Workshop on Mitigation of Earthquake Disaster by Advanced Technologies (MEDAT-2)," edited by M. Bruneau and D.J. Inman, 7/23/01, (PB2002-100434, A16, MF-A03).

MCEER-01-0003 "Sensitivity Analysis of Dynamic Systems Subjected to Seismic Loads," by C. Roth and M. Grigoriu, 9/18/01, (PB2003-100884, A12, MF-A03).

MCEER-01-0004 "Overcoming Obstacles to Implementing Earthquake Hazard Mitigation Policies: Stage 1 Report," by D.J. Alesch and W.J. Petak, 12/17/01, (PB2002-107949, A07, MF-A02).

MCEER-01-0005 "Updating Real-Time Earthquake Loss Estimates: Methods, Problems and Insights," by C.E. Taylor, S.E. Chang and R.T. Eguchi, 12/17/01, (PB2002-107948, A05, MF-A01).

MCEER-01-0006 "Experimental Investigation and Retrofit of Steel Pile Foundations and Pile Bents Under Cyclic Lateral Loadings," by A. Shama, J. Mander, B. Blabac and S. Chen, 12/31/01, (PB2002-107950, A13, MF-A03).

MCEER-02-0001 "Assessment of Performance of Bolu Viaduct in the 1999 Duzce Earthquake in Turkey" by P.C. Roussis, M.C. Constantinou, M. Erdik, E. Durukal and M. Dicleli, 5/8/02, (PB2003-100883, A08, MF-A02).

MCEER-02-0002 "Seismic Behavior of Rail Counterweight Systems of Elevators in Buildings," by M.P. Singh, Rildova and L.E. Suarez, 5/27/02. (PB2003-100882, A11, MF-A03).

MULTIDISCIPLINARY CENTER FOR EARTHQUAKE ENGINEERING RESEARCH

A National Center of Excellence in Advanced Technology Applications

University at Buffalo, State University of New York
Red Jacket Quadrangle ▪ Buffalo, New York 14261-0025
Phone: 716/645-3391 ▪ Fax: 716/645-3399
E-mail: mceer@acsu.buffalo.edu ▪ WWW Site: http://mceer.buffalo.edu

University at Buffalo *The State University of New York*

ISSN 1520-295X